

School of Civil and Mechanical Engineering

**Machinability Improvement of Hard-to-Machine Materials by
Monitoring and Controlling Laser Heating**

Ouf Abdulrahman Shams

**This thesis is presented for the Degree of
Doctor of Philosophy
of
Curtin University**

January 2020

Abstract

In product manufacture, machining of hard metals such as titanium alloys tends to produce poor surface quality with accelerated tool wear and low material removal rate, due to the generation of large cutting forces, excessive workpiece temperatures and chemical reactivity resulting from high yield stress and low thermal conductivity. In overcoming these manufacturing challenges, industry practice upheld by current research identifies significant potential benefits from Thermally-Assisted Machining (TAM) techniques to improve machinability of titanium-based alloys whereby the application of localised workpiece heating temporarily reduces metal hardness at the cutting point and lessens cutting forces. Reduced workpiece hardness due to localised heating also facilitates higher material removal rate and extends cutting tool life whilst resulting in better surface finish. Such techniques under consideration are: heating by laser beam, plasma torch heating and heating by induction coil. Research investigations recognise that the Laser-Assisted Machining (LAM) could reduce cutting forces by 30% to 60% and tool wear by 90%. With Plasma-Assisted Machining cutting forces are reduced by 20% to 40% and enhances the tool life by 150 times. Additionally, the Induction-Assisted Machining is observed to reduce cutting force by 36% to 54% while increasing the tool life by 206.

The laser-assisted technique (LAM) is recognised to be more cost-effective and productive for improving the machinability of titanium alloys than other localised heating techniques. LAM is a widely-used and growing method for controlled preheating of workpiece to reduce cutting forces and promote machinability in metal machining, thereby enhancing manufacturing quality and productivity. In setting LAM parameters, the current practice typically relies on trial-and-error approaches. A clear understanding of workpiece thermal behaviour under laser spot heating is pivotal to developing a systematic basis for determining required preheating levels and optimised cutting variables for LAM. Moreover, the intensity of this thermal penetration dictates the potential degree of ‘thermal softening’ (or increased ductility) achievable in the workpiece, facilitating enhanced LAM process. In achieving this, the experimental methods are recognised to be largely impractical, if not tedious, due to the instrumentation limitations and lack of suitable non-intrusive measuring methods. Conversely, numerical methodologies do

provide precise flexible and cost-effective analytical options, for deriving an insightful understanding of the transient thermal impact from laser preheating on rotating workpiece in machining. Therefore, the numerical simulation is required to study the transient thermal behaviour of a rotating cylinder heated by a laser beam as a heating source.

The research discussed in this thesis presents an investigation, where a finite-volume-based numerical simulation is developed through ANSYS/FLUENT solver for examining the thermal response of a rotating cylinder subjected to localised laser preheating. The uncertainties thereof could lead to adverse outcomes in product manufacture, and would negate the potential benefits of this machining method. On a rotating frame of reference, the numerical model is formulated, considering transient heat conduction into the cylinder body and the combined convection and radiation losses from the cylinder surface. Comprehensive parametric analyses and model validations are carried out to ascertain the accuracy and applicability of the numerical simulation. Based on neural network principles, a preheating parametric predictor for LAM is synthesised using steady state temperature data from the model and incorporating the Levenberg-Marquardt algorithm. This predictive tool is trained and verified as a practical preheating guide for LAM for a range of operating conditions.

The findings of this study have multiple benefits in reassuring the industrial community of using LAM technique in machining hard-to-machine alloys requiring high cost and cutting time. The experimental data provide significant input for developing the three-dimensional numerical model, which allows simulating the transient thermal behaviour of the rotating cylindrical workpiece heated by low-power laser. The numerical model generates data to obtain laser preheating levels to achieve required depth of material softening at the workpiece surface before machining.

In summary, this research examines the practical benefits of localised surface heating of workpiece material with a laser source to reduce local surface hardness and improve machinability to overcome machining challenges of hard alloys in the manufacturing industry. The investigation develops a three-dimensional numerical simulation of laser preheating on a rotating metal cylinder with experimental

validation for examining the thermal response and to identify the strong correlation between laser preheating levels and metal cutting parameters, as applied to hard metal machining processes.

Acknowledgements

Over the past years I have had the opportunity to work with many extraordinary people both inside and outside the Department of Mechanical Engineering and have been blessed with a tremendous amount of support.

First, I sincerely show my gratitude for the grateful support and inspired over these years of my supervisor Dr. Alokesh Pramanik. His expertise, input and advice have been ordinarily valuable for my whole research program.

I would also like to extend my most sincere thanks to Head of Mechanical Engineering Department Professor Tilak Chandratilleke (Co-Supervisor) for all his guidance and help during the years taken to complete this research. He constantly gave me valuable advice and significant support with his kindness, excellent research and abundant experience.

I would like to thank my Co-Supervisor, Dr. Nima Nadim, who introduced me to the laser-related research, guided me in Ph.D. program, and continually supported and inspired me over these years. He provided many brilliant ideas and valuable suggestions to improve and complete this research.

I would also like to sincerely thank Professor Ian Howard (Chairperson) for his unwavering support and encouragement to me. He always emphasised my strengths and show great open-mindedness and warmth, and always made time for me whenever I needed any help.

I also thank technicians David Collier, Graeme Watson, Hamish Thava, and Adam Frew for their assistance during the many hours of testing and manufacturing of the test rig used in this research. Without them, I probably would not achieve this goal.

I would like to give special thanks to my parents, my brothers for their unconditional love and continual support over the years. They always encouraged me to strive to be the best I could and to produce the best work I could. Without their support, patience, and encouragement, it is impossible for me to make it this far.

Finally, I thank with high regard to God who is unconditional love forever. He is always my excellent supporter, who always loves, inspires, encourages, motivates, and strengthens me.

Publications

A list of papers in which some of this work has been published is provided

The following publications are associated with this research:

Book Chapter

- 1- O. A. Shams, A. Pramanik, and T. Chandratilleke, Thermal-Assisted Machining of Titanium Alloys, Advanced Manufacturing Technologies, Springer, p. 49-76, 2017, https://doi.org/10.1007/978-3-319-56099-1_3.
- 2- O. A. Shams, A. Pramanik, T. Chandratilleke, and N. Naim, Comparative Assessment and Merit Appraisal of Thermally Assisted Machining Techniques for Improving Machinability of Titanium Alloys, Introduction to Mechanical Engineering, Springer, p. 297-331, 2018, https://doi.org/10.1007/978-3-319-78488-5_10.

Article Journal

- 3- N. Naim, O. A. Shams, T. Chandratilleke, and A. Pramanik, Preheating and Thermal Behaviour of a Rotating Cylindrical Workpiece in Laser-Assisted Machining, Journal of Engineering Manufacture. p. 49-76, 2019, <https://doi.org/10.1177/0954405419863597>.

Table of Contents

Declaration	Error! Bookmark not defined.
Abstract	II
Acknowledgements	V
Publications	VI
List of Tables	XI
List of Figures	XII
Nomenclature	XVI
Chapter 1	1
Introduction	1
1.1 General Background	1
1.2. Titanium and Titanium Alloys	2
1.3 Machinability of Titanium Alloys	4
1.4 Thermally Assisted Machining (TAM)	5
1.5 Problem Statement	7
1.6 Significance and Contribution of this Study	8
1.7 Objectives of Research	8
1.8 Organization of Thesis	9
Chapter 2	11
Literature Review	11
2.1 Introduction	11
2.2 Background	11
2.3 Machining Difficulties and Issues with Titanium Alloys	20
2.4 Thermally Assisted Machining (TAM)	29
2.5 Effects of Preheating Temperature	31
2.6 Thermally Assisted Machining Techniques	37
2.6.1 Laser-Assisted Machining (LAM)	37
2.6.2 Plasma-Assisted Machining (PAM)	50
2.6.3 Induction-Assisted Machining (IAM)	52
2.7 Laser-Assisted Machining of Rotating Workpiece	56
2.8 Concluding Remarks	61
Chapter 3	63
Experimental Methodology	63
3.1 Introduction	63

3.2 Objectives.....	63
3.3 Design of Experimental	64
3.4 Test-Rig Components.....	67
3.4.1 Mechanical Design Consideration.....	67
3.4.2 Control system (Mechatronics) design.	69
3.4.3 Fabrication Problems	71
3.5 Workpiece Material	74
3.6 Laser System	76
3.7 Temperature Measurement Method	82
3.7.1 FLIR ThermoVision™ A40V Camera	83
3.7.2 ThermaCAM™ Researcher	84
3.8 Reflection Test	86
3.9 Emissivity Test.....	88
3.10 Summary	98
Chapter 4	100
Experimental Analysis.....	100
4.1 Introduction	100
4.2 Emissivity and Temperatures Correction.....	101
4.3 Discussion and Parametric Analysis.....	107
4.3.1 Thermal effect of laser power.....	107
4.3.2 Thermal effect of rotational speed	110
4.3.3 Thermal effect of scanning velocity	116
4.4 Summary	118
Chapter 5	119
Numerical Simulation Methodology	119
5.1 Scope of Chapter.....	119
5.2 Introduction	120
5.3 Numerical Method.....	121
5.4 Ansys FLUENT.....	122
5.4.1 FLUENT setup stages.....	123
5.5 Finite Volume Method (FVM)	123
5.6 Properties of Discretization Schemes	127
5.6.1 Conservative.....	128
5.6.2 Bounded.....	128

5.6.3 Transportive	129
5.7 Discretization	129
5.8 Quadratic Upwind Interpolation for Convection Kinematics Scheme	129
5.9 Modelling Flow in Moving Zone.....	131
5.10 Single Rotating Reference Frame (SRRF)	134
5.11 Numerical Model Geometrical Configuration and Boundary Conditions.....	134
5.12 Governing Equations of Heat Transfer.....	136
5.12.1 Heating by Laser Beam.....	137
5.12.2 Convective Heat Fluxes	138
5.12.3 Radiative Heat Fluxes.....	139
5.13 Modelling Design Considerations	140
5.14 Results of Numerical Model.....	141
5.15 Model Validation and Sensitivity Evaluation	144
5.15.1 Laser Power Profile	144
5.15.2 Transient Surface Thermal Response	145
5.15.3 Influence of Laser Beam Characteristics.....	146
5.16 Deploying the Model.....	148
5.17 Stationary Laser Heating and Thermal Equilibrium	148
5.18 Artificial Neural Network	150
5.18.1 Learning of Neural Networks.....	153
5.18.2 Laser Preheating Parametric Predictor.....	154
5.18.3 Artificial Neural Network Fitting and Discrete Prediction	156
5.19 CFD Analysis of Titanium Alloy Heating	159
5.19.1 Setup and Conditions.....	159
5.19.2 Numerical challenges and strategy.....	160
5.19.3 Simulation Results.....	160
5.20 Summary	164
Chapter 6	167
Conclusions and Recommendations.....	167
6.1 Introduction	167
6.1.1 Thermal Assistance Method	168
6.1.2 Thermal Assistance Techniques.....	169
6.2 Experimental Work	171
6.3 Numerical Work.....	172

6.4 Achievements.....	175
6.5 Suggested Improvements and Recommendations for Future Research Interests....	177
References	179
Appendix A	193
Appendix B	201

List of Tables

Table 1. 1 Thermal and mechanical properties of elemental titanium (5, 6, 19).	4
Table 2. 1 Summary of research works on dry machining different alloys using several types of cutting tools.....	12
Table 2. 2 Machining conditions for no Built-up Edge development.....	24
Table 2. 3 Summary of LAM of titanium alloys.....	46
Table 2. 4 Summary of past work on IAM of titanium alloys	55
Table 2. 5 Comparison of preheating techniques used in machining of titanium alloys	56
Table 2. 6 Summary of significant LAM studies and key aspects.....	60
Table 3. 1 Setup parameters of the experiment stages	66
Table 3. 2 Chemical composition (Wt %) of titanium alloy Ti-6Al-4V (240).	74
Table 3. 3 Physical and Thermal properties of titanium alloy Ti-6Al-4V (6, 19, 240).	74
Table 3. 4 List of Mechanical properties of titanium alloy Ti-6Al-4V (6, 19, 240)..	75
Table 3. 5 Characteristics of K-Type Thermocouple.....	92
Table 5. 1 The comparison between three styles of the study	122
Table 5. 2 The advantages and disadvantages of three numerical methods.....	124
Table 6. 1 Summary of TAM techniques used in titanium alloys machining.....	170

List of Figures

Figure 1. 1 Thermally assisted machining using gas torch as external heating source (33) with kind permission from Elsevier	6
Figure 1. 2 Flow chart of the thesis outline.....	10
Figure 2. 1 Cracks at cutting edge after machining Ti-555 alloy on a heavy-duty lathe machine (76).....	21
Figure 2. 2 Damaged cutting tool edge in machining Ti-6Al-4V alloy at speed and feed of 100 m/min and 0.25 mm/rev respectively (56).....	22
Figure 2. 3 Build-up Edge (BUE) at cutting tool edge (70).....	23
Figure 2. 4 Crater wear at cutting edge in machining titanium alloy (Ti-555) (76) ..	25
Figure 2. 5 Delamination of coated cutting tool (WC-Co) in machining Ti-6242S alloy (68).....	25
Figure 2. 6 Adhesion at cutting edge during machining of Ti-6Al-4V alloy (58).....	26
Figure 2. 7 Wear and adhering workpiece material at rake face while high-speed milling of Ti-6Al-4V alloy (59).....	27
Figure 2. 8 Geometrical features of segmented chip formation (127).....	27
Figure 2. 9 Types of chip microstructures in conventional machining of titanium (Scale bar represents 100 μm) (129).....	28
Figure 2. 10 Preheating workpiece during turning process.....	30
Figure 2. 11 Preheating workpiece during milling process (143).....	31
Figure 2. 12 Relationship between temperature and mechanical strength of selected hard-to-machine alloys (143).....	32
Figure 2. 13 Reduction rate of machining force while machining Ti-6Al-4V alloy at feed (a) 0.1 mm/rev, and (b) 0.2 mm/rev (153) with speed 40 and 80 m/min and cutting depth 1 mm (153).....	33
Figure 2. 14 Tool damage (a) rake face (b) flank face of cutting tool inserts at speed 160 m/min with laser heating, and (c) rake face (d) flank face of cutting tool inserts under similar machining circumstances under without laser heating (155).....	34
Figure 2. 15 SEM views of chip sections at varying laser powers at speed 40 m/min and feed 0.2 mm/rev (a) no laser (b) 500W (c) 1000W, (d) schematic chip morphology (153).....	35
Figure 2. 16 (a) and (b) Chip Microstructures formed in laser-assisted machining at speed 7 m/min, (c) and (d) SEM secondary electron images of dendrites at the same chip surface (129).....	36
Figure 2. 17 Illustration of laser beam position (perpendicular to the feed direction) in turning.....	39
Figure 2. 18 Relative position of the laser beam during turning operation: (a) end-view and (b) side-view (185), with kind permission from John Wiley and Sons.....	39

Figure 2. 19 Residual stresses as a function of depth during machining with and without laser heating, a axial residual stresses and b circumferential residual stresses (161)	41
Figure 2. 20 Distribution shape of laser energy density, (a) Gaussian distribution and (b) Top-Hat distribution (176)	42
Figure 2. 21 Chip morphologies of titanium metal matrix composite: a with LAM, $V_c = 100$ m/min, $T_s = 500$ °C, and, b conventional machining, $V_c = 100$ m/min, RT (188) with kind permission from Elsevier	44
Figure 2. 22 The micrograph of the machined surface (300 m/min, 0.4 mm/rev) under: (a) conventional and (b) LAM machining conditions (189) with kind permission from Elsevier	45
Figure 2. 23 Illustration set-up of PAM (164) with kind permission from Elsevier..	51
Figure 2. 24 A schematic drawing of plasma torch (164) with kind permission from Elsevier.....	51
Figure 2. 25 Experimental set-up of (a) induction-assisted turning, and (b) induction-assisted milling.....	54
Figure 3. 1 The Experimental rig	65
Figure 3. 2 A functional diagram of the DC spinning motor control circuit.	68
Figure 3. 3 Motor for the Shaft Spinning.....	68
Figure 3. 4 Pillow Blocks with Concentric Locking and Cast-Iron Housing Bearing	68
Figure 3. 5 Steel Timing Belt Pulley.....	69
Figure 3. 6 Contitech Synchrobelt HTD, Timing Belt.....	69
Figure 3. 7 The functional diagram of DC transition motor control circuit.....	70
Figure 3. 8 (a) Lever SPDT Momentary Solder Tail Micro Switch and (b) Single DPDT Relay Board	70
Figure 3. 9 DC Motor Speed Control Driver	70
Figure 3. 10 (a) Pocket Digital Laser Tachometer and (b) Contrast Spot.....	71
Figure 3. 11 The Power Supply for The Electrical Control Circuits	71
Figure 3. 12 Test Rig with One Bearing	72
Figure 3. 13 Pillow Blocks Bearing without Shield.....	73
Figure 3. 14 The 3827 6400RPM, DC 24V, 5.6 A MAX motor	73
Figure 3. 15 Geometry of the experimental sample test	75
Figure 3. 16 Photon Machine (C-55L CO ₂ laser) (241).....	76
Figure 3. 17 Fusions 10.6 Series installed inside glass container	77
Figure 3. 18 Schematic diagram of a Laser Stepped Heating System (241)	78
Figure 3. 19 The front and back panels for the laser power module.....	79
Figure 3. 20 The motion control tower of Fusions 10.6 Series.....	80
Figure 3. 21 The main window of Chromium software.....	80
Figure 3. 22 The move stages dialog in Chromium software 2.2	80
Figure 3. 23 (a) The laser control window in Chromium software (2.2).....	81
Figure 3. 24 The ThermoVision™ A40V Camera.....	84

Figure 3. 25 Main Window ThermaCAMTM Researcher.....	85
Figure 3. 26 Preparations for Reflection Test	87
Figure 3. 27 Laser Reflection Sign	88
Figure 3. 28 Sand blaster machine	91
Figure 3. 29 TalySurf device to measure surface roughness	91
Figure 3. 30 The precision reference specimen	92
Figure 3. 31 (a) The heating gun and (b) The thermometer.....	93
Figure 3. 32 Setup to measure the emissivity of titanium alloy workpiece	94
Figure 3. 33 Measuring surface temperature.....	95
Figure 3. 34 The relation between temperature and emissivity of the shiny surface.	95
Figure 3. 35 The relation between temperature and emissivity of the black surface.	96
Figure 3. 36 The relation between temperature and emissivity of the roughed surface	97
Figure 4. 1 The Experiment Setup	100
Figure 4. 2 Flow diagram of the emissivity and temperatures correction.....	102
Figure 4. 3 Camera images for heating sandblaster (Ti-6Al-4V) workpiece by moved laser (a) at 100 rpm, 50 % LP, 40mm/min, 35 sec; and (b) at 500 rpm, 50% LP, 20mm/min, 65 sec	102
Figure 4. 4 Camera images for heating sandblaster (Ti-6Al-4V) bar by stationary laser: (a) at 100 rpm, 20 % LP, 310 sec; (b) at 200 rpm, 30 % LP, 310 sec; (c) at 500 rpm, 40% LP, 310 sec; and (d) at 1000 rpm, 50 % LP, 250 sec	103
Figure 4. 5 Camera images for heating painted (Ti-6Al-4V) workpiece by stationary laser: (a) at 100 rpm, 10 % LP, 310 sec; (b) at 200 rpm, 20% LP, 310 sec; (c) at 500 rpm, 30 % LP, 310 sec; and (d) at 1000 rpm, 40 % LP, 220 sec	103
Figure 4. 6 Black-painted workpiece heated with different laser power (LP) at 100 rpm	104
Figure 4. 7 Black-painted workpiece heated with different laser power (LP) at 1000 rpm	104
Figure 4. 8 Sandblaster workpiece heated with different laser power (LP) at 100 rpm	105
Figure 4. 9 Sandblaster workpiece heated with different laser power (LP) at 1000 rpm	105
Figure 4. 10 Sandblaster workpiece heated with moving laser at 100 rpm & 50% W	106
Figure 4. 11 Sandblaster workpiece heated with moving laser at 20 mm/min & 50% W	106
Figure 4. 12 Corrected surface temperatures for black-painted workpiece heated with different laser power (LP) at 100rpm.....	108
Figure 4. 13 Corrected surface temperatures for black-painted workpiece heated with different laser power (LP) at 1000rpm.....	108
Figure 4. 14 Corrected surface temperatures for sandblaster workpiece heated with different laser power (LP) at 100 rpm.....	109

Figure 4. 15 Corrected surface temperatures for sandblaster workpiece heated with different laser power (LP) at 1000 rpm.....	110
Figure 4. 16 Comparison of transient surface profile, Black-painted surface at various rotational speeds	113
Figure 4. 17 Comparison of transient surface profile, roughed surface at various rotational speeds.....	116
Figure 4. 18 Corrected surface temperatures for sandblaster workpiece heated with moving laser at 100 rpm & 50% W	117
Figure 4. 19 Corrected surface temperatures for sandblaster workpiece heated with moving laser at 20 mm/min & 50% W	117
Figure 5. 1 A typical CV and neighbouring nodes.....	126
Figure 5. 2 CV used in the QUICK scheme.....	130
Figure 5. 3 Stationary and Rotating Reference Frames	133
Figure 5. 4 Schematic of laser assisted pre-heating configuration, applied for numerical model.....	135
Figure 5. 5 Evaluation laser distribution functions for 3D numerical model	138
Figure 5. 6 Transient temperature visualisation of heated rotating workpiece in: (a) workpiece surface, (b) mid-plane through workpiece axis, and (c) inside cross section of workpiece; at: LP=500 W, $D_L=3$ mm, $V_T=100$ mm/min, $\omega=1000$ rpm.	143
Figure 5. 7 Evaluation the three profiles of laser intensity: uniform, linear and exponential, Temperature at M2: LP=500 W, $D_L=3$ mm, $V_T=100$ mm/min, $\omega=1000$ rpm (184).....	145
Figure 5. 8 Validation of the surface temperature with previous experimental data (184), LP=500 W, $D_L=3$ mm, $V_T=100$ mm/min, $\omega=1000$ rpm.....	146
Figure 5. 9 The effect of variation power of laser beam on workpiece surface temperature, at M2: $D_L=3$ mm, $V_T=100$ mm/min, $\omega=1000$ rpm (184).....	147
Figure 5. 10 The effect of variation laser scanning velocity on workpiece surface temperature at LP=500 W, $D_L=3$ mm, $\omega=1000$ rpm (184).....	148
Figure 5. 11 Typical temperature over time for non-traversing laser $D_L=2$ mm, $V_T=100$ mm/min, $\omega=1000$ rpm	149
Figure 5. 12 A general neuron model of an ANN.....	150
Figure 5. 13 Activation Functions in ANN.....	152
Figure 5. 14 Temperature of selected points at the heating cross section for the discrete thermal summary: (a) temperature points across critical section, (b) discrete thermal summary at point 1 (LP=40W, $\omega=500$ rpm, and $D_L=2$ mm)	155
Figure 5. 15 Framework and examination of ANN fitted through MATLAB, (a) network diagram, (b) regression plots of ANN fitting	157
Figure 5. 16 LOFF prediction of temperature at TR1, (a) $D_L=2$ mm, varying LP and ω , (b) LP=20W varying D_L and ω	158
Figure 5. 17 Comparison of surface temperature at 45° trailing the laser heating point, $\omega=100$ rpm	162
Figure 5. 18 Steady-state thermal diffusion patterns and intensity, $\omega=100$ rpm.....	164

Nomenclature

Symbol	Description	unit
$A_{Exposre}$	Area of laser exposure	m^2
a_e	Radial depth of cut	mm
a_p	Axial depth of cut	mm
C_p	Thermal capacity	kJ/kg.K
C_T	Laser transmission coefficient	(-)
D	Tool or workpiece diameter	mm
fz	Feed per tooth	mm
fr	Feed per revolution	mm
F	Machine linear feed, similar to the translational velocity of the plasma torch	N
Gr	Grashof number $\frac{g\beta(T_s - T_f)D^3}{\nu^2}$	(-)
h	Enthalpy	kJ/kg
h_j	Jet heat transfer coefficient	W/m ² K
I	Plasma intensity	A
L	Length of workpiece	mm
L_2	Lens-workpiece distance on chamfer surface	mm
L_1	Tool-laser beam distance on the surface of workpiece	mm
P	Laser power	W
P_r	Prandtl number	(-)
p	Pitch (distance between two tops of chip)	mm
P_{CO2}	Power of CO2 laser	kW
\dot{Q}_L	Laser surface heat flux	W/m ²

R	Laser radius	mm
Re_j	Jet Reynolds number	(-)

Symbol	Description	unit
Re_w	Rotational Reynolds number = $\frac{\pi\omega D^2}{\nu}$	(-)
\vec{r}	Distance vector	mm
r	Distance from centre of laser	mm
RT	Room temperature	°C
S	Source term	(-)
T	Temperature	°C
T_{mr}	Material removal temperature	°C
T_o	Initial workpiece bulk temperature	°C
T_s	Surface temperature	°C
V_c	Cutting speed	m/min
V_T	Translational velocity of laser beam	m/s
Z	Number of teeth of the milling tool	(-)

Greek symbols

α_l	Angle between workpiece axis and beam axis	(degree)
α	Absorptivity	(-)
ν	Kinematic viscosity	m ² /s
ρ	Density	kg/m ³
ω	Rotational velocity	rad/s
Γ	Diffusion coefficient	(-)

Chapter 1

Introduction

1.1 General Background

A tremendous growth has been noted in the use of advanced materials for improving technical efficiency and cost-effectiveness in engineering applications. In complying with industry needs, high-performance materials are constantly developed to satisfy superior products quality with extended dimension accuracy and surface finish. Some applications need to alloys have light-weight, higher strength, and stable properties at elevated service temperatures and harsh environments. Among many advanced engineering materials used, titanium alloys are at the forefront of technical choice for these applications due to their extraordinary material properties that surpass traditional steel and aluminium alloys (1-3). Some such application examples are the product design in automotive, aerospace, marine and power generation industries, where the system efficiency, reliability and fuel economy largely dependent upon the strength-to-weight ratio of alloys used and their operating longevity.

Machinability is the term describing the ease or difficulty of the machining processes of certain engineering materials. Machining (turning, milling, drilling) is the critical metal shaping operation carried out in many manufacturing facilities in most economically developed countries. Several references are able to give a clear picture of the processes of materials machining. This process includes removing unwanted layers from the material of the workpiece to get the desired shape of products. According to Sandvik Coromant's definition (4), there are many hard-to-machine (HTM) materials because of their high hardness, which ranged between 42 HRC and 65 HRC. Generally, the most demanded alloys classified as HTM are high-speed steels, Inconel, ceramic, and titanium alloys. In the last decades, the use of titanium alloys extensively has been increased in two major areas of industrial fields: corrosion-resistant service and strength-efficient structures, for instance, aerospace, automotive and medical applications. Titanium and its alloys have exceptional properties at room and elevated temperatures, such as high specific strength and superior resistance to fatigue and corrosion.

The cost of machining these alloys components is extremely high, compared to machining other alloys like aluminum alloy components. That is because of difficulties encountered during the machining process include tool wear, low metal removal rates, etc. These difficulties will lead to high cutting temperature, low machining speed, an elevated level of tool vibration, and short tool life. These problems are attributed to some undesirable mechanical and thermal properties, for instance, high hardness, low elasticity modulus, high chemical reactivity, and low thermal conductivity. Therefore, many research studies have paid special interests in four topics to overcome the major difficulties that occur in the machining of titanium alloys. These topics are (i) development of new cutting tool materials, (ii) improvement of the tool design, (iii) investigation the right combination of cutting tool, machine tool and cutting parameters, and (iv) development and implementation of advanced hybrid machining processes e.g cryogenic, cooling and lubrication systems, and preheating methods.

1.2. Titanium and Titanium Alloys

Ti - titanium is a shiny metal with dark grey colour and was initially discovered in the eighteenth century by William Gregor, 1791. This metal has been used widely in the second half of the 20th century. Because titanium is seldom found in high concentrations and never found in a pure state, therefore, the difficulty in processing the metal makes it expensive. Titanium has density approximately (60%) of that of steel or nickel-based alloys, which makes titanium strengthened greatly by alloying and deformation processing. In addition, this metal has exceptional corrosion resistant and relative strength advantages which are over competing materials such as stainless steel and aluminum. Table 1.1 includes the thermal and mechanical properties of elemental titanium. Therefore, it justifies why titanium and titanium alloys are a wise selection to be used primarily in several advanced engineering applications that need materials with extraordinary properties. There are many alloys-based titanium such as, Ti-64, Ti-6242S, Ti-4.5Al-4.5Mn, and Ti-6Al-7Nb. Amongst these alloys, the Ti-6Al-4V (one of titanium aluminides alloys) was covered more than 45 % of usage in various industrial fields because it has widespread advantages. These excellent properties explain their good workability and preferential use in many engineering applications.

Titanium alloys, as with other materials, among the most important and can be crystallized in various elemental crystal structures. These structures are the hexagonal close packed (HCP), the body centered cubic (BCC) and the face centered cubic (FCC) (5, 6). Depending on the number of slip system, plastic deformation increases from the titanium of structure (HCP) to the titanium of structure (BCC) to the titanium of structure (FCC). In temperatures below 882 °C, the crystal structure of titanium will be HCP while the structure transformed to BCC above 882 °C. According to that, there are four main groups of titanium alloys as follows: alpha (α), near-alpha, alpha-beta (α - β), and beta (β) (5, 6). Titanium alloys properties are essentially determined by two factors: the chemical compositions (the percentage of additive elements) and the microstructure of the alloy. Adding certain elements to titanium such as Aluminum (Al) and Vanadium (V), alter the phase transformation temperature, which in turn affects the crystal structure and mechanical properties of titanium. Based on the alloying condition and possible additive elements, many categories of titanium alloys have been discovered and around 30 kinds have reached commercial status.

Titanium alloys offer a unique combinations of exceptional mechanical properties and superior physical characteristics of high resistance to corrosion, fatigue and oxidation, underpinning the alloys' popularity as highly sought-after lightweight alternative (7, 8). In particular, Ti-6Al-4V alloy is widely utilized as important components in the aerospace sector for higher ratio of strength-to-weight and in heat exchangers (9-12) for high temperature and corrosion tolerance. Chemically inertness and stable physical properties make titanium alloys highly attractive and biocompatible for producing biomedical implements for diseased bone replacement, cartilage and spinal fixation (13-17), and in food processing industries. In producing modern aircraft such as Boeing 787, titanium alloys have become even more attractive due to their similar thermal expansion coefficients to common aviation materials of aluminium and graphite (3, 11, 18) with the added benefits of superior galvanic resistance and excellent creep resistance.

Table 1. 1 Thermal and mechanical properties of elemental titanium (5, 6, 19).

Property	Description or value
Density	4510 Kg/m ³ (0.163 Ib/in. ³)
Melting point	1668 °C (3035 °F)
Solidus/liquidus	1725 °C (3135 °F)
Boiling point	3260 °C (5900 °F)
Thermal conductivity	11.4 W/m.K
Specific heat	0.5223 kJ/kg.K
Hardness	70 – 74 HRB
Tensile strength	240 MPa
Young's modulus	120 GPa

1.3 Machinability of Titanium Alloys

Generally, machining process is governed by many various contributing factors beside mechanical properties. Among the mechanical properties, strength and hardness have the highest effect on the machinability of alloys, therefore, classified as the HTM. Machinability of any alloy is ordinarily specified based on several criteria such as cutting tool life, chip formation, cutting temperature, machining dynamics, and surface finish of workpiece. The key issues with conventional (dry) machining of titanium alloys are: (1) cutting edge wear, (2) built-up-edge (BUE), (3) increasing cutting forces, (4) high-temperature and high pressure on tool, and (5) vibration cutting tool and holder. These problems occur due to titanium and its alloys inherent properties, such as low thermal conductivity leading to high cutting temperature, their chemical reactivity with almost all tool materials at high-temperature, high hardness at elevated temperature and low modulus of elasticity. Furthermore, the ability to change the phase of titanium alloys makes the deformation process more complex. Therefore, more attention has been spent to overcome these issues by finding suitable solutions.

A group of the experimental studies concerned on finding suitable types of cutting tools to machine titanium alloys. In these studies, many tool materials have been used to machining these alloys such as, uncoated and coated cemented carbides (WC/Co), polycrystalline diamond (PCD), and polycrystalline boron nitride (PCBN)

and cubic-boron-nitride (CBN). The results illustrate a slight improvement in machining life of the cutting tool and surface integrity of workpiece. Another group of the studies focuses on the cutting tool cooling strategy such as cryogenic cutting high-pressure coolant, rotary tool turning, to improve the machinability of titanium alloys (10, 11, 20). This strategy leads to good prolong tool life with a better surface finish at various machining parameters (16, 21). On the other hand, in the traditional machining, the major problem of using massive amounts of cutting fluids has been ignored, which leads to serious environmental issues as well as health concerns for the machine operators. Being aware of this, manufacturers worldwide have been trying to minimise or eliminate the use of liquid coolant during metal cutting. This gives rise to manufacturers incorporating a limited amount of dry machining into the manufacturing processes.

The third part of studies is about applying another strategy includes preheating workpiece before/during cutting process to improve the machinability of titanium alloys by reducing the cutting pressure. Positive results in terms of the longer tool life, lower cutting forces, smoother machined surface and increased material removal rate have been reported when using thermally assisted techniques. Thermally assisted techniques are divided into three heating methods (22-24): induction-assisted method, plasma-assisted method, and laser-assisted method. In this research, more attention to employ the laser-assisted technique to improve titanium alloys machining.

1.4 Thermally Assisted Machining (TAM)

Improvements in the machinability of hard and HTM materials have been a subject of interest for the past decades. Several assisting techniques including hot machining or (TAM) have been proposed and attempted on “hard-to-machine” materials to ease shear characteristics and thereby to reduce tool wear and enhance machining speed. TAM is not a new concept and originated out of applications with low-temperature heat sources (25-28). In 1898 Tilghman (29) filed a US patent to use electrical resistance for preheating a workpiece during machining. Since then, many researchers have followed Tilghman approach and investigated many possible alternatives heat sources such as gas torches, laser beams and plasma arcs, etc.

The concept of TAM is based on the principle that the yield strength and hardness of materials decrease with the increase of temperature whilst other properties do remain relatively unaffected. In this, an external heat source is deployed to preheat the workpiece surface during machining without heating the cutting tool (23, 30-32) as illustrated by figure 1.1 (33). For any given work material, TAM requires appropriate control of workpiece temperature to keep cutting forces within an optimum regime (34), hence to achieve the best surface integrity and extended tool life (35, 36).

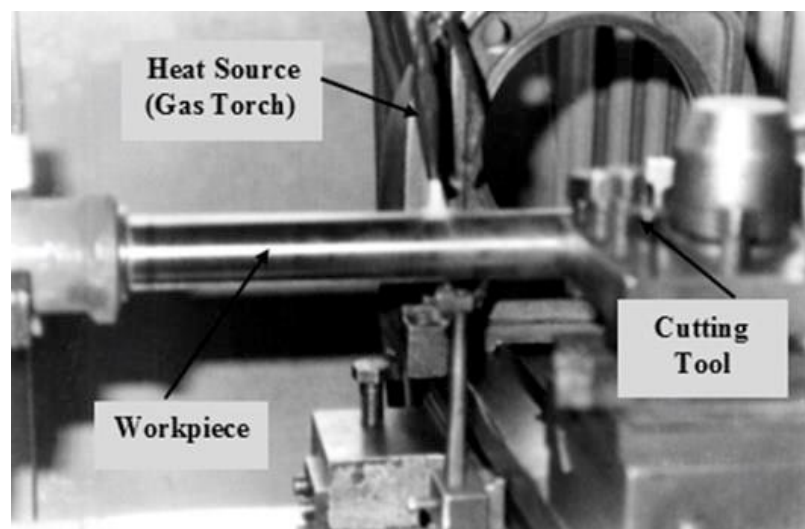


Figure 1. 1 Thermally assisted machining using gas torch as external heating source (33) with kind permission from Elsevier

The basic requirements identified for TAM of HTM materials are given below (23, 27):

- The external heat source should be localised at the shear zone;
- The heating area should be limited to a small zone;
- Heating method is to be incorporated with a temperature-regulating device;
- Overheating of machined surface is to be avoided to prevent any potential metallurgical changes to the uncut workpiece;
- External heat source must be of adequate intensity to produce a large heat output for imparting rapid temperature rise in advance of the cutting point.

1.5 Problem Statement

The dynamic nature of the industry, as well as developments of manufacturing systems, can and will continue to affect the future of the titanium industry. The performance of titanium-based alloys machining in terms of dimension accuracy, good surface finish, and short machining time is defined by their mechanical properties and machining setup. Improvement of titanium alloys machining is depended mainly on the overcoming the complexities associated with the inherent properties of these alloys. LAM has been used for these issues. This method is one of the various techniques of TAM, which involves many operating parameters. It has been reported from many studies that there are positive influences of LAM parameters on the machining of titanium alloys. LAM diffuses laser with high-power focussed at a small spot on the cutting zone to preheat upstream of tool path surface during conventional machining.

Rising preheating temperature with laser power causes a decrease the microhardness at cutting zone, thereby reducing the cutting tool pressure on the workpiece surface. Subsequently, this leads to a significant reduction in cutting force and flank wear, thereby increasing cutting tool life. Moreover, the chip formation during LAM is continuous because of preheating temperature improves the deformability of workpiece surface layer near to cutting zone (30, 37). Furthermore, lowering down dynamic cutting forces and hardness near the cutting surface leads to much smoother machined surface with very few defects such as material build-up and grain pull-out (38, 39). Thus, LAM effectively improves the machinability of titanium alloys even at high cutting speed.

According to that, there are two groups of parameters effect on machinability of these alloys namely, (1) parameters associated with laser and (2) parameters associated with machining. The first group mainly includes: preheating time, laser power, laser beam diameter, laser scanning speed, laser beam/cutting tool lead distance, laser focusing lens/workpiece distance and induction beam/workpiece axis angle. While the second group mainly consists of feed, depth of cut, cutting speed and laser-tool lead. Therefore, the selection of appropriate operating in the LAM for titanium alloys is a big challenge to be controlled, since both thermal and machining aspects should be considered.

1.6 Significance and Contribution of this Study

Research on improving the machinability of HTM engineering materials have primarily focused on the application of new types of cooling liquids and cutting tools as well. While the existing studies concentrate on the application of TAM mechanisms in the HTM alloys machining. These studies showed excellent results in terms of surface finish, cutting tool life, and machining time. Nevertheless, many aspects of TAM methods especially laser technique are still not understood and need extensive study. According to that, this present work is a thermal study to investigate numerically and practically the pre-heating process of Ti-6Al-4V alloy workpiece by the laser beam. The overall contributions that will result from the research are:

- Emulating the laser assisted pre-heating and establishing a method of thermography for accurate measurement. The experiment will be conducted to assess thermal response of Titanium within the applied range of parameters. This will improve the experimental insight of process and offer a benchmark for numerical verifications.
- Improving the existing state-of-art in numerical modelling of laser assisted heating. This urges a better understanding of key parameters, issues related to the numerical stability and wider range of validation. Finite volume method is designated as the numerical scheme which is widely and increasingly applied in commercial solvers.
- Utilising and combining both analyses to predict conditions required for the best results of LAM where the softening is achieved in the desired vicinities without exposing micro-structure damage to the remaining areas. Such prediction could be carried directly through simulation of the given case or by fitting low-order models (e.g. ANN fitting), for estimation with low-computational resources.

1.7 Objectives of Research

Due to titanium alloys wide application in many industries and the difficulties during machining processes, it rarely attracts the interest of researchers. Besides, these problems also related to the thermal properties like low thermal conductivity, which discourage the researchers from applying traditional machining as the manufacturing process for these alloys. The present research work focusses mainly on the

improvement of current cutting methods by adding a cooling system and/or aided heat to enhance the machining process. This study aims to provide a better understanding of the improvement of titanium alloys machining. Hence, the detailed objectives of this study are as follows:

- 1) To gain a clear understanding of the thermal assisted techniques which have been used to overcome several difficulties that occurred during traditional machining of titanium alloys.
- 2) To develop a three-dimensional (3D) numerical model of a rotating workpiece subjected to localised laser preheating, where a finite-volume based numerical simulation using ANSYS/FLUENT solver for examining the thermal response.
- 3) To provide unique analytical and practical benefits for applications involving laser-assisted machining processes.
- 4) To predict the cutting performance and optimise machining parameters that would eventually lead to improved machinability and productivity, as well.

1.8 Organization of Thesis

The outline of the thesis is showed in Figure 1.2, which describes the content covered in the seven chapters that make up the thesis. An overview of each of the chapters is presented below:

In **Chapter 1 (Introduction)**, the background to the research topic, and the scope and aims of the research are introduced to justify the reason for undertaking this research.

In **Chapter 2 (Literature Review)**, the past works are reviewed to understand the state of the art regarding complexities of titanium alloys machining and the effects of TAM techniques to reduce these problems. The last part of this extensive survey is about the thermal behaviour of a rotating cylinder that is heated by the laser beam.

Chapter 3 (Experimental Methodology), elaborates all details about the stages of the test rig manufacturing. Additionally, a detailed explanation of the laser machine, ThermaCAMTM Researcher software, and thermal camera describe in this chapter. Then, this chapter covers all preparation tests for experiments. Finally, the experimental results of heating titanium alloy (Ti-6Al-4V) workpiece employing the methodology

Chapter 4 (Numerical Modelling), covers the numerical method (Finite Volume Method) and computational fluid dynamics software (FLUENT CFD Software), that used in the modelling process. Thereafter, the development of a 3D model of the rotating workpiece, then, validation this model with previous experimental work, are introduced in detail. Then, a low order estimation explains by employing machine learning and an artificial neural network (ANN). Finally, use the developed numerical (CFD) model of the heated rotating workpiece to simulate various scenarios of heating Ti-6Al-4V workpiece. Followed that, compared the results of the CFD model with the experimental results presented in Chapter 3.

In **Chapter 5 (Results and Discussions)**, the results of empirical work and numerical simulation are present with a highlight of important discoveries through an in-depth comparison between both sets of results in detailed.

In **Chapter 6 (Conclusions and Recommendations)**, the conclusions from the whole thesis are display with highlight achievement of this research. The last part of this chapter provides proposals for future research interest in improving titanium alloys machining. Some selected information required during the study can be found in the appendices.

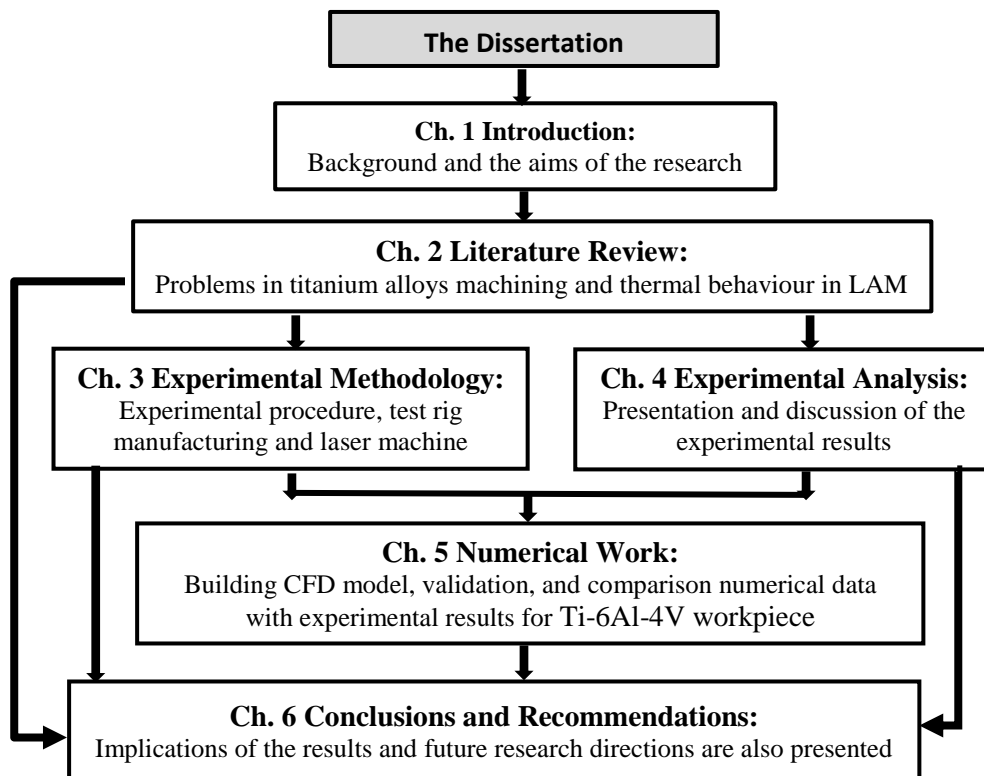


Figure 1. 2 Flow chart of the thesis outline

Chapter 2

Literature Review

2.1 Introduction

As indicated in Chapter 1, the objective of this literature review is to give a clear view to understand the machining processes of titanium alloys through over 200 publications. This chapter starts with the problems and difficulties have occurred during machining of titanium-based alloys. After that, the chapter explains the effects of thermally assisted machining (TAM) methods on improving the machining process. Further, this review carries out an extensive survey of recent advances in methodology and appraises preheating to the TAM techniques that have used for titanium alloys. Finally, the experimental and numerical previous studies about the heated rotating workpiece by the laser beam have reviewed and presented.

2.2 Background

In recent decades, an extensive use and increasing demand of components for titanium alloy manufacturing are witnessed due to steadily developing growth in applications requiring metal components having high strength, light-weight and excellent corrosion resistance (1, 21, 40). Due to their extraordinary physical properties and mechanical stability at elevated temperatures, titanium alloys are primarily considered for special applications such as, automotive, aerospace, petroleum refinery and nuclear reactors, etc. (9, 12, 41, 42). However, titanium alloys are well recognised for being hard-to-machine (HTM), because such alloys inherently possess low thermal conductivity and elastic modulus, and high chemical reactivity at elevated temperature (43-45). These properties significantly lead to increase the manufacturing cost of titanium alloys components compared to other conventional alloys (41, 46, 47). Low thermal conductivity of titanium alloys impedes dissipation of heat generated during machining, causing steep rise in tooltip temperature, hence adversely affecting the tool life, resulting in poor surface finish and dimensional inaccuracies (1, 20, 48, 49). High chemical reactivity of titanium alloys tends to rapidly dissolves and degrades the cutting tool during machining to result chipping and early tool failure. These attributes significantly impair the

titanium alloy machinability with low production rate and high manufacturing cost (20, 45, 50).

Under dry conditions, Table 2.1 outlines numerical and experimental studies involving the machining of titanium alloys for comparative assessment and merit appraisal of techniques for improving machinability. These studies aptly recognise titanium-based alloys to be extremely HTM, especially at higher surface speed, even by latest cutting tools and methods (21, 40). It is observed that poor surface finish quality is evidently noticeable at rather low machining speeds between 60 m/min to 120 m/min and beyond (51). Such machining issues are attributed to excessive cutting forces generation at tool tip due to high material hardness that also leads to elevated workpiece temperatures contributed by lower thermal conductivity of these materials. Tool chatter arising due to large machining forces leads to rough surface finish which is further compounded by chemical reactivity due to high cutting temperatures (41, 45). These effects are exaggerated with increasing cutting speeds, making it very complex for machining titanium to a precise size and shape at higher cutting speed (52, 53), hence imposing limits on production economy and efficiency. Therefore, the present industry trend is to search for effective approaches or methods for improving machinability of these alloys.

Table 2. 1 Summary of research works on dry machining different alloys using several types of cutting tools

Author/ Publication	Titanium Alloy	Aim of Investigation	Outcomes/Findings
Komanduri et al., (54)	Ti-6Al-4V	Chip formation mechanism during turning.	<ul style="list-style-type: none"> - Rapid flank wear - Uninterrupted contact at/near the cutting tool tip - Higher reactivity to most tool materials - High temperature near shear bands

Hartung et al., (55)	Ti-6Al-4V	Determine the wear mechanism during titanium alloy turning machining	<ul style="list-style-type: none"> - Rapid dissolution or chemical reaction occurs during machining process between titanium alloy and two conventional cutting tool materials including C2 grade (Carboloy 820) and C3 grade (Kennametal K68)
Dornfeld et al., (44)	Ti-6Al-4V	<p>Examine the effects of tool dimensions and machining conditions on</p> <p>the burr cross-section shape during drilling</p>	<ul style="list-style-type: none"> - During dry machining, four shapes of burr were formed, such as a uniform, roll back, lean back and roll back with expanded exit - Roll back phenomena happened because of the thermal expansion due to increasing local temperature at the inside burr face - During wet machining, there three types of burr observed namely, standard even burr, burrs with a drill cap, burrs ring shaped burr - Depending on the drill types, smaller burrs are produced by helical point drill while
Jawaid et al., (56)	Ti-6246	Investigate the grooved carbide cutting tool wear during turning.	<ul style="list-style-type: none"> - The rate of flank wear was increased rapidly when the feed and speed were increased - High cutting temperature facilitates diffusion wear which smoothens the worn area - Higher speed and feed cause chipping of cutting tool - A significant increasing in tool life achieved during dry machining when the feed and speed were 0.25 mm/rev and speed 60 m/min respectively

López de lacalle et al., (11)	Ti-6Al-4V & Inconel 718	Study the influence of uncoated hard cutting tools [quality (K10) microgram] and coating tools [titanium carbide (TiC) and titanium-aluminium nitride (TiAlN)] with milling machining parameters on the machinability	<ul style="list-style-type: none"> - The chip thickness was enlarged with rising depth of radial cut and decreasing feed when using uncoated tool -The development in the cutting tool life was achieved with using uncoated tools at the range of clearance angle from 18° to 20° - The coating material caused a delay the wear in flank
Nabhani (57)	TA48	Experimentally study the work quality of the polycrystalline diamond (SYNDITE) cutting tool in turning titanium alloy	<ul style="list-style-type: none"> - -SYNDITE PCD is the most functional cutting tool due to its minimum wear rate and better surface finish
Che-Haron (53)	Ti-6Al-2Sn-4Zr-6Mo	Investigate wear of tool and integrity of machined surface during turning	<ul style="list-style-type: none"> - Straight grade cemented carbides tool is more convenient to machine this type of alloys - Chipping and wear in flank face are key reasons for the failure of tools. - Machined surface contains austere tearing and plastic deformation
Wang et al., (58)	Ti-6Al-4V	Investigate the effect of binder of cubic boron nitride tools during high speed milling	<ul style="list-style-type: none"> - The wear in the flank is not even and it dominates the wear of binder-less tools. - The binder-less performed better during titanium alloys machining - The optimal machining with use BCBN tools at depth of cut 0.075 mm, speed 400 m/min, and feed 0.075 mm/rev
Wang et al., (59)	Ti-6Al-4V	Examine the wear characteristics of cubic boron nitride tool without binder while milling at high speed	<ul style="list-style-type: none"> - Grooves of micro size appear on the flank during the initial cutting stage owing to the abrasion - Workpiece material diffuses from the tool into chip

Che-Haron (60)	Ti-6Al-4V	Investigate the surface integrity during turning with uncoated carbide of ISO label cutting tools, CNMG 120408-883- MR4 and CNMG 120408-890- MR3	Surface finish is slightly worse at slower speed, whereas surface finish improves when the speed rises. - Surface microstructure experiences plastic flow and tearing when the tool fails - Machined surface has higher hardness than that of original material
Nouari et al., (61)	Ti-6242S	Study the effect multilayer CVD-coating during end milling	- The local wear dominates tool performance - Higher speed, lower feed and a smaller depth of cut give improved finish of machined surface
Che Haron et al., (62)	Ti-6246S	Examine the influence of using the alloyed carbide tools on the end milling	- The uncoated carbide and CVD-coated carbide tools are better for titanium alloys milling
Nurul amin et al., (63)	Ti-6Al-4V	Compare the tool wear, surface finish while using polycrystalline diamond (PCD) and uncoated tungsten carbide-cobalt (WC-Co) during end milling	- Faster machining and longer tool life with uniform wear in PCD compare to that of uncoated WC-Co - To avoid tool wear, the allowed speed should be below 120 m/min for PCD, while for WC-Co is up to 40 m/min - Because of the better tool performance and lesser chatter in PCD, the surface roughness is lower.
Jianxin et al., (64)	Ti-6Al-4V	Investigate diffusion wear during turning	The tool wear is accelerated due to the element diffusion to and from the chips and tool.

Dargusch et al., (65)	Grade 2 unalloyed Titanium (99.8% Ti)	Study the effect of end-milling without and with lubricant on the deformation zone depth	<ul style="list-style-type: none"> - Residual compressive stress increases with while the speed rises during dry machining - Deeper deformation layer and higher sub-surface twin density observed during dry machining than machining with lubricant at higher cutting speed (48.3 m/min) - Micro-hardness of the machined surface without lubricant is increases slightly with the increase of compressive residual stresses
Ibrahim et al., (66)	Ti-6Al-4V	Analyse the surface integrity after turning with coated carbide cutting tools.	<ul style="list-style-type: none"> - Better surface with acceptable, cracks and tears was achieved at 95 m/min speed, 0.35 mm/rev feed and 0.1 mm cutting depth - Higher surface roughness (4.31 μm) at initial machining then regularly decrease until the surface become smoother (2.92 μm) at the end.
Sun et al., (67)	Ti-6Al-4V	Understand the chip formation and machining force generation during turning	<ul style="list-style-type: none"> - At high feed rate and low machining speed, both the continuous and segmented chips are generated due to a static force and a recurring force, respectively - the slip angle is lower in continuous chips than that in the segmented chip
Abdel-aal et al., (68)	Ti-6246S	Effect of thermal conductivity of cutting tool material on alloyed carbide (WC-Co) cutting tools during turning	<p>The cutting temperature and thermodynamic forces such as stress, strain rate, and temperature gradient, are led to anisotropy of the tool material's thermal conductivity - The high gradient of flank wear was noted at machining speed 150 m/min when cutting with tool without coating - The flank wear is noted at the edge of the tool during machining by coated cutting tool at 125 m/min and 0.2 mm/rev speed and feed respectively.</p>

Fang et al., (69)	Ti-6Al-4V & Inconel 718	Study the machinability in term of force ratio (cutting force/thrust force) during high speed turning	<ul style="list-style-type: none"> - Machining forces reduces at the rise of speed, whereas the force ratio increases - Increasing feed caused increasing forces as well as force ratio
Armendia et al., (70)	Ti-6Al-4V & Ti54M	Compare the Ti-6Al-4V machinability with Ti54M machinability during the turning	<ul style="list-style-type: none"> - Ti54M alloy machines better than Ti-6Al-4V - The lower crater and flank wear rates are noted easily during machining of Ti54M owing to its microstructure - The machining forces of Ti6Al-4V are larger than those of Ti54M - In speeds 50 – 60 m/min, both the titanium alloys showed adiabatic shear bands during chip
Özel et al., (71)	Ti-6Al-4V	Investigate the effect of single and multi-layered coatings of cBN and TiAlN on tungsten carbide cutting tools during turning	Both coatings show decreasing cutting forces at around 50 m/min speed, while, increased near to 100 m/min speed due to larger edge radius, especially in multi-layer coated tool
Dass et al., (72)	(Grade 5) alloy (89.75% Ti)	Explore the influence of cutting depth, speed, approach angle as well as feed on the surface finish and machining forces while turning	<ul style="list-style-type: none"> - The decreasing of feed affects more substantially than other variables on the reduction of force and roughness - On the contrary, increasing approach angle has a slight effect on the improvement of surface finish
Honghua et al., (73)	TA15	Compare the performance of polycrystalline cubic boron nitride (PCBN) as well as polycrystalline diamond (PCD) in terms of surface finish, tool wear, wear morphology and tool life while milling	<ul style="list-style-type: none"> - At higher cutting speeds, PCBN shows short tool life compared to the PCD - Non-uniform flank wear occurred for both two types of tools

Mhamdi et al., (74)	Ti-6Al-4V	Investigate the influence of hemispherical shape of tool, speed and feed on the machined surface of during milling	<ul style="list-style-type: none"> - The significant improvement of surface roughness was achieved during cutting upward and downward surface with hemispherical tool compared when machining at the top of concave surface - The increment in speed feed (900 mm/min) leads to increase the roughness of the surface
Ugarte et al., (75)	Ti-6Al-4V, & Ti-5553	Study the machinability of two titanium alloys during three different operations, such as face milling, interrupted cutting and orthogonal milling	<ul style="list-style-type: none"> - Adhesion wear is appeared very clearly in Ti-5553 machining compared with Ti6Al-4V machining. -Machining forces while machining Ti-5553 alloy are larger than the forces of Ti6Al-4V alloy - The cutting temperature for Ti-5553 alloy was greater than the temperature for Ti6Al-4V alloy - Due to higher segmentation and higher temperature during machining, the Ti6Al-4V alloy machinability is greater than those of Ti-5553 alloy
Nouari et al., (76)	Ti-6Al-4V & Ti-555	Study the effect of microstructure of workpiece material on tool wear as well as stability of the turning process	<ul style="list-style-type: none"> - The Ti-6Al-4V has higher thermal softening sensitivity than that of Ti-555 alloy - Due to a nodular structure and fine grains (1 μm) of Ti555, it is harder to machine compare to Ti-6Al-4V alloy - Adhesive wear is higher during Ti-6Al-4V machining compare to that during machining of Ti-555
Balaji et al., (77)	Grade 2 unalloyed Titanium (99.8% Ti)	Examine the effects of rake angle, speed and feed on machining forces, temperature and chips generation in turning	higher speed with positive rake angle leads to reduced forces, cutting tool wear and temperature

Cotterell et al., (78)	Ti-6Al-4V	Investigate the shear strain and cutting temperature during milling	<ul style="list-style-type: none"> - The shear strain increased with cutting speed increases, while, slight changes in shear strain noticed with a variation of feed rate value - Temperature at cutting zones increases with increasing cutting speed - Increase cross section of the chip due to increase cutting feed rate chip section which in turn increases friction between chip and tool
Shetty et al., (79)	Ti-6Al-4V	Determine optimum drilling parameters for the better hole quality and chip type	<ul style="list-style-type: none"> - The shape of chip at low cutting speed is spiral cone with minimum thickness. - The size of formation burr was minimum at reduced cutting speed - Surface finish was better at high speed (20 m/min) because of increased heat generated which is lead to softening the material of workpiece at the top layer
Li et al., (80)	Ti-6Al-4V	Study the effect of deep submillimeter-scaled texture on the cutting forces and the friction properties	<ul style="list-style-type: none"> - Implanted three types of texture on rake faces of cutting tools caused a substantial influence on the distribution of stress and therefore affects tool life

As illustrated from Table 2.1, the traditional methods, such as, new design and using new alloys for cutting tools, have not been enough to improve the machinability for these alloys in terms of the production cost and manufacturing time. Therefore, several investigations have been dedicated to the development and implementation of technological innovations (47, 81) in overcoming operational challenges and enhance performance capabilities (39). At the forefront of such techniques is TAM, that increase ductile deformation in the cutting zone (23, 35). In this, the workpiece surface is heated just before machining and the material temperature is raised to reduce yield strength locally within the deformation zone at the cutting tool edge, thus minimising cutting forces (29). TAM process requires operating conditions to

be managed inside an optimal domain for a certain workpiece material for obtaining the desired outcome, such as expected surface integrity and extended cutting tool life (35, 36).

For machining titanium alloys, TAM technique has been attempted with different heating sources and configurations, namely high-frequency induction coil (82-85), plasma (86, 87), and laser beam (37, 38, 88-90). These studies have reported potential improvement in the machinability of titanium-based alloys. This chapter provides an exhaustive compilation and a detailed review of these investigations, identifying specific issues related to titanium alloys machining and the merits of various TAM approaches, including workpiece preheating before/during the machining. Specific emphasis is placed on the reduction of machining forces, surface roughness and tool wear. The following section presents a detailed discussion on the difficulties and issues associated with machining of titanium-based alloys.

2.3 Machining Difficulties and Issues with Titanium Alloys

Titanium and its alloys have extraordinarily hard mechanical properties and poor thermal characteristics in maintaining production efficiency and cost-effectiveness. In a practical sense, titanium machining brings about operational challenges because of the manufacturing needs to achieve higher cutting speed and material removal rate (91, 92).

During machining of titanium alloys, excessively large cutting forces are produced along with vigorous tool chatter due to very high yield stresses of these alloys, whilst highly elevated tool/workpiece temperatures are generated from unyielding plastic deformation under low ductility. These interactive effects lead to poor surface finish, which is adversely affected by increasing cutting speeds and rate of material removal. Additionally, reduced ability to conduct heat hinders heat dispersion and creates highly concentrated temperature rise within the cutting zone and at the tool tip. Consequently, high-temperature chemical reactivity is triggered at the machining surface whilst the tool tip undergoes burnout reducing tool life (5).

Each property of titanium has different effects on the machinability (5, 41). Past studies identify that, when machining titanium alloys, the workpiece surface undergoes work hardening process at the cutting edge, making the material harder

than normal for the cutting tool. Increased cutting force arising from this effect is detrimental to the machining process and leads to very high cutting tool wear rate. Moreover, it has been reported that both compressive and tensile residual stresses may present on the machined surface in titanium alloys machining (93) depending on the machining processes. The tensile stresses are not beneficial and should be minimised while compressive stresses are useful for fortifying fatigue strength (94). TAM techniques enable to release these in varying degrees.

Upon applying cutting tool pressure, machining processes generate large cutting forces and strong friction at the tool tip from plastic deformation at the workpiece-tool contact interface (95). Intense heat is also invariably produced at the cutting zone, largely from plastic deformation and to a lesser extent by tool tip friction (72, 96). Cutting forces and heat generation are acutely stronger with titanium alloys having higher hardness and high-temperature strength (97). It has been observed that owing to elevated cutting zone temperature, a built-up edge is formed on cutting tool as a protective layer of workpiece material (98). Thickness of this layer tends to decrease with increasing cutting speed, causing higher rate of tool wear. Additionally, high temperature and resulting thermal stresses over workpiece-tool contact length is a known major reason for micro/macro crack development along the cutting edge, which is designated as edge depression (99). Figure 2.1 typically illustrates cracks developed at the tool's cutting edge during machining of Ti-555 alloy.

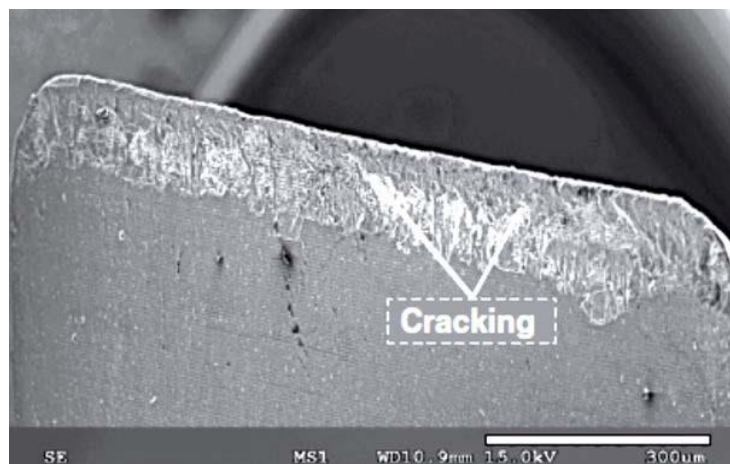


Figure 2. 1 Cracks at cutting edge after machining Ti-555 alloy on a heavy-duty lathe machine (76)

In machining, cutting zone temperature plays a crucial role in determining product surface quality, manufactured tolerances and tool wear (100). Typically, in machining, 90% of the work expended on plastic deformation is transformed to heat creating intense temperature rise within the cutting zone (29). 75 % - 80 % of this heat is captivated in cutting tool (45, 55) whereas the rest of heat is taken away by the chips and workpiece. In easy-to-machine materials, chips may remove up to 25 % of the generated cutting heat (101).

Titanium alloys tend to have poor thermal conductivity values (65, 102) because of the constrained molecular slip in hexagonal crystal microstructure of these alloys. This naturally hinders the heat diffusion process within the workpiece and creates highly-concentrated thermal stresses and steep temperature rise in the cutting zone (6, 65, 79, 103, 104). Affected by elevated temperatures and compressive stresses the plastic deformation occurring within the primary cutting region produces adiabatic shear bands (46, 96, 105, 106).

At high cutting speeds, rapidly forming chips would have lesser contact length with the tool face and somewhat lower friction coefficient. However, resulting from reduced heat removal by chips (45, 55, 79), the cutting temperature is significantly elevated over the small interface between the tool face and chips (20, 101). This tends to severely damage the tool cutting edge, as shown in Figure 2.2. With titanium alloys machining, higher localised tool temperature is a serious and concerning issue, especially at large cutting speeds.



Figure 2. 2 Damaged cutting tool edge in machining Ti-6Al-4V alloy at speed and feed of 100 m/min and 0.25 mm/rev respectively (56)

Retention of high yield strength at higher temperature with lower elastic modulus adversely affects the titanium alloys machinability (53, 92, 103). With such conditions, cutting tool pressure would deflect the workpiece significantly leading to tool chatter/vibration and undercut (107, 108), hence creating detrimental effects of poor surface quality and tolerance. It has also been noted that, under the compressive force exerted by the tool, high cutting zone temperature would weld some workpiece material to the tool edge. This welded material is Built-up Edge (BUE) (84). Figure 2.3 demonstrates the BUE which was generated during machining titanium alloys with cemented carbide (WC/Co) tools at machining speed of 60 m/min (98).

Chemical reaction initiates BUE formation at the tool-chip contact zone, which induces chamfering and chipping of the cutting edge (44, 109). This increases the cutting forces eventually beginning to deflect the workpiece (109). Therefore, BUE is regarded as a root cause for producing unacceptable surface finish and poor dimensional accuracy (42, 70, 110). The development of BUE is influenced by speed, machining temperature, workpiece material and the tool. A stable BUE plays the significant role of acting as a protective layer for the cutting edge (24). To the contrary, an unstable BUE adversely impacts on both the cutting tool and surface finish. Trent (111) has stated that the BUE reduces the contact length, implying high cutting temperature and high stress concentration simultaneously occur restricted to a minor region at the cutting edge (within 0.5 mm) (112). This increases pressure load on the tool edge while machining of titanium alloys (51). Under limited machining situations, machining of titanium-based alloys shows no tendency for BUE to form, depending on the titanium alloy type, see Table 2.2.

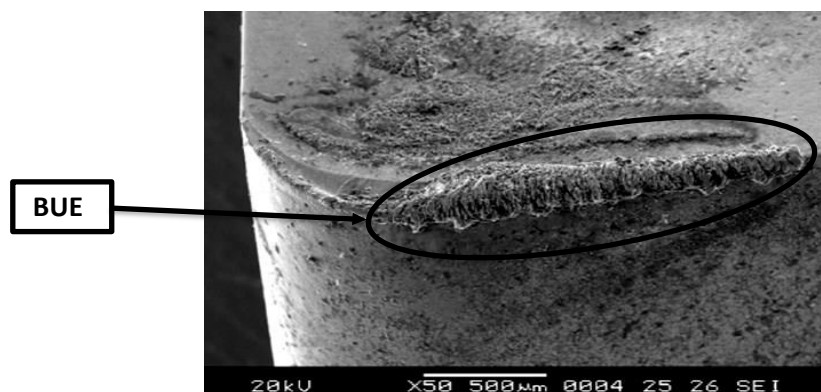


Figure 2. 3 Build-up Edge (BUE) at cutting tool edge (70)

Table 2. 2 Machining conditions for no Built-up Edge development

Author/ year	Titanium Alloy	Cutting Tool	Speed (mm/min)	Feed (mm/ tooth or mm/rev)	Depth of Cut (mm)	Machining Type
Nurul Amin A.K.M. 2007 (113)	Ti-6Al- 4V	Uncoated cemented carbide WC/Co and polycrystalline diamond (PCD)	160	0.1	1.0	Milling
Armendia M. et al 2010 (70)	Ti-54M & Ti6Al- 4V	Uncoated cemented carbide WC/Co	80	0.1	2.0	Turning
Rahman Rashid R.A. 2012 (114)	Ti- 6Cr5Mo- 5V4Al	Uncoated tungsten carbide	160	0.19	1.0	Turning
Jawaid A. 1999 (56)	Ti-6246	tungsten carbide CNMG 120408- (890 & 883)	100	0.25	2.0	Turning
Ugarte A. et al 2012 (75)	Ti-6-4 MA	PVD coated (TiAlN- TiN) cemented carbide	40	0.15	2.0	Milling
	Ti-6-4 STA		40			
	Ti-5553		25			
Wang Z.G. et al. 2005 (58)	Ti-6Al- 4V	Cubic boron nitride (CBN) and Binderless CBN (BCBN)	350	0.1	0.1	Milling

On the other hand, it was noted that cutting tools are very rapidly consumed owing to adhesion between workpiece and the cutting tool while machining of titanium alloys (53, 102). This is attributed to prevalent wear mechanisms, such as attrition, dissolution-diffusion and adhesion at contact length between workpiece and cutting tool face. Tool wearing triggers different types of tool failure (115, 116), as presented in Figures (2.4 - 2.7). These wear mechanisms do occur due to micro hardening and topography of material beneath the machined surface in machining of titanium alloys (116, 117).

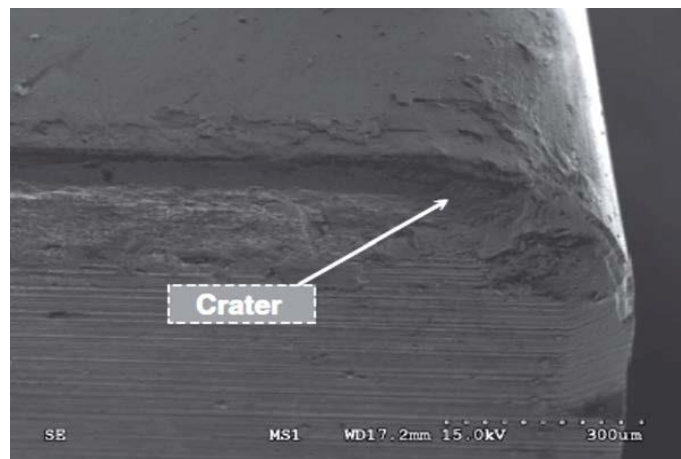


Figure 2. 4 Crater wear at cutting edge in machining titanium alloy (Ti-555) (76)

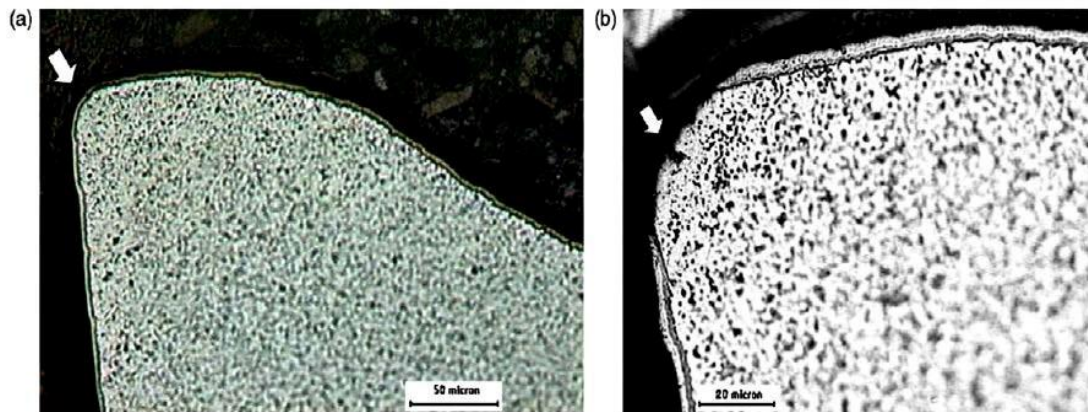


Figure 2. 5 Delamination of coated cutting tool (WC-Co) in machining Ti-6242S alloy (68)

Coated tools may get delaminated at the cutting edge making it blunt (73, 118), as illustrated in Figure 2.5, because of incompatibility in thermal expansion coefficients of coating and tool materials (118, 119). Ezugwu et al. (120) have identified that poor thermal diffusion leading to higher machining zone temperature is the main

reason of tool consumption during machining of Ti-6Al-4V. Amalgamation of increased machining load as well as elevated temperature at upper speeds cause rapid chipping on tool edge (52, 121, 122), as shown in Figure 2.6. High cutting temperature also produces adhesion of small morsels of workpiece material on cutting tool (68, 103), such as depicted in Figures 2.5.

The adhesion erodes the tool flank material, and such effects are accelerated when the cutting depth and machining speed rise in high speed milling with PCD/PCBN tools (73). Repetitive adhesion of workpiece material promotes BUE formation that gradually alters the cutting edge geometry (70). For these reasons, it is hard to machine titanium alloys with HSS steel cutting tools at speed above 30 m/min and by tungsten carbide tools at above 60 m/min. Ceramic and cubic boron nitride tools are not appropriate for machining titanium alloys since these react with titanium alloys (106).

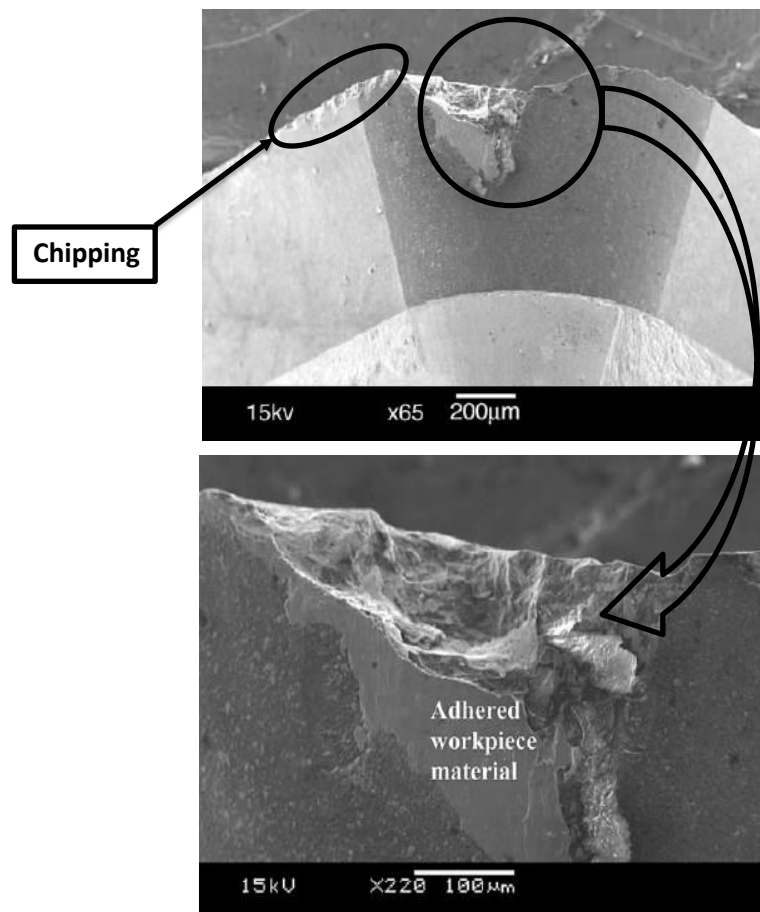


Figure 2. 6 Adhesion at cutting edge during machining of Ti-6Al-4V alloy (58)

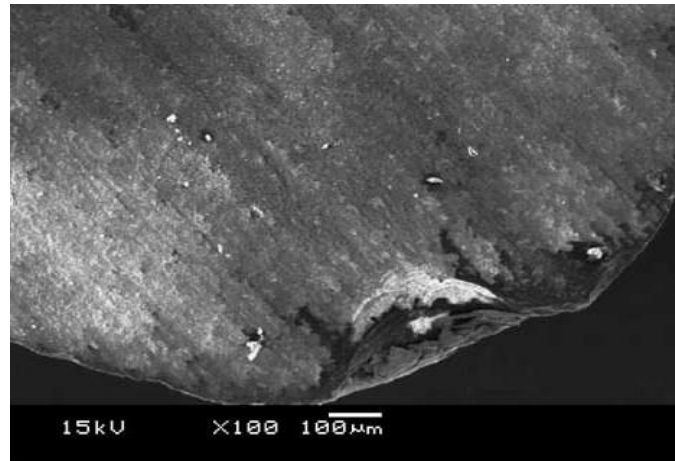


Figure 2. 7 Wear and adhering workpiece material at rake face while high-speed milling of Ti-6Al-4V alloy (59)

Titanium alloys react with many cutting tool materials, such as CBN and PCBN at elevated (cutting) temperatures typically above 500 °C (3, 101). In this thermally-triggered reaction, the cutting tool material is removed on an atomic scale (68, 123), producing a Tribochemical wear process. This mechanism can occur as molecular-mechanical wear or corrosive wear or as a combination of both (99, 102). Such fast reactivity between workpiece and tool causes smearing, galling and chipping of the machined surfaces (68, 124) as well as fast cutting tool wear (5), as depicted in Figure 2.7. Additionally, at elevated cutting temperatures, titanium alloys undergo oxidation forming compounds (125), while chips may get welded on to the cutting tool face and machined surface (61, 66, 76, 126), causing machining issues.

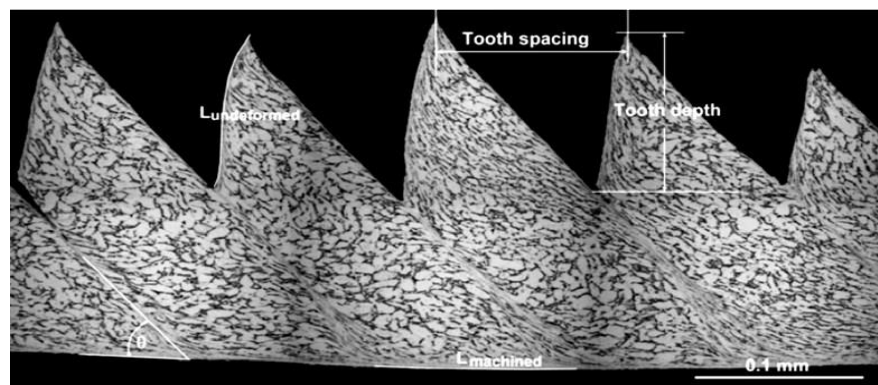


Figure 2. 8 Geometrical features of segmented chip formation (127)

Chip formation in machining is categorised to be (i) continuous chip, (ii) continuous chip with BUE and (iii) discontinuous chip (3, 128). Chips produced during titanium machining are observed to be discontinuous or segmented (98), particularly at lesser speed around 40 m/min (128, 129), as illustrate by Figure 2.8. This is because, with titanium alloys, the plastic deformation within the primary cutting zone is very difficult and said to undergo “Catastrophic thermos plastic shear” (70, 101), where the process is unstable and nonhomogeneous (105) due to extreme material hardness of these alloys. Consequently, the chip formation occurs with cyclic frequent chip breakage (105) and increased flank wear.

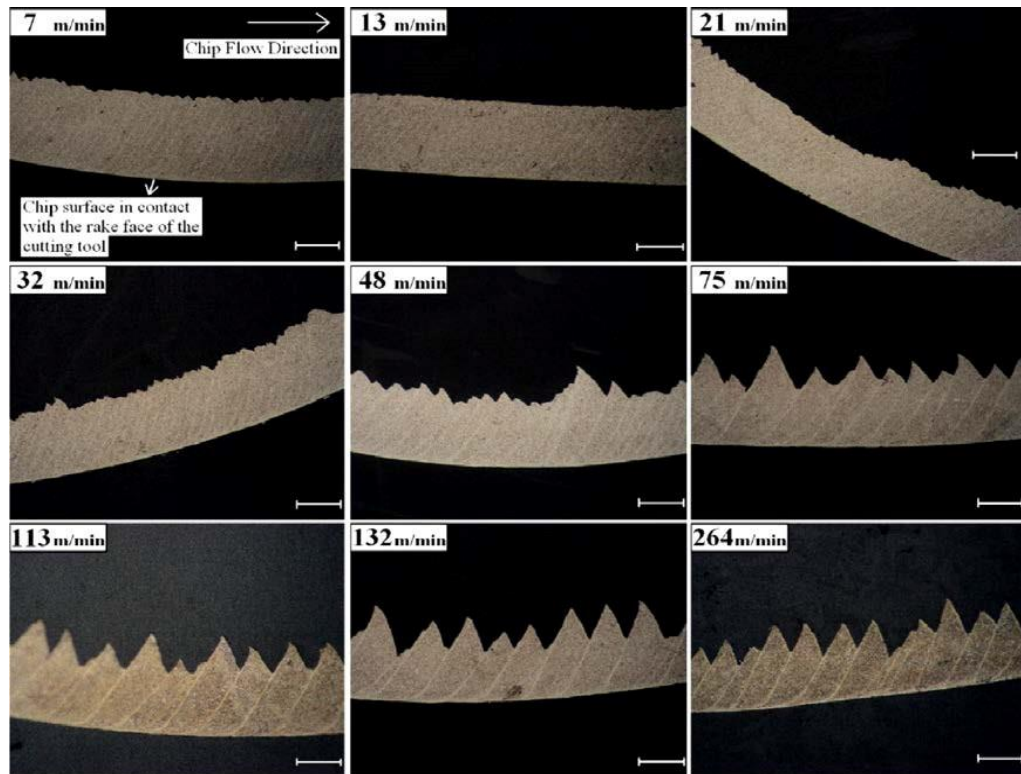


Figure 2. 9 Types of chip microstructures in conventional machining of titanium (Scale bar represents 100 μ m) (129)

Discontinuous chips are observed to have much shorter contact length with tool face compared to a continuous chip-approximately one third length (5, 51, 54). Pramanik et al, (42) have stated that the microstructure of titanium alloy determines the cutting speed at which segmented chip formation would begin. For titanium alloys, Figure 2.9 illustrates various chip formation shapes/types associated with

different cutting speeds (54, 70). Discontinuous chips have tendency to induce fluctuations in cutting forces, especially when alpha-beta alloys are machined (112). Shivpuri et al (125) have reported that the phenomenon of chip segmentation would limit the metal removal rates during cutting operation and causes cyclic vibration of forces.

The self-excited vibration significantly affects the formation of chips as well as machined surface, which often referred to as chatter (98, 130). The changing frictional force due to chip flow on tool face generates shear localisation and also contributes to forced vibration and self-excited chatter (45, 131). These vibrations can lead to catastrophic tool failure. It has been observed that the tool vibration and chatter from segmented chip are associated with the thrust components of the cutting forces and the periodic oscillation during machining (20, 63). Also, the serration chip intensity increases the fluctuations of cutting forces and induces dynamic stresses at the cutting tool, triggering high tool wear (51, 132). Chip formation instability induced by high cutting temperature and the micro-fatigue loading thus applied on the tool tip are accountable for austere wear in flank and decreased cutting tool life (133, 134), in titanium alloy machining. These invariably affect the stability of the cutting edge leading to sub-surface defects and inaccurate dimensions of the machined surface (107, 120, 135).

In machining hard titanium alloys, extraordinarily high cutting temperatures are encountered owing to the combined effects of difficult plastic deformation, segmented chip formation, poor workpiece thermal conductivity and self-induced tool chatter, resulting in unacceptable machined surface quality and various forms of cutting tool damage to shorten tool life. All these detrimental effects lead to machining process inefficiencies and higher manufacturing product cost. The following section examines the status-quo in methods to increase the machinability of titanium alloys, based on TAM approaches.

2.4 Thermally Assisted Machining (TAM)

Over the last four decades different techniques have been considered and applied in overcoming problems associated with surface quality and tool wear during titanium alloy machining (118). Among these methods, TAM has emerged as a forerunner,

which involves workpiece preheating with precisely coordinated external heat sources. This technique was first devised by Tigham in 1889 and since then has evolved to use heating methods incorporating plasma, laser and induction coil systems with varying degrees of thermal generation intensities (136).

Conceptually, TAM approach applies localised heating in advance of the cutting point to soften the workpiece surface layer that reaches cutting tool for machining (137). The external heating locally improves ductility of workpiece and reduces forces required for plastic deformation, thus potentially alleviating the concerning issues of high temperature rise and tool chatter (20, 138, 139). Figure 2.10 schematically shows a TAM configuration, where the heat source position and power are essentially dependent on machining variables and the distribution of temperature to be achieved in workpiece. In some cases, instead of the workpiece, the cutting tool is heated to manage the behaviour of work material (140, 141).

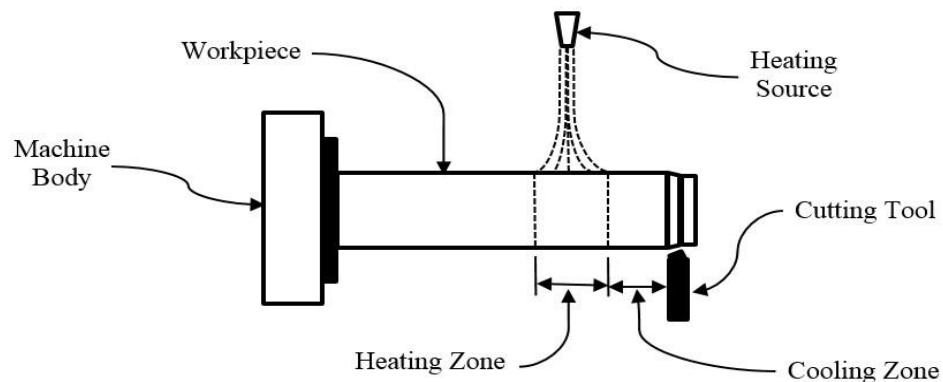


Figure 2. 10 Preheating workpiece during turning process

Due to low thermal conductivity and material hardness, in machining titanium alloys, TAM requires careful and appropriate selection of preheating method based on source heating power, source position, machining speed, depth of cut and feed. Also, the material of tool should be capable to endure more than 300 °C surface temperatures and have steady chemical and thermal behaviours, and adequate resistance to wear. It is noted that the heating strategy for turning process is slightly different to that of milling, due to rotational differences in the cutting configurations of the two methods. In turning, the cutting area is repeatedly heated (118) therefore

would require less heating intensity compared to milling, where the cutting area does not move as fast as in turning. A typical TAM arrangement for milling is shown in Figure 2.11 along with workpiece temperature distribution.

In TAM, the effectiveness of the approach is critically dependent on the preheating temperature, which requires careful control to prevent overheating of the workpiece and material deformation (136, 142). In selecting external heating, considerations should include not to over soften the surface layer in the primary cutting zone, which can lead to unwanted deformation that can bring about other machining complexities (3, 37).

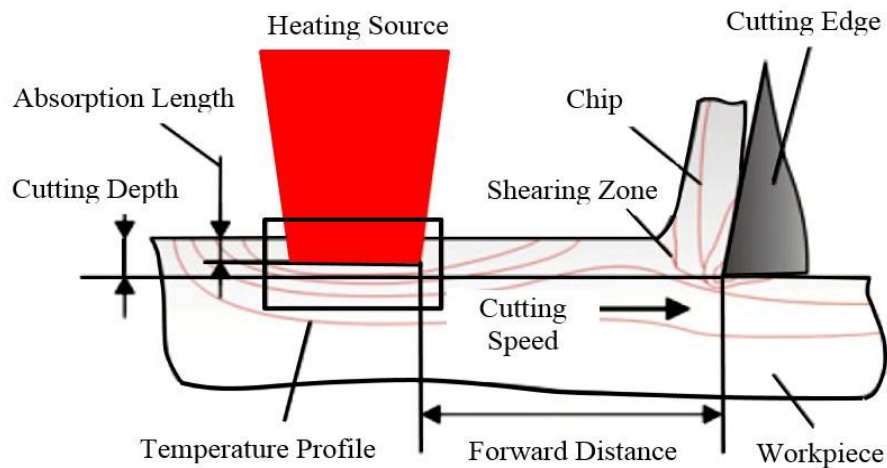


Figure 2. 11 Preheating workpiece during milling process (143)

2.5 Effects of Preheating Temperature

Figure 2.12 presents the influence of temperature on mechanical strength of some selected HTM materials (143), where it is noted that heating generally weakens materials by reducing stress and strain hardening rate. This effect, which is known as thermal softening (42, 118), is the principle behind TAM technique. In TAM, workpiece temperature within the primary shear zone is raised above the recrystallization temperature by external heating to reduce the workpiece yield strength (144, 145). This assists plastic deformation, and reduces work hardening effects and cutting force requirements in machining processes (146, 147). Thus, power consumption is reduced while material removal rate and productivity (142, 148) are increased. This approach is particularly beneficial for HTM materials such

as, titanium-based alloys, where TAM makes machining of these alloys much easier (37, 149). For TAM to be operated effectively, the preheating temperature must be controlled and kept within a range not affecting microstructural change of the workpiece (118). In this regard, Machado and Wallbank (101) reported that the preheating temperature of titanium alloys needs to be maintained below 882 °C to prevent phase transformation. Also, it has been observed that rate of strain hardening decreases significantly between temperatures 200°C to 734°C (143).

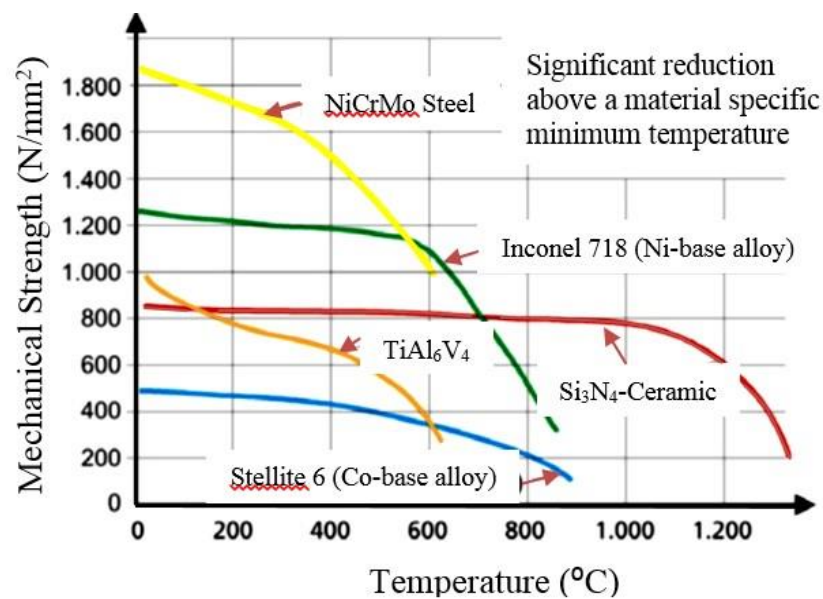


Figure 2. 12 Relationship between temperature and mechanical strength of selected hard-to-machine alloys (143)

With preheating, force components in the machining such as cutting force, feed force, normal force, and thrust force, are dramatically reduced which reduces the dynamic impact on the tool and advances tool's mechanical and thermal fatigue characteristics, operational life and machining cost-effectiveness (42, 150). Amin (151) studied the influence of whole workpiece preheating in furnace on machinability of high-temperature resistant steel and titanium alloy BT6 (Russian Standard). It has been found that the preheating tends to stabilise chip formation process and increases interaction length between cutting tool and chip.

Sun et al. (152) explored the influence of laser preheat in milling of Ti-6Al-4V. They noticed significant reduction of feed force within 200 to 450°C temperature. Ayed et al. (153) observed reduced machining forces with the laser

power up to a certain value. Heating beyond this adversely affected because of chip melting and melted chips sticking to the tool rake face, especially when the laser-cutting tool clearance was 3 mm. Figure 2.13 illustrates the cutting force reduction with the applied laser power for preheating. It is noted that a more than 50% reduction in machining forces was achieved when the laser beam and cutting tool gap 5 mm. However, increased feed and speed impart opposite effect on the reduction of machining forces. It is concluded that a substantial decrease of forces is generally possible with higher levels of external heating.

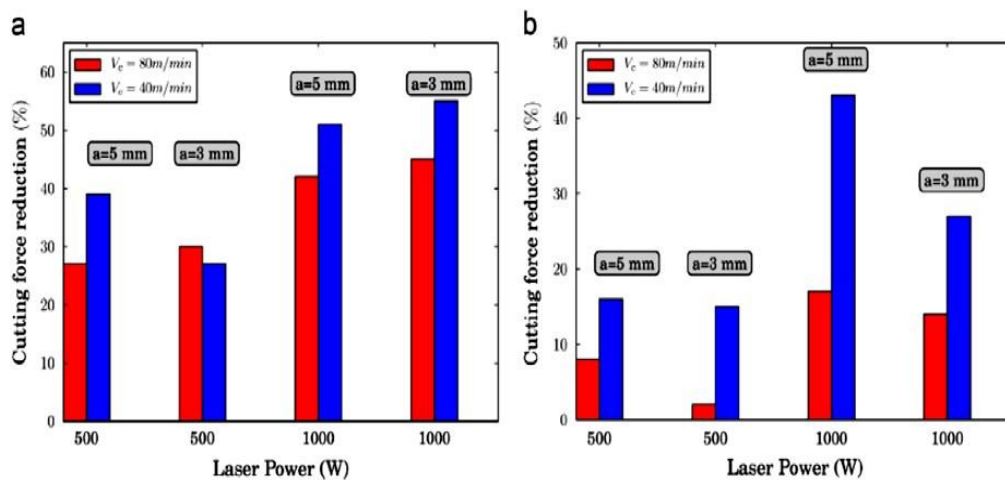


Figure 2. 13 Reduction rate of machining force while machining Ti-6Al-4V alloy at feed (a) 0.1 mm/rev, and (b) 0.2 mm/rev (153) with speed 40 and 80 m/min and cutting depth 1 mm (153)

The machining force is linearly proportional to the variation of feed and/or depth-of-cut (154) in the course of laser assisted machining of titanium alloys (Ti-6Cr-5Mo-5V-4Al) (155) and (Ti-10V-2Fe-3Al) (129). During turning of (Ti-6Cr-5Mo-5V-4Al) alloy, the cutting forces decrease by about 15% at laser power of 1200 W, feed 0.15 to 0.25 mm/rev and speeds within 25 to 100 m/min. Whereas, the percentage of decrease in machining forces during machining of (Ti-10V-2Fe-3Al) alloy is between 10 to 13 % in machining speed range of 45 – 70 m/min. Due to thermal softening, workpiece preheating also reduces the amplitude of force fluctuations, which in turn dampens tool vibration (28, 156). Hence, damages to rake and flank faces are lessened, as illustrated by Figure 2.14.

Dandekar et al., (150) studied machinability of Ti-6Al-4V alloy in terms the specific machining energy, tool life, and surface roughness with laser assistance.

A marked decrease in the rate of tool wear was noted with increasing material removal temperature (T_{mr}) up to ($250\text{ }^{\circ}\text{C}$). At this temperature, cutting tool life increased by about 1.7 times at machining speed below 107 m/min compare to that of conventional machining. The wear rate of tool started to increase with the rise of workpiece temperature over $250\text{ }^{\circ}\text{C}$.

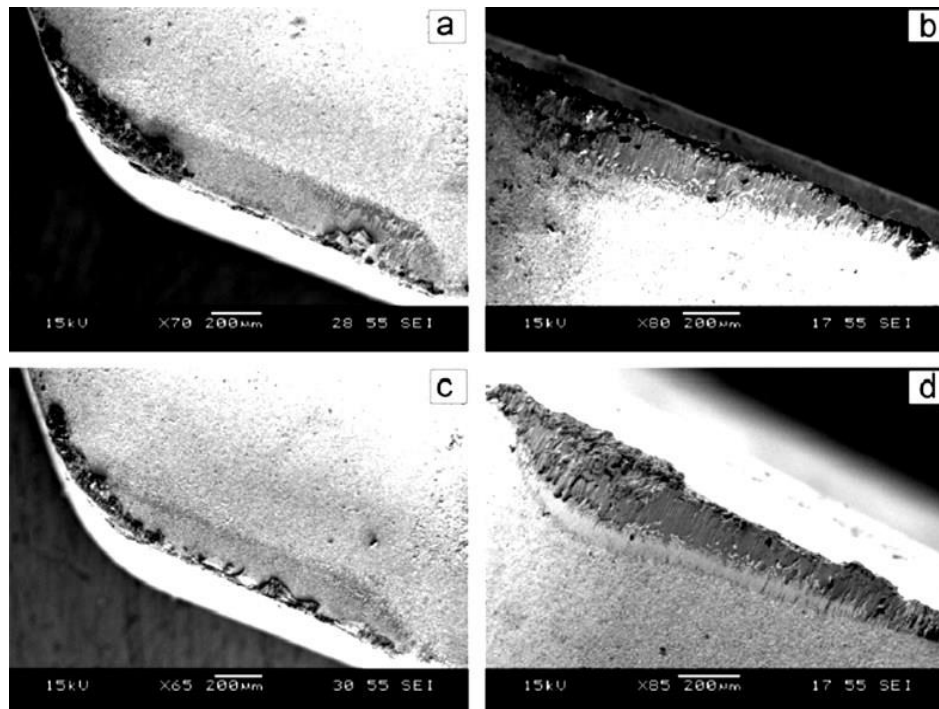


Figure 2. 14 Tool damage (a) rake face (b) flank face of cutting tool inserts at speed 160 m/min with laser heating, and (c) rake face (d) flank face of cutting tool inserts under similar machining circumstances under without laser heating (155)

TAM offers further benefits in reducing the occurrence of adhesion of chip fragments and BUE at the tool cutting edge, which are direct implications of high temperature build up in the plastic deformation zone. With thermal softening induced by preheating, TAM improves surface finish with fewer surface cracks and less porosity than in traditional machining (157). This is further evident from the fact that the microhardness at the surface layer is decreased with higher levels of preheating temperature because of the reduced density of dislocation (158). The increased preheating temperature stimulates grain growth and larger grains stay close to the heated surface of the workpiece. Increased grains size reduces strain hardening effect, and as a result, the hardness increases as the distance from the

workpiece surface rises along the depth. Several variables influence the yield strength of the workpiece during TAM and affect the machined surface. These variables are heat source power, the gap between heat source and tool, and the distance and angle between the workpiece surface and heat source. Germain et al., (159) observed a slight reduction in the surface roughness between $0.3\ \mu\text{m}$ and $0.6\ \mu\text{m}$, when the laser power was between 500 W and 1000 W while machining of Ti-6Al-4V alloy at speed of 26 m/min and 54 m/min.

Localised heating softens the surface and changes the material removal mechanism. These affect the morphology and microstructure of the chips in TAM where the chips are formed with clearer edges, uniform thickness and homogeneous segmentation (152). Due to high temperature in TAM, the chip morphology changes from sharp saw-tooth (brittle fracture type) to a continuous chip (plastic flow type). This is represented by the significant difference in both the depth of saw-teeth and segment spacing, as shown in Figure 2.15. The formation of continuous chips reduces the surface roughness and minimises self-induced vibration (135, 160). The segmented chip is occasionally found at low cutting speed. With increasing preheating temperature, the deformability of work material at heated surface improves. Hence, continuous chips are produced at higher machining speeds. It has been noted that the localised melting in chips occurs at less than 20 m/min speeds, as illustrate in Figure 2.16. It is also reported that the increase surface temperature raises chip thickness and reduces the distance D_c (shown in figure 2.15) and shear angle (153). All these increase the frequency of the chip segmentation.

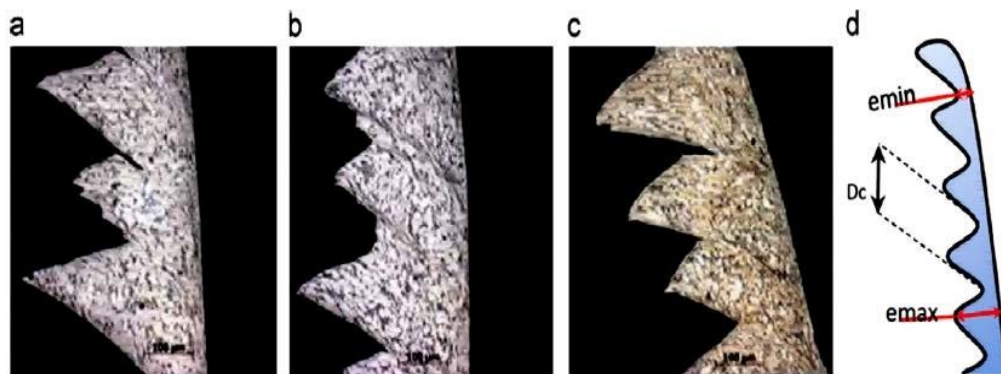


Figure 2. 15 SEM views of chip sections at varying laser powers at speed 40 m/min and feed 0.2 mm/rev (a) no laser (b) 500W (c) 1000W, (d) schematic chip morphology (153)

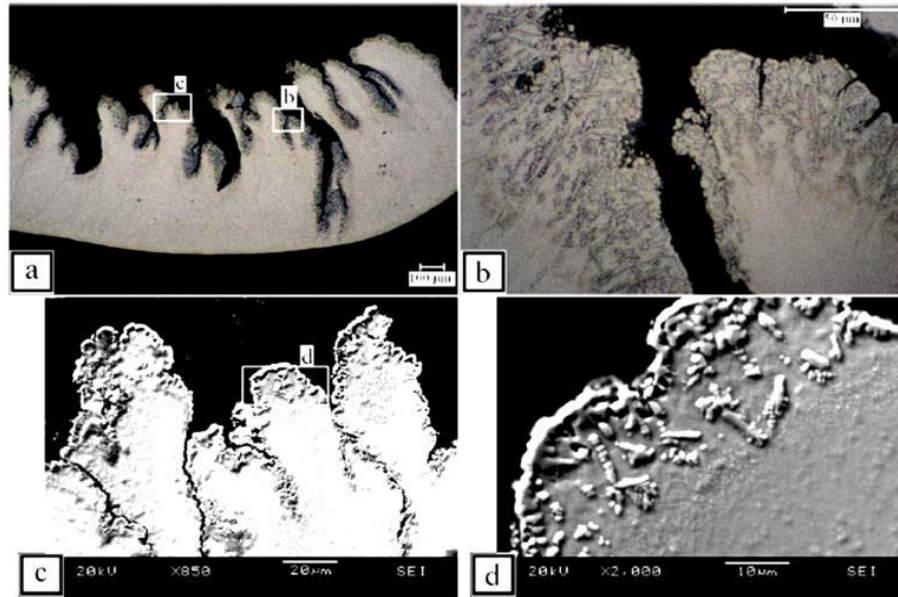


Figure 2. 16 (a) and (b) Chip Microstructures formed in laser-assisted machining at speed 7 m/min, (c) and (d) SEM secondary electron images of dendrites at the same chip surface (129)

Using laser of 1500 W, Braham-Bouchnak et al., (161) have observed semi-continuous and continuous chips owing to the increase of sawtooth frequency. It is also reported that the chip shrinkage coefficients decreased with higher heating temperature that increases chip length (162), or the reduction in chip shrinkage coefficient leads to stable and thinner chip. Using polycrystalline diamonds (PCD) inserts for machining, Ginta et al., (162) have noted that TAM reduces vibration amplitude from 53% to 86% due to preheating at 650 °C.

Above review identifies that TAM decreases the flow stress and strain hardening of workpiece material, hence significantly suppresses tool chatter/vibration and improves tool life. Elevated temperature in TAM facilitates smoother material flow over the flank as well as rake faces of the cutting tool thereby improves the machined surface. Chips formed under proper thermal conditions tend to be thin, long and continuous. These would increase the chip-tool contact length compared to those produced in conventional machining. This longer contact length decreases the stresses at tool face and extend cutting tool life. Thus, the TAM technique represents an effective solution to machining HTM materials with an acceptable cost with improved productivity and quality.

2.6 Thermally Assisted Machining Techniques

Some recent research works have been focused on the development of TAM techniques for improving titanium alloys machining. For example, Bermingham et al. (139) measured both tool life and wear mechanisms after preheating the workpiece in a conventional furnace prior to machining of titanium alloy (Ti-6Al-4V) at three workpiece temperatures with two carbide cutting tools. A 30 % reduction in the cutting forces was achieved in addition to 7 % improvement in tool life, compared to that offered by cooling technologies under identical experimental conditions. Current state of the art identifies high-end thermal-assisted techniques, such as induction-assisted machining (82-85), plasma-assisted machining (86, 87, 163-166), and laser-assisted machining (37, 38, 88-90) are more promising contenders that significantly improve the overall machinability of titanium alloys with recognized benefits of high MRR and economics of machining.

2.6.1 Laser-Assisted Machining (LAM)

Recently, LAM has been used as an auxiliary process for machining various HTM materials and alloys as well as alloys possess high melting point, and composites. LAM deploys a high-power laser focussed at a certain spot on the workpiece to preheat upstream of tool path surface during traditional machining (167-170). The laser heating point in turning is confined to less than 3 mm diameter (171, 172). This localised heating lowers the yield strength of HTM at elevated temperature, thus reducing cutting forces and tool wear to improve surface finish quality and cut down the machining time (39, 169, 173). However, the intense laser heating causes oxidation, melting and/or vaporization of the workpiece surface while the transient thermal response of the workpiece would potentially induce uneven thermal expansion of the material (29, 170, 174). The performance of laser preheating technique depends on the laser attributes such as laser power, beam diameter, scan speed and approach angle (tool-beam distance), as well as the machining parameters such as cutting speed, feed rate and depth of cut. Therefore, LAM is rather complex to control for as it is governed by many parameters and their mutual interactions (150, 171, 175). Nonetheless, this technique has been widely extended to various machining operations such as milling, grinding and turning, etc. (176), recognising its many advantages: (i) adaptability to different types of machining processes, (ii)

localization of high temperature and (iii) process stability (39), etc. This technique offers flexibility in machining of HTM material as it allows adjusting of input parameters to reduce machining time, thus yielding a significant reduction in production cost, as much as 60 % – 80 % (27, 34, 161, 177).

LAT centre consists of three main components, where the first component contains a high-power continuous-wave laser to supply strong, localized and controlled heating to the workpiece; the second part is a system of optics for guiding the laser beam from the lasing chamber to the workpiece; and the third component contains machine tool, i.e. lathe itself (89). The position of a laser beam is arranged in such a way that the temperature distribution remains uniform into the cutting zone (149). It uses two control systems namely, revolver-kind optics and auto focusing to control the laser beam size (176). The revolver-kind optic system is equipped with various lenses that process selectively, while in auto focusing, the laser beam diameter and the focal length are set by automatic focusing system. The laser beam can be transferred from its module to a specific machining zone by using optical fibres or mirrors (176).

In LAT, the workpiece rotates at high speed and while it is being subjected to cyclic heating at a specific rotating point via a laser beam focused on an area ahead of the cutting edge. The workpiece temperature gets progressively elevated at the heated point and shows slight cooling when laser spot moves away along the cutting path (178-180). Generally, a continuous-wave beam with a Gaussian distribution is useful to minimise the thermal shock. To the contrary, with a pulsed-wave mode laser, heating and cooling tend to be more rapid at the workpiece, leading to a workpiece surface hardening process that adversely affects the machining performance (180). The convection and conduction heat transfers processes impact considerably on the temperature distribution in the cutting zone (178, 180, 181).

It has been found that arranging the laser beam perpendicular to the feed direction is more effective for not heating the machined surface and makes machining easier (167), see Figure 2.17. In addition, in this method, the laser output is regulated by a pyrometer, allowing a constant temperature to be achieved in the component (182). However, the temperature at a depth of machining may not be enough for a deeper cut and the measurements do not warrant recording such

temperature for precise determination of effective cutting depth (38, 182-184). Whilst LAM can be practically used for machining titanium alloys, this technique is observed to be difficult for cutting straight holes or pear-shaped holes (39, 169).

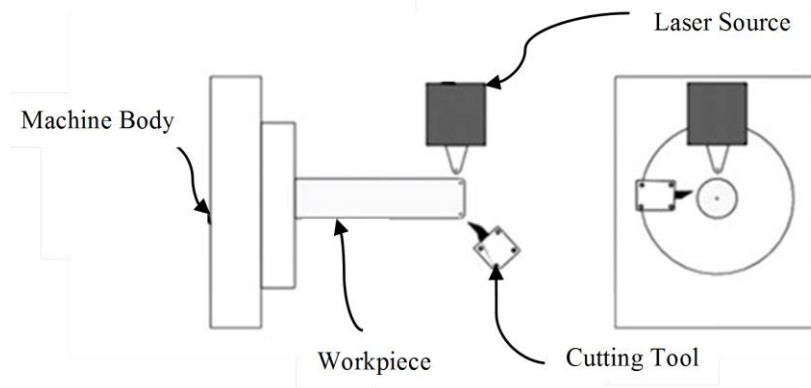


Figure 2. 17 Illustration of laser beam position (perpendicular to the feed direction) in turning

Another possible arrangement of the laser beam is to set its vertical orientation to the workpiece chamfer surface during turning operation (89, 149), as illustrated in Figure 2.18. This reduces the components of cutting forces significantly (30, 183, 185), hence minimising the chances of any mechanical and/or thermal issues. For uniform reduction of cutting forces, it is essential that the laser spot size should completely cover the chamfer surface, so that the softening of plastic deformation zone by the laser becomes easy. This will reduce the shear-generated heat to level below conventional machining (38).

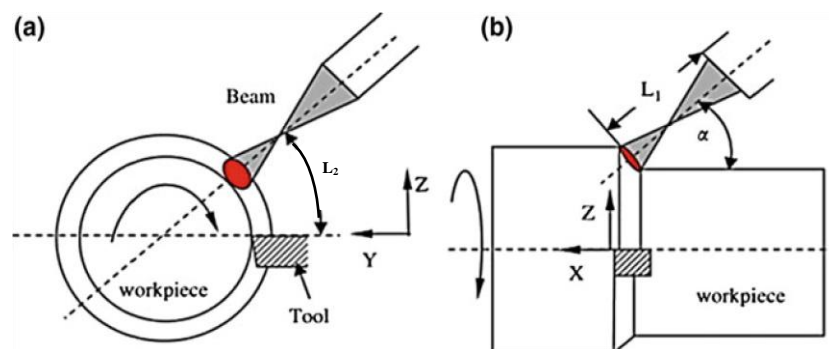


Figure 2. 18 Relative position of the laser beam during turning operation: (a) end-view and (b) side-view (185), with kind permission from John Wiley and Sons

In laser-assisted milling operation, multiple laser beams can be used in various orientations over the cutting area, because a large zone is covered by cutting tool (90, 186). The temperature at the laser spot depends on (i) the heating duration, (ii) the laser power density distribution and (iii) the number of heating/cooling cycles (38). Due to the ability to control spot size and laser power density, the thermal distortion and heat-affected area are generally small in LAT methods. Therefore, intense thermal gradient is confined to a very thin surface layer at the workpiece, enabling machining without interfering on the integrity of workpiece subsurface. According to many studies (174, 187), the temperature gradient at the cutting zone is important to understand the mechanism of chip formation, investigate the thermo-mechanical characteristics in LAM, and to determine the reduction values of cutting forces (188).

The effectiveness and benefits of LAM for various HTM materials are reported in literature, identifying a significant reduction in cutting forces, tool wear, chatter and producing better machined surface and increased MRR, such as for steels (38, 189-192), inconel 718 (189, 193-196), nickel alloys (197, 198), waspaloy alloy (199), ceramics (172, 174, 179, 200-202), magnesium alloys (203, 204), and metal matrix composites (48, 178, 188, 205, 206). There have been many investigations in recent years examining the feasibility of LAM for titanium alloys.

Hedberg et al. (207), experimentally studied the improvement in the machinability of titanium alloy (Ti-6Al-4V) by using LAM technique. It was determined from the study that the flank wear and compressive residual stresses of the machined surface were decreased by 10% and cutting speed was increased around 35% in LAM compared with conventional process to machine Ti-6Al-4V. Furthermore, increasing cutting speed showed a 33% reduction in cost in spite of the additional cost of laser equipment. Germain et al. (159) investigated the effect of LAM on residual stresses of machined bearing steel (100Cr6) and titanium alloy (Ti-6Al-4V). This study indicated that the higher laser power reduces the cutting forces and increases the residual stresses towards tensile or positive stresses at the surface layer. Braham-Bouchnak et al. (161) studied the improvement in productivity of titanium alloy (Ti555-3) through LAM to improve chip formation by a thermal softening phenomenon. It was identified that a reduction of surface temperature and the change of chip formation mechanisms are achieved by increasing the frequency

of sawtooth. Furthermore, the surface integrity of workpiece was modified in terms of strain hardening and residual stresses, as shown in Figure 2.19. Dandekar et al. (150) investigated the effect of LAM with hybrid machining on titanium alloy (Ti-6Al-4V) machinability. The results show that it is possible to increase the cutting speed during machining (Ti-6Al-4V). Moreover, the cutting forces were reduced with reasonably higher MRR.

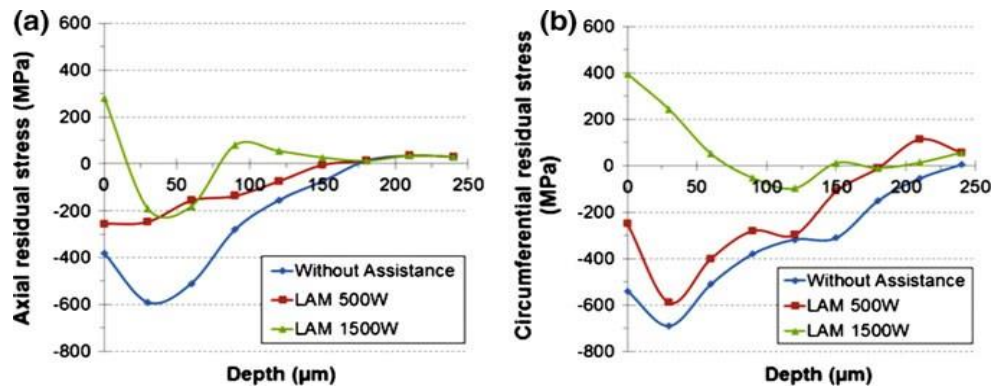


Figure 2. 19 Residual stresses as a function of depth during machining with and without laser heating, a axial residual stresses and b circumferential residual stresses (161)

Rashid et al. (155) studied the effects of LAM on machining of the beta titanium alloy (Ti-6Cr-5Mo-5V-4Al), by comparing cutting temperatures and cutting forces during LAT and conventional machining at different values of feed rates and cutting speeds. This comparison showed that the cutting forces reduced by 15 % in LAM.

The results show that the optimum cutting speed range of 25–100 m/min is suitable to avoid chip/tool welding; and leads to acceptable characteristics of surface integrity. Furthermore, the optimum range of cutting temperatures was found to be 1050–1250 °C causing a moderate reduction in cutting forces. Sun et al. (152) reported that local heating by a laser beam in front of the cutting tool during laser-assisted milling of titanium alloy (Ti-6Al-4V) caused a dramatic reduction in cutting forces, especially feed force at 200–450 °C. This higher temperature at tool/chip interface zone may accelerate the dissolution/diffusion and adhesion wear, thereby leads to softening the cutting tool (152, 208). Therefore, the maximum tool life achieved between 230 and 350 °C for LAM with compressed air delivered through the spindle during laser-assisted milling of Ti-6Al-4V (152). It was noted that both the cutting tool life and tool failure modes depend on the temperature at cutting zone.

LAM of HTM materials produces a dense layer with fine grains which improves the hardness of the surface during the phase change and fast solidification in the surface area (209, 210). The most widely used laser sources that have been investigated as preheating media in LAM experiments are a neodymium-doped yttrium aluminium garnet laser (Nd:YAG), carbon dioxide laser (CO₂) and high-power diode laser (HPDL) (176, 211, 212). Fundamentally, Nd:YAG laser is a solid-state laser that emits a wavelength of 1.064 μm (213, 214). However, CO₂ laser is a gas laser that emits a wavelength of 10.64 μm , which is ideal for optimum absorption. The CO₂ laser produces spot size 10 times larger than that produced by Nd:YAG laser, when both types are used in the same machine set-up. HPDL laser has broader wavelength bands than others and emits a wavelength from 0.808 to 0.980 μm (215, 216). Nd:YAG laser is ideally used for metals and coated metals, while CO₂ laser is best suited for organic materials for example wood, paper, plastics, glass, textiles and rubber. The CO₂ laser has limitations, where it requires a beam transfer technique using a mirror compared to other types of the laser using fibre optic cables (180, 212, 215). In HPDL laser, the laser energy density has uniform geometry in Top-Hat shaped, which represents much better results than the Nd:YAG and CO₂ lasers that have a Gaussian distribution (176, 215, 217), see Figure 2.20. The Nd:YAG laser is most useful on most of the HTM materials like hardened steel and titanium alloys due to the shorter wavelength (12, 171, 192). On the other hand, HPDL laser shows an absorption rate of about 40% at the surface of metals, thus making this type being largely suited for most metallic materials and better beam stability in LAT (216-218).

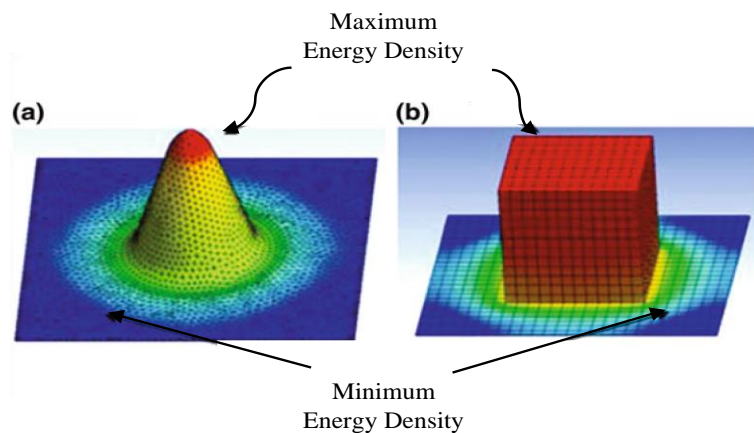


Figure 2. 20 Distribution shape of laser energy density, (a) Gaussian distribution and (b) Top-Hat distribution (176)

Rashid et al. (114) have studied the effects of laser power on the beta titanium alloy (Ti-6Cr-5Mo-5V-4Al) machining and noted that the optimum range of laser power is 1.2–1.6 kW to reduce cutting forces significantly at cutting speed ranging from 25 to 125 m/min. The influence of laser power on residual stresses during LAT of AISI 4340 steel via finite element analysis have examined by Nasr and Balbaa (208). The results showed that surface tensile residual stresses decrease with the increase of laser power. At lower laser power, limited preheating in front of the cutting tool causes easier compressive deformation. Higher laser power produces mostly thermal deformation, which leads to minimizing the material resistance of workpiece at cutting zone and causes tensile residual stress at the machined surface. The effect of laser power and cutting speed on the machining of Inconel 718 superalloy have been investigated (219). It was noted that the surface temperature increases with higher laser power and falls when the approach angle increases.

Kannan et al. (220) investigated the LAM feasibility of machining alumina ceramics over a range of laser scan speeds on cutting tool wear. The results showed that the surface temperature fluctuates around 1250 °C when the laser scan speed is around 35–55 mm/min at a laser power of 0.35 kW. The cutting forces and flank wear decreased significantly at this temperature. However, above this range of laser scan speeds, the cutting forces and flank wear were observed to increase. This is because of the reduction of laser-material interaction time at the higher speed of laser scan. Subsequently, the temperature at the depth of cut would be much less than the softening temperature. Sun et al. (127) analyzed the influence of the laser beam diameter on chip formation during machining titanium alloy (Ti-6Al-4V) at various machining speeds. This investigation showed segmented chip formation at low and high speeds. Continuous chips are formed at intermediate speeds because of the thermal softening at the shear zone, which causes ductile deformation.

The surface layer of workpiece needs to be heated to a temperature that will cause ductile deformation of material during the machining operation. Due to high temperature during LAM, the continuous chip is formed, indicating plastic deformation rather than brittle fracture (37, 182). Chips thus formed have a highly irregular segmentation pattern, that is distinguished by larger fluctuations in segment height (h) and pitch (p) compared to the one that formed in conventional machining, as illustrated in Figure 2.21. As a principle requirement, the heating temperature

must not be high enough to change the bulk material properties of workpiece and/or soften of the cutting tool (182). Therefore, laser heating needs to be confined to the workpiece surface and should be readily removed before heat propagates into the bulk of workpiece (50). This results in reduction of surface roughness, as shown in Figure 2.22, and lessen tool wear by about 90% when compared with traditional machining (182, 189).

The distance from cutting edge to laser beam is a critical factor during preheating by laser. This determines the time interval between heating and machining processes, therefore the temperature distribution at the machining zone [34]. During machining commercially pure titanium, Sun et al. [67] noted that the highest reduction of cutting forces occur when the laser spot position is nearest to the cutting edge. However, the distance between tool and beam must not be very close to prevent cutting tool damage by overheating [63]. High laser heating temperatures may prematurely degrade the cutting edge, leading to subsurface damage of workpiece [59].

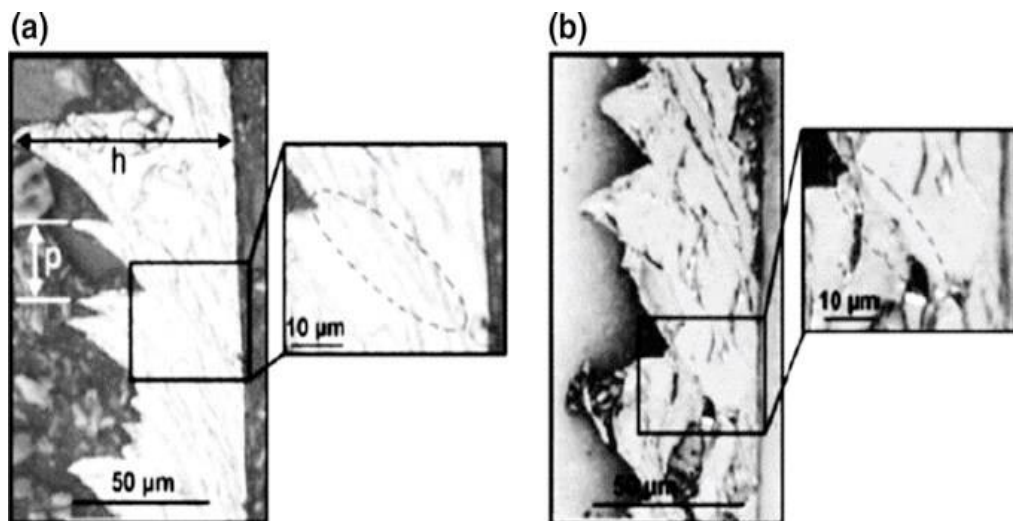


Figure 2. 21 Chip morphologies of titanium metal matrix composite: a with LAM, $V_c = 100$ m/min, $T_s = 500$ °C, and, b conventional machining, $V_c = 100$ m/min, RT (188) with kind permission from Elsevier

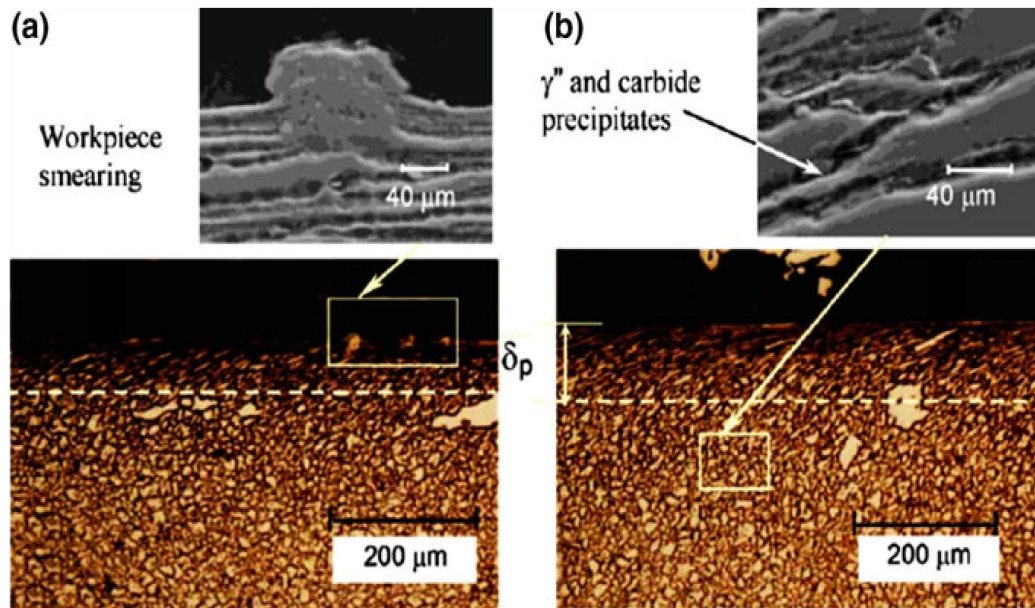


Figure 2. 22 The micrograph of the machined surface (300 m/min, 0.4 mm/rev) under: (a) conventional and (b) LAM machining conditions (189) with kind permission from Elsevier

The material removal temperature is an important variable that requires to be controlled to prevent metal melting and/or undesirable microstructure change during machining (38). The material removal temperature can be obtained empirically for turning Ti-6Al-4 V with single CO₂ laser from Eq. (2.1) (150):

$$T_{mr} = \frac{e^{3.4} P_{CO_2}^{0.66}}{f_r^{0.31} D^{0.34} V_c^{0.31}} \quad (2.1)$$

Equation (2.1) shows that the material removal temperature increases with higher laser power. However, this temperature decreases with increasing cutting speed and workpiece diameter, owing to the reduced interaction time between the laser beam and the workpiece. Therefore, increasing rotating speed leads to a reduction in both the cutting force and cutting tool life (38, 185). Attia et al. (189) stated that MRR and the surface finish improve approximately by 800% and 25%, respectively, during LAT compared to those with conventional turning. The past work on the effect of LAM on the machinability of titanium alloys is summarized in Table 2.3.

Table 2. 3 Summary of LAM of titanium alloys

Author	Type of study	Workpiece material	Machining process	Process parameters	Objectives	Results and conclusions
Rajagopal et al. (89)	Experimental	Inconel 718 & Ti-6Al-4V	Turning	Laser power, Feed rate	To study the influence of Laser beam/cutting tool distance on the machining efficiency and tool wear.	Significant reduction in tool wear and cutting forces.
Germain et al. (159)	Experimental	Bearing steel (100 Cr6) & Ti-6Al-4V	Turning	Cutting speed, Feed rate, Depth of cut, Laser power	To analyse the effect of effect of process parameters on fatigue strength in LAM, and to further optimize them.	<ul style="list-style-type: none"> - Significant reduction in cutting forces and surface roughness -Improvements in residual stresses. -Slight reduction in the fatigue strength.
Sun et al. (185)	Experimental	Pure Titanium	Turning	Laser beam-tool lead distance, Laser focusing lens-workpiece lead distance, Incident beam/workpiece axis angle, Laser power, Cutting speed, Feed rate	To investigate the effect of LAM on the cutting forces and chip formation.	<ul style="list-style-type: none"> - Low cutting forces - Smoother surface finish - Continuous chip formation

Sun et al. (127)	Experimental	Ti-6Al-4V	Turning	Cutting speed, Laser power	To investigate the influence of laser beam on chip formation.	- Continuous chip formation at higher laser power and cutting speed
Dandekar et al. (48)	Numerical & Experimental	Ti-6Al-4V	Turning	Tool material, Cutting speed, Material removal temperature	To study the enhancement in MRR and cutting tool life	- Significant enhancement in MRR and cutting tool life. - Low machining costs.
Yang et al. (221)	Numerical & Experimental	Ti-6Al-4V	Without machining	Laser power, Laser scanning speed, Laser spot size, Angle of incidence	Characterization of heat affected area produced by laser heating.	- Increasing width and depth of the heat affected area with laser power increases and laser spot size decreases.
Sun et al. (152)	Experimental	Ti-6Al-4V	Milling	Cutting speed, Feed rate, Depth of cut, Laser power, Cutter axis/laser spot centre distance	Analysing the influence of LAM on cutting forces and cutting tool wear.	- Dramatic decrease in feed force -Significant reduction in tool chipping.
Rashid et al. (155)	Experimental	Ti-6Cr-5Mo-5V-4Al	Turning	Cutting speed, Feed rate	To analyse the effects of cutting speed and feed rate on cutting forces and cutting temperatures.	- Reduction in cutting forces. - Cutting temperature decreased with increasing cutting speed.
Zamani et al. (222)	Numerical & Experimental	Ti-6Al-4V	Milling	Cutting speed, Laser power, Feed rate	Investigating the effect of machining and laser parameters on cutting forces.	-Significant cutting forces reduction in three directions (X, Y and Z). -Increasing cutting tool life.

Rashid et al. (114)	Experimental	Ti-6Cr-5Mo-5V-4Al	Turning	Cutting speed, Laser power	To analyse the influence of laser power on cutting forces and cutting temperature.	- Reduction in cutting forces at high laser power and moderate to high cutting speeds.
Zamani et al. (223)	Numerical	Ti-6Al-4V	Milling	Feed rate, Laser power	To analyse the influence of feed rate and laser power on the cutting speed and cutting tool.	-Appreciable reduction in cutting forces and tool wear.
Rashid et al. (203)	Experimental	Ti-10V-2Fe-3Al	Turning	Cutting speed, Feed rate	To study the effect of cutting speed and feed rate on cutting forces, cutting temperature and chip formation.	- Low cutting forces and temperature. -Cutting temperature is greatly dependent on the cutting speed and feed rate. - Continuous chip was formed at moderate cutting speed and segmented chip at high cutting speed.
Braham-Bouchnak et al. (161)	Experimental	Ti555-3	Turning	Cutting speed, Feed rate, Depth of cut, Laser power,	Investigating the effect of LAM on cutting forces, chip formation and machining productivity.	- LAM has small effect on surface roughness criteria. -Increasing frequency of discontinuous chip with increase in laser power.

Joshi et al. (224)	Numerical	Ti-6Al-4V	Without machining	Laser power, Laser spot diameter, Rotation speed	To analyse the temperature distribution inside the workpiece heated in LAM.	-The surface temperature increases when laser power increases and laser spot diameter decreases. -The surface temperature decreases with increase in scanning speed.
Rashid et al. (156)	Experimental	Ti-10V-2Fe-3Al	Turning	Cutting speed, Laser power	To investigate the effect of laser power on machining parameters during LAM.	- Optimum value of laser power resulted in reduction of cutting forces and improvement in surface finish. - Optimal range of cutting speed helps to avoid force fluctuations during LAM.
Xi et al. (225)	Numerical	Ti-6Cr-5Mo-5V-4Al	Turning	Laser scanning speed, Rotation speed	Simulation of LAM using traditional finite element method and Split Hopkinson Pressure (SPH) method.	-Significant reduction in temperature is achieved with increase in laser scanning speed.
Ayed et al. (153)	Numerical & Experimental	Ti-6Al-4V	Turning	Laser power, Cutting speed, Feed rate, laser beam/cutting tool distance	To study the effects of machining and laser parameters on cutting forces and chip formation.	-Increase in laser power minimizes the shear angle and reduces the chip thickness -Significant reduction in the cutting forces.
Hedberg et al. (207)	Experimental	Ti-6Al-4V	Milling	Laser power	To study the machinability of Ti alloy	Significant reduction in flank wear and cutting forces.

2.6.2 Plasma-Assisted Machining (PAM)

PAM is another technique that is recommended for machining of HTM materials such as Ti-6Al-4V that undergo change in mechanical properties at high temperature (11, 87, 164). PAM is an economical option for heating work material because the cost of heat generation is much lower than the laser technique (164). PAM has the ability to generate and transfer required amount of heat to the workpiece by a plasma torch to improve machinability (164, 165, 226). This technique elevates temperature locally ahead of the cutting tool edge and can raise workpiece temperature to 400–1000 °C by convective plasma energy transformation (163, 227). Although, plasma-heating operates with the same principle as laser heating, but the power density obtained from plasma is less than that of laser (23, 180).

A PAM set-up consists of a conventional machine tools (i.e. lathe and milling machines), a plasma-heating platform with a torch and a control unit. The layout of PAM and plasma torch is illustrated in Figures 2.23 and 2.24, respectively. In this, the thermal arc generator has two parts such as electrode and nozzle, as shown from Figure 2.24. A critical issue with PAM is the difficulty to keep the localized heating temperature constant in the allocated cutting zone. Direct current is used to generate arcs from the reaction between plasma gas and electrode sparking to produce equilibrium or thermal plasma (164, 180). In this preheating technique, the heat spot diameter is around (4–5 mm) and can be located at machining zone near the cutting tool. The electrode is generally made of tungsten and acts as a cathode. The plasma gas flows through the nozzle that works as an anode when machine nonconductive materials. However, the workpiece serves as an anode for conducting materials machining (164, 227). Extremely localised energy is obtainable at low gas flow rates when PAM of materials that have a good electrical conductivity (226, 227). When cutting is performed nearer to the chuck, a special enclosure is attached to the chuck to minimize the turbulent air flow effects generated by the chuck rotation (164, 227).

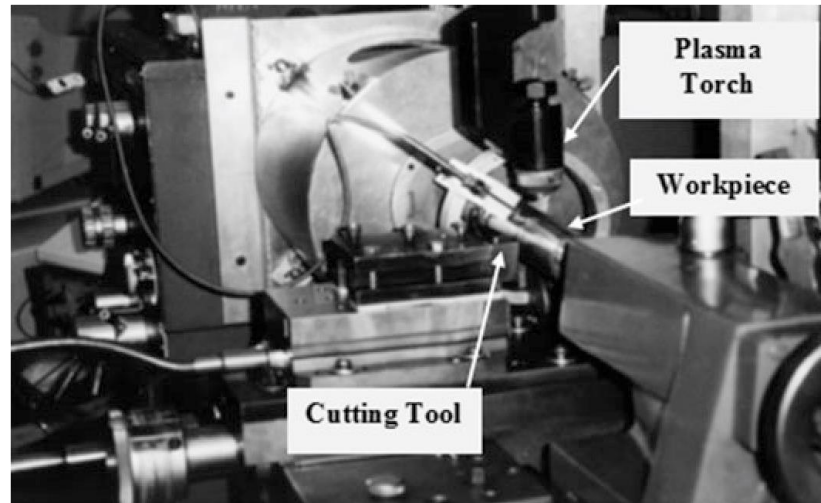


Figure 2. 23 Illustration set-up of PAM (164) with kind permission from Elsevier

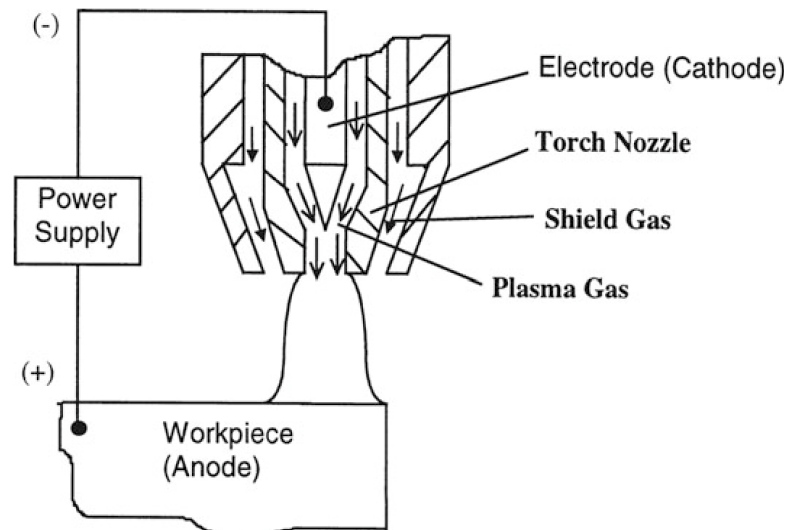


Figure 2. 24 A schematic drawing of plasma torch (164) with kind permission from Elsevier

There are many technical considerations affecting the selection of cutting parameters (163), where PAM technique has inherent difficulties in controlling the hotspot diameter. The size of heating spot influences the process parameters fz and a_e . The surface temperature of workpiece can be obtained from the empirical Eq. (2.2) (228), with fixed values of the cathode setback, the plasma gas flow rate and the shield gas flow rate. The axial depth of cut, a_p is directly related to the temperature distribution under the surface layer of the workpiece. The machining parameters namely, fz , V_c , a_p and a_e have direct effect on the operation performance and cutting tool behaviour.

Equation (2.3) (163), shows a cross relationship between heating parameter (F) and machine parameters (f_z, V_c, z, D):

$$T_s = 80.3275 \frac{l^{0.584} T_0^{0.06}}{V_c^{2.206} D^{0.405} f_r^{0.2026}} \quad (2.2)$$

$$F = \frac{f_z 1000 V_c z}{\pi D} \quad (2.3)$$

Applying plasma technique enables high MRR and increased cutting tool life (164). PAM is widely used only for turning operations because of the difficulties with plasma heating in end-milling operation (166, 180).

During PAM, the formed chip morphology transformed from segmented chip (brittle fracture type) to continuous chip (plastic flow type) due to increased heating temperature (142). Additional, the chip temperature that formed in this technique tends to be higher than in traditional machining, leading to higher flank wear rates (70, 163). The cutting forces in this method are substantially lower around 20–40% with the elevated surface layer temperature until a critical temperature is reached at the chip deformation zone (163-165). Besides the reduction in cutting tool wear, the PAM technique also improves the surface finish of the workpiece without occurring much defects (23, 165, 166).

2.6.3 Induction-Assisted Machining (IAM)

IAM is a new approach in thermal-assisted machining, where a high-frequency induction coil is used as an external heat source to preheat workpiece at localised areas or surface zones adjacent to the coil. Unlike other methods, the coil generates heating along a line on the workpiece, not at a localised point. Thus, the heating region tends to be much wider in IAM compared to other methods. Nonetheless, this method is capable of quickly achieving high temperatures that are controllable and stable (180, 229). Depending on the machining application of turning or milling

processes, IAM induction coil is configured to match the operational requirement, as illustrated by Figure 2.25. In these, the heating device consists of three main components, namely (i) matching transformer and condenser, (ii) high-frequency transformer (invertors) and (iii) cooling unit. The induction coil is energized by high frequency alternating electric current to create a magnetic field, thereby generating intense heating. This heating is achieved without any contact between the induction coil and the workpiece while the rate of heating is determined by parameters such as, material magnetic permeability, frequency and intensity of electric current and, material electrical resistance and specific heat (82-85).

Induction workpiece preheating reduces tensile strength and strain hardening (180, 230), and softens the work surface layers (28, 82, 113), hence decreasing the cutting forces. A past work conducted on induction-assisted milling of (Ti-6Al-4V) at 650 °C, thermal softening resulted in cutting force reduction from 338.2 N to 265.6 N (84). Baili et al. (230) studied the effect of preheating by induction coil on machinability of titanium alloy (Ti-5553). They reported that the components of cutting forces remain constant at a temperature lower than 100 °C while for a temperature between 100 and 500 °C, about 10% force reduction was observed. Then this reduction increases significantly when the temperature exceeds 500 °C (230). However, the thermal stresses encountered in induction coil heating are higher than that for laser technique (28).

With IAM, reduced tool wear dramatically extends the cutting tool life, much similar to other workpiece preheating techniques (28, 82, 84, 229). At moderate cutting speeds in end-milling process, titanium alloy preheating by IAM increased the cutting tool life around 80% (229). In end-milling of Inconel 718, tool life improvement of 83% is noted at the lowest cutting feed while around 28% is observed at the highest feed (110). With high-frequency induction heating, tool vibration and chatter are also reduced to acceptable levels (28, 229). Ginta et al. (84) have observed 67% reduction in vibration amplitude when the titanium workpiece was heated to 420 °C led to enhance machinability. Additionally, their results show (28) 88% less amplitude acceleration for Ti-6Al-4V with IAM at workpiece temperature of 650 °C. Furthermore, the vibration suppression minimizes dynamic loads on the cutting edge, thereby reduces flank wear (83-85, 229).

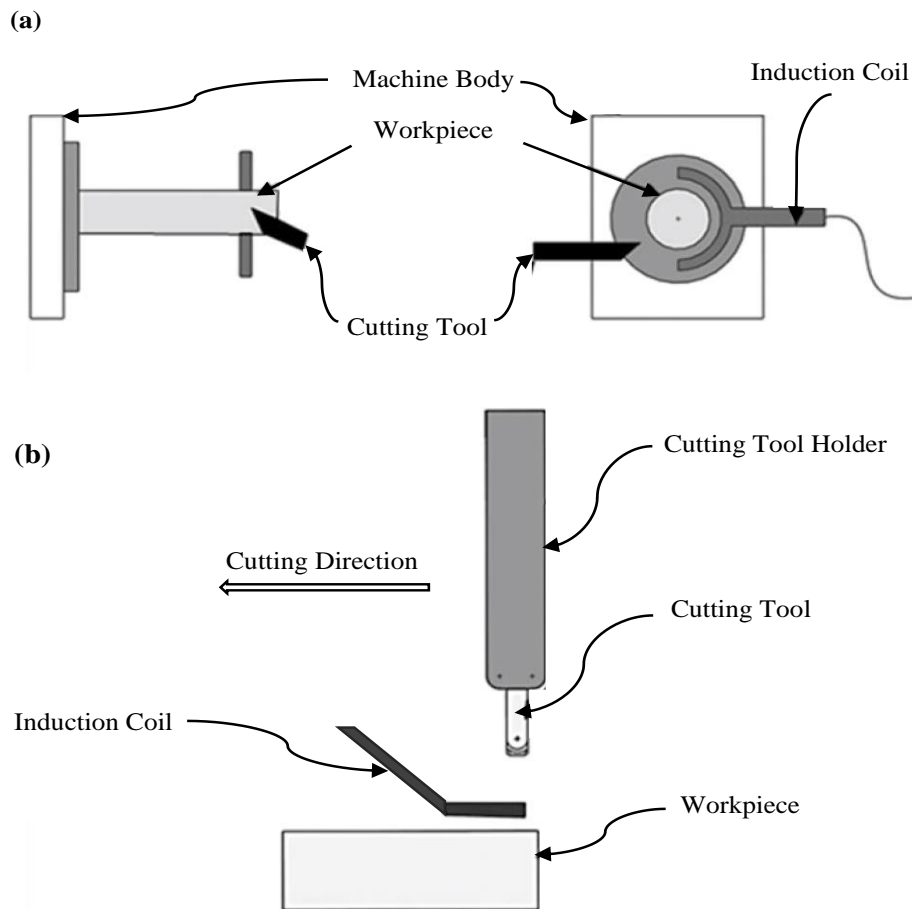


Figure 2. 25 Experimental set-up of (a) induction-assisted turning, and (b) induction-assisted milling

During machining titanium alloys, the BUE is considered as a major factor that affects surface quality. The formation of BUE depends on the chemical reactivity between chip and cutting tool materials, which in turn depend on the preheating temperature (110). The size of BUE increases with increase in temperature during IAM, until it reached a certain size, then pass off with a chip (84). In end-milling of Ti-6Al-4V, the temperature generated is basically responsible for the built-up of chip fragments on the machined zone that finally depreciates the surface finish (158). The temperature generated during cutting process is rationally adequate as a driving force to enhance annealing arrangements during IAM. The driving force increases with the increase of preheating temperature, thereby leading to lower microhardness (158). With this condition, initiation and establishment of grain growth happen,

causing hardness reduction of materials (158). IAM produces lower surface roughness compared to that achieved in machining process at room temperature (113, 230). Previous studies on the effect of IAM on the machinability of titanium alloys are summarized in Table 2.4. A comparison of all the heating techniques applied in the machining of titanium alloys has made in Table 2.5.

Table 2. 4 Summary of past work on IAM of titanium alloys

Author	Workpiece Material	Machining Process	Variable Process Parameters	Objectives	Results and conclusions
Hossain et al. (229)	Ti-6Al-4V	End-Milling	Cutting speed, Feed rate	To study the influence of induction assistance on the surface integrity in milling process.	-Tremendous increment in tool life. -Significant reduction in cutting forces. - Reduced chatter and vibrations.
Ginta et al. (84)	Ti-6Al-4V	End-Milling	Preheating temperature	Investigating the effect of workpiece heating on the tool life.	-Increased cutting tool life. -Significant reduction in cutting forces. - Reduced machining vibrations.
Ginta et al. (28)	Ti-6Al-4V	End-Milling	Preheating temperature	To study the effect of workpiece heating by induction source on the machinability in milling process.	- Significant reduction in cutting forces. - Improvements in the tool life. - Reduced chatter and vibrations.
Baili et al. (230)	Ti-5553	Turning	Preheating temperature	To enhance the machinability of Titanium.	- Low cutting forces. - Improvements in surface integrity.
Ginta et al. (158)	Ti-6Al-4V	End-Milling	Depth of cut, Preheating temperature	To study the influence of IAM on the surface integrity during end-milling process.	-Decrease in microhardness with increase in preheating temperature.

Table 2. 5 Comparison of preheating techniques used in machining of titanium alloys

Description	LAM	PAM	IAM
Heating source	Laser	Plasma	Electric current
Heating tool	Laser beam	Plasma torch	Induction coil
Heating tool movement	Unlimited movement of heating tool	Unlimited movement of heating tool	Limited movement of heating tool
Complexity of the components	Complex components	Less complex components	Simple components
Heating area	Localised point	Localised point	Line
Degree of heat concentration	High degree	High degree	Low degree
Controlling heat source	Easy control of heat source	Impossible to precisely control	Easy to use
Cost of equipment	High cost	Medium cost	Low cost

2.7 Laser-Assisted Machining of Rotating Workpiece

As mentioned in section 2.6.1, a laser spot beam in LAM is applied to preheat the moving workpiece surface in advance of the cutting tool. This localised heating intends to create sufficient thermal penetration into the workpiece and reduce material yield stress up to the cutting depth, thus improving ductility and reducing cutting forces. With material “softening” in the cutting region, tool vibration is lessened, hence resulting in better product surface finish and dimensional tolerances whilst prolonging tool life. These benefits of LAM are essentially derived through correct levels of preheating, where inadequate application would give rise to excessive cutting temperatures, imparting adverse changes to surface microstructure and tool life as well, while over preheating would irreversibly compromise workpiece strength.

For harnessing preheating benefits, a clear understanding of the thermal penetration into the workpiece is essential, allowing accurate determination and optimisation of cutting parameters in LAM. However, the scientific investigation of this thermal situation is inherently complex due to highly transient and non-uniform workpiece temperature fields. Therefore, the schema for determining LAM preheating parameters remains grossly underdeveloped and the current practice heavily relies on trial-and-error approaches that bring about operational uncertainties.

The experimental methods provide limited scope for improved understanding on thermal impact from laser preheating on workpiece owing to impractical or tedious instrumentation requirements and lack of suitable non-intrusive measuring methods. On the other hand, analytical methods involving appropriate numerical modelling processes offer high precision and flexibility to accommodate mechanistic complexities and generate accurate parametric predictions in a cost-effective manner, thus leading to formulation of a systematic foundation for LAM.

Literature on LAM reports some limited research attempts that consider the classic heat transfer problem of point source surface heating on a rotating workpiece, and heat dissipation to the ambient by combined modes of heat transfer. In these, Gecim and Winer (231) applied an integral transformation technique to analyse the steady-state thermal behaviour of a rotating workpiece, subjected to a moving heat source and convective heat loss. They obtained the temperature distribution analytically, and simplified the analysis by neglecting axial and circumferential conduction, and assuming constant thermal conductivity and convective heat transfer coefficient with uniform heat flux. A thermal source term was deployed to represent the frictional heat generated by the cutting tool that increased with the workpiece rotational speed whilst the workpiece temperature observed to fall due to improved convection. Pioneering experimentation in this field, Pfefferkorn et al. (232) have investigated surface temperature of a rotating workpiece heated by a linearly moving laser beam. Using air cooling nozzles to enhance convection, a parametric analysis was performed with shaft dimensions, angular velocity, laser point translational speed, laser power and the laser pointer size. Instead of contact thermocouples for measurements, they utilised a more advanced method of laser pyrometric technique for simultaneous measurement of surface temperature and emissivity of the workpiece, hence examining qualitative and quantitative appraisal of surface thermal behaviour against key operational parameters.

Extending this work, Rozzi et al. (184) performed similar experimental measurements to validate their analytical model that accounted for heat transfer modes of conduction, convection and radiation. This model assumed constant thermal properties and deployed empirical correlations for jet impingement cooling. The reported results indicated good matching for surface temperature at various laser

power, and rotational and translational velocities. Subsequently, Rozzi et al. (233), added a cutting tool to their experiment and considered material removal process with laser heating. A substantial surface temperature rise was observed due to the additional heating from cutting friction. Through simultaneous laser heating and material removal process, this research demonstrated the critical need to achieve softening temperature in the workpiece prior to reaching the cutting tool interface, and the importance of thermal penetration depth as a key aspect of LAM process.

Thermal behaviour of heated rotating cylinders has been numerically examined as multi-mode transient transfer problems using Finite Element Method (FEM), Finite Volume Method (FVM) and explicit dynamic approaches. Rozi et al. (233, 234) developed a numerical model for simulating heat transfer in a rotating cylinder during LAM process and used their experimental data for validation. This parametric study identified laser power, laser-to-tool distance and transitional velocity as the most influential parameters while the effects from rotational velocity (and radial temperature gradient) were described as marginal. Anderson and Shin (190) highlighted the importance of LAM application for hard-to-machine material such as high-nitrogen, nickel-free stainless steels and conducted an experimental investigation to determine the parametric map of machining enhancement. They also performed a microstructure analysis and indicated how far from surface the material remains intact and hence raised the importance of achieving informed and controlled temperature profile towards core area.

Samanta et al. (235) experimentally studied the influence of micromachining LAM operation on cutting force and residual stress in Inconel 625 samples. The results show reduction in cutting force (by 25%) and increase in normal compressive residual stress (up to 50%), which reveals combined favourable and adverse effect. This could potentially set a trade-off pattern to be optimised for each material, dimension and heating intensity where the key input is an accurate three-dimensional temperature profile. Sun et al. (152) showed that not only the LAM preheating assists material softening and accordingly reduces the cutting forces but also such effectiveness could be correlated with surface front temperature and optimised. As a demonstration, they determined an optimised range of surface temperature for Ti-6Al-4V, suggesting a minimised cutting force and thermal damage to the cutting

tool. Shi et al. (236) developed a three-dimensional FEM model for investigating an Inconel 718 rotating cylinder, which is being heated by a laser source and tool-chip interface friction. They simulated the laser beam as a moving heat source, calibrating it with the experimental values. The numerical validation was performed by comparing workpiece temperature at various feeding rates and cutting speeds. This numerical model was used for the investigation of plastic deformation due to combined thermal and mechanical stresses, and the predictions were made for LAM operation.

Based on FVM through FLUENT software package, a simulation model was attempted by Abdulghani et al. (237) for analysing a rotating workpiece subjected to a localised laser heat source with Gaussian distribution function. The study examined the influence of laser power, laser scanning and rotational speed on machining parameters for AISI51 50H steel. This work has clearly identified the simulation possibility for modelling the transient thermal problem associated with heated rotating workpieces. Nonetheless, the model validation was limited to data at low rotational velocity (6 rpm), hence comprehensive analysis could not be performed.

Thermal modelling with rotational workpiece poses considerable numerical complexities and challenges. In technically overcoming these, LAtHEM approach (LAsER THERmal Modelling), a methodology developed by the University of the Basque Country) has been considered, which converts the combined workpiece rotational and transitional velocities into equivalent single linear motion. Numerical simulation is then performed using the transient conduction equation on a flat workpiece with reduced complexities. Arrizubieta et al. (238) also reported an extended numerical study on a heated rotating workpiece developed using LAtHEM methodology albeit with simplifying assumptions. The LAtHEM approach essentially converts the combined rotational and transitional velocity of workpiece into equivalent single linear motion and solves the transient conduction equation on a flat workpiece with reduced complexities. With satisfactory validation using experimental data, this work concluded that this approach and the assumptions are extendable for analysing rotating workpiece preheated behaviour in LAM. Table 2.6 summarise the current significant studies involving rotating workpiece and their key

contributions in LAM, along with the typical parametric ranges and aspects for further investigation.

Table 2. 6 Summary of significant LAM studies and key aspects.

Author	Workpiece Material	Setup Parameters	Comments	Study Pattern
Pfefferkorn (232)	Ceramic	Dp=6.35 mm, P=300-500W, ω =500-1500 rpm, D _L =2-4 mm	No cutting / Laser pyrometer is used	Experimental
Rozzi et al. (233)	Silicon Nitride	Dp=8.46 mm, P=400-600W, ω =500-1500 rpm, D _L =3 mm	With and without cutting / Laser pyrometer is used	Numerical and Experimental
Shi et al. (236)	Inconel 718	Dp=60 mm, P=3kW / ω =4000 rpm, D _L =2 mm	Sharp cutting tool / Thermography is used FEM model using package DEFORM 3D V6.0	Numerical and Experimental
Rahman et al. (129)	Beta Titanium alloy	P=1.2kW, D _L =2 mm	Cutting near the laser point / Thermography	Experimental
Rozzi et al. (234)	Silicon Nitride	Dp=8.46 mm, P=400-600W, ω =500-1500 rpm, D _L =3 mm	Control volume method with separated phases	Numerical
Abdulghani et al. (237)	Steel	Dp=20 mm, P=200-1000W, ω =100-900 rpm, D _L =5 mm	FVM using FLUENT package	Numerical
Arrizubieta et al. (238)	Bi-material (Steel and WC-17Co)	Dp=39.6 mm, P=600-1000W, D _L =5 mm	LATHEM	Numerical and
Mostafa et al. (239)	DIN 1.7225 Carbon Steel	Dp=32 mm, P=275W&300W, ω =115 rpm, 300rpm, D _L =4 mm	Green's function with Visual Studio platform and FEM model using ABAQUS/STANDARD	Numerical and Experimental

2.8 Concluding Remarks

The rise requests for special alloys such as titanium alloys in the manufacture of engineered components have substantially increased the innovations and developments in machining techniques. From the literature review presented in this chapter, there has been enormous progress in the development of titanium alloys machining. The review provides a comprehensive appraisal of the current state of development in TAM techniques for improving the machinability of a board range of HTM materials, including titanium alloys. It is identified that the main strategy of TAM is to reduce yield strength and the work hardening effects of the workpiece. Preheating of workpiece before initiating cutting process has indicated much more effectiveness in increasing the machinability than other techniques used for HTM materials. With appropriate workpiece heating in TAM, plastic deformation is promoted in the cutting zone to reduce shear resistance at the cutting edge thereby lessening the cutting force and specific cutting energy while improving surface finish and tool life.

A detailed description (working principle, mechanism and research progress and development) of three important TAM techniques (LAM, PAM and IAM) used for titanium alloys can be summarised as follows:

- (a) All three preheating techniques lead to a cutting forces reduction, extended tool life and improved surface quality at different levels during machining of titanium alloys;
- (b) LAM is capable to reduce the generation of cutting forces up to 60%, decrease tool wears about 20–30%. Furthermore, the surface quality obtained by LAM is equivalent to those obtained by grinding process;
- (c) LAM and PAM offer the advantages of rapid and localized heating with sharp temperature rise in workpiece compared to induction heating techniques;
- (d) Laser or plasma beam offers the best controlling possibility and flexibility of heat distribution in the workpiece.
- (e) PAM is capable of decreasing cutting force up to 25%, with up to 40%extension in tool life with reasonable improvement in surface finish when compared with conventional machining;

- (f) Induction-assisted machining produces high capacity preheating, but unable to provide concentrated and localized workpiece preheating;
- (g) To Control preheat rate is quite easier in LAM than PAM and IAM.

TAM techniques have proven viability with improved machinability for Titanium alloys and a board range of other HTM metals and polymers. LAM is noted to offer the “best option” as a heat source for achieving highly localized and intense power density for workpiece preheating requirements with the advantage of output controllability. In essence, it can be concluded that the heating ability of LAM with its focused beam is ideally suitable for machining Titanium alloys and other hard materials. This technique allows a significant improvement in the machinability with low cutting forces, increased MRR, less heat-affected zone, increased tool life and superior workpiece surface integrity.

On the other hand, prevention of workpiece overheating is critical for successful implementation of TAM that is to be ensured by estimating the peak preheating temperature. As such, careful analysis of surface temperature and workpiece temperatures distribution forms an essential research element in studies to determine optimum preheating conditions and machining parameters. In achieving these objectives, predictive thermal models are viewed to be essential for a clear understanding of heat transfer processes associated with TAM, supported by further experimentation. Therefore, this work presents experiments of heated a rotating Ti-6Al-4V workpiece by using the CO2 laser machine in Chapter Three. After that, Chapter Four presents the development of a numerical simulation to describe the preheating thermal behaviour of a rotating workpiece subjected to laser spot as a surface heat source in LAM.

Chapter 3

Experimental Methodology

3.1 Introduction

The experimental methodology of the current study is presented in this chapter. This methodology includes details of the setup for each experiment. Then, an illustrative description of the laser machine and surface temperature measurement technique are also included. Finally, the reflection and emissivity tests are explained, and associated results demonstrated.

3.2 Objectives

A literature review has shown that getting traditional titanium alloys machining is never achieved without difficulties, due to the unacceptable thermal properties of these alloys for instance, low thermal conductivity. Therefore, some methods have to be used to reduce obstacles during machining of titanium-based alloys. In Chapter two, three different techniques of TAM have been presented in detail. These techniques have been applied to the machining of titanium-based alloys to improve the machinability of these alloys. LAM has been selected to provide pre-heating to the workpiece as this method has been proven effective in preheating in machining many other HTM alloys. The PAM and IAM, on the other hand, have had limited practical applications compare with LAM. The challenge for applying TAM is to know the required surface temperature at the cutting zone that is as close to – or better – than traditional dry machining.

This work aims to present a comprehensive understanding of heating the rotating cylinder, by studying the temperature distribution at the surface during the heating of the rotating metallic workpiece. Many researchers have reported different methods to measure surface temperature in LAM. These studies were concluded at a high range of generated power for laser beam starting from 500 W up to around 1200 W, with different degrees of success. In current study, the new technique has utilized to simulate LAM for titanium alloy workpiece without cutting process. A Laser Stepped Heating System located in the John de Laeter Centre at Geology Department/Curtin University has been used as a thermal-assisted technique to heat

specimens. This laser apparatus generates a laser beam with low power up to 55 W. Based on the space under the laser nozzle, a small-scale rig has been designed and manufactured at workshop of the Mechanical Department, to simulate the turning process without cutting. To achieve the main research objectives outlined in Section 1.7, a number of experiments had been carried out. These experiments include heating Ti-6Al-4V alloy cylindrical workpiece using laser beam with low power, during rotating at different speed.

3.3 Design of Experimental

Three titanium alloy (Ti-6Al-4V) solid workpieces are prepared with different surfaces and positioned in the developed test rig one by one, to model the small-scale turning process. This method is adopted for the heated rotating cylinder to measure a temperature of the surface and analyse the temperature distribution, as well as providing variable heat transfer data of the heating process. The experimental apparatus consists of the following parts: workpieces, test rig, laser machine, laser control unit, IR camera, and IR camera control unit. Figure 3.1 indicates the positions of each part of the apparatus inside the laser lab. The workpiece was clamped between bearing and the DC spinning motor. To achieve a comprehensive monitoring during the experiments, IR camera was used for detecting the temperature at a surface of the workpiece. Additionally, the control system (mechatronics) of the test-rig was designed to control a speed of the workpiece and aperture base in one dimension.

Previous researchers had carried out experiments under a high value of laser power to analyse the heating process during the laser-technique for titanium alloys. Due to some technical faults in the laser machine, the maximum value of the generated power could be from 5.5 W to 27.5 W. Therefore, the experiments of this research was conducted under low laser power. Prior to starting any experiment, the setup parameters of both test-rig and a laser machine such as laser power, spot laser diameter, laser scanning velocity, and rotation speed, are prepared at the desired requirements for each experiment scenario. Each test includes shooting down a laser beam to the workpiece's surface during its rotation. After a few seconds, the corresponding value of the surface temperatures was measured using the thermal

camera and its software. All measurements were made following the same procedure, excepted the time between measurements. Furthermore, the camera is set at emissivity value (0.5) and (0.5 m) the distance between the camera and titanium alloy workpiece.

The experimental part of this work described in this chapter is split into four stages. The setup parameters of these stages are listed in Table 3.1. The following steps sequences are scheduled to carry out studying the distribution of temperatures at the heated rotating surface. In the first stage, the workpiece of the painted surface is heated with five values of the laser power at two different rotation speeds. The thermal picture is taken every ten seconds by IR camera along the heating period. The second stage is the same procedure as the first stage but for a sandblaster workpiece. At the third stage, the sandblaster workpiece is heated by laser at power 13 W while moving the base of the test-rig at different linear speeds. Finally, in the fourth stage, the laser power and laser scanning velocity are constant at 13 W and 20 mm/min, respectively; during heating sandblaster workpiece at various rotating speeds.

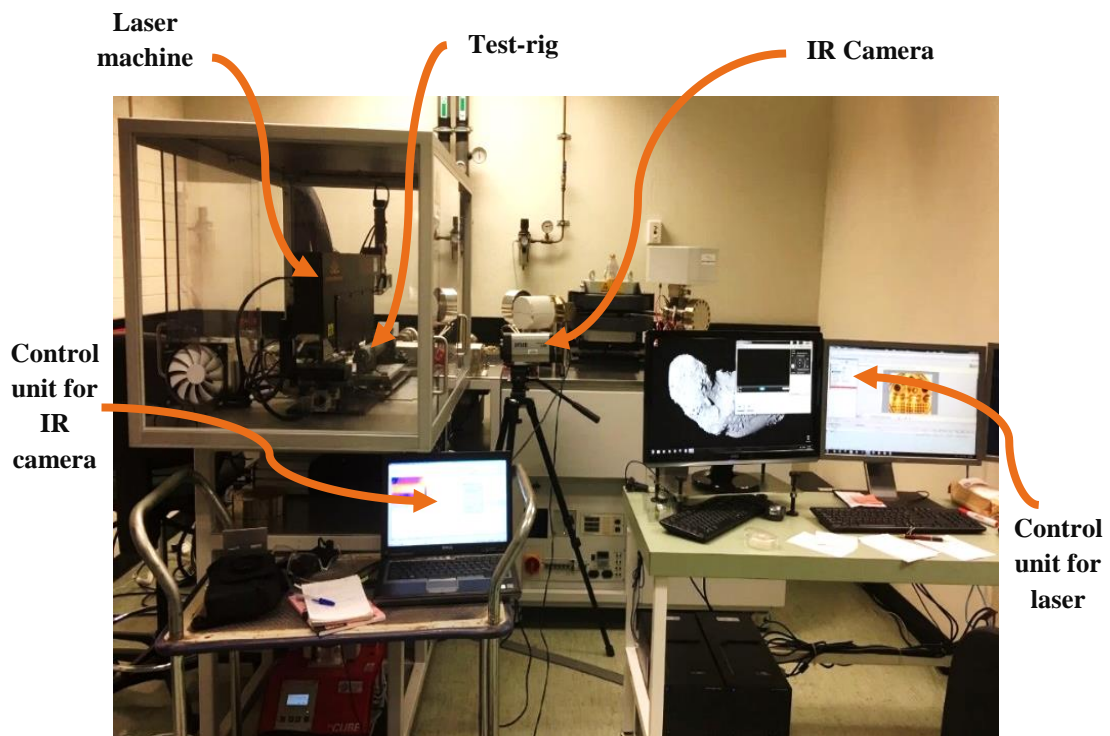


Figure 3. 1 The Experimental rig

Table 3. 1 Setup parameters of the experiment stages

Stage -1-				
Workpiece Type	Painted surface	Heating Style	Fixed laser beam	
Spindle Speed (r.p.m.)	Percentage of Laser Power		Measuring Time (Sec.)	
100	10 %		600	
	20 %		600	
	30 %		600	
	40 %		420	
	50 %		360	
1000	10 %		600	
	20 %		600	
	30 %		600	
	40 %		420	
	50 %		360	
Stage -2-				
Workpiece Type	Rough surface	Heating Style	Fixed laser beam	
Spindle Speed (r.p.m.)	Percentage of Laser Power		Measuring Time (Sec.)	
100	10 %		600	
	20 %		600	
	30 %		600	
	40 %		480	
	50 %		480	
1000	10 %		600	
	20 %		600	
	30 %		600	
	40 %		480	
	50 %		480	
Stage -3-				
Workpiece Type	Rough surface	Heating Style	Moving laser beam	
Percentage of Laser Power	50 %	Heating Length (mm)	40	
Spindle Speed (r.p.m.)	100			
Scanning Speed (mm/min)	20	30	40	50

Measuring Time (Sec.)	120	72	60	48
Stage -4-				
Workpiece Type	Rough surface	Heating Style	Moving laser beam	
Percentage of Laser Power	50 %	Heating Length (mm)		40
Scanning Speed (mm/min)	20	Measuring Time (Sec.)		120
Spindle Speed (r.p.m.)	100	200	500	1000

3.4 Test-Rig Components

This alternative test-rig is manufactured to simulate the preheating process of rotating cylindrical workpiece. The test-rig for this research is consisted of two sections, the first one mechanical and the other is mechatronics. These sections are assembled together to achieve double movement (linear and rotational). According to these two motions, many different scenarios can do to study the temperature distribution at the workpiece surface.

3.4.1 Mechanical Design Consideration

Figure 3.2 describes the principle control circuit of the DC rotating motor, that responsible for cylinder rotation in terms of increase or decrease the rotational speed. At the beginning stage of manufacturing test rig, the mechanical section is including the DC spinning motor (see Figure 3.3), a cylindrical workpiece from titanium alloy with length (250 mm) & diameter (50 mm), and two set-screw locking bearings (UCP 210 type) that clarified in Figure 3.4. All these parts are installed on the movable metal base (upper base) that in touch with steel timing belt pulley (Figure 3.5) by the timing belt (Figure 3.6). On the other side, this pulley in touch with the fixed metal base (bottom base) by a timing belt. The transition DC motor is connected with the bottom base to transfer the motion to the timing pulley and thus moving the upper base.

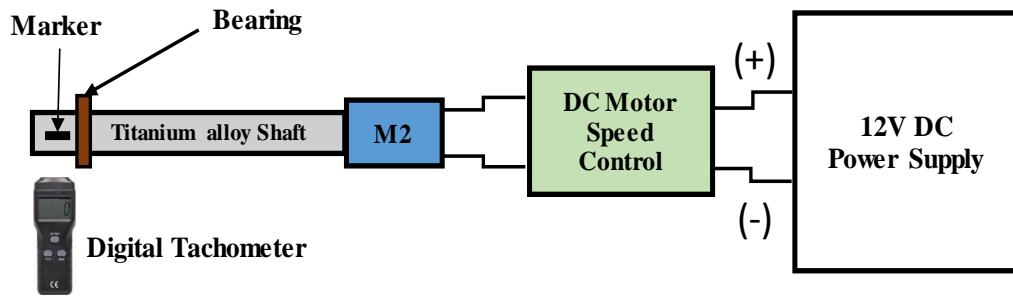


Figure 3. 2 A functional diagram of the DC spinning motor control circuit.



Figure 3. 3 Motor for the Shaft Spinning



Figure 3. 4 Pillow Blocks with Concentric Locking and Cast-Iron Housing Bearing



Figure 3. 5 Steel Timing Belt Pulley



Figure 3. 6 Contitech Synchronbelt HTD, Timing Belt

3.4.2 Control system (Mechatronics) design.

Figure 3.7 characterizes the functional diagram of mechatronics section, that responsible for rotating speed and linear motion within a certain distance in x-direction. The lever SPDT momentary switches and single DPDT relay board, illustrated in Figure 3.8, are used to eliminate the movement of the movable base to the right and left directions. To control the DC motors, two of the speed control drivers, illustrated in Figure 3.9, are used to turn on/off both DC motors and to increase/decrease the rotation speed for both. The desired spin speed determined by measuring the number of cylinder revolution per a minute (rpm) via using digital non-touch laser tachometer shown in Figure 3.10 (a). The detector of tachometer detects changes in the frequency of the reflected infrared light as reflected alternately by the contrast spot (black marker). In this experiment, the workpiece end is covered with black adhesive tape to represented as contrast spot, as illustrated in Figure 3.10 (b). The rotation speed measured according to the number of frequency changes per unit time. Both the electrical control circuits described in Figures (3.2) & (3.7) provided with electric power by utilizing (12 V DC) power supply and illustrated in Figure 3.11.

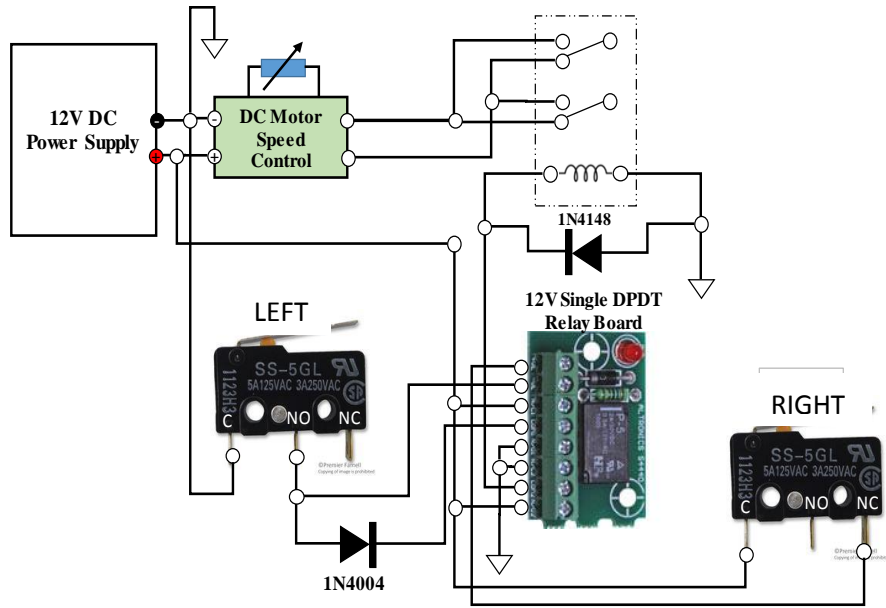


Figure 3. 7 The functional diagram of DC transition motor control circuit

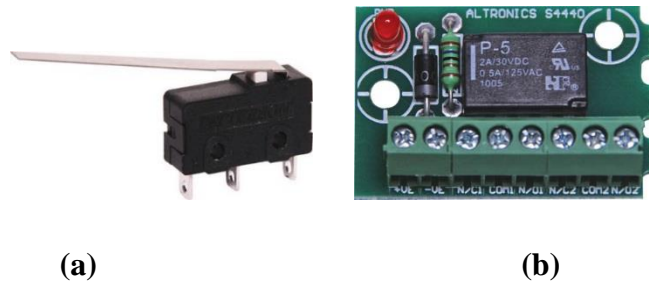


Figure 3. 8 (a) Lever SPDT Momentary Solder Tail Micro Switch and (b) Single DPDT Relay Board

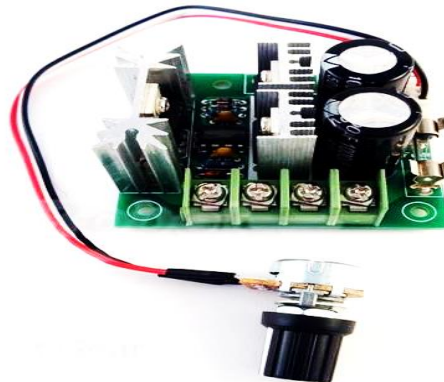


Figure 3. 9 DC Motor Speed Control Driver

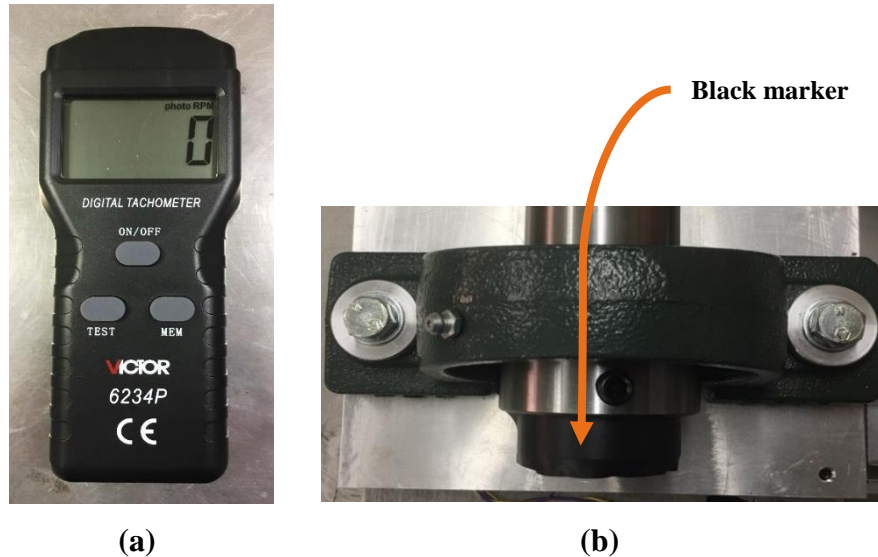


Figure 3. 10 (a) Pocket Digital Laser Tachometer and (b) Contrast Spot



Figure 3. 11 The Power Supply for The Electrical Control Circuits

3.4.3 Fabrication Problems

There are many problems that occurred during the manufacturing process of a test-rig. The following is an explanation of these issues and the timely solutions to reduce their effects.

It was noticed during connecting workpiece with two bearings, that the diameter of one ends of the shaft bigger than the other end. This workpiece came from the supplier company with these inaccurate dimensions in the diameters. This leads to making one of the bearings cannot install it with the workpiece. Moreover, the not uniform shape (unsymmetrical mass) of the shaft will lead to unstable rotating around the rotation axis. Therefore, the surface of the workpiece from the end of (51.5 mm) has been machined and make the diameter equal (50 mm) by using lathe machine.

In the beginning of manufacturing process, the standard (high power) DC motor 9700 rpm for high speeds was used to rotate the workpiece around the x-axis. However, this motor showed an inability to rotate the shaft more than 85 rpm. Due to high torque requirement for rotating the workpiece. Consequently, it needs to replace this motor with another one has torque higher than the torque of the first motor. The standard motor has been replaced by Parvalux Brushed DC motor (90 W, 12 V dc, 3000 rpm) but the problem remained so that the motor cannot be spin with high speed as required for more than 1000 rpm. According to all that, the choice is made on using COMO drills DC motor (36.88 W, 12 V dc, 82.08 gcm, 4289 rpm). This motor connected with workpiece through its small shaft with a diameter (6.35 mm), and spinning it with rotating speed up to 2150 rpm.

When assembling all parts and turn on the test-rig, it was noted that a clear vibration during workpiece rotation. This vibration is unwanted because of its effects on the stability of the heating spot over the surface, thereby leads to inaccurate results. According to this, three things have been done to reduce vibration as much as possible. Firstly, a length of the shaft (500 mm) is decreased and become (250 mm) to minimise the sample mass. Secondly, one of the two bearings have been removed as shown in Figure 3.12, which was helped to reduce friction between bearings and titanium shaft. Finally, to slash the friction more, it was noted that removing the contact seal from bearing, as illustrated Figure 3.13, led to the better result decreasing of friction.



Figure 3. 12 Test Rig with One Bearing

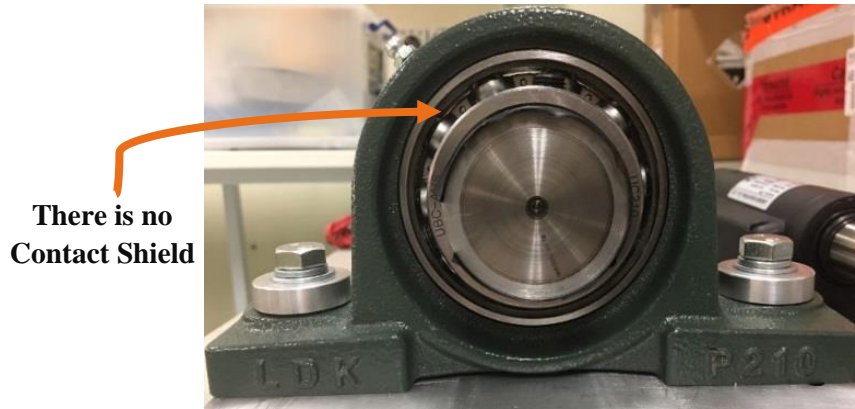


Figure 3. 13 Pillow Blocks Bearing without Shield

The laser machine has a nozzle with a limit movement in four directions. In the same time, the experimental procedure of some tests needs moving laser nozzle. According to this situation, the nozzle is installed, and workpiece moved linearly by making the upper base moves via using Como Drills DC Geared Motor, Brushed, 12 V nominal, 6 -12 V dc, 20000 gcm, 55 rpm, 41.3 W. After performing the trial operation of the test-rig, it was noted that speed of the upper base faster than the speed that wanted for experiments. Therefore, the DC motor is replaced with the motor its type is 3827 6400RPM, DC 24V, 5.6 A MAX, as illustrated in Figure 3.14. A JAEGER INDUSTRIAL Company manufactured this type of motor, which has stroke length 69 mm and with speed of 8.5 mm/sec. By this motor, the slow speed required is achieved.

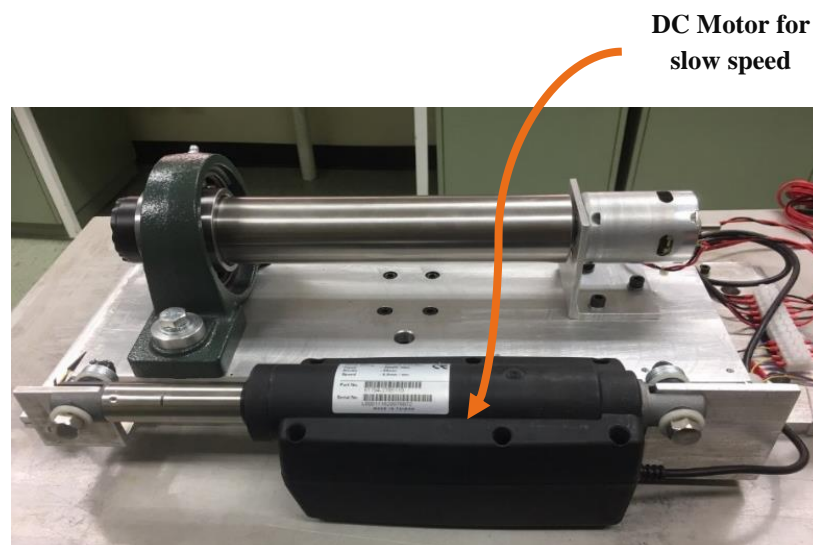


Figure 3. 14 The 3827 6400RPM, DC 24V, 5.6 A MAX motor

3.5 Workpiece Material

Titanium alloy Ti-6Al-4V (Grade 5) is chosen as the workpiece material because it is readily available and most widely used in the industry. It is also generally accepted as difficult-to-machine due to its unique thermo-mechanical properties. Table 3.2 shows the chemical composition of Ti-6Al-4V alloy. This alloy features good machinability and unique in combines attractive properties such as, high strength-to-weight ratio and its exceptional corrosion resistance. The physical, thermal and mechanical properties are listed in Table 3.3 and Table 3.4, respectively. These properties with inherent workability make Ti-6Al-4V lead to reliable and economic usage. Moreover, the Ti-6Al-4V offers the best all-round performance for a variety of weight reduction applications in different fields such as, chemical industry, biomechanical, marine, and direct manufacturing of parts for aerospace. Specimens test component are used for this experimental purpose. The shape of this specimen is sold shaft with dimensions (50 mm) diameter and (250 mm) length, as shown in Figure 3.15.

Table 3. 2 Chemical composition (Wt %) of titanium alloy Ti-6Al-4V (240).

O	N	C	H	Fe	Al	V	Ti	Others/total
0.20	0.05	0.10	0.0125	0.30	5.5-6.75	3.50-4.50	Up to 90	0.4

Table 3. 3 Physical and Thermal properties of titanium alloy Ti-6Al-4V (6, 19, 240).

Physical Properties	
Density	4.43 g/cc
Melting Range	1538 °C – 1649 °C
Thermal Properties	
Specific Heat Capacity	0.5263 J/g- °C
Thermal Conductivity	6.7 W/m-K
Melting Point	1604 °C – 1660 °C
Solidus	1604 °C
Liquidus	1660 °C



Figure 3. 15 Geometry of the experimental sample test

Table 3. 4 List of Mechanical properties of titanium alloy Ti-6Al-4V (6, 19, 240).

Mechanical Properties	
Hardness, Rockwell	36
Hardness, Brinell – Estimated from Rockwell	334
Hardness, Vickers – Estimated from Rockwell	349
Hardness, Knoop – Estimated from Rockwell	363
Tensile Strength, Ultimate	950 MPa
Tensile Strength, Yield	880 MPa
Elongation at Break	14 %
Reduction of Area	36 %
Modulus of Elasticity	113.8 GPa
Compressive Yield Strength	970 MPa
Notched Tensile Strength	1450 MPa
Ultimate Bearing Strength	1860 MPa
Bearing Yield Strength	1480 MPa
Poisson's Ratio	0.342
Charpy Impact	17 J
Fatigue Strength	240 MPa
Fracture Toughness	75 MPa-m ^{1/2}
Shear Modulus	44 GPa
Shear Strength	550 MPa

3.6 Laser System

Heating surface of titanium alloy shaft is achieved by using the laser machine Fusions 10.6 Series. The photon machine is a Laser Stepped Heating System which originally designed for geochronology analysis of minerals. This device (Diamond C-55 Series) utilizes the carbon dioxide laser source (CO₂) which produces a high intensity laser beam with specific wavelength 10.6 μm. The machine has the capacity to irradiate circle surface area in diameter up to (6 mm) by using a field-proven in the near infrared (IR) with output power from 2.5 W to 55 W. The power becomes more stable after a few seconds from laser running.



Figure 3. 16 Photon Machine (C-55L CO₂ laser) (241)

The Fusions 10.6 Series is connected with PC computer to control the input parameters (laser power, laser spot size, coordinates of the heating spot in (X, Y, Z)) to the photon machine. The laser of Fusions 10.6 Series classified as category of Class 4 according to the US Food and Drug Administration. Thereby, this device presents permanent damages to the eye (blindness) and skin (increased risk of cancer) from direct or reflected laser beam exposure. Therefore, laser machine installed inside a protective housing to protect persons who work close to it from unnecessary laser radiation, as shown in Figure 3.16 ("Fusions 10.6 Series User Manual," 2010). The protective housing is fixed and not prepared to be removed by the operator during operation or maintenance as well. For more safety, Fusions 10.6 Series installed inside glass container to protect from any laser reflection during the heating process, as illustrated in Figure 3.17.



Figure 3. 17 Fusions 10.6 Series installed inside glass container

The photon machine includes three subassemblies, coaxial beam delivery unit (laser module), controller, and laser power module. This beam delivery unit consists of many elements such as video/laser combing block, 6X motorized zoom magnification video microscope, built-in power meter, laser and laser beam delivery

optics, and a ring light. The assembly of laser module merges the CO₂ laser with the video microscope imaging, laser targeting, spot size adjustment and lighting with the (X, Y, Z) stages as shown in Figure 3.18, which in turn help to facilitate the purpose of this machine. The Fusions 10.6 Series machine provides coaxial and coinciding focal planes performance due to the independent focusing and alignment capability of each the essential functions, imaging and lasing. This laser machine represented as a unique beam-flattening technology because it converts the usual Gaussian beam profile to a flat and uniform energy distribution across the test piece. There is no any escape of laser light during heating process because the CO₂ laser burns immediately into the completely enclosed beam delivery unit. The flexible control on the movement of both the expander lens and focusing lens inside combining block leads to adjust laser spot size from 0.1 mm to 6.0 mm in diameter. The test piece lighted by the ring light powered by a 150 W illuminator, thereby eliminates shadows that can happen around heating area. The power needs for the laser of the Fusions 10.6 Series is provided by laser power module illustrated in the Figure 3.19, with inputs 240 VAC, 50/60 Hz and 6.3 A.

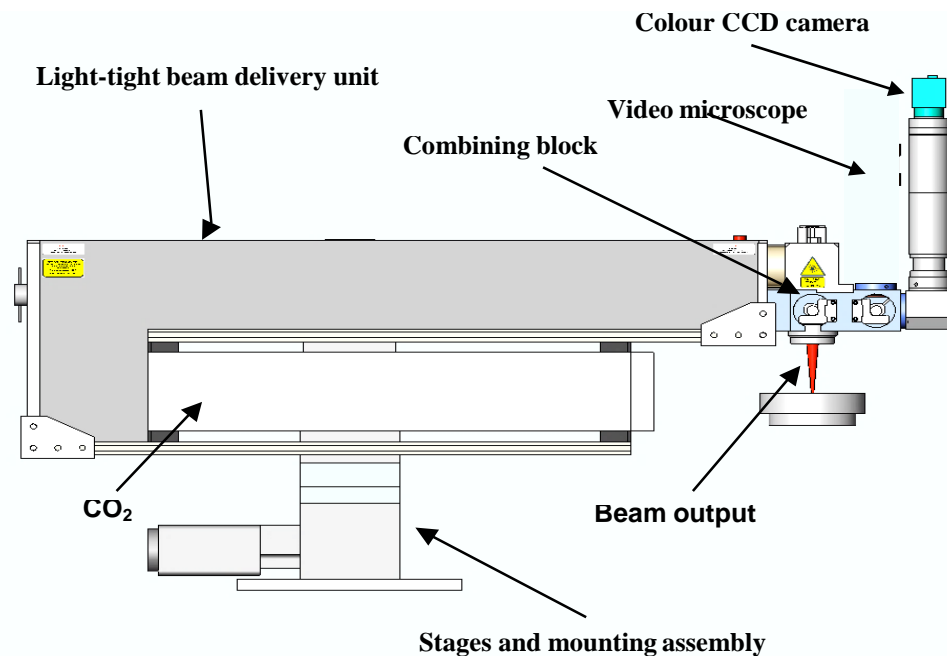
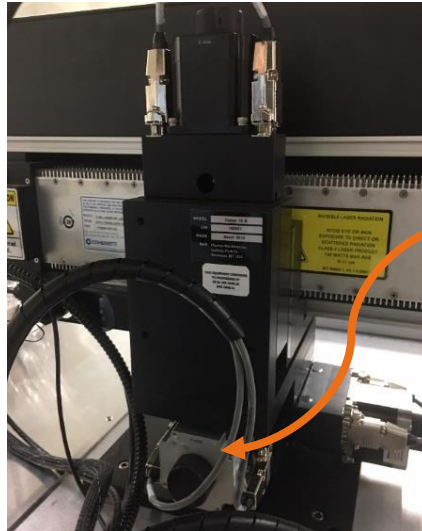


Figure 3. 18 Schematic diagram of a Laser Stepped Heating System (241)



Figure 3. 19 The front and back panels for the laser power module

The laser module assembly has a limited motion (50 mm) on all axes (X, Y, Z) above the test specimen (titanium alloy shaft) by using motion control tower, see Figure 3.20. This tower houses all electronics parts that necessary to support the laser module and all drivers requisite to control the motion in three directions as well. The controller tower supports subassemblies of photon machine, power meter, variable focusing lens unit, and video zoom microscope by an umbilical cable. The inputs required for controller are 110 - 240 VAC, 50/60 Hz, and 3 A. Photon machine (Fusions 10.6 Series) is runs and control on its motions by using Chromium 2.2 software, which installed on a desktop computer. This software is most powerful packages available today and plays a role as a third party to integrate the controller and driver to control the encoded and DC servo motors. Through this Laser Ablation software package, the variable of illumination intensity can be controlled. The main screen of Chromium software illustrated in Figure 3.21. The heating point of the laser beam over the sample surface determines by inserting the values of three coordinates X, Y, and Z in Position portion. The next step selecting the units of dimensions (μm or mm) which done through the Unit partition, then, pressed on the (Go to) button and the navigating process finished, as shown in figure 3.22. The laser module is navigated easily due to use the window of coordinates (Move Stages) illustrated in Figure 3.23.



Z axis knob

Figure 3. 20 The motion control tower of Fusions 10.6 Series

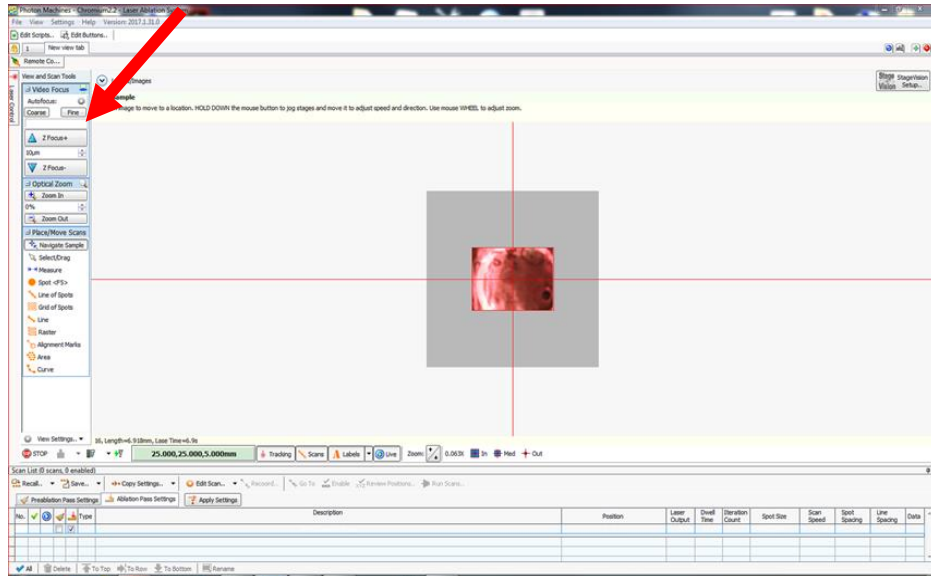


Figure 3. 21 The main window of Chromium software

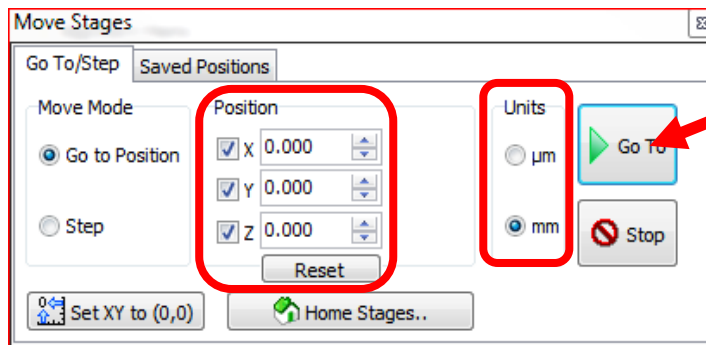


Figure 3. 22 The move stages dialog in Chromium software 2.2

In the Laser Control window of Chromium software (2.2) shown in Figure 3.23 (a), the setup parameters of the heating process such as fire mode, laser power, and spot size can be managed. This window appeared and activate after click on the line titled "Laser Control" positioned in the left edge of the main page of a software, see Figure 3.7. Through line labelled "Laser Energy" laser energy is given as a percentage of the total energy value produced by this laser device, which is equally as mentioned earlier 55 W. Chromium software provides many types of scanning by the laser beam namely spot, line, area, and other types as depicted in Figure 3.23 (b). Furthermore, the slider bar titled "Max Power Limit" played a good role to control the power output of the laser, which is rescaled and keep it under the specified value.

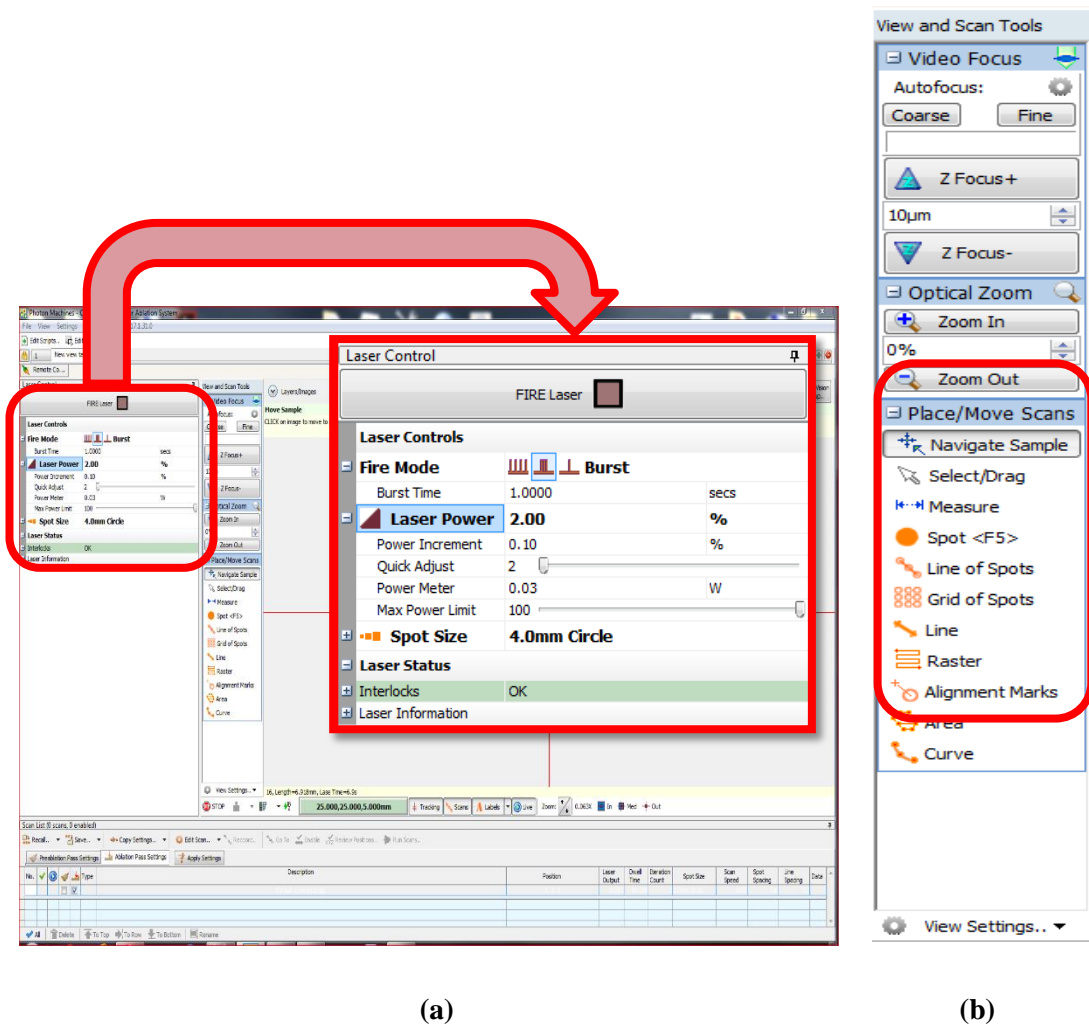


Figure 3. 23 (a) The laser control window in Chromium software (2.2)

(b) The side tool bar that contains "Place/Movie Scenes" window

3.7 Temperature Measurement Method

There are many techniques to measure surfaces temperatures of objects such as thermocouples, resistance temperature detectors (RTDs), thermistors and integrated circuit (IC). Thermocouples are a simple technique and widely used to measure surface temperature and inside temperature distribution for material objects as well. Diverse types of thermocouples classified according to the measured range of temperatures and measurement accuracy like (type J), (type K) and so on. These types can measure temperatures over wide ranges, completely inexpensive. Moreover, they are a very rugged sensor, however, they are a comparatively less accurate comparison with other types of sensors, because of its lowest sensitive of the output versus temperature change. On the other hand, thermocouples are least stable as measuring tool especially in case of moving surfaces like rotating cylinder even when using the slid bearings. This because of it difficult to keep the thermocouples stationary due to centrifugal force resulting from rotation.

The operation principle of the RTDs is based on the electrical resistance of material changes as its temperature changes. RTDs are stable, accurate and linear more than thermocouples, yet it is less rugged and more expensive. In addition, this technique can be used to measure a range of temperature from $-200\text{ }^{\circ}\text{C}$ to $800\text{ }^{\circ}\text{C}$. While, thermistors tend to produce a high signal outputs and rapid response time because of its small sizes which permit fast response to temperature changes. The output of thermistor depends on the fact that the resistance changes in a metal-oxide-semiconductor material as its temperature changes. However, this technique typically can be used to measure a limited range of temperature ($-45\text{ }^{\circ}\text{C}$ - $260\text{ }^{\circ}\text{C}$) with better accuracy than it with a thermocouple. Finally, IC is the newly developed technique to measure temperatures. This type of temperature sensor designed to produce an extremely linear voltage or current proportional to temperature. Nevertheless, IC sensors have a limited temperature range and typically are used to measure temperatures from $-45\text{ }^{\circ}\text{C}$ to $150\text{ }^{\circ}\text{C}$.

From all the above and according to nature of the experiment test (space under laser machine, the range of measured, temperature, and workpiece stability), it can be noted that the four types of sensors are not suitable to use in this experiment. Therefore, the focus is turned on using a non-contact technique to measure surface

temperatures distribution. Non-contact measurement techniques are now established throughout the entire world. This measurement method is the preferred technique for moving and inaccessible objects; and dynamic processes that require a fast response; and temperature more than 1000 °C. The thermographic camera FLIR ThermoVision™ A40V is chosen for use as a non-contact tool in this work to measure temperatures on a spin cylinder surface while heated by external heating source. This thermal infrared camera is an intelligent infrared imaging camera for accurate temperature distribution measurement. In addition, the program ThermaCAM™ Researcher is adopted to establish a connection between software and the camera, which is also used to monitor the recorded data.

3.7.1 FLIR ThermoVision™ A40V Camera

Recently, IR thermal camera is a well-established tool throughout the entire world for the inspection of thermal events. The infrared camera is still the largest application of thermography. The IR thermal imager serves as a quick temperature scanning tool to identify hot spots on target objects. These cameras cannot discriminate energy at 7 μm from energy at 14 μm the way the human eye can distinguish various wavelengths of light as colours. ThermoVision™ A40 Series of infrared cameras are a non-contact device affordable and precise solution for industrial product and process monitoring. The A40 series can measure subtle temperature variations, which is undetectable by any other means. Moreover, A40 cameras can find and resolve problems at an early stage, which improves product quality and cut down on scrap or warranty expense. Thermal imaging camera has a special lens used to focus the infrared light emitted by all the bodies in view. A phased array of infrared-detector elements converts the detected focused light into a very detailed temperature pattern (electronic signals). These signals are treated to produce high-resolution and stand out clearly infrared images, which perform temperature distribution and thermal calculations. Thermal imaging camera ThermoVision™ A40V is one from this series with a fully-integrated system, as shown in the Figure 3.24.

The A40V camera delivers crisp and longwave images in a multitude of palettes because it has detector technology type of Focal Plane Array (FPA)

uncooled microbolometer. This camera features plug-and-play setup which makes it simply connect to standard monitor and produce real-time thermal images with spatial resolution (IFOV) 1.3 mrad. The infrared images accurately show heat patterns and thermal anomalies. Due to onboard logic and menu-driven configuration controls, it is easy to select and control many parameters, such as target spots, temperature range, and image colour palettes. The lightweight (1.4 Kg) with the compact design granted A40V camera flexibility to mount in various remote locations, which possibly represent the optimal sites for data collection. The thermal sensitivity at rated frequency (50/60 Hz) for A40V camera is 0.08 °C at 30 °C. Furthermore, the focusing process controlled by a built-in focus motor and done within a spectral range from 7.5 μm to 13 μm.



Figure 3. 24 The ThermoVision™ A40V Camera

3.7.2 ThermaCAM™ Researcher

ThermaCAM™ Researcher is an official program in world of infrared imaging and measurements. It is compatible with wide variety types of infrared cameras, and Figure 3.25 shows the main window of this program. The main reason for using this program is deal with live infrared images, which received through a camera interface or from other media, such as PC-Card hard disks from ThermaCAM cameras. Researcher program supports four hardware configurations namely: PC-Card camera interface, parallel camera interface, a FireWire interface, and an IRFlashLink interface. The running of this program requires specific versions of Microsoft Windows such as Windows 95/98/ME, Windows NT 4.0 (service pack 3 or higher), and Windows 2000/XP (depend on the type of interface). The program can display

infrared images, record them on disk and analyse them afterwards during their replay. In addition to that, providing directly values of the measurement result from the live stream of images that do not need to record. The information could extract from this program by using an automatic way of transferring information which is known as OLE. OLE is a Microsoft standard that helps to link and automatic updating data between image and temperature information from Research program into other compliant applications, for example, Excel and Word.

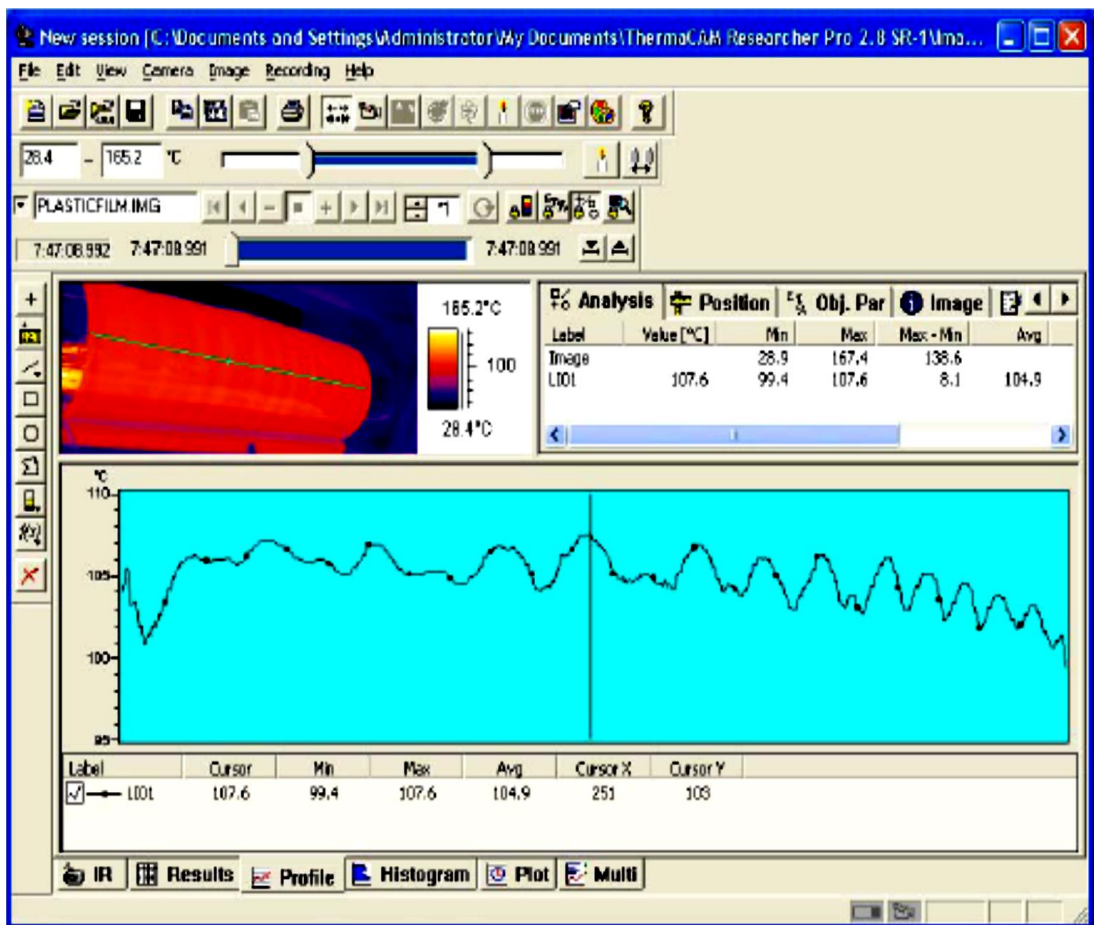


Figure 3. 25 Main Window ThermoCAM™ Researcher

ThermoCAM™ Researcher uses a set of predefined screen layouts, one for each type of thermal information, therefore, it has a powerful analyse thermal performance. The built-in measurement functions in this program provide extensive temperature analysis tools namely: (i) isotherm, (ii) spot measurements, (iii) area and line

measurements. The results that come from these tools can be shown within the infrared images and many windows, such as profile window, histogram window, result table window, plot window. All temperature results and image properties are analysed by using custom mathematical formulas. Furthermore, Researcher program can fully control on all functions of infrared camera, such as focus, level and span adjustment, temperature range adjustment, and colour palette; from the moment connected to a PC displaying a live image. This program has the capability to stores and retrieves temperature information digitally, such as static and real-time infrared images, live IR video sequences, and dynamic high-speed events. All these can get it directly from ThermaCAM cameras, thereby allowing in-depth and precise analysis of thermal events. Thus, ThermaCAMTM Researcher provides an automation interface through its functions that makes it ideal for integration into automation/machine vision applications.

3.8 Reflection Test

As mentioned in section (3.6), dealing with a laser (class 4) needs high-level of safety to avoid numerous health and safety hazards. Therefore, special precautions must be observed when operating a laser machine (Fusions 10.6 Series). One of these precautions is to test the reflection of the laser beam after it is hitting the surface of the workpiece. Reflection test is an essential technique to assess knowing laser beam reflection by installing white sheets around the workpiece underneath the laser nozzle as shown in Figure 3.26. After that, the laser machine has been turned on with laser power; starting at 5 % till reached 45 % of the total power without rotating workpiece (static test). In each heating trial, the laser power is increased 5 % with a constant distance between laser nozzle and workpiece. In the same time, the white sheets have been examined visually by a naked eye, looking for any burning effects due to the reflection of the laser beam on it. Then, the same procedure was repeated but with rotating the workpiece during preheating shots.

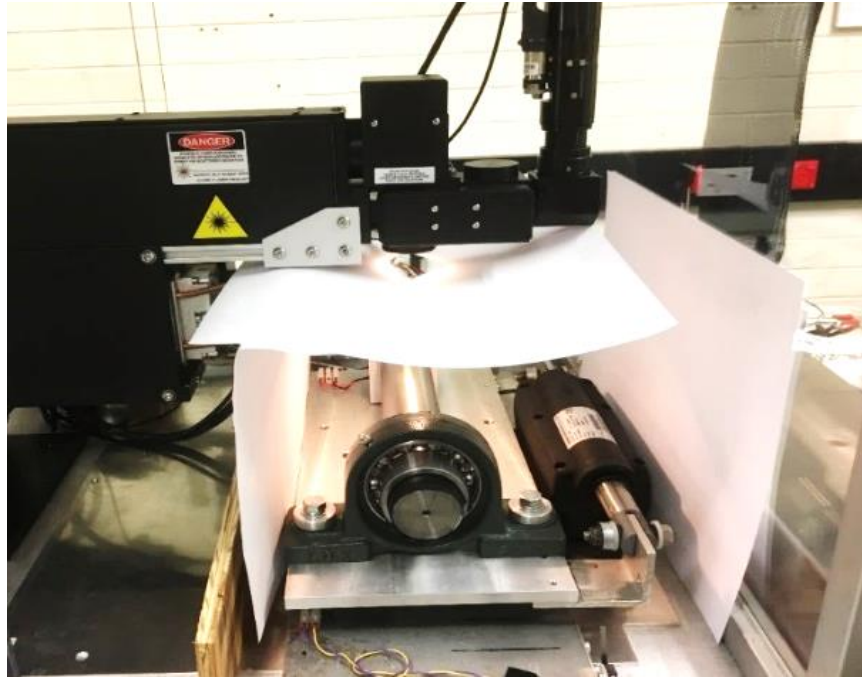


Figure 3. 26 Preparations for Reflection Test

The results of the visual inspection showed no any burned spot or line appeared in white papers. That means there is not any laser reflection occurred during the heating process until used laser with power 50 % or more. Which the burned lines, illustrated in Figure 3.27, appeared because of the presence of scratches and cavities on the workpiece's surface, which have higher emittance values compered to flat surfaces on the same workpiece. The degree of surface finish plays an important role in increasing or decreasing the emissivity of the workpiece surface, at the same time, the reflection of laser beam. The reflection of most laser power from the surface is mean; a small amount of laser power will transfer to inside the workpiece. As a result, the surface temperature will not rise, and the surface of workpiece remains cold. This indeed what happened after the test of the laser beam reflection. According to this, the surface of a workpiece was machined by using CNC lathe machine to remove all scratches. On the other hand, the surface finish improved more causing increase the surface emissivity, which led to increasing the reflection of laser beam when repeat this test.



Figure 3. 27 Laser Reflection Sign

3.9 Emissivity Test

Knowledge of surface emissivity (by scientific convection properly called emittance) is important both for accurate non-contact surface temperature measurement and for heat transfer calculations. Emissivity is a complex term describing the efficiency with which a material radiates infrared energy in a defined waveband and at a given temperature. Emissivity is defined as the ratio of the energy radiated from a material's surface to that radiated from a blackbody (a perfect emitter) at the same temperature and wavelength and under the same viewing conditions. Most solid objects exhibit very low transmission of infrared energy, therefore, the majority of incident energy is either absorbed or reflected.

The objects that do not transmit energy have a simple balance between emissivity and reflectivity. The infrared energy emitted by a body differs according to the composition of the body and to the physical condition of the surface (19). For instance, a clean and polished metal surface will have a low emissivity (emit inefficiently), whereas the oxidised metal surface has a better value of the emissivity (more efficient emitters). The material emissivity depends on the nature of the surface. Thermal emissivity strongly depends on numerous factors including workpiece condition, the workpiece temperature, the wavelength of radioactive waves, the surface of the object that considered form and general geometrical features and of course the thickness of the object when it is translucent (242).

Moreover, emissivity is related to the optical and electrical properties of the materials, and it is a key parameter required in heat transfer calculations for several industrial applications, for example, in aerospace and aircraft components (19, 243).

Many facilities about emissivity measurement have been described in the literature over the past decades. The methods of these facilities can be broadly classified into two categories: indirect and direct emissivity measuring methods. Indirect measuring refers mainly to the reflection method in which the emissivity can be calculated based on the Kirchhoff's law by measuring the reflectivity and the transmissivity of the sample. Direct emissivity measuring method is based on the definition of emissivity by measuring the radiance of the sample and blackbody at the same conditions (e.g. temperature, wavelength and angle), in which the emissivity is computed as the ratio of the two measuring values.

On heat transfer occasions the surface emissivity can be used as a property that can be measured by a non-contact technique. Although most often used as an off-line measurement, it has occasionally been used in. As a non-contact mainstream method, radiation thermal camera is widely used in many industrial applications due to its advantages of high response speed, high accuracy, and non-contact measurement. IR camera is one of a few methods to estimate or measure the emissivity value of an object's surface. The accuracy of this camera mainly relies on the emissivity of the surface of the object. Uncertainty in the emissivity measurement could cause a large error in monitoring the temperature (244, 245). Emissivity of a sample should, therefore, be measured during the temperature measurement process and the effect of nature and type of the surface on the emissivity needs to be taken into account.

As a result of the reflection test, the emissivity value of the workpiece surface must be measured, improved to reduce the reflection of laser beam after heating workpiece. No measurements can be found about the effect of surface nature on the normal spectral emissivity of Ti-6Al-4V titanium alloy. However, a number of observations can be available about the effect of surface oxidization on the spectral emissivity of this titanium alloy in the literature (242), in which some strong oscillations were observed during the heating period. To increase the emissivity for

any material surface, there are different methods have been used for the emissivity evaluation, which is listed as follows:

- 1) Apply a thin layer of tape
- 2) Stratify a thin layer of paint, lacquer, or other high emissivity coating
- 3) Apply a thin coating of baby powder or foot powder
- 4) Stratify a thin layer of oil, water, or other high emissivity liquid
- 5) Apply a surface treatment such as anodizing
- 6) Roughen the surface (may require substantial roughening)

For this work, two of the above methods (2 & 6) have been used to develop the thermal emissivity of titanium alloy workpiece. In addition to the shiny workpiece, two other titanium alloy workpieces have been made with black-painted surface and roughed surface. The shiny surface was made after polishing the workpiece with Wet & Dry P1200 emery paper grits, then it was buffed with a cloth & brass compound. The sand-blaster machine, illustrated in Figure 3.28, has been used to produce rough surface for the second workpiece. For the sandblaster, the grit size 100/300 microns of silica sand was used at 90/100 psi operating pressure. The surface roughness of a second workpiece is 5.61 μm , which is measured by using TalySurf device and the precision reference workpiece, shown in Figures 3.29 and 3.30 respectively. While the roughness of the polished surface is 0.2 μm . The third workpiece of Ti-6Al-4V alloy was painted with heat resistant paint black colour for high temperature. This type of paint is heat resistant 100% silicone based flat finishing coat especially designed for use on metal surfaces subject to extreme heat up to 540 °C. The surface was thoroughly cleaned and free from dirt, rust scale, and other contaminants. Where it wiped the surface with mineral turps and allow to dry before painting at the room temperature.



Figure 3. 28 Sand blaster machine

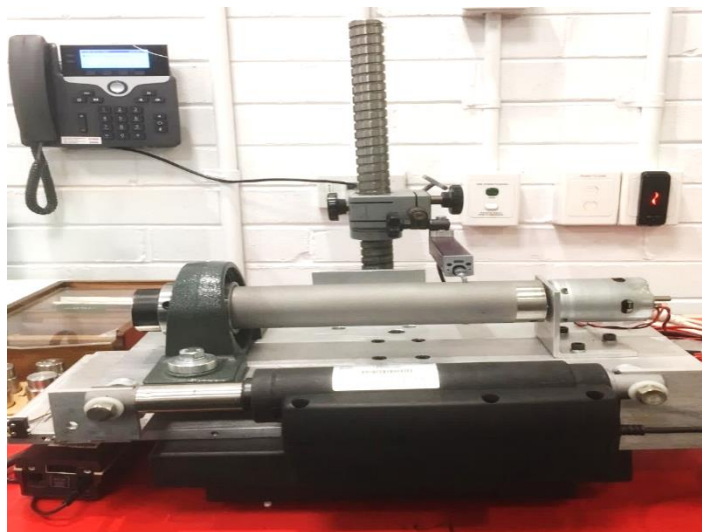
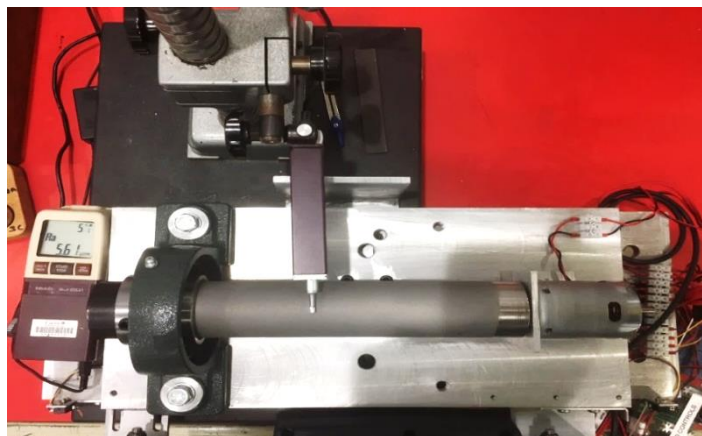


Figure 3. 29 TalySurf device to measure surface roughness

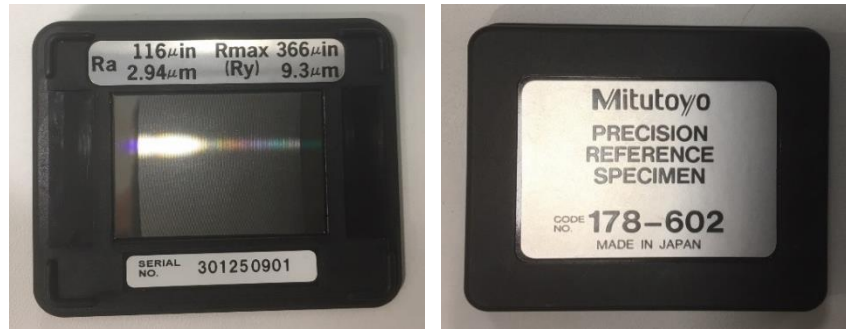


Figure 3. 30 The precision reference specimen

There have been many studies of titanium alloy emissivity, but the heating modes, wavelengths of the infrared measuring temperature, and temperature ranges differed from those used in this test (245), so it was difficult to choose a published emissivity value to calculate the temperature. The manner of making the test is extremely simple. This test includes measuring thermal emissivity of three workpieces of Ti-6Al-4V alloy with different surface such as, shiny, rough and painted. In this empirical test, emissivity evaluation of a commercial Ti-6Al-4V workpiece is attempted using a thermocouple (type K) and thermometer-based temperature measurement system. As illustrated in Table 3.5, thermocouple (type K) is the most common general-purpose thermocouple with a sensitivity of approximately $41 \mu\text{V}/^\circ\text{C}$. A high accuracy infrared thermo camera of type ThermoVision™ A40V is used to obtain the emissivity of the workpiece's surface. Finding the unknown thermal emissivity value of a target object has always been a test challenge when performing IR thermography analysis.

Table 3. 5 Characteristics of K-Type Thermocouple

Type	K
Material	Chromel-alumel
Temp. range °C (continuous)	0 to +1100
Temp. range °C (short-term)	-180 to +180
Tolerance class One (°C)	± 1.5 between -40°C and 375°C $\pm 0.004 \times T$ between 333°C and 1200°C
Tolerance class Two (°C)	± 2.5 between -40°C and 333°C $\pm 0.0075 \times T$ between 333°C and 1200°C
Curie Point	354

A simple method is set up to quickly test the emissivity with an infrared thermal imaging system within a small distance according to the theory of measuring temperature by infrared system. A heated element radiates heat down onto the surface and the surface layer of workpiece reflects the heat toward a lens of the thermal camera. The amount of heat reflected is dependent upon the type and the structure of the surface. The emissivity test includes heating titanium alloy (Ti-6Al-4V) shaft with hot-air by using a heating gun shown in Figure 3.31 (a). Then, thermometer with a thermocouple (type K) are used to measure the temperature of the workpiece surface, see Figure 3.31 (b). Finally, the ThermoCAM™ Researcher is used to calculate the emissivity between 25 °C and 120 °C from an adjacent distance (0.5 m) between the IR camera and workpiece. Emissivity test is practical and easily implemented and includes three stages, the first stage contains heating workpiece with a shiny surface. The second stage concentrates on the heating workpiece that its surface roughed by Sandblaster. While the third stage dedicates on the heating workpiece after painting the surface by black paint.



Figure 3. 31 (a) The heating gun and (b) The thermometer

This kind of spectral emissivity measurement can be easily done when there is some kind of contact-type- temperature sensing acquisition working in parallel with the IR thermal imager. The emissivity values of the workpieces are carried out on a self-made, and the schematic diagram of the spectral emissivity measurement device is

shown in Figure 3.32. The procedure for this test is as follow: clean the workpiece's surface from any dirt or stains if possible, using a piece of dry cloth. Next, start heating at a certain selected point on the surface of the workpiece, as illustrated in Figure 3.32. The heating process was an intermittent process, at each stop the surface temperature has been measured manually, as shown in Figure 3.33. This temperature has been inserted into the camera software, at the same time, the radiation emitted by the workpiece surface is detected by a lens of the thermal camera. The ThermoVision™ A40V has been setup at emissivity (1.0) and (0.2 m) distance between the IR camera and specimen. The above procedure is the same to calculate the emissivity for all three workpieces surfaces.

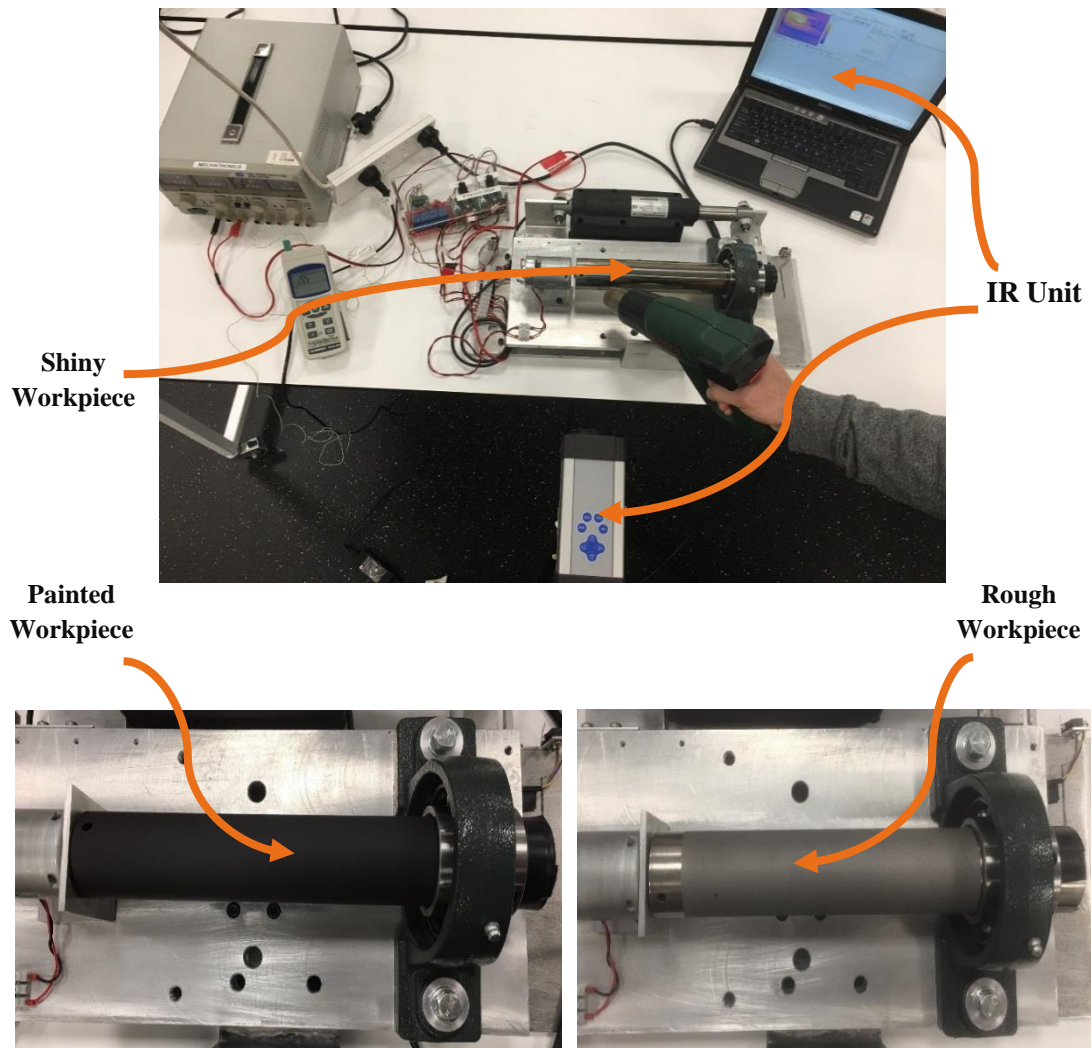


Figure 3. 32 Setup to measure the emissivity of titanium alloy workpiece

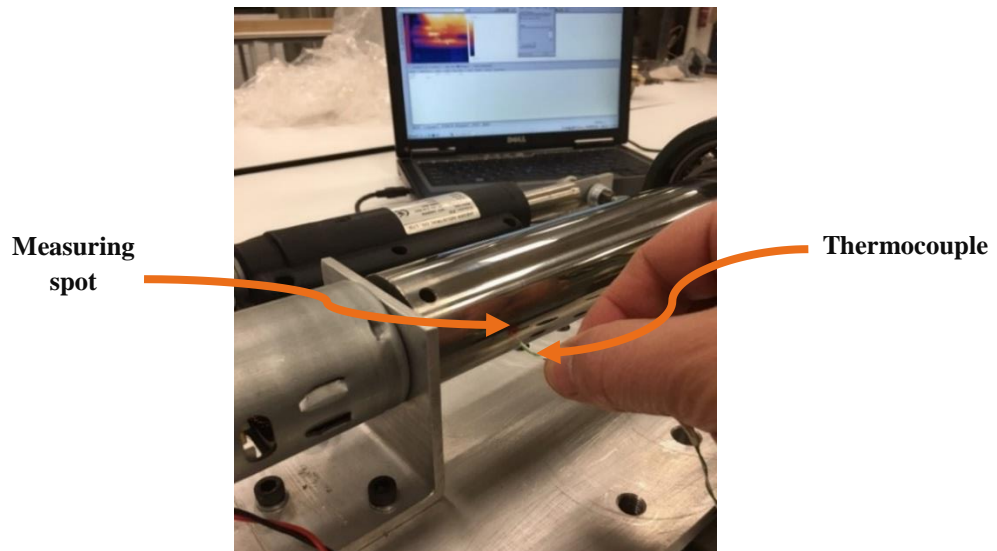


Figure 3. 33 Measuring surface temperature

According to the principle of emissivity measurement introduced earlier, the results are show temperature – emissivity relation. Figure 3.34 shows the relation between the temperature at the polished (shiny) surface and the emissivity of this surface. From this figure, it can be noted that the emissivity starts with a small value (0.26) and gradually decreased with increasing surface temperature. This is attributed to the condition of the surface, which is quite clean and bright like a mirror, therefore, it emits low levels of radiant thermal (heat) energy.

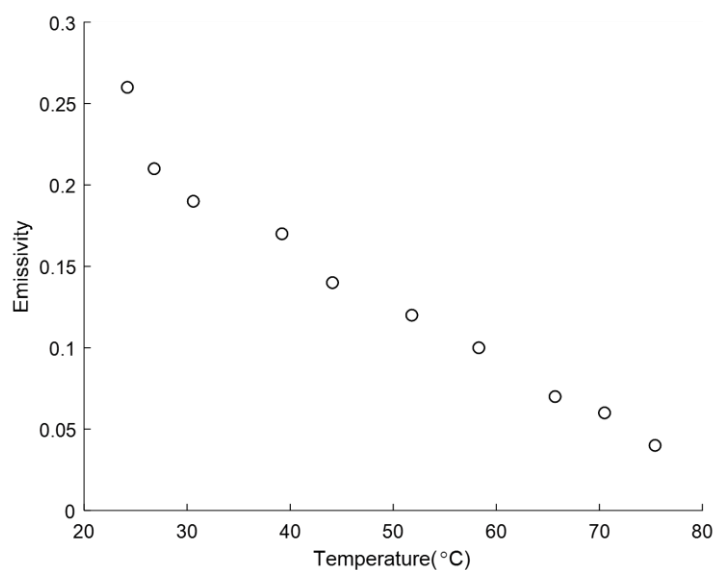


Figure 3. 34 The relation between temperature and emissivity of the shiny surface

On the other hand, Figure 3.35 illustrates how the normal spectral emissivity of the painted surface changed with increasing the surface temperature. From this figure, it can be seen that the surface emissivity increased with increasing the temperature of workpiece surface till reached up to 0.91 at temperature around 64 °C. Above this temperature the emissivity starts decreasing sharply in the same time of temperature rising. This could be attributed to differences in the structure of the black paint layer.

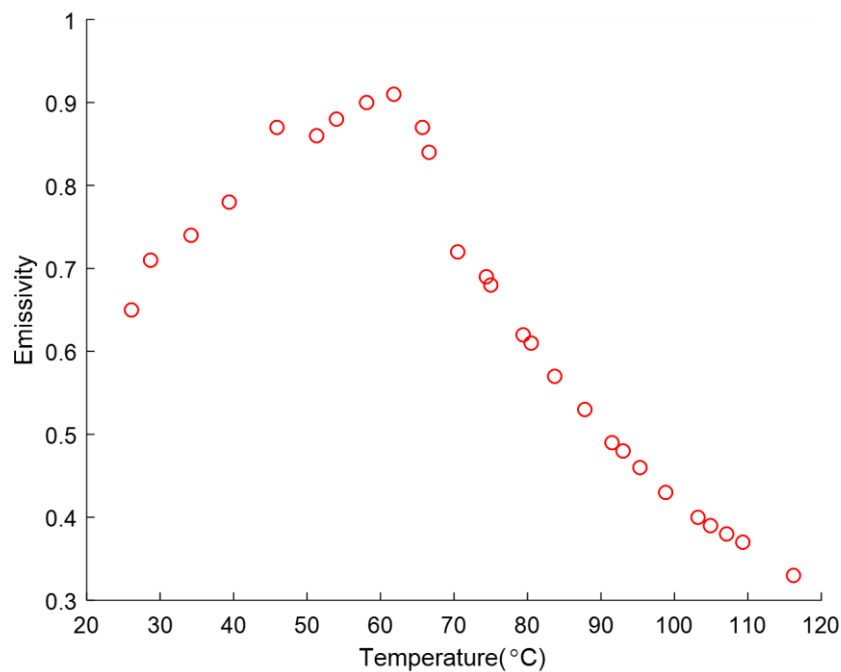


Figure 3. 35 The relation between temperature and emissivity of the black surface

Finally, Figure 3.36 illustrates the variation in the emissivity values by increasing the surface temperature of the Ti-6Al-4V alloy workpiece that has a rough surface. It can be noted that the emissivity increased with increasing of temperature till reached to 0.63 at temperatures around 75 °C. However, the emissivity value decreases significantly after this temperature with increasing surface temperature. A slight peak is found at about 64 °C and 75 °C in Figures (3.35) & (3.36), respectively. In overall, the rising and decreasing of thermal emissivity for both painted and rough surfaces of this alloy look similar. However, there is a clear difference in the shape

of the increasing part, where there is fluctuation in emissivity values with the surface temperature increases. The possible reasons for the changes in emissivity were generally considered to be variation of composition, change in surface morphology. It is worth noting that, the emissivity at the given temperature in 25 °C - 120 °C approximately follows a linear rule as a function of temperature.

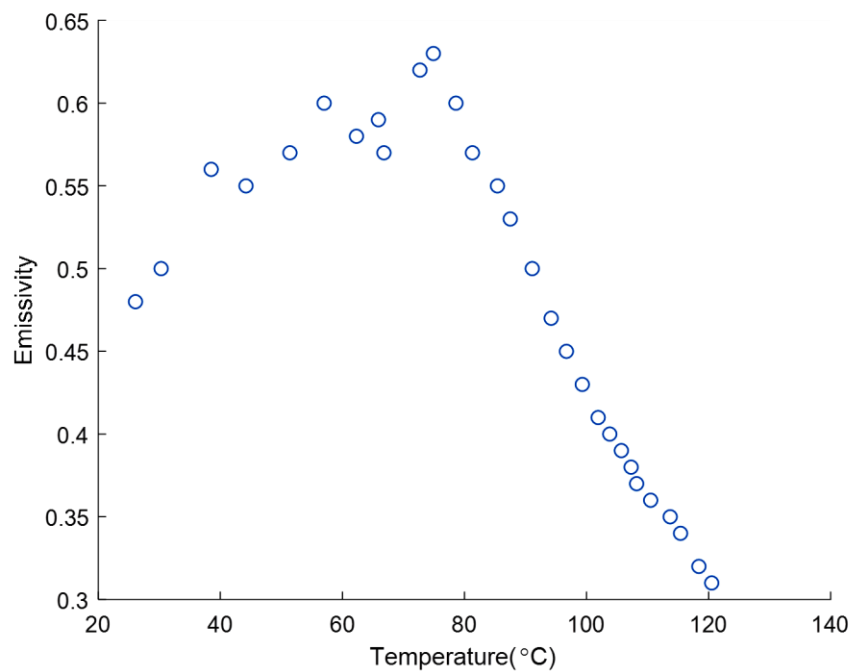


Figure 3. 36 The relation between temperature and emissivity of the roughed surface

In conclusion, this test has studied the behaviour of spectral emissivity as a function of surface temperature using the present experimental setup. According to the principle of emissivity measurement introduced earlier, the results are shown in Figures (3.34), (3.35) and (3.36). As expected, the normal spectral emissivity for the shiny workpiece was small value and this explain why most laser beam reflected from the surface during reflection test. While a quite difference in the experimental values were found between black-painted and roughed workpieces with similar range of the temperatures. The physical surface change that can explain this apparently anomalous behaviour is the presence of surface stresses generated during the

machining and grinding of the workpieces. Finally, black-painted surface has higher emissivity and absorptivity than the roughed surface.

3.10 Summary

In this chapter, a small rotating shaft test-rig has been created for heating condition monitoring based temperature distribution measurements. This set up has been designed to facilitate improvements in condition monitoring methods for the early estimation of the heating temperature of the laser-assisted technique. Thereby it will help to estimate the depth of cut for the lathe process. The test-rig instrumentation includes the provision of techniques for surface temperature measurements for monitoring heating rotated subject as well as the possibility of developing advanced methods for understanding temperature distribution behaviour during various preheating scenarios.

In order to check the variation of the emissivity during the heating process, a simple experimental method for infrared spectral emissivity measurement which consists mainly of the following three parts: Ti-6Al-4V alloy workpiece with a test-rig, simple heating tool (thermal gun) and Thermo-Camera. The emissivity measurements of this titanium alloy are performed at different temperatures and different types of surfaces, and the data trend is well consistent with the general rule of metal emissivity. The spectral emissivity for several temperatures has been plotted in figures (3.34), (3.35) and (3.36). It is remarkable that, between 25 °C and 117 °C, the emissivity goes through a maximum up to 0.91 for painted, while it is 0.63 for surface treated by sandblaster.

All experimental work presented in this study were conducted on a Laser Stepped Heating System manufactured by Photon Machines Inc., USA. It is a three-axis machine with (50 x 50 x 50) mm axis strokes along the *x*-, *y*-, and *z*-axes respectively. This machine utilizes a CO₂ laser source which can produce a high-intensity laser beam in the near infrared portion of the spectrum. The influence of heating rotating solid cylinder by laser beam on the surface condition has been presented in this chapter. Two workpieces with diameter (50 mm) and length (250 mm), have been utilized for modelling small-scale turning process. One workpiece has been painted with heat resistant paint black colour for high

temperature, while the other workpiece has been carried out on sandblaster machine to get rough surface.

Through the aforementioned scenarios of the experimental study, it is clear that the experimental method has provided limited scope for improved comprehending of the thermal impact from laser preheating for a rotating workpiece. Thus, it is difficult to understand the preheating thermal behaviour of a rotating workpiece subjected to laser spot as a surface heat source, and heat dissipation to the ambient by combined modes of heat transfer in LAM. Therefore, in the next chapter (Chapter Five), appropriate numerical modeling processes have used to offer high precision understanding and flexibility to predict the accurate setup of LAM.

Chapter 4

Experimental Analysis

4.1 Introduction

This chapter displays the results for each experiment of heating titanium alloy (Ti-6Al-4V) workpiece by a laser beam during the rotation. Then, the underlying trends of the analysis present experiments identified and discussed, as well.

The present experiments are designed to investigate the effect of LAM parameters, such as laser power, rotating speed, and heating style, on temperatures distribution and heat transfer rate at the rotating surface. The Ti-6Al-4V cylindrical workpiece has heated by a laser machine that generating a laser beam with low power (up to 27.5 W). Surface temperature measurements have been monitored and measured through the ThermoVision™ A40V Camera, which is placed 500 mm away from the rotating workpiece, as illustrated in Figure 4.1.

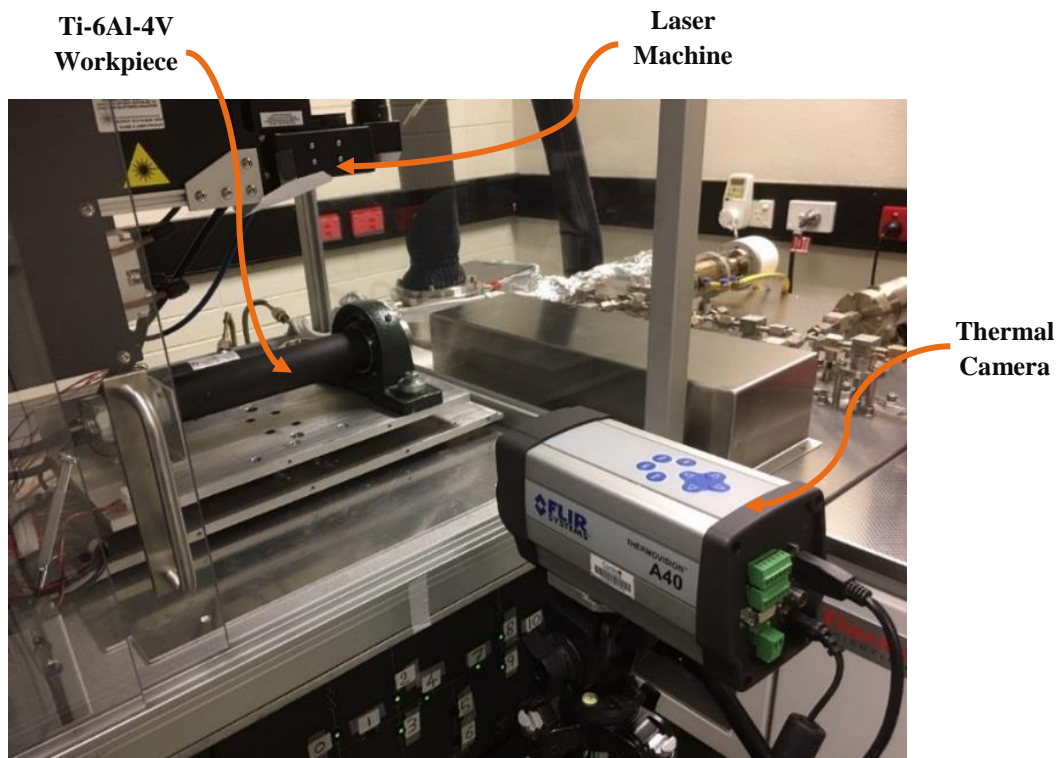


Figure 4. 1 The Experiment Setup

Two workpieces of titanium alloy with different surfaces (rough and black-painted) are used for this empirical work. All experiments included heating the surface layer by a low power laser beam during rotation of the workpiece. Additionally, two scenarios are followed in these current experiments, namely as stationary laser heating and moved laser heating. For the remainder of the experiments of the current research (section 3.3), the experiments conducted in four stages: the first stage includes heating rotating painted workpiece by a stationary laser. The second stage comprises heating a rotating rough workpiece by a fixed laser beam. Whereas, the third stage includes heating a rough workpiece by moving a laser beam with various scanning velocities. Finally, the fourth stage conducts heating with constant scanning velocity and at different rotation speeds for a rough workpiece.

4.2 Emissivity and Temperatures Correction

All experiments have conducted at a constant value of thermal emissivity (0.5). Consequently, a correction of the practical results was performed to obtain more accurate values. The correction process for the current work has been conducted in two stages, as illustrated in Figure 4.2. The first stage includes thermal emissivity correction, while the second stage contains surface temperature correction. Emissivity correction has started with fitted the spline for rough and painted surfaces through the datasets of the emissivity test (section 3.9). The data of surface temperatures have collected through converting thermal camera images into Excel data. Some of the thermal images are shown in Figures (4.3), (4.4), and (4.5), which have taken at different values of the setup parameters such as, spinning speed, scanning speed, laser power, and heating time. Further, Figures 4.6 to 4.11 show the results of laser experiments for both sandblaster surface and black painted surface. By using MATLAB, the local emissivity values were estimated utilizing data of laser heating tests with a fitted spline. After that, the local thermal emissivity has been used to estimate the correction factor, which in turn utilized to calculate the corrected surface temperatures. The corrected temperatures are presented and discussed in the following section.

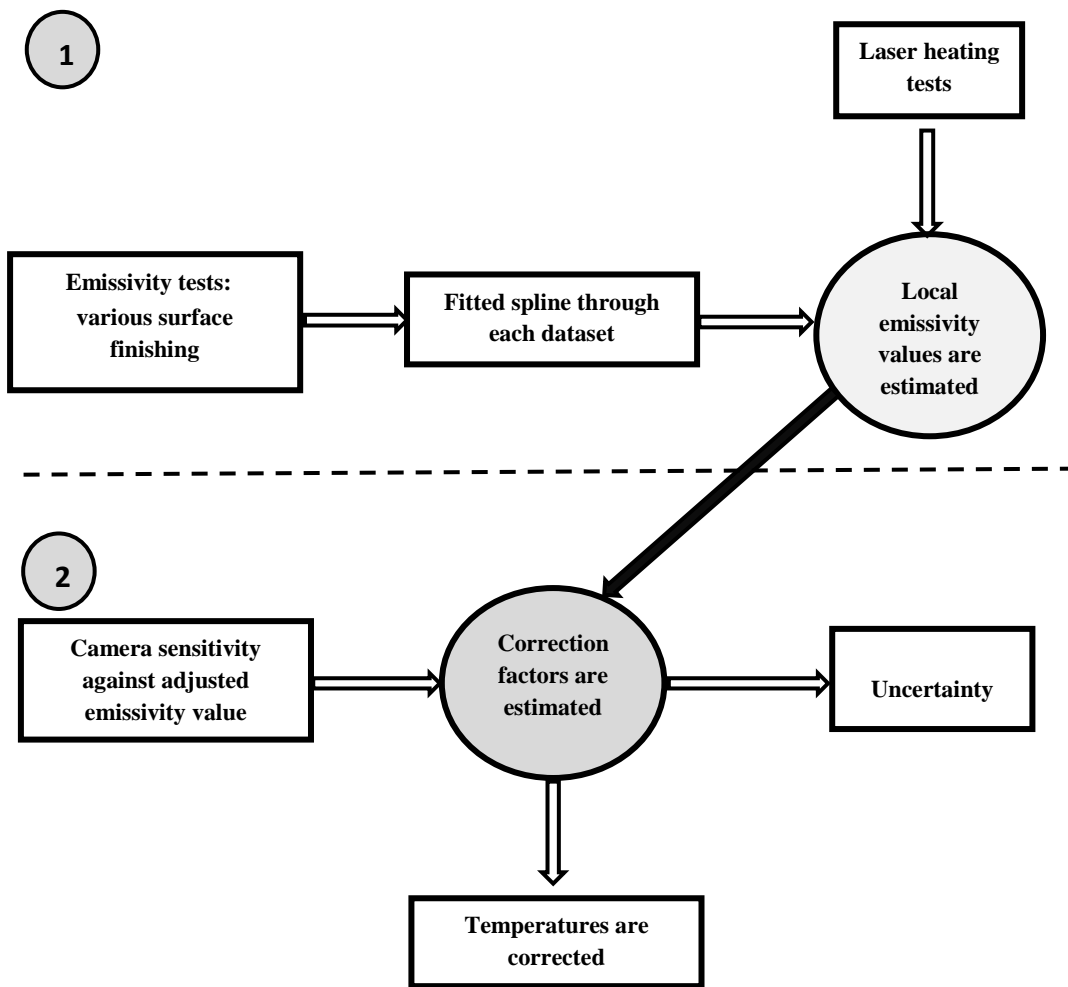


Figure 4. 2 Flow diagram of the emissivity and temperatures correction

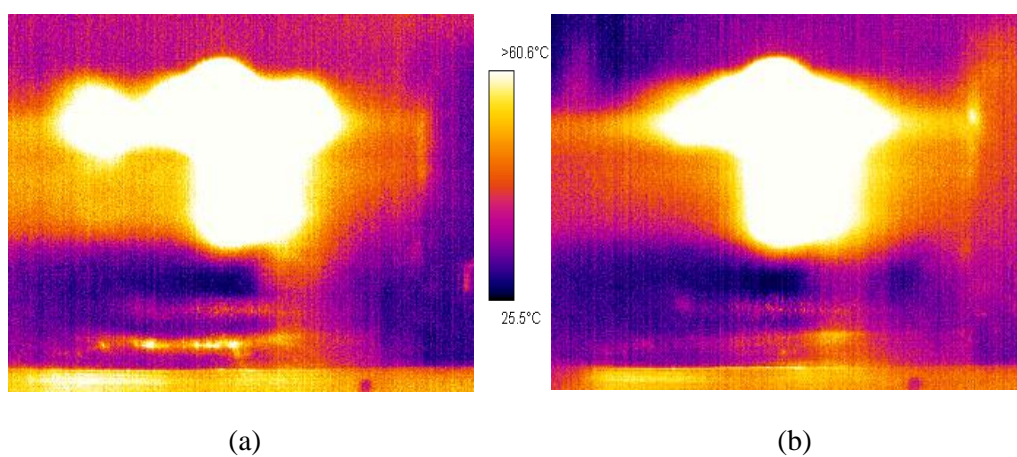


Figure 4. 3 Camera images for heating sandblaster (Ti-6Al-4V) workpiece by moved laser (a) at 100 rpm, 50 % LP, 40mm/min, 35 sec; and (b) at 500 rpm, 50% LP, 20mm/min, 65 sec

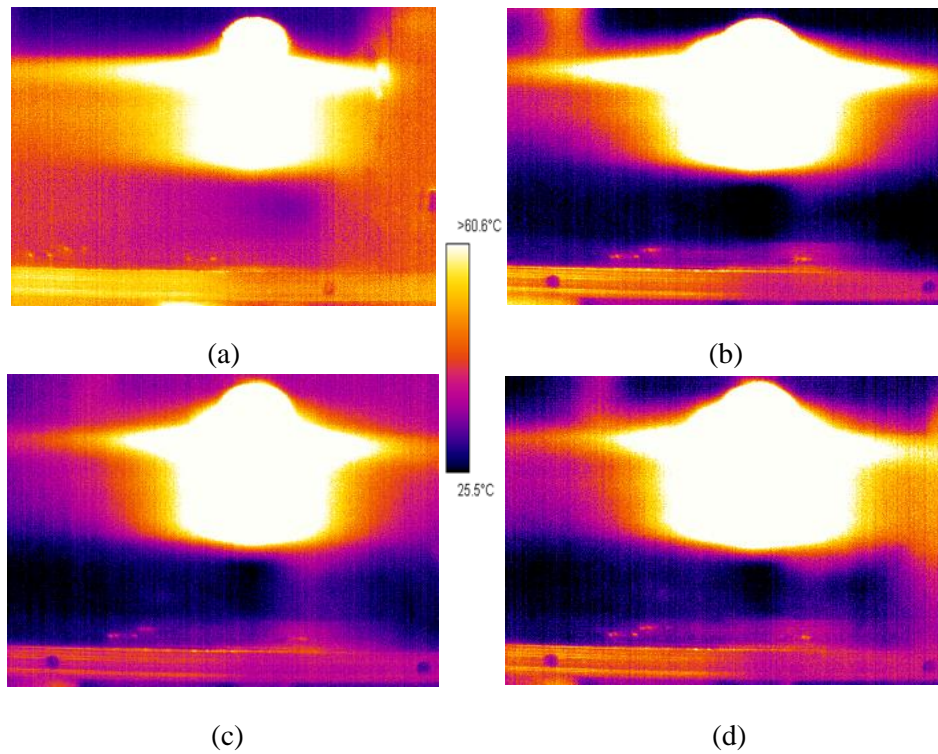


Figure 4. 4 Camera images for heating sandblaster (Ti-6Al-4V) bar by stationary laser: (a) at 100 rpm, 20 % LP, 310 sec; (b) at 200 rpm, 30 % LP, 310 sec; (c) at 500 rpm, 40% LP, 310 sec; and (d) at 1000 rpm, 50 % LP, 250 sec

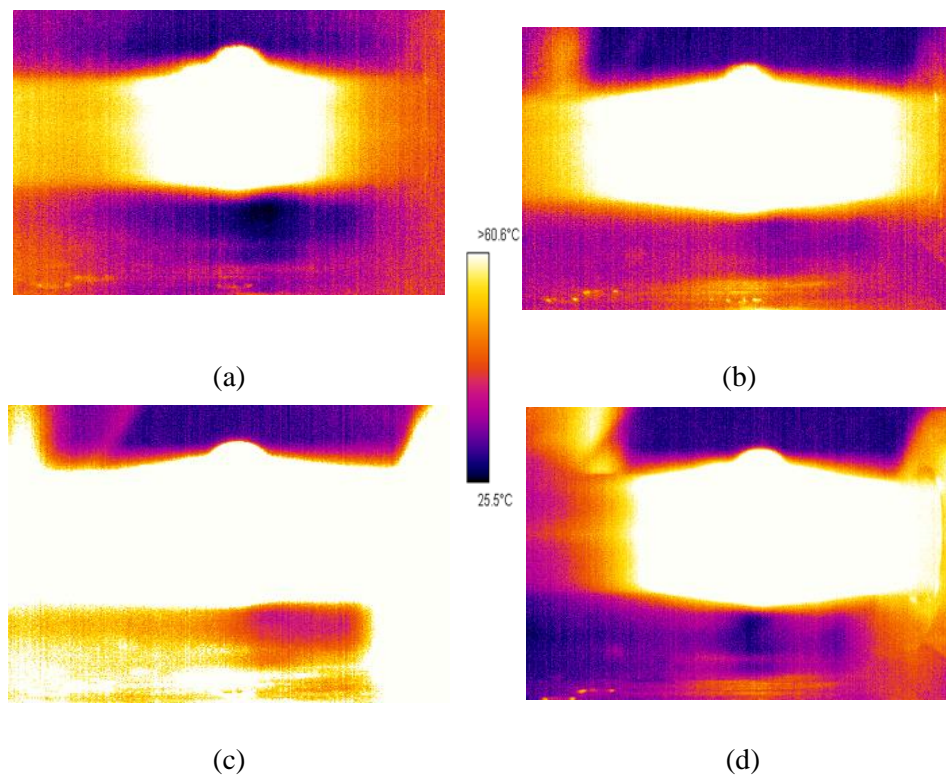


Figure 4. 5 Camera images for heating painted (Ti-6Al-4V) workpiece by stationary laser: (a) at 100 rpm, 10 % LP, 310 sec; (b) at 200 rpm, 20% LP, 310 sec; (c) at 500 rpm, 30 % LP, 310 sec; and (d) at 1000 rpm, 40 % LP, 220 sec

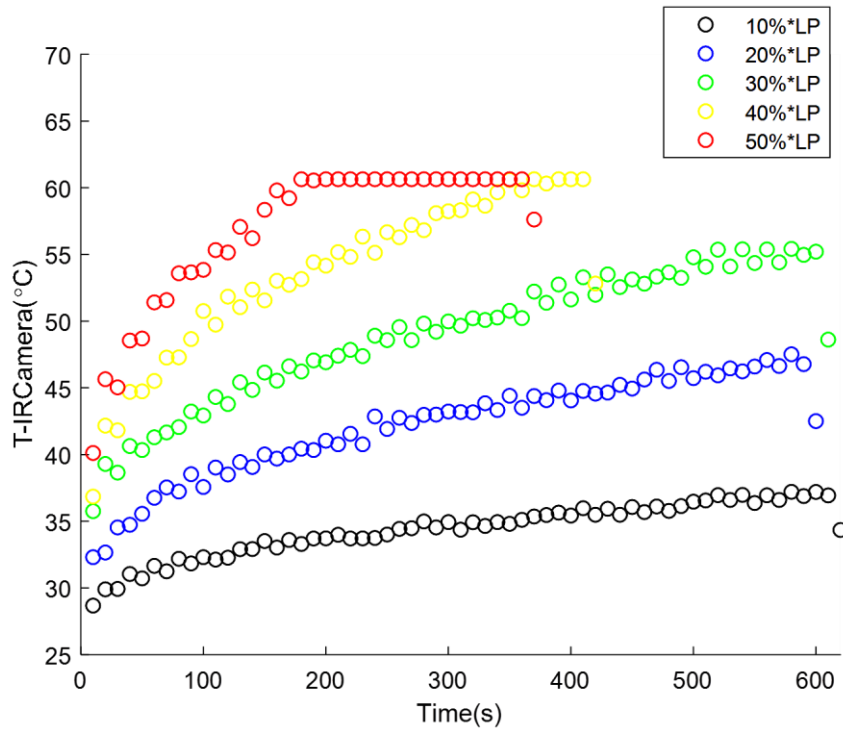


Figure 4. 6 Black-painted workpiece heated with different laser power (LP) at 100 rpm

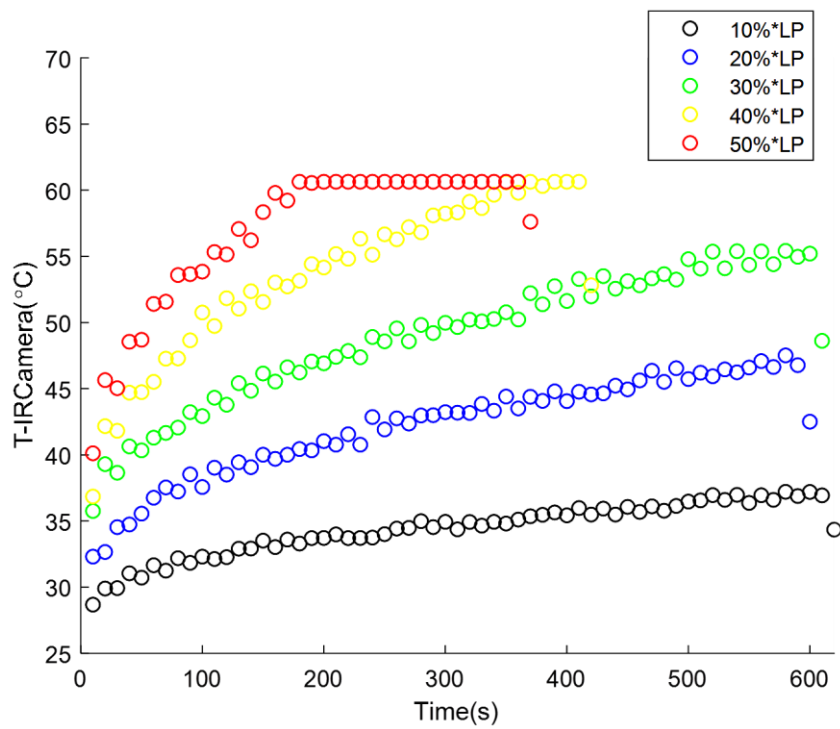


Figure 4. 7 Black-painted workpiece heated with different laser power (LP) at 1000 rpm

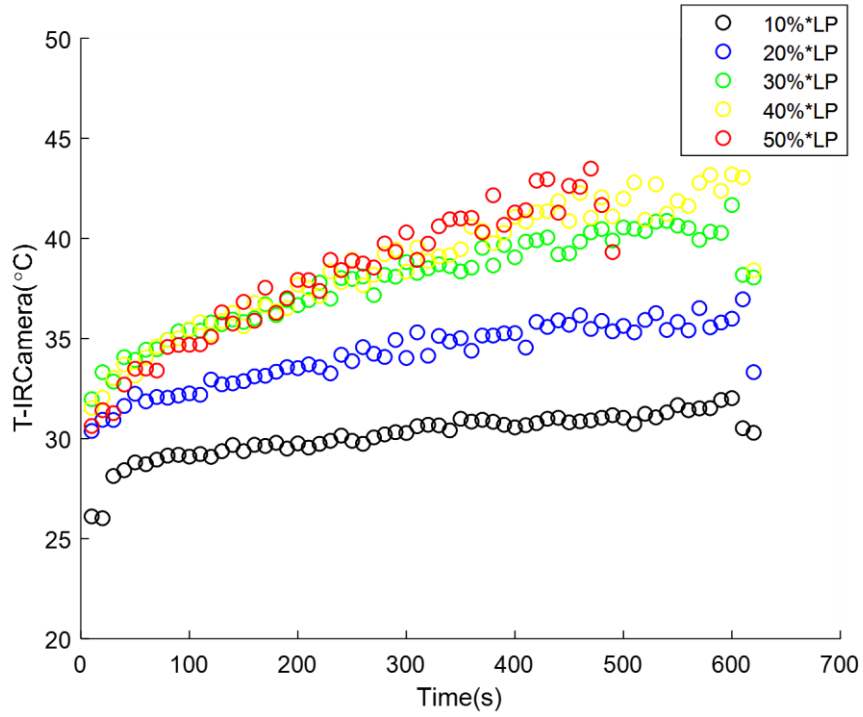


Figure 4. 8 Sandblaster workpiece heated with different laser power (LP) at 100 rpm

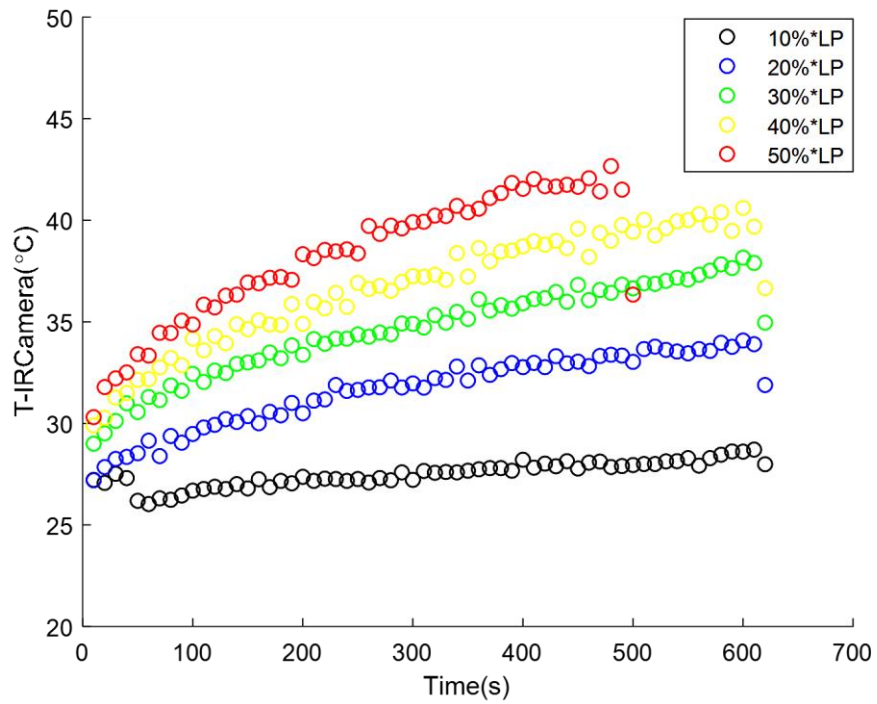


Figure 4. 9 Sandblaster workpiece heated with different laser power (LP) at 1000 rpm

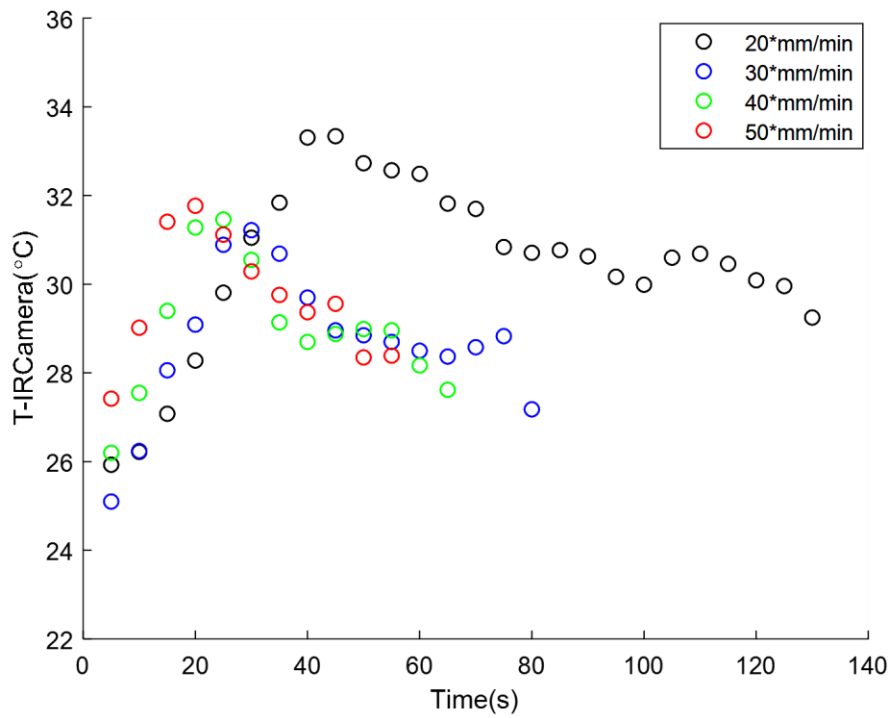


Figure 4. 10 Sandblaster workpiece heated with moving laser at 100 rpm & 50% W

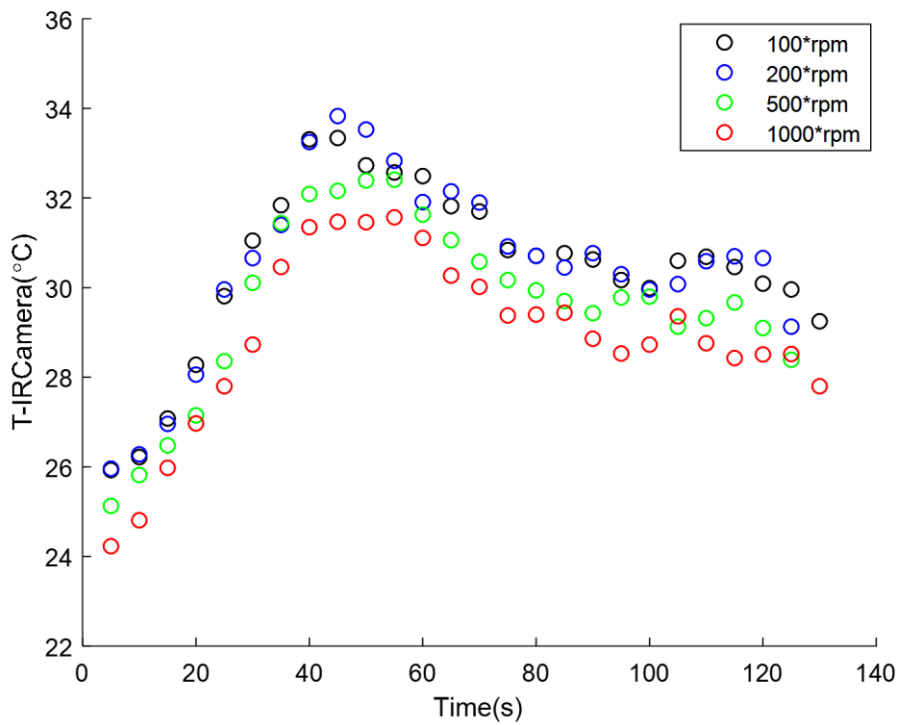


Figure 4. 11 Sandblaster workpiece heated with moving laser at 20 mm/min & 50% W

4.3 Discussion and Parametric Analysis

Generally, it is expected that an increase in the laser power and rotating speed gives rise to a corresponding increase in the rate of heat transfer. The increase in surface temperature is equivalent to an increase in laser power, while, increasing the rotation speed is accelerating heat transfer especially convection heat transfer. The analysis of current experimental data of workpiece surface temperatures is achieved through three sections to study the effect of laser power, rotation speed, and scanning velocity of the laser beam, as shown below:

4.3.1 Thermal effect of laser power

At first, the analysis is simplified by examining only a value of the presented laser power, limited to a rotating speed and laser spot diameter. Figures (4.12) and (4.13) show the variation of surface temperatures with heating time for rotating titanium alloy workpiece painted with Black paint, at 100rpm and 1000rpm, respectively. These figures clearly show the temperature has increased with increasing the power of the laser beam from 10 % to 50 % of the total power (55 W) that generates by laser machine. This increase in surface temperature with increasing of time is attributed to the increase in the exposure time of a workpiece surface by the laser beam, which occurs during constant rotating speed. Further, it can be observed a slight fluctuation in increase the temperature due to the possibility of the presence of some scratches or dust. Lastly and most importantly, at the highest laser power, it is evident that there is thermal equilibrium in the region of the heating. Means the heat that hits on the workpiece surface through a laser beam equal the heat transfer inside the workpiece (conductive heat) and thermal loss from the surface (convection and radiation heat). Therefore, no reduction or increase in the heat transfer rate at that value of laser power.

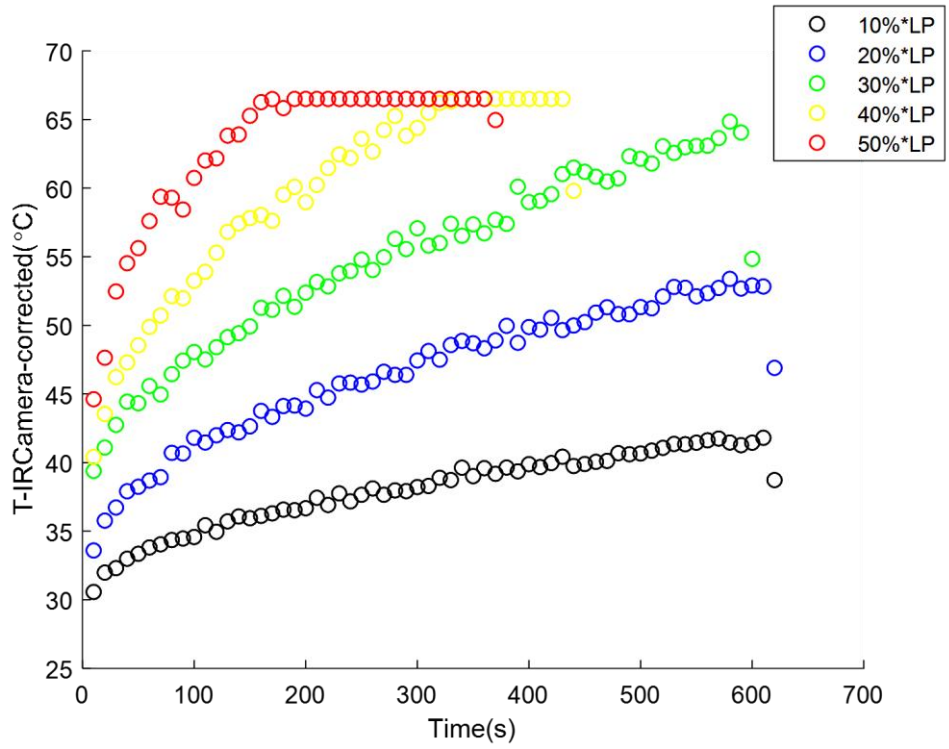


Figure 4. 12 Corrected surface temperatures for black-painted workpiece heated with different laser power (LP) at 100rpm

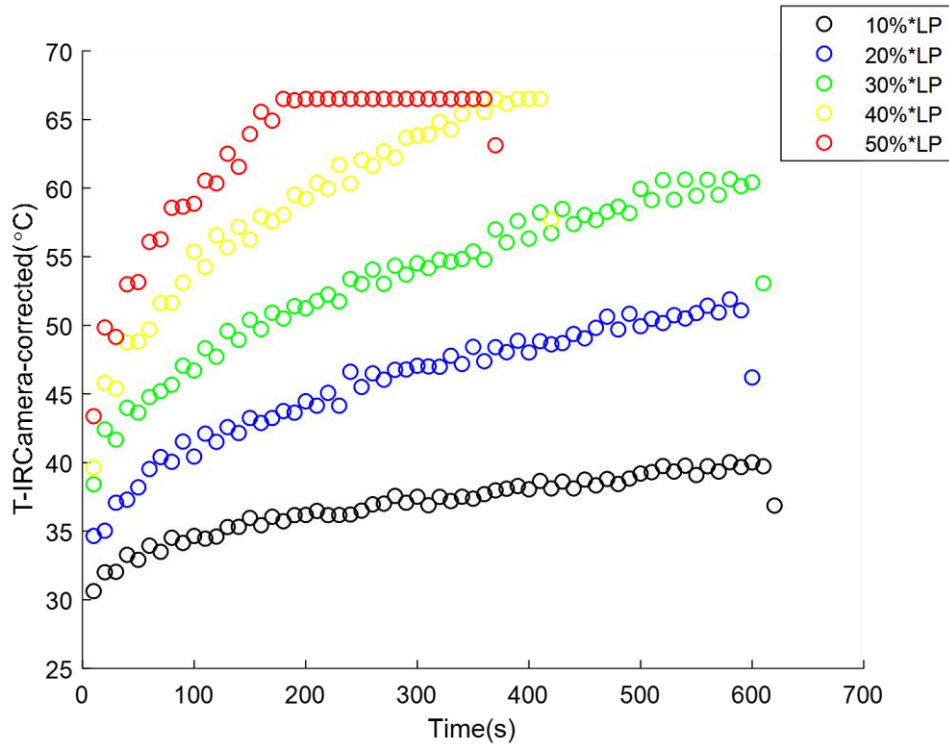


Figure 4. 13 Corrected surface temperatures for black-painted workpiece heated with different laser power (LP) at 1000rpm

Figures (4.14) and (4.15) illustrate the behaviour of surface temperature during heating a workpiece has a sandblasted surface, and which, spinning at two different speeds. Obviously, from these figures, the sandblaster surface temperatures are lower than the temperature of the black-painted surface and take a longer time to rise. The shape of the curves of increasing surface temperature quite different from those curves for workpiece has black-painted surface. Additionally, a clear fluctuation can be observed in temperature increases compared to the black-coated surface due to the rough surface nature. Finally, the last point of each curve in Figures (4.5 – 4.10) and (4.12 – 4.15) represents the surface temperatures, immediately after turning off the laser beam.

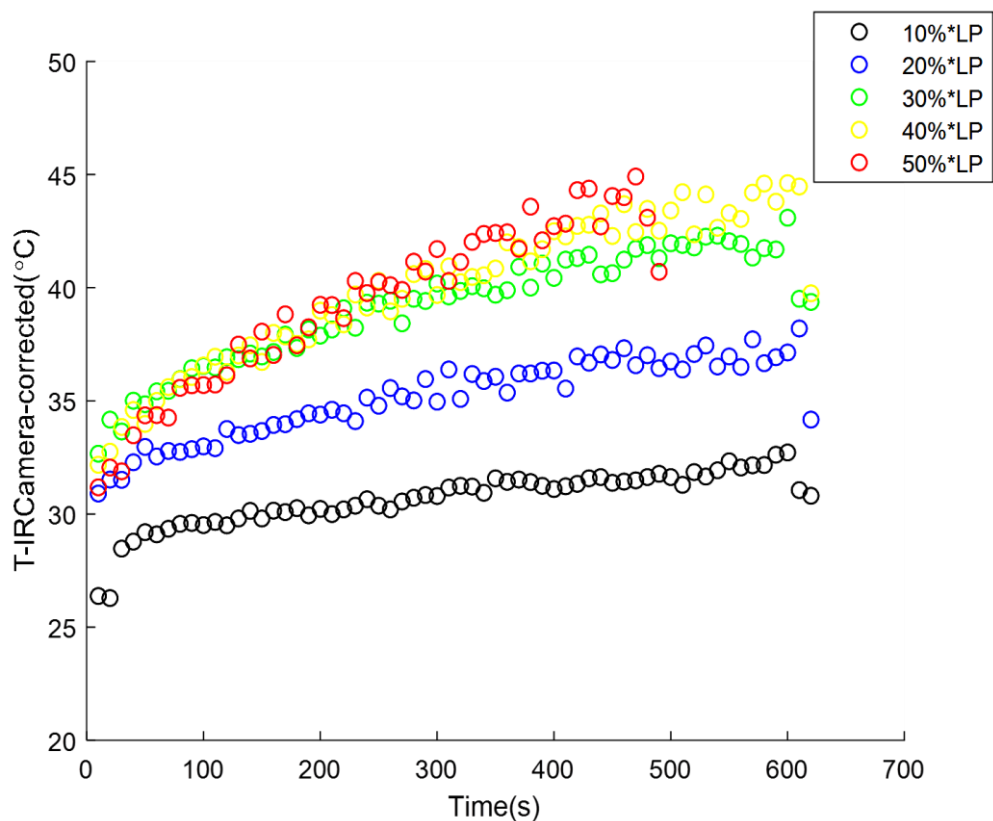


Figure 4. 14 Corrected surface temperatures for sandblaster workpiece heated with different laser power (LP) at 100 rpm

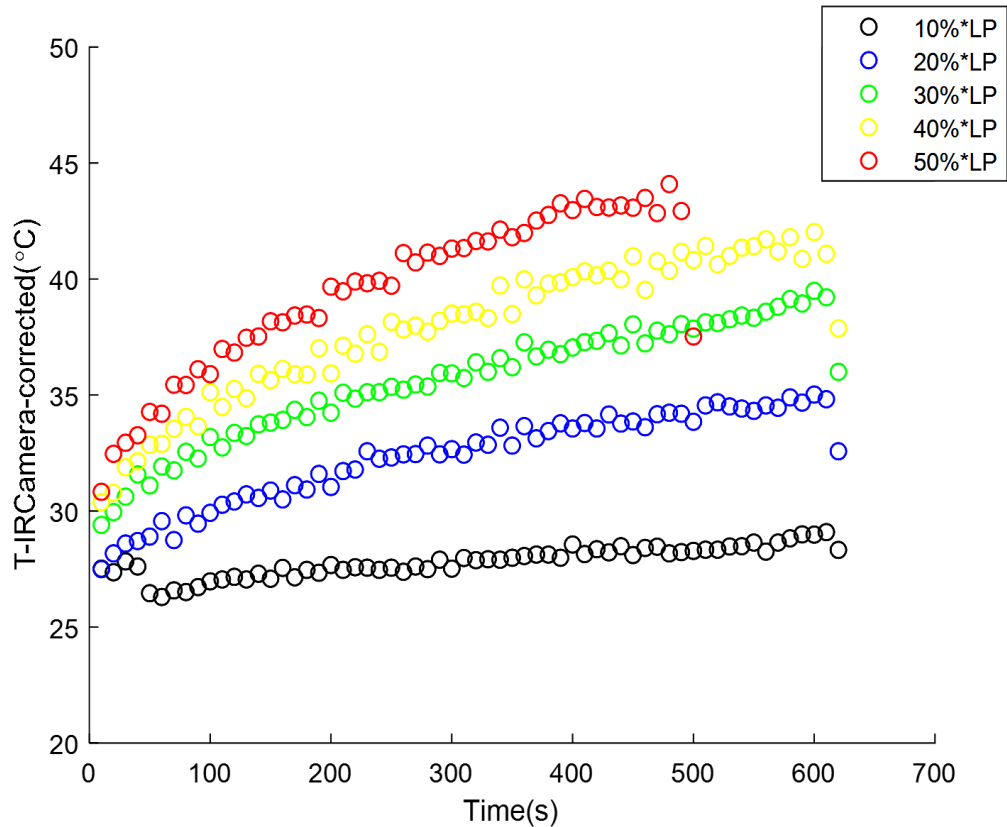


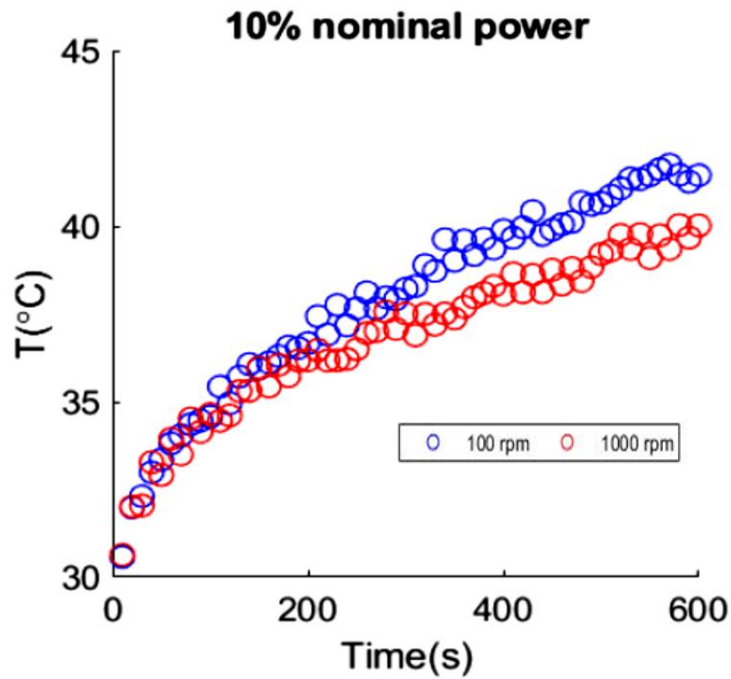
Figure 4. 15 Corrected surface temperatures for sandblaster workpiece heated with different laser power (LP) at 1000 rpm

4.3.2 Thermal effect of rotational speed

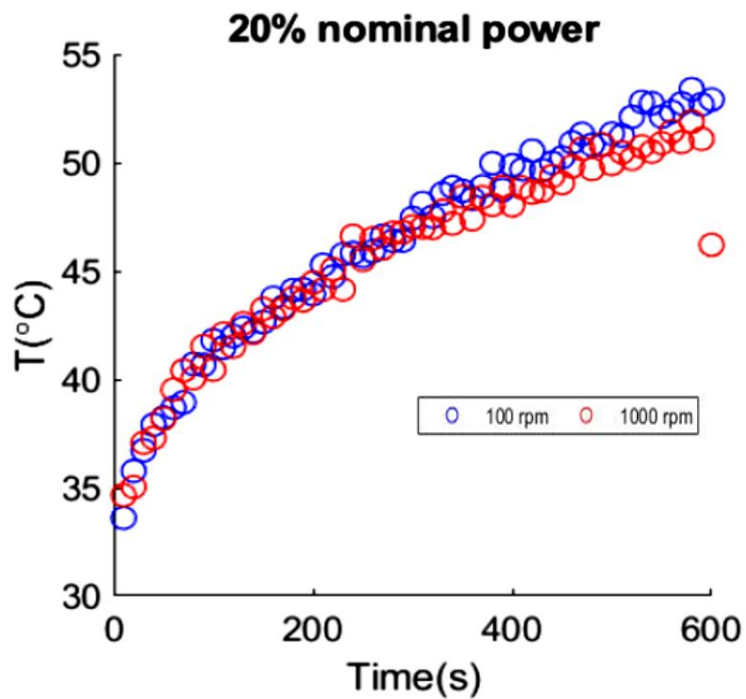
The thermal behaviour of the process is majorly determined by influence of the laser heating and convective loss, due to rotation. The convection intensity is a variable which could be adjusted within functionality of the apparatus. Considering the uncertainties involved in the test procedure, the small surface temperature variations are expected to be overshadowed with lack of accuracy and therefore the distinction should be large enough to be clearly discerned. The test was carried out for (100, 200, 500 and 1000) rpm and results indicated comparison between 100 rpm and 1000 rpm exhibiting sufficient deviation to explain the effectiveness of convection.

Figure 4.16 represents the transient surface temperature of black-painted workpiece for various laser powers and rotational speeds. The black-painted surface, as earlier mentioned, has higher emissivity and absorptivity and therefore the laser source has higher heating influence. Lower laser power and heating intensity allows the effect of convective cooling to be distinguishable. Observing the case with 10 % laser

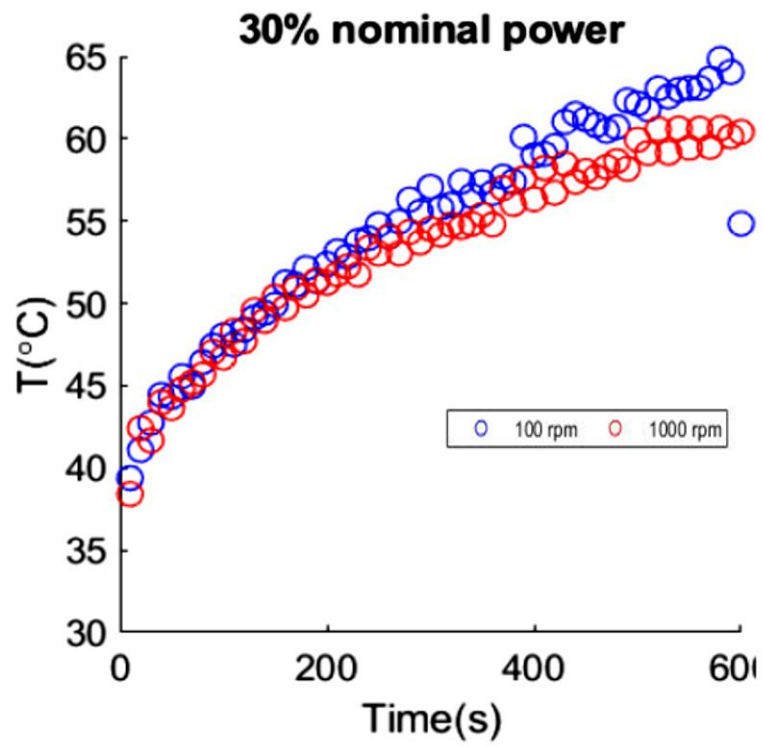
nominal power, workpiece with 1000 rpm rotational speed is found to have a lower surface temperature. Nevertheless, as heating power ramps up heating is becoming more dominant and the distinction is gradually less observable, within operating conditions and reading accuracy.



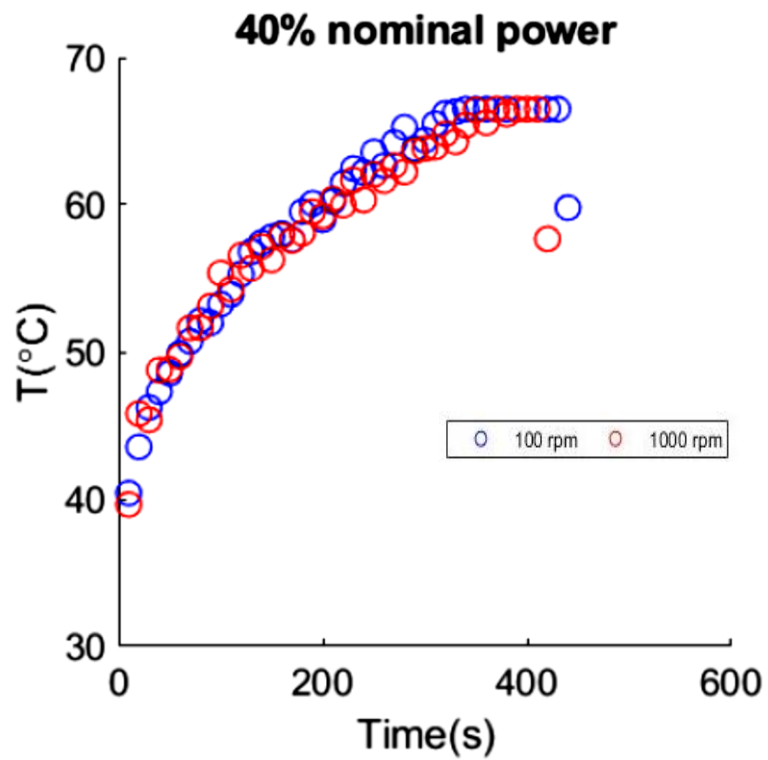
(a)



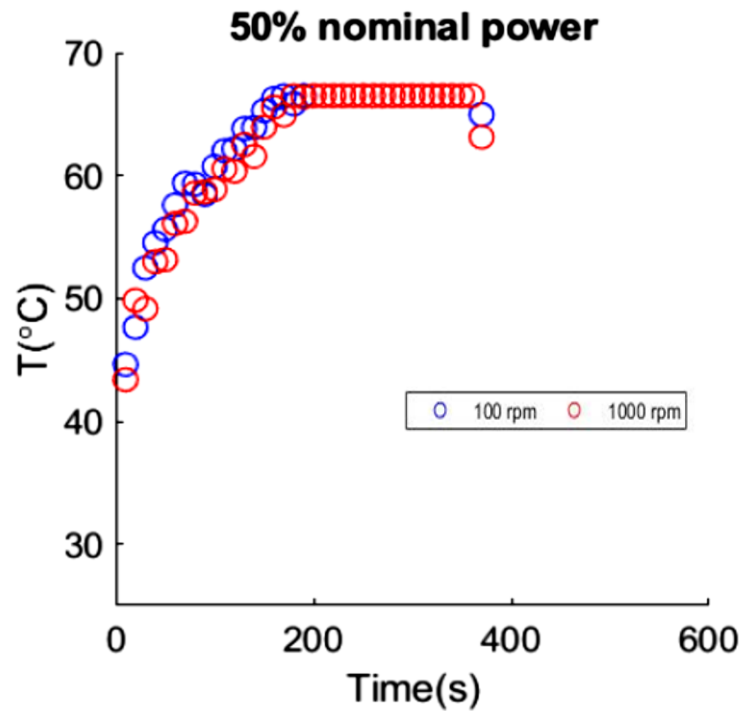
(b)



(c)



(d)

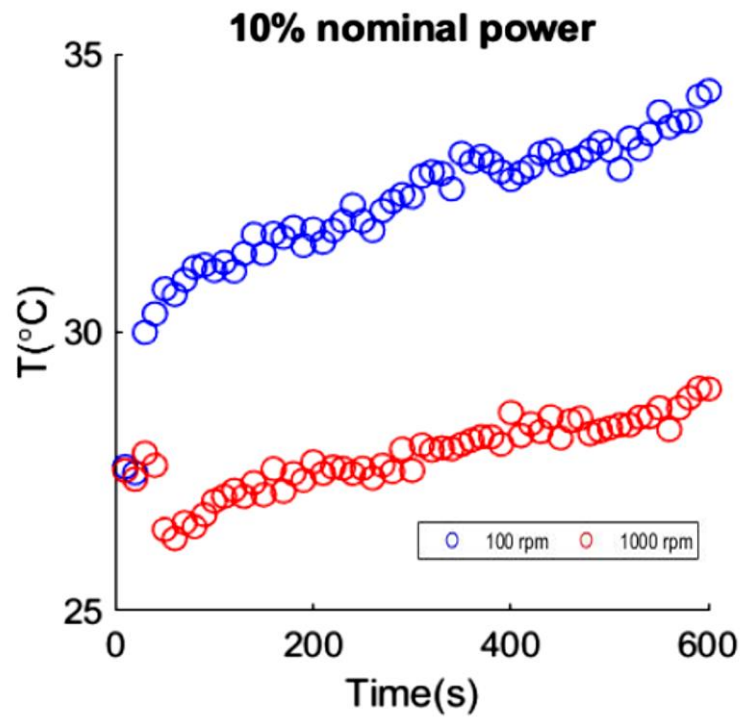


(e)

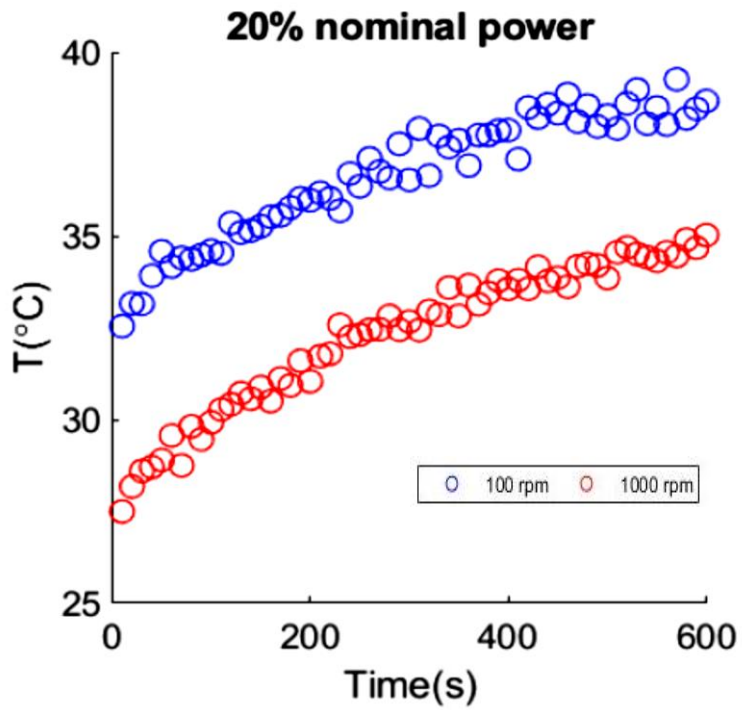
Figure 4. 16 Comparison of transient surface profile, Black-painted surface at various rotational speeds

The results of black-painted sample broadly signal the contribution of comparison is more observable at the lower surface temperature meaning when the heating power or surface absorptivity are lower. This conclusion is reconfirmed when the roughed (sandblaster) surface sample, with lower absorptivity, was examined under the similar conditions. Figure 4.17 compares thermal behaviour of sandblaster surface sample while rotational speed and laser power are varying.

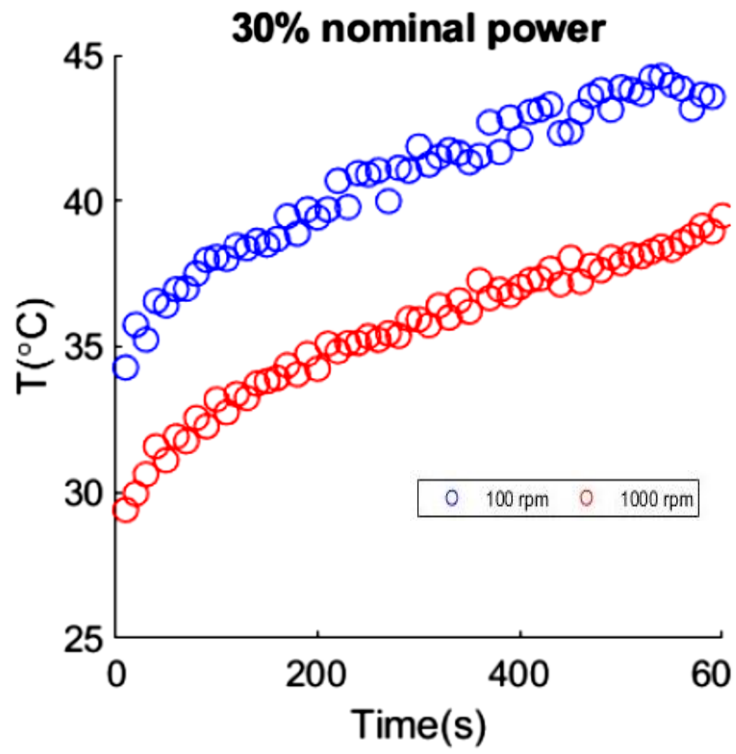
The result for this test clearly exhibits more effective convection at the higher rotational velocity, as theoretically expected. The enlarged gap between two cases of rotational speed gradually shrinks as the heating (i.e. laser) power is intensified; yet, effectiveness of convective cooling, at higher rotational speed is well evident.



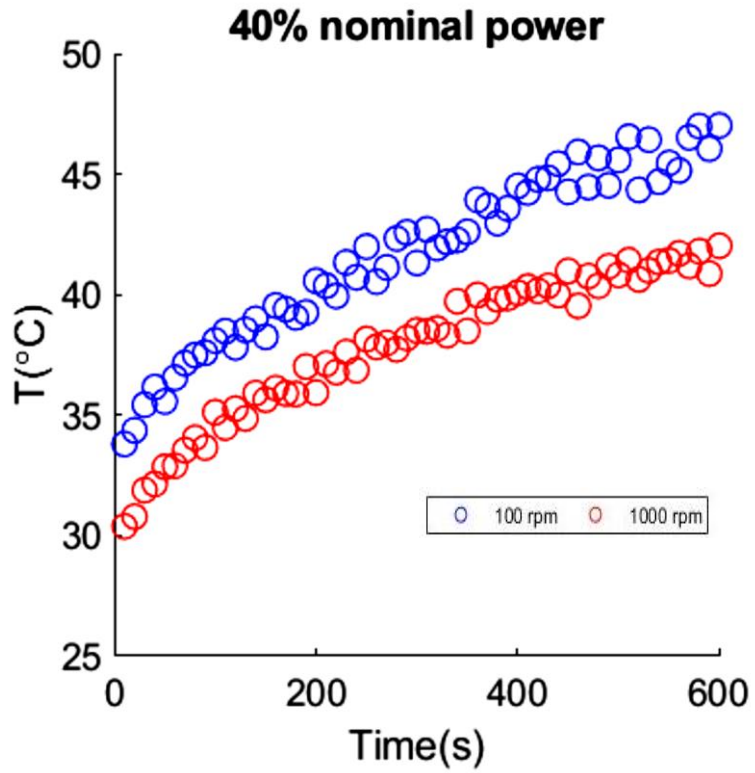
(a)



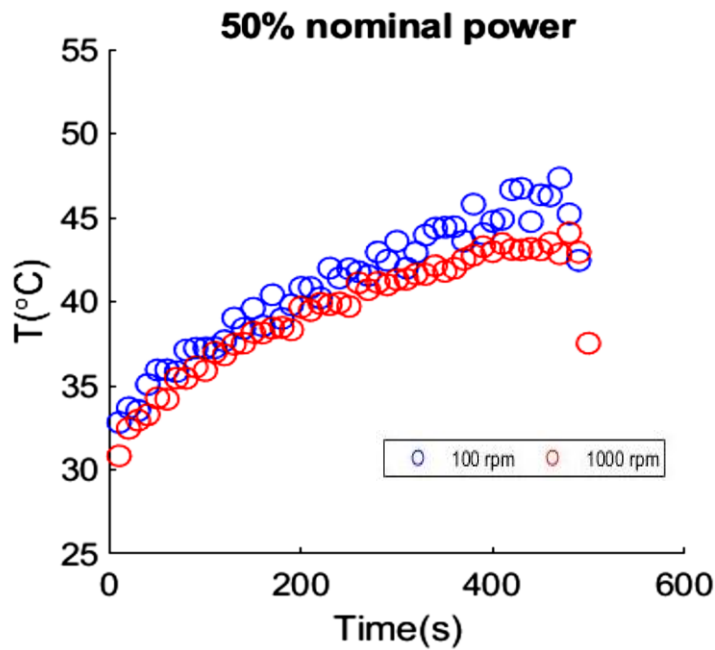
(b)



(c)



(d)



(e)

Figure 4. 17 Comparison of transient surface profile, roughed surface at various rotational speeds

4.3.3 Thermal effect of scanning velocity

To identify the temperatures variation during moving laser beam, Figures (4.18) and (4.19) illustrate the increase and decrease surface temperatures during heating roughed workpiece. Figure 4.18 shows the variation in rotating surface temperature heated by moving a laser beam with different scanning velocities, while, Figure 4.19 illustrates the changes in temperatures during increase rotation speed. From Figure 4.18, it is noted that the curves are shifting to the left, this attributed to shortening the heating course with increased scanning velocity for the laser beam. The temperature decreases with increasing scanning speed due to a decrease in laser projection time, thereby, decreases the amount of heat transferred to the workpiece surface. Moreover, the highest temperatures have been achieved during scanning a laser at speed of 20 mm/min.

Figure 4.19 shows the change in rotating speed has a pronounced effect on increases and decreases of the surface temperatures. The increasing in rotation speed caused decreasing the surface temperature, due to increasing air velocity over the workpiece surface, that way, increase the heat transfer rate (convection heat transfer). Furthermore, it can see that the maximum temperatures have recorded at

the period from the 40 s to 60 s from the time of the entire course of laser scanning. After that, away from laser heating, the temperature has gradually decreased because of the workpiece surface undergoes cooling, which is primarily controlled by surface thermal radiation and rotational heat convection.

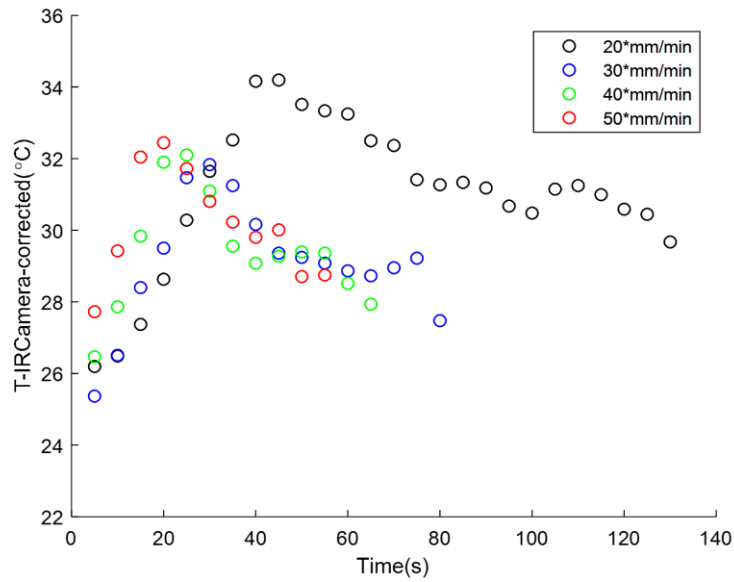


Figure 4. 18 Corrected surface temperatures for sandblaster workpiece heated with moving laser at 100 rpm & 50% W

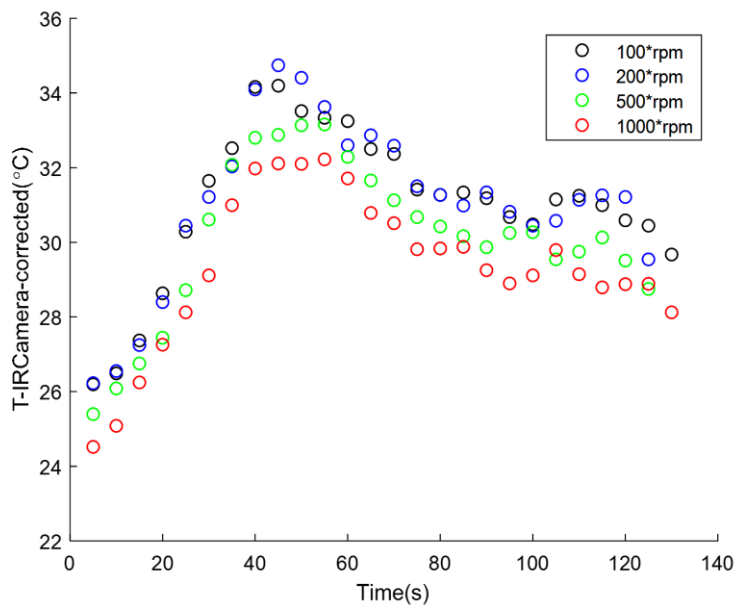


Figure 4. 19 Corrected surface temperatures for sandblaster workpiece heated with moving laser at 20 mm/min & 50% W

The figures (4.5) to (4.10), however, demonstrate the corrected surface temperature behaviour during all three experiments. Comparing with the results of the tests (section 4.3), there is no significant difference can be observed in increasing or decreasing for the temperatures. Which in turn confirms the accuracy of the results obtained from experiments.

4.4 Summary

At instances when the workpiece surface exposed to laser heating, the magnitude of temperature peak is predominantly determined by the combined effect of heat absorption at the heated area and the heat penetration into the Ti-6Al-4V workpiece body. This increase in workpiece surface temperature was observed for both cases heating black-painted surface and rough surface. The transient behaviour of workpiece surface temperatures depicted in Figures (4.12) to (4.15) clearly linked to the operating heat transfer modes. As expected, the surface temperature has increased with increasing the power of the laser beam. The increase in laser power has accompanied with an increase heating time, which have had a positive effect on increasing surface temperatures. From Figure 4.18, it observed that the peak surface temperature decreases with the increased laser traverse velocity. This follows the physical trend as faster laser scanning velocities provide shorter surface exposure to laser heating, thus giving decrease to lower local temperatures. Moreover, the increase in rotating speed has a similar effect of increasing the laser traverse velocity on the peak surface temperature. This follows the physical trend as slower workpiece rotating speed provide a slower air-cooling, thereby, reducing the effect of convection.

Chapter 5

Numerical Simulation Methodology

5.1 Scope of Chapter

A proper understanding of heat transfer phenomena and appropriate prediction of thermal behaviour is a key concern for a wide range of manufacturing processes such as during preheating in LAM processes. Temperature range, in such application, is commonly high enough to originate significant micro-structural influence and cause variation in material properties, machining results and production outcome. As illustrated from the experimental work in the Chapter Three, experimental techniques are not sufficient method for measurement of the thermal and structural parameters, since the experimental accessibility is limited, and variations have a significantly fast rate. Overcoming the current experimental limitations, the current study develops a new three-dimensional numerical model, which is validated against published data. This model is utilised to investigate transient thermal behaviour of the rotating cylindrical workpiece heated by a laser beam as a heating source.

This chapter introduces the theoretical background associated with the research topic and involves the use of ANSYS FLUENT along with finite volume method (FVM), modelling flow in a moving zone and artificial neural network (ANN). The modelling requirements and associated sensitivities are discussed in detail considering parametric variations, followed by validation of the model against the previous experimental data. The thesis's emphasis is on the manifesto of valid numerical modelling. The importance of this 3D model is to obtain not only the surface thermal profile but also the thermal diffusion pattern inside the workpiece, which is crucial for manufacturing and quality assurance. Utilising the thermal computational model (TCM), feasibility and accuracy of the artificial neural network (ANN) model have examined as an alternative to regression. The low-order function fitting (LOFF) tool has been trained by TCM results and allows fast, lower computational resources and accurate thermal mapping.

5.2 Introduction

Review of experimental studies (section 2.7) reveals the thermal behaviour of a rotating workpiece, heated by a laser beam, is influenced by a wide range of parameters such as material properties, operational parameters, and laser characteristics. These parameters are obviously cannot be investigated simultaneously through an empirical procedure. Many studies have been conducted toward the development of reliable analytical models by simplifying the problem at the cost of assuming some thermal and material details as negligible. Numerical modelling study classified and considered as the most versatile, comprehensive and affordable tool of analysis. To achieve an optimised level between accuracy and computational resources, the solver elements and setup must be tested for verification, validation and sensitivity analysis.

The current research applies one of the most robust and reliable discretisation methods for computational analyses, which is a FVM, to estimate thermal conduct of a LAM rotating workpiece. The FVM and Ansys FLUENT as the choice of framework and platform respectively and utilises the model to carry out a thermal analysis. FVM method has been appraised and cited as one of the best schemes for handling conservation equation including energy diffusion with embedded heat sources. More specifically to the current application, a rotation of the field could be well simulated by application of single rotating reference frame (SRRF) for a sole diffusion heat transfer problem through a solid medium. The sole thermal diffusion is sufficient to emulate physics of the three-dimensional solid zone of solution whereas combined thermal boundary condition (i.e. convective and radiative cooling) requires a more complex temperature dependent formulation. Beyond numerical accuracy and robustness, Ansys FLUENT is utilised for the ease of implementation, compatibility of the solver with other multi-physics platforms (e.g. FEA modules for thermos-structural behaviours) and versatility of the applied code for essential customisation are the other anticipated benefits from the package.

In the next sections, the modelling requirements and associated sensitivity are discussed in details and followed by performing validation against experimental measurement in various locations, laser power, and rotational velocities.

5.3 Numerical Method

The several of numerical methodologies, mentioned earlier in the literature, portrays the wide range of options available to be adopted based on the computational needs and level of physical details to be considered. Among them, the current analysis favours the Computational fluid dynamics technology. Computational fluid dynamics (CFD) software is a group of numerical methods utilised to acquire approximate solutions of fluid dynamics problems involving heat-transfer, fluid flow and associated phenomena like chemical reactions. This numerical method is highly-scalable, allowing for effective parallel calculations on many of processing cores. Table (5.1) shows the advantages and disadvantages of the possible methods to study any single engineering problem, espial in thermo-fluids and heat transfer fields.

Use of ANSYS package enable investigation of thermal stresses on an integrated platform coupled with CFD results. Moreover, this software has ability to study large systems with extensive detail of results, which are difficult or impossible to use analytical or experimental approach. According to that, since the 1990s, CFD has been increasingly used as a vital component in the simulation of industrial processes and products (246). The numerical algorithms are applied in CFD software packages which are used to tackle heat transfer and fluid flow problems. These codes include three major elements namely: (1) A pre-processor, (2) A solver, and (3) A post-processor. It can access to these three elements from WORKBENCH of Ansys software. Thus, the user of this software has a wide range of choices to determine the level of detail obtained in the result. However, the results of CFD need to be validated against third party results.

Through the element “Pre-Processor”, the geometry of the domain is defined and sub-divisions of interest domain are meshed into cells of various types[control volumes (CVs)] (247). Additionally, the domain boundary and appropriate boundary conditions are specified to ensure realistic simulation of the physics. While the element “solver” supports integrating the governing equations over the field all the CVs of domain. That means the CFD codes have ability to predict and estimate the transport behaviour of a certain scalar by balancing convection, diffusion and the rate of change over the time with the source terms. The third

element “Post-Processing” is visualise the quantitative results in form of illustrative graphics such as 2D and 3D surface plots, vector plots, colour postscript output (247). Moreover, Post-Processor has animation facilities for dynamic result display and data export facilities for further manipulation.

Table 5. 1 The comparison between three styles of the study

	Experimental	Analytical	CFD
Advantages	<ul style="list-style-type: none"> - More realistic - Allows complex problems and cases 	<ul style="list-style-type: none"> - Simple application - General validity - Understanding and interpretation of phenomena 	<ul style="list-style-type: none"> - Not limited to linear cases - Allows complex problems - Stationary and non-stationary - Relatively affordable cost - Integration in the project chain
Disadvantages	<ul style="list-style-type: none"> - Need for instrumentation - Scale effects - Difficulty in measurements of perturbations - Operational Costs 	<ul style="list-style-type: none"> - Limited to simple cases - Typically linear problems 	<ul style="list-style-type: none"> - Errors: discretization, truncation - Difficulty in boundary conditions - Simplifications needed - Time for setup & run - Difficult interpretation

5.4 Ansys FLUENT

Ansys FLUENT software is one of the most popular CFD solvers, enabling the valid and efficient thermos-fluid optimization. FLUENT is the preeminent tool for fluid flow analysis, and it is integrated into Ansys-Workbench which promotes multi-physics simulations. Workbench is a platform to interconnect and synchronise various numerical simulators such as CFD and FEA solvers. This software contains well-validated physical modelling capabilities to deliver fast, accurate results across the widest range of CFD and multi-physics application (248). It has ability to simulate reliable physical cases for industrial applications, such as turbulent flows, heat transfer, multiphase flows, chemical mixing, and reaction flows. In addition,

FLUENT offers a wide range of numerical and discretisation schemes and user-defined boundary conditions which has been advantageous to the current problem. In this software pack, FVM is utilised in solving process through using solution-adaptation of the mesh. The graphic results of Ansys FLUENT of CFD illustrates how fluid and particle flow, heat transfer, chemical reactions, combustion, and other parameters evolve with time.

5.4.1 FLUENT setup stages

The process of setting up a simulation in FLUENT complies with the general workflow of CFD analysis and could be briefed into:

1- Step One: Pre-Processor

- a. **Pre-analysis:** preparing boundary condition to represent the actual case (system) under the study. Also, collecting corresponding theoretical or experimental results for comparison.
- b. **Geometry:** making the geometry by using Ansys design modeler from Workbench or any other computer aided design software, like AutoCAD, SolidWorks, CATIA, AutoCAD Inventor etc.
- c. **Meshing:** discretising the domain into a finite number of cells. The simulation outputs depend on Mesh type (high quality Mesh can produce accurate simulation results).

2- Step Two: Solver

- a. **Physical Setup:** understanding and performing physical setup through giving inputs for solution accuracy, such as boundary condition, material physics properties of involved, etc.

3- Step Three: Post-Processing

- a. **Numerical Solution:** analysing the simulation results and data.
- b. **Verification & Validation:** checking whether the laws of basic physical are maintained or not, for instance, does simulation solution satisfy transport energy equation.

5.5 Finite Volume Method (FVM)

The FVM is a method for representing and evaluating coupled non-linear partial differential equations in the form of algebraic equations. This method is one of the developed numerical solution techniques that is used in computational fluid

dynamics packages. The “Finite volume” is referred to the small volume surrounding each node point on a mesh and the way discrete form of equations are derived. Similar to the finite difference method (FDM) or finite element method (FEM), the physical domain is discretised into a number of contiguous cells (control volumes) defined by a numerical grid. The principle advantage of the FVM is that it ensures conservation of variables over each discrete cell, rather than over the global domain as is the case with the FEM, in which a functional form of the governing equations is minimised over the entire domain (249). The summary of the advantages and disadvantages of a numerical methods (FDM, FEM, FVM) that mostly used to analyse engineering and industrial problems were listed in Table (5.2).

Table 5. 2 The advantages and disadvantages of three numerical methods

	FDM	FEM	FVM
Advantages	<ul style="list-style-type: none"> - Relatively easy implementation - Good results and efficiency on simple geometries - Several high-order schemes available 	<ul style="list-style-type: none"> - Integral formulation: valid for shocks and discontinuities - Flexible for complex geometries - Straightforward high-order - Very rigorous mathematical foundation 	<ul style="list-style-type: none"> - Directly apply the integral spatial discretization in the physical space (no coordinate transformation to a computational space) - Flexible for complex geometries: both structured and un-structured meshes - Mass, momentum and energy are conserved by definition
Disadvantages	<ul style="list-style-type: none"> - Generally limited to structured meshes - Conservation property is not guaranteed in general - For non-uniform grids, a coordinate transformation to the “computational space” has to be considered and discretised 	<ul style="list-style-type: none"> - Higher computational effort - Conservation not always guaranteed 	<ul style="list-style-type: none"> - Historically, less developed mathematical framework - More difficult to attain high-order accuracy, especially for unstructured meshes

General equations of conservation (transport) for mass, momentum, energy, species etc., are solved on this set of CVs. In FVM, the volume integrals in a partial differential equation that contain a various term are converted to surface integrals. This means the governing equations are integrated over each of these cells; the terms appearing after integration are then approximated with finite-difference type schemes. Then, these terms are evaluated as fluxes at the surfaces of each finite volume. The result of this discretization process is a system of (N) algebraic equations, where N is the number of discrete cells, which are solved using the different theorem.

The FVM is based on integral conservation law rather than partial differential equation. The integral conservation law is precise enough for small CVs. The governing equation of steady diffusion can easily be derived from the general transport equation of the property ϕ by assuming the transient and terms to be zero. The CV integration, which determines of the final FVM formulations distinguishes it from all other CFD techniques, gives the following equation (250):

$$\int_{CV} \text{div}(\Gamma \text{grad } \phi) dV + \int_{CV} S_{\phi} dV = \int_A n \cdot (\Gamma \text{grad } \phi) dA + \int_{CV} S_{\phi} dV = 0 \quad (5.1)$$

Consider the steady state diffusion of property ϕ in a three-dimensional domain. The process is governed by the following form (250):

$$\frac{\partial}{\partial x} (\Gamma \frac{\partial \phi}{\partial x}) + \frac{\partial}{\partial y} (\Gamma \frac{\partial \phi}{\partial y}) + \frac{\partial}{\partial z} (\Gamma \frac{\partial \phi}{\partial z}) + S_{\phi} = 0 \quad (5.2)$$

The CV including node G has six neighbouring nodes specified as west, east, south, north, bottom, and top (W, E, S, N, B, T), see Figure 5.1. The notations (w, e, s, n, b, t) are utilised to indicate to the west, east, south, north, bottom and top cell faces respectively. There are three steps in FVM, as follow (250, 251):

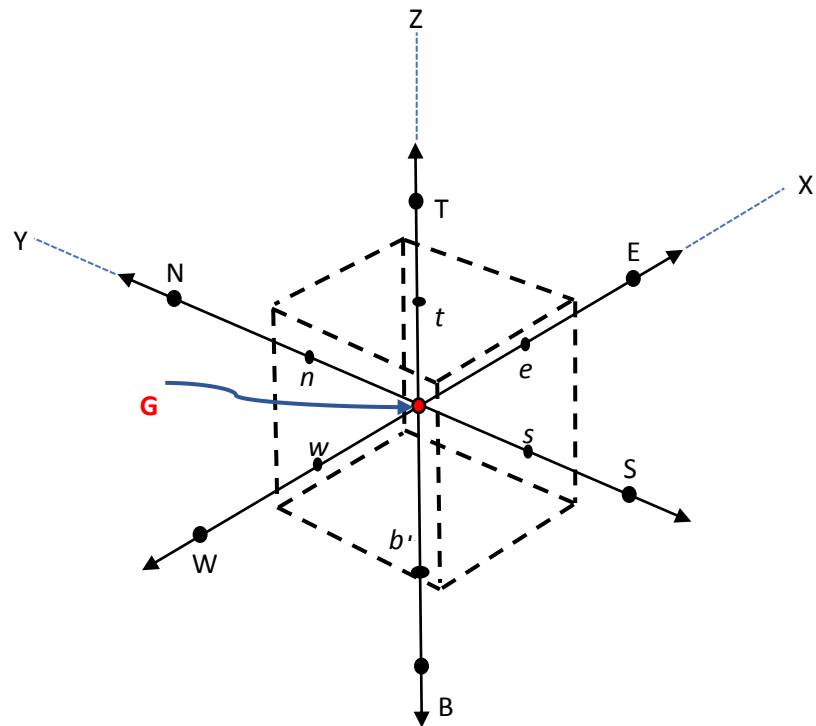


Figure 5. 1 A typical CV and neighbouring nodes

The first step: Grid generation

This step involved dividing the domain through placing a number of nodal points; each node is surrounded by a control volume or cell. The faces (or boundaries) of CVs are positioned mid-way between adjacent nodes. Commonly, it is set up CVs near the edge of the domain in such a way that the physical boundaries coincide with the CV boundaries.

The second step: Discretisation

This step represents the key of the FVM. In this step, the governing equations (Equation 5.2) are integrated over CVs to produce the equation of discretised at its nodal point G. The general discretised equation (Equation 5.3) is a very attractive feature in FVM because it gives an obvious physical interpretation. This equation constitutes a balance equation for ϕ over the CV, which is mean the diffusive flux of

ϕ leaving the east face minus the diffusive flux of ϕ entering the west face is equal to the generation of ϕ .

$$[\Gamma_e A_e \frac{(\phi_E - \phi_P)}{\delta x_{PE}} - \Gamma_w A_w \frac{(\phi_P - \phi_W)}{\delta x_{WP}}] + [\Gamma_n A_n \frac{(\phi_N - \phi_P)}{\delta y_{PN}} - \Gamma_s A_s \frac{(\phi_P - \phi_S)}{\delta y_{SP}}] + [\Gamma_t A_t \frac{(\phi_T - \phi_P)}{\delta z_{PT}} - \Gamma_b A_b \frac{(\phi_P - \phi_B)}{\delta z_{BP}}] + (S_u + S_P \phi_P) = 0 \quad (5.3)$$

The third step: Solution of equations

Two types of solution techniques are used to solve the linear algebraic equations are (i) Direct Methods and (ii) Indirect (Iterative) Method.

From a general transport equation (Equation 5.4), the steady convection – diffusion equation can be derived for a general property ϕ as.

$$div(\rho \phi u) = div(\Gamma grad \phi) + S_\phi \quad (5.4)$$

Integration over a CV gives equation of the flux balance in a CV:

$$\int_A n \cdot (\rho \phi u) dA = \int_A n \cdot (\Gamma grad \phi) dA + \int_{CV} S_\phi dV \quad (5.5)$$

The calculation of transported property ϕ is the essential problem in the convective discretisation terms at CV faces and its convective flux across these boundaries.

5.6 Properties of Discretization Schemes

In most heat transfer problems, the truncation error of central differencing could be a potential issue and should be considered when deciding the discretisation schemes.

Theoretically, numerical results should be accurate solution of the transport equation when number of computational cells is infinitely large, regardless of the applied discretisation method. However, as fundamental properties of discretisation scheme, only a finite (sometimes extremely small) number of cells is utilised. This means that conservative solutions can be obtained on relatively coarse numerical grids. The use of coarse grids will however introduce numerical errors which will reduce the accuracy of the simulation. In general, there are three requirements for a differencing scheme (248, 250):

- Conservativeness
- Boundedness
- Transportiveness

5.6.1 Conservative

The integration over a finite number of CVs for the convection-diffusion equation produces equations set of discretised conservation involving fluxes of the transported property ϕ through CV faces. The flux out of a CV should be the same as that into the neighbour CV to ensure the conservation of ϕ for the entire solution domain, for instance the flux out of cell i through its face e should be the same as that into cell $i + 1$ through its face w).

5.6.2 Bounded

The absence of sources the internal nodal values of property ϕ should be bounded by its boundary values. For the east face, for instance, this means that temperature (T_e) must not be smaller (or larger) than cell values used to compute T_e . It is satisfied if all coefficients are positive. Furthermore, another essential requirement, all coefficients of the discretised equations should have the same sign which is usually all positive. Thus, this implies (physically) that an increase in the variable ϕ at one node should result in an increase in ϕ at neighbouring nodes. If the scheme of discretisation not satisfies, the boundedness requirements it is possible that the solution will not converge at all, or, if it is, that it contains wiggles.

5.6.3 Transportive

The transportive property of a fluid flow is clarified through considering the effect at a point (G) due to two constant sources of ϕ at nearby points (W) and (E) on either side. Also, the scheme should reflect the method information is transported. The method information is transported through face (e), for instance, is dependent on the ratio between convection and diffusion the Peclet number $Pe_e = (\rho U \delta x / \Gamma)_e$.

5.7 Discretization

There are many solution methods in CFD software to solve the steady convection-diffusion equation. Several of the utilised methods such as upwind scheme, hybrid scheme, power-law scheme, and QUICK scheme are the central differencing scheme. The accuracy of upwind and hybrid schemes is only first-order in terms of Taylor series truncation error. The upwind schemes are quite stable and comply the transportiveness requirement, however, the first-order accuracy makes them prone to numerical diffusion errors. The number of these errors can be minimised by employing higher-order of discretisation. This is due to the many neighbour points engaged together in schemes have higher-order, which are produced reducing discretisation errors by bringing in wider impact. The central differencing scheme has second-order accuracy, and proved to be unstable and does not have the transportiveness property. Formulations that do not take into account the flow direction are unstable and, therefore, more accurate schemes of higher-order, which preserve upwinding for stability and sensitivity to the direction of flow, are needed. Every simulation presented in this Thesis used the QUICK discretization scheme for thermal diffusion in a rotational frame. More detail on this scheme, which used in the present work, is given in the following sections.

5.8 Quadratic Upwind Interpolation for Convection Kinematics Scheme

The quadratic upwind interpolation for convection kinematics (QUICK) scheme is a method used in numerical methods in CFD for convection-diffusion problems. It is denoting as one of the simplest and most stable discretization methods for solving hyperbolic partial differential equations. However, this scheme is more dissipative

against the simulated stream. The upwind scheme was first proposed by Brian P. Leonard together with the QUICKEST (QUICK with Estimated Streaming Terms) scheme in 1979 (252). QUICK is presented the transportiveness property as a higher order differencing scheme with numerical diffusion reduced to minimum. Basically, it uses the values upstream to evaluate the property on the boundaries of the cell and then use them to compute the value at the centre of the cell. This scheme assumes a quadratic upwind interpolation for the face value of the scalar variable by assuming a second order polynomial (parabola) through the downstream, upstream and one node further upstream nodes of the cell face in question. A second order polynomial is fitted through W, P and E (Figure 5.2).

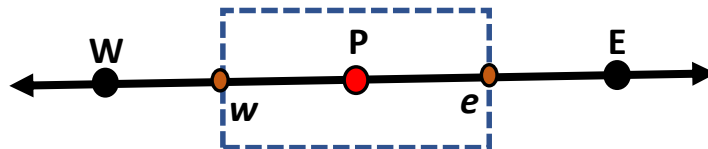


Figure 5. 2 CV used in the QUICK scheme

$$T(x) = ax^2 + bx + c \quad (5.6)$$

The conditions below are used to determine the coefficients a, b and c. So that at e :

$$T_{(x = 1.5 \delta x)} \equiv T_e = (3/4)T_P + (3/8)T_E - (1/8)T_W \quad (5.7)$$

This approved that QUICK scheme is third-order accurate and unbounded scheme because it takes the second-order derivative into account and disregards the third-order derivative. The QUICK scheme is used to solve the equations of convection-diffusion, using the second-order central variation for the diffusion term and the convection term, the scheme is third-order accurate in space and first-order accurate in time. Moreover, this scheme is most appropriate for steady flow or quasi-steady

highly convective elliptic. The QUICK scheme displays increased accuracy when compared to the upwind scheme due to the higher order truncation error (253, 254). The main disadvantage of the QUICK scheme, however, is that it can become unbounded – particularly when the source term variation, and hence the variation of T , is large.

5.9 Modelling Flow in Moving Zone

As mentioned before in this chapter, Ansys FLUENT solves the fluid flow equations and heat transfer, by default, in a fixed reference frame. However, there are many problems where it is required to solve the equations in a moving reference frame. Typically, a wide range of engineering cases include non-stationary objects such as rotating blades, impellers, and similar types of moving surface, and it is the flow around these non-stationary parts that are of interest. In many problems, the moving objects render the problem unsteady when viewed from the stationary frame. With moving reference frame, however, the flow around the moving object can be modeled with specific limitations as a steady-state problem with respect to the non-stationary frame.

The modelling capability of moving reference frame in Ansys FLUENT allows the user to model different problems, including moving objects by allowing a user to activate moving frames in selected cell zones. When a moving reference frame has activated, the motion equations are modified to incorporate the additional acceleration terms. These additional terms occur due to the transformation from the stationary to the moving reference frame. The fluid flow around a moving object can be modeled through solving the motion equations in a steady-state manner. In moving reference frames, the solution of flows is required the use of moving cell zones. The motion of these cell zones is explained as the reference frame motion to which the cell zone is attached. With this capability, many different cases that involve moving parts can be setup and solved using FLUENT. In Ansys FLUENT, the capability of moving cell zones provides a powerful set of features for solving problems in which the domain or parts of the domain are in motion. There are two kinds of flow problems that can address as following:

- Thermo-Flow problems in a single rotating reference frame.
- Thermo-Flow problems in multiple rotating and/or translating reference frames

For many problems, it may be possible to refer the entire computational domain to a single moving reference frame. This is known as the single reference rotating frame (SRRF) approach (255). The benefit of using the SRRF approach is provided the geometry meets specific requirements. However, it may not be possible to utilise an SRRF for more complex geometries or multi-stage rotational behaviours. In such conditions, the designer breaks up the problem into multiple cell zones, with well-defined interfaces between the zones. In this class of problem, the manner of treating the interfaces leads to two steady-state modelling methods namely, the multiple reference frame (MRF) approach and the mixing plane approach. The essential reason to use a moving reference frame is the problem of unsteady in the stationary (inertial) frame steady with respect to the moving frame. For constant rotational speed case (steadily rotating frame), the transformation a fluid motion equations to the rotating frame such that steady-state solutions will be possible. However, in case of not constant rotational speed, additional terms have included in the transformed equation which is not included in Ansys FLUENT formulation. Thus, it is obligatory to work an unsteady simulation in a moving reference frame with constant rotational speed.

As illustrated in Figure 5.3, consider a coordinate system which is rotating steadily with rotation speed $\vec{\omega}$ relative to a stationary (inertial) reference frame. The origin of the rotating system is situated by a position vector \vec{r}_o . The rotation axis is defined by a unit direction vector \hat{a} such that:

$$\vec{\omega} = \omega \hat{a} \quad (5.8)$$

The computational domain for the CFD problem is defined with respect to the rotating frame such that an arbitrary point in the CFD domain is located by a position vector \vec{r} from the origin of the rotating frame (see Figure 5.3). Moreover, the fluid velocities can be transformed from the non-moving frame to the rotating frame using equation (5.9):

$$\vec{v}_r = \vec{v} - \vec{u}_r \quad (5.9)$$

where: $\vec{u}_r = \vec{\omega} \times \vec{r}$

In the above equation, \vec{v}_r is the relative velocity (the velocity viewed from the rotating frame), \vec{v} is the absolute velocity (the velocity viewed from the stationary frame), and \vec{u}_r is the “whirl” velocity (the velocity due to the moving frame).

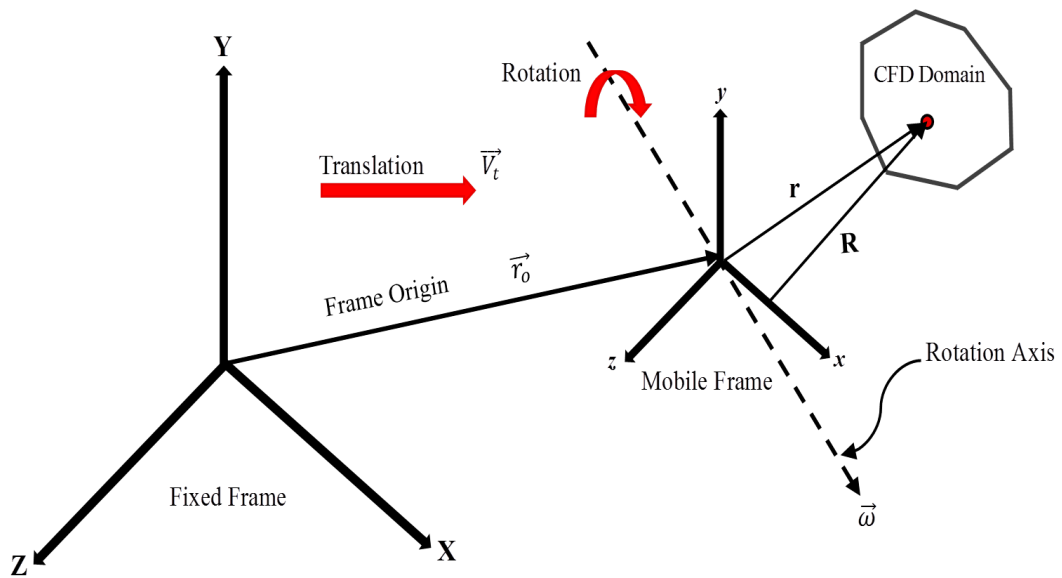


Figure 5. 3 Stationary and Rotating Reference Frames

There are two exact forms of the governing equations, formulated according to relative velocity and absolute velocity as illustrated in equations (5.10) & (5.11), respectively (255).

$$\frac{\partial}{\partial t}(\rho E_r) + \nabla \cdot (\rho \vec{v}_r H_r) = \nabla \cdot (k \nabla T + \vec{\tau}_r \cdot \vec{v}_r) + S_h \quad (5.10)$$

$$\frac{\partial}{\partial t} \rho E + \nabla \cdot (\rho \vec{v}_r H + p \vec{u}_r) = \nabla \cdot (k \nabla T + \vec{\tau} \cdot \vec{v}) + S_h \quad (5.11)$$

5.10 Single Rotating Reference Frame (SRRF)

The SRRF option can be used to model flows of many problems which involve rotating components such as turbo-machinery, mixing tanks, and related devices. In each of these cases, the flow field is unsteady in an inertial frame (i.e., a domain fixed in the laboratory frame) because the rotor / impeller blades sweep the domain periodically. SRRF is used to convert unsteady flow to steady with respect to the moving frame. This moving reference frame is associated with a single fluid domain. FLUENT has the ability to model flows in a non-accelerating and an accelerating reference frame. There are many types of flows can be modeled in a coordinate system that is moving with the rotating objects and thus experiences a constant acceleration in the radial orientation. When some problems are defined in a rotating reference frame, the rotating boundaries become non-moving relative to the rotating frame, since they are moving at the same speed as the reference frame.

Particularly, there are some requirements must the surface boundaries adhere to it:

- Any moving surfaces with the reference frame can assume any shape, for instance, the blade surfaces associated with a pump impeller. Further, on the moving surfaces, the no-slip condition is located in the relative frame such that the relative velocity is zero.
- Surfaces are non-moving with respect to the stationary coordinate system can be defined, however, these surfaces must be surfaces of revolution about the rotation axis. Here the so slip condition is defined such that the absolute velocity is zero on the walls. An example of this type of boundary would be a cylindrical wind tunnel wall which surrounds a rotating propeller.

5.11 Numerical Model Geometrical Configuration and Boundary Conditions

The preheating process of LAM commonly consists of a cylindrical rotating workpiece which is heated by a laser beam, moving along the workpiece. Figure 5.4 schematically shows such typical configuration of laser preheating process in advance of the cutting process (without having cutting tools applied). This modelling configuration is used as a benchmark for evaluation of the current numerical model. In this configuration, the solid cylinder rotates at angular speed (ω) while the surface being heated at spot by laser beam that traverses at velocity

(V_t) along the cylinder axis. To allow model validation the modelling parameters of laser properties, cylinder dimensions, cutting variable and locations of temperature recording are chosen according to those of a previous experimental study (184). The three temperature recording locations (P_1 , P_2 and P_3) are evenly distanced along a surface line which is radially located 67.7° CCW of the laser transverse line. The initial temperature of workpiece is assumed to be uniform and equal to the ambient temperature.

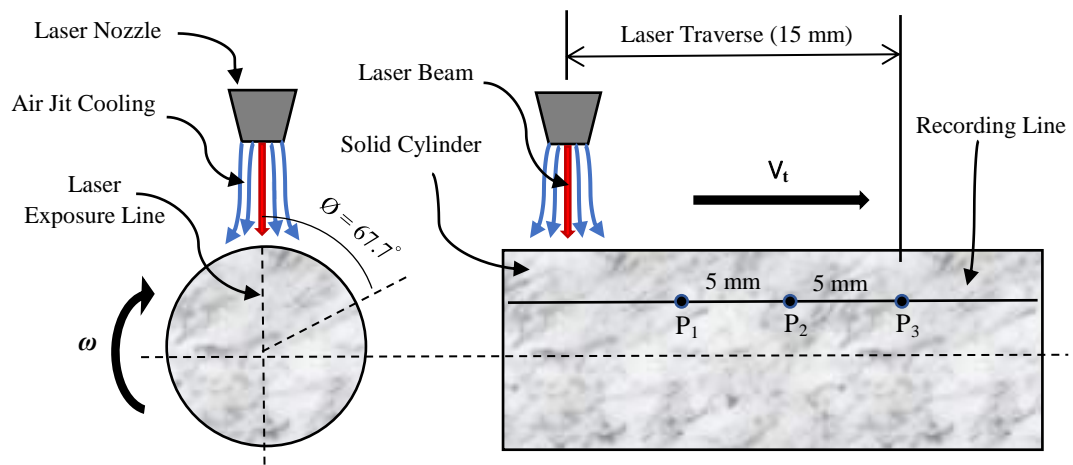


Figure 5. 4 Schematic of laser assisted pre-heating configuration, applied for numerical model

This problem has various numerical and physical sensitivity issues that are crucial for obtaining valid results. A combined workpiece rotation and the laser transverse motion impart a unique fluctuating temperature profile that propagates into the material of workpiece. The intensity of this thermal penetration dictates the potential degree of ‘thermal softening’ (or increased ductility) achievable in the workpiece, facilitating enhanced LAM process. As the intended purpose, the numerical model is set up only to inspect the requirements of laser preheating technique for appraising the material softening potential in preparation for the subsequent machining operation. Hence, the heat generated from cutting operation is not included in the current study, allowing the examination of preheating thermal behaviour in isolation of the cutting tool integration. In addition, as illustrated in Figure 5.4, an air jet impingement system is incorporated in the simulation modelling to regulate

excessive local temperature build-up in the vicinity of the laser projection area. In the subsequent thermal process, the numerical modelling accounts for the radiative heat absorption over the laser spot, the combined convective and radiative surface heat losses from the entire surface of the workpiece and the cooling effect from jet impingement.

5.12 Governing Equations of Heat Transfer

The computational domain is restricted to the rotating cylinder whereas the surface heat dissipation is deemed as boundary conditions and hence the advection term is eliminated from energy equation. The rotating cylinder locally absorbs heat through the laser exposure area and overlay losses heat through convection and radiation mechanisms. The configuration of solution field and boundaries indicate dependency of all three mechanisms and their associated parameters (e.g. heat transfer coefficient and emissivity) to the surface temperature. This sets a unique scenario where the transient behaviour of boundaries and their conditions are more complicated than heat diffusion in a rotating domain. Therefore, the model consists of a diffusion equation, in SRF, to solve a three-dimensional equation of conduction in a solid domain as shown in equation below:

$$\frac{\partial}{\partial t} \rho h + \nabla \cdot (\vec{\omega} \times \vec{r}) \rho h = \nabla \cdot k \nabla T + S_h \quad (5.12)$$

Where $\vec{\omega}$ and \vec{r} represent rotational velocity and distance from the axis of rotation respectively. Source term of S_h accounts for the laser heating which is incorporated as an energy source term (defined within laser exposure area). Measurements, used for validation, recorded temperature variation up to 1200 K and hence, estimation of material properties as function of temperature could potentially be critical to the accuracy of predictions. Utilising Equation 5.12 to determine three-dimensional, transient thermal diffusion, the laser exposure closure, surface convection and radiation are other key elements of the current model to be determined.

5.12.1 Heating by Laser Beam

Laser exposure is modelled by incorporating a volumetric heat generation source within the laser point area, projected on the rotating circumferential area of the cylinder. The curved rotating boundary is considered as a wall with non-zero thickness which enables implementation of heating condition as a volumetric source term, beneficial to the solution stability and convergence. Mean intensity of heat generation rate in is correlated as laser power divided by total area of exposure. The nominal laser power, measured at laser device, indicates energy level of the laser beam as departing the source. Nevertheless, loss of energy is inevitable through the process of laser transmission and accordingly a percentage of dispatched energy would be delivered to the rotating surface. The loss of source energy is accounted by a defined transition coefficient (C_T) which is calibrated empirically. Equation 5.13 represents the function of laser heat flux, applied on laser exposure area as:

$$\dot{Q}_L = \frac{C_T P \alpha}{A_{Exposure}} f\left(\frac{r}{R}\right) \quad (5.13)$$

Laser initial power is transmitted (C_T) and absorbed (α) through the area of laser pointer projected on the cylinder surface ($A_{Exposure}$) where $f\left(\frac{r}{R}\right)$ determines the laser intensity profile and found to have a remarkable influence on the thermal response. There are three types of laser power profiles, uniform, linear and exponential distributions, have been examined. The resulted transient temperature profiles are compared with experimental measurements to estimate the effectiveness and select the most accurate function. Figure 5.5 illustrates profiles of these three distribution functions with some adjustments of the range for enhanced visualisation.

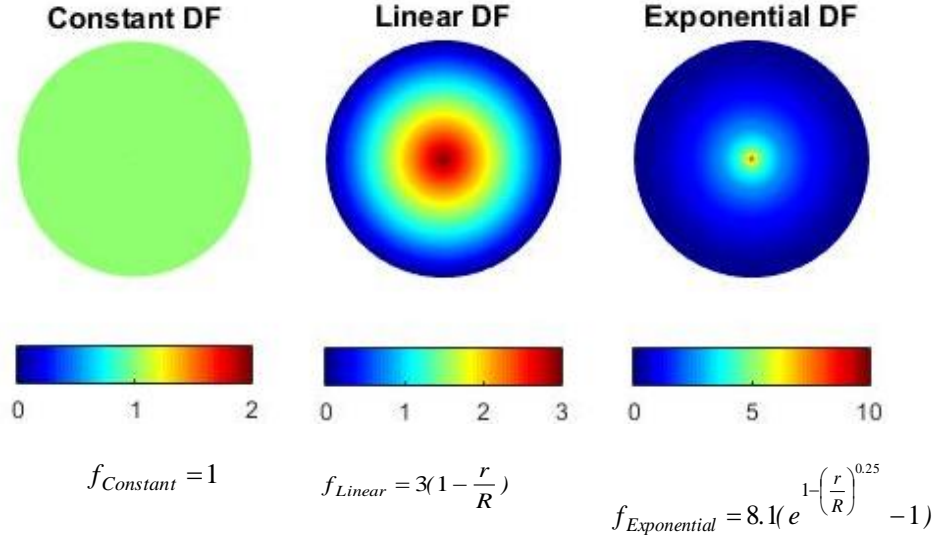


Figure 5. 5 Evaluation laser distribution functions for 3D numerical model

Formula and constants of all three functions are determined to generate required profile while maintaining area integral-averaged value of heat flux equal same as mean value (i.e. $\frac{\int_A f dA}{A} = 1$).

5.12.2 Convective Heat Fluxes

To simulate experimental conditions, three major convective streams of laser jet cooling, convective losses from circumferential surface and convective losses from flat surfaces (located at two ends) of the cylinder are considered. The jet cooling is an air impingement exposed to a small area, almost overlapped with laser projection vicinity. The cooling effect of this air jet, at given as conditions of $Re_j=15,900$ and $H/D=10$, was estimated as $h_j=3200 \text{ W/m}^2\text{K}$, using empirical correlation proposed by El-Genk et al. (256). The loss from the circumferential area of rotating cylinder has the largest value amongst convective streams. Owing to sensitivity of the model to this term, Grashof number is determined locally (with reference to a film and surface temperature) and used for local estimation of convective heat transfer coefficient. Considering the geometry and range of operational parameters, heat transfer coefficient, in circumferential area of the cylinder, is determined as below (257):

$$h_{rc} = 0.135 \frac{k}{D} \sqrt{(0.5 Re_\omega^2 + Gr) Pr} \quad (5.14)$$

Convective stream from end planes is considered as loss from rotating disks, which could be determined from Equation 5.15:

$$h_{rd} = 0.36 \sqrt{\frac{\omega D^2}{\nu}} \quad (5.15)$$

Schemes applied for convection losses are empirical (having alternative closures) which could be replaced according to the range of operating parameters (mostly decided by Re_ω). Properties of air, required for calculation of heat transfer coefficient, are estimated with reference to the locally estimated film temperature assuming the ambient temperature to be constant at 300 K.

5.12.3 Radiative Heat Fluxes

The contribution of radiation in heat transfer process, under the given conditions, is significant and requires certain physical and numerical consideration to be accurately modelled. Equation 4.16 is the common expression of radiative heat flux where shape factor is assumed to be one for each boundary cell. This assumption is valid as the boundaries have cubic cells with square differential faces.

$$\dot{Q}_R = \sigma \varepsilon_T (T_w^4 - T_{ambient}^4) \quad (5.16)$$

The main physical concern to be considered in radiation scheme is the dependency of emissivity to the material temperature (assuming constant surface characteristics), as this property could be severely affected across the high-temperature variation range. The measurement of emissivity through pyrometer tests indicates maximum uncertainty of 15% (mostly in high temperature) for silicon nitride, as the material applied for the current test and validation practice. To implement Equation 5.16 as a dynamically adjusting boundary condition (combined with other implemented modes) face values are to be used as wall temperature (T_w) while ambient temperature is constant at 300K.

5.13 Modelling Design Considerations

The numerical simulation is required to study transient thermal behaviour of a rotating cylindrical workpiece heated by a laser beam and exposed to the air as a coolant. To achieve a converging, stable and valid simulation, the developed 3D model needs to conform to some critical setting requirement. Despite the exclusion of advection term, the transport equation is theoretically prone to unboundedness and truncation error. The numerical instability has been prominently observed for the cases of implementing a low-order discretisation scheme (e.g. first order upwind) or insufficient mesh refinement. This could be related to the large spatial and temporal gradients across the domain which in some extreme cases push the solver into a fast divergence.

5.13.1 Grid generation

The meshing strategy is set according to general and specific requirements. The first general requirement is to ensure the meshing resolution is high enough to minimise mesh-oriented truncation error and results are physically reliable. Such resolution varies according to the intensity of operating parameters (e.g. heat flux and temperature gradient) and hence mesh uniformity would be the second general requirement. Uniformity of the grid is evaluated by aspect ratio and skewness factor which both are ideally desired to be close to one.

Besides, the specific requirements related to the physics and operations of rotational cylinder heated with a laser beam could be briefed to:

- 1) The small surface area, which is heated by the laser beam (all the investigated cases have laser diameter smaller than 4mm), is crucially important and enough surface resolution is necessary to capture accurate heat source,
- 2) Temperature gradient toward the surface is larger and insufficient refinement leads to divergence, high Courant number (for a given time resolution) and physically incorrect results,

- 3) Mesh resolution in radial direction also needs to be examined for each case to ensure transient thermal exchange is not missed over spatial and/or temporal discretisation,
- 4) Toward the cylinder core gradients are reduced and it would be possible to gradually reduce mesh density to optimise computational resources.

Grid generation is initially set by global estimation of relative truncation error (as the function of average grid spacing) and accordingly, the further refinement was applied on boundaries. Sufficient resolution is essential in boundaries to effectively and smoothly incorporate the laser intensity profile and convection loss across the curved boundary. Presence of a large energy source within a small area of boundary also implies high spatial temperature gradient. To avoid the mesh-oriented nonlinearity, in such high temperature gradient and rotating zone, the radial resolution should also be refined toward the curved surface. The growth rate is applied across five layers of cells arriving in courser core cells, to ensure a smooth transition across the mesh. The sensitivity originated by the ratio of angular mesh resolution and rotational velocity has also been taken into account as a temporal criterion of grid generation and refinement was applied to have not less than 1-degree angular refinement and (0.1 mm) within laser motion course. The final mesh consists of 858,231 hexagonal cells. Temporal refinement of (0.01 s for the first set of results) is applied for the current set of cases which is robust enough, even for the maximum Courant number (based on heat flux estimations), since an implicit time scheme is utilised. QUICK formulation is used for spatial discretisation of energy equation to be used with a second order implicit temporal discretisation. Application of discretisation scheme with higher than first order accuracy is necessary for both convergence and validity.

5.14 Results of Numerical Model

The SRRF method with FVM model is used to simulate the transient thermal behaviour of a heated, rotating workpiece as is locally heated by a laser beam. Scenarios have been set up according to the dimensions described in Figure (5.4) and material properties of Silicon-Nitride ($\rho= 3440 \text{ kg/m}^3$, $C_p=110 \text{ J/kg.K}$, $k=15$

W/m.K). Additionally, the operating parameters have been set according to the experimental benchmark (184).

Figure (5.6) illustrates the thermal response of a rotating cylinder heated by a laser beam with given characteristics. Temperature contours are illustrated on the circumferential surface and inside the rotating cylinder, at three-time steps. This visualisation assists to interpret the transient thermal field and also highlights the benefit of utilising a full-scale numerical model, as compared to experimental measurement. As a prime advantage of using the numerical model, Figure 5.6(d-i), has visualised temperature inside the cylinder which is not easily feasible to measure experimentally.

The circumferential surface temperature of the rotating workpiece as the laser beam is moving along the axis of the workpiece depicts in Figure 5.6(a-c). A rotation speed of workpiece and translational motion velocity of laser source are maintained steadily at constant values. The entire heat absorption process takes place during exposure of laser to cylinder surface, as the displacement of the projection area is progressively captured. Naturally enough, the laser exposure area has the highest temperature of the field, slightly exceeding 1500 K for the represented scenario. The cylinder rotational motion induces convective cooling streams and therefore cylinder undergoes heat dissipation (cooling) process through the surface area. The rotational trailing area remains also relatively in high temperature as it is cooling down and approaching a quasi-steady temperature. The behaviour is described as quasi-steady since time scale of cooling from peak temperature to the given temperature is much smaller than the time required for the surface to approach ambient temperature.

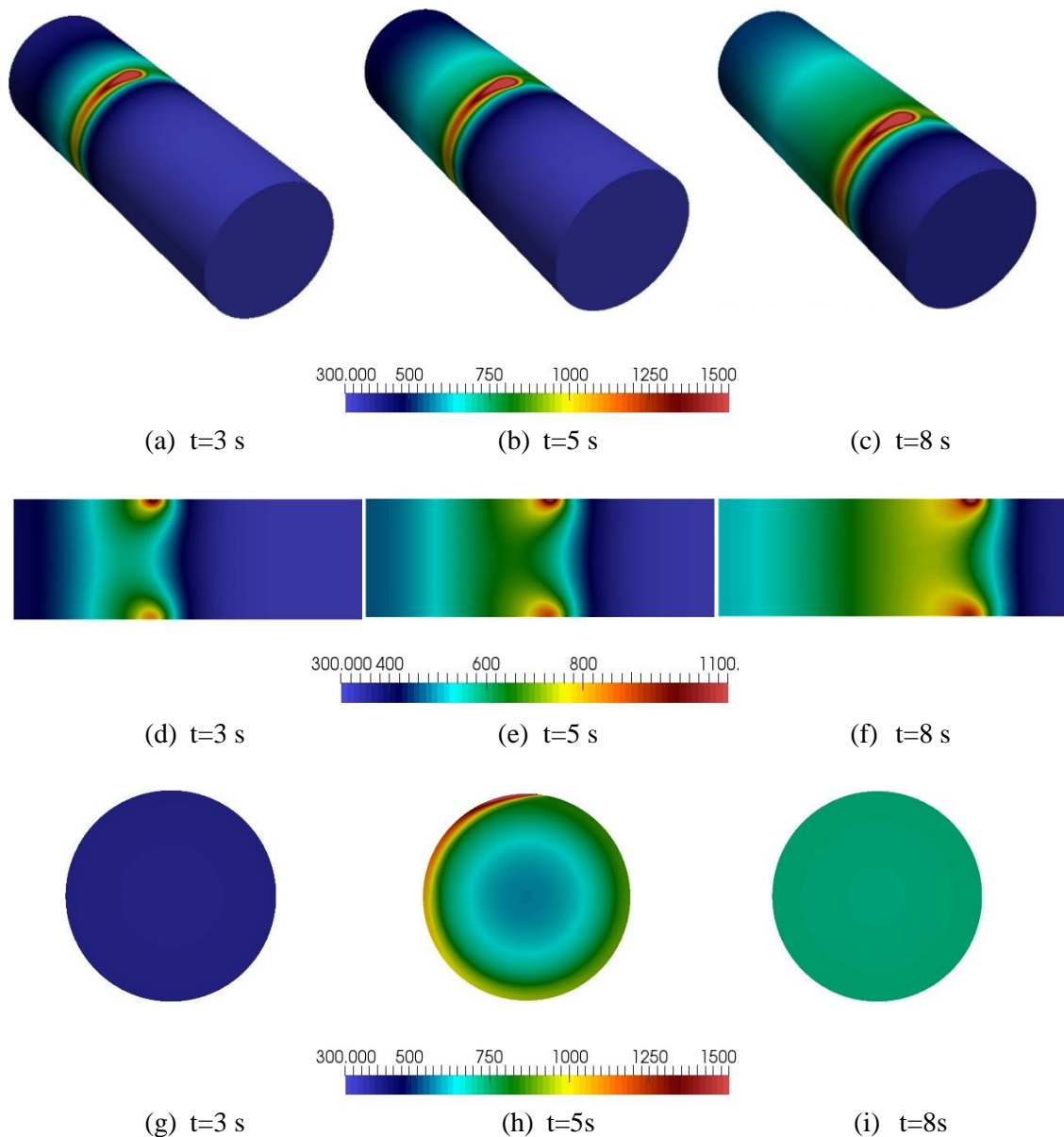


Figure 5.6 Transient temperature visualisation of heated rotating workpiece in: (a) workpiece surface, (b) mid-plane through workpiece axis, and (c) inside cross section of workpiece; at: $LP=500$ W, $D_L=3$ mm, $V_T=100$ mm/min, $\omega=1000$ rpm

Figures 5.6(d-f) visualise the temperature distribution, on a mid-plane aligned with axis of the cylinder, where the laser is exposed on top side. A hot ring generated through the laser exposure point is obvious in these contours where laser translation could be clearly tracked in three consecutive time-steps. This thermal preview could give an estimation of heat diffusion through the cylinder both toward the axis and along the cylinder. Figures 5.6(g-i) represent a mid-plane having normal vector, aligned with axis of cylinder. The plane is almost on its initial temperature (around 300K), at $t=3$ s, when the laser exposure has not reached to this point which means

conduction is initially not the most effective mechanism in the time scale of seconds. Consequently, at $t = 5$ s, laser reached to this cross-section and exposes right at the crown of this circular cut-through. Local heating, rotational convection cooling and resulted thermal diffusion are illustrated in preview of this cross-section at the given snapshot. The laser point has moved over the cross section, in the following time step, when a more uniform temperature is captured. This uniform field is in the range of so-called quasi-steady temperature, which was earlier mentioned.

5.15 Model Validation and Sensitivity Evaluation

Temperature field could be partially (i.e. surface temperature) compared against the experimental measurements to examine validity, sensitivity and accuracy of numerical assumptions and associated results. This is carried out in the current section as initially three aforementioned laser intensity profiles are compared and discussed and then the best distribution function is applied for the parametric validation tests.

5.15.1 Laser Power Profile

The most accurate laser profile and its influence on heat transfer process need to be initially determined to accordingly examine sensitivity and validity of model throughout geometry and for various key parametric changes. Three laser profiles, estimating power intensity distribution, are proposed for comparison, as depicted in Figure 5.7. Coefficients and constants of these functions are obtained by equating the area-averaged values (integral over area divided by area) to one, ensuring the mean heat flux value is not influenced by the distribution function. The surface temperature is monitored at M_2 (i.e. the middle point) as the area of interest and three temperature curves, resulted from uniform, linear and exponential functions are plotted against experimental measurements (184) of pyrometer technique, in Figure 5.7.

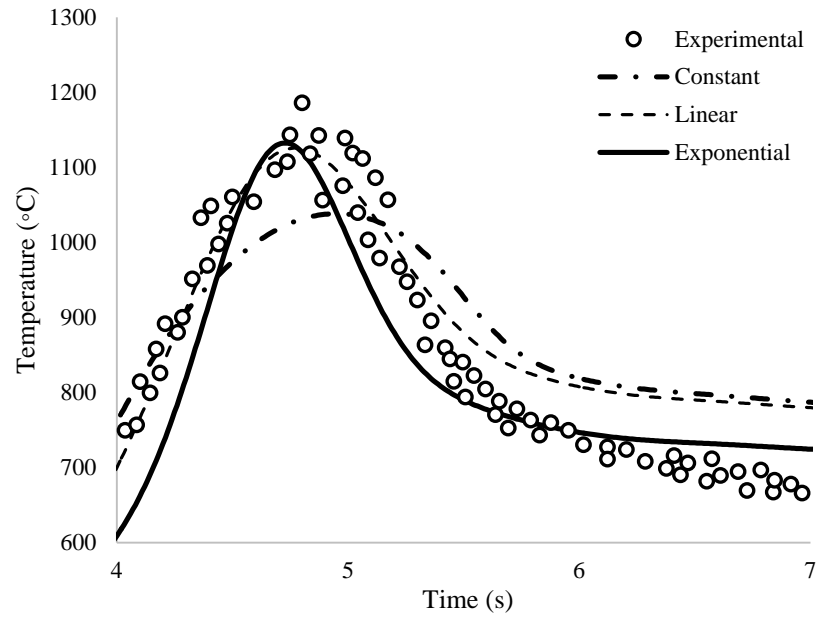


Figure 5. 7 Evaluation the three profiles of laser intensity: uniform, linear and exponential, Temperature at M2: LP=500 W, $D_L=3$ mm, $V_T=100$ mm/min, $\omega= 1000$ rpm (184)

This very illustrative graph visually explains the importance of laser profile during the laser heating process. Comparing demonstrated power density profiles, it is clarified why from uniform to exponential functions, the bell-shaped graph is pushed to have a higher pick point and lower trailing temperature value. The significance of variation is more obvious where pick and trailing values have over 150 K difference between the best and worse temperature prediction. Based on this analysis, exponential distribution, with function given in Figure 5.5, is decided as the best laser power intensity profile and is accordingly used the rest of investigation.

5.15.2 Transient Surface Thermal Response

Surface temperature is experimentally measured at three points of M_1 - M_3 , specified in Figure 5.4, over the course of heating which is set to be 10 s for the validation scenarios. This comparison between experimental measurements and numerical results (with exponential laser profile) is referred as the main validation test where satisfactory matching (i.e. within the reported experimental accuracy) is achieved.

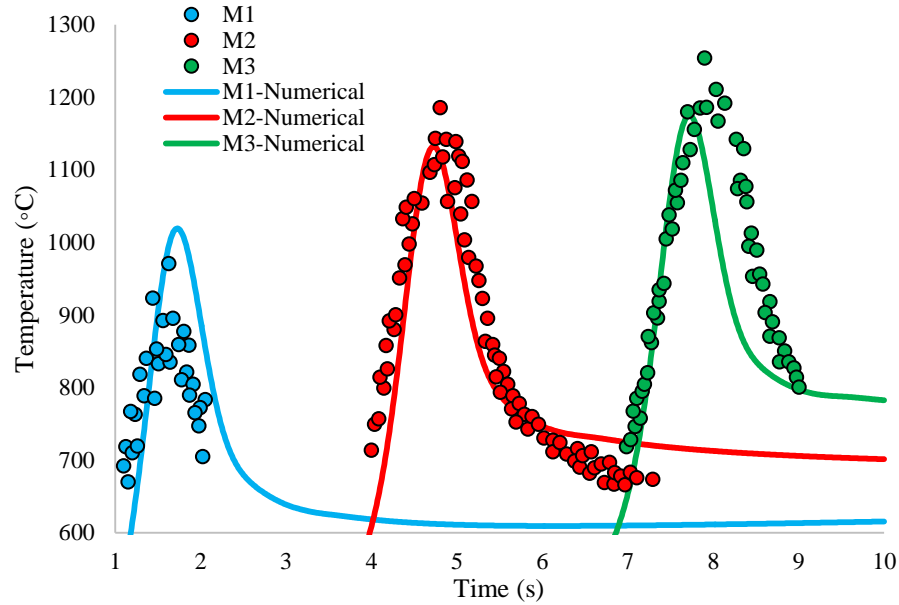


Figure 5.8 Validation of the surface temperature with previous experimental data (184), LP=500 W, $D_L=3$ mm, $V_T=100$ mm/min, $\omega=1000$ rpm

The obtained validated results are strictly bond to the calibration of all three modes of heat transfer and their associated parameters. For instant, growth of temperature from one pick to the consecutive one is controlled by temperature dependent thermal diffusion coefficient while the local magnitude of this pick correlated to absorption of heat in the exposure area is highly sensitive against the combination of absorptivity and thermal diffusion. Following the temperature pick, there will be a cooling process which is determined by rotational convection and radiation. Therefore, the tail section of each graph could be associated with accuracy and validity of convection-radiation cooling closures which indicated a good agreement here.

5.15.3 Influence of Laser Beam Characteristics

The numerical model has been also parametrically tested to ensure it responds as expected against LAM operational variable. The laser power and translational speed are two additional parameters, examined experimentally and hence the associated thermal measurements could be used for verification of the numerical model. Figure 5.9 compares experimental and numerical values of temperature at M_2 point for three laser powers of 400, 500 and 600 W. The general temperature growth and

temporal distribution patterns are corresponding well and hence the model could be approved for the parametric analyses associated with laser power. The more evident deviated numerical estimation and also more scattered experimental measurements, in the cases of higher power lasers, remarks uncertainty of surface characteristics and radiation parameters which are assumed, according to the available range of measurements.

The third and last validation comparison graph examines sensitivity and validity of numerical model against laser translational speed whilst all other characteristics are maintained constant. It takes the laser point just more than two seconds to reach M_2 , as it travels at the fastest speed of 200 mm/min. This time linearly increases with velocity, for two slower cases, as shown in Figure 5.10. The overall heating is found to be inversely proportional to laser translational speed as deduced from the surface temperatures. This is clearly indicated in Figure 5.10, as pick temperature of lowest and fastest travelling lasers demonstrate more than 500 K difference. This comparison concludes numerical validation in a relatively wide range of parameters.

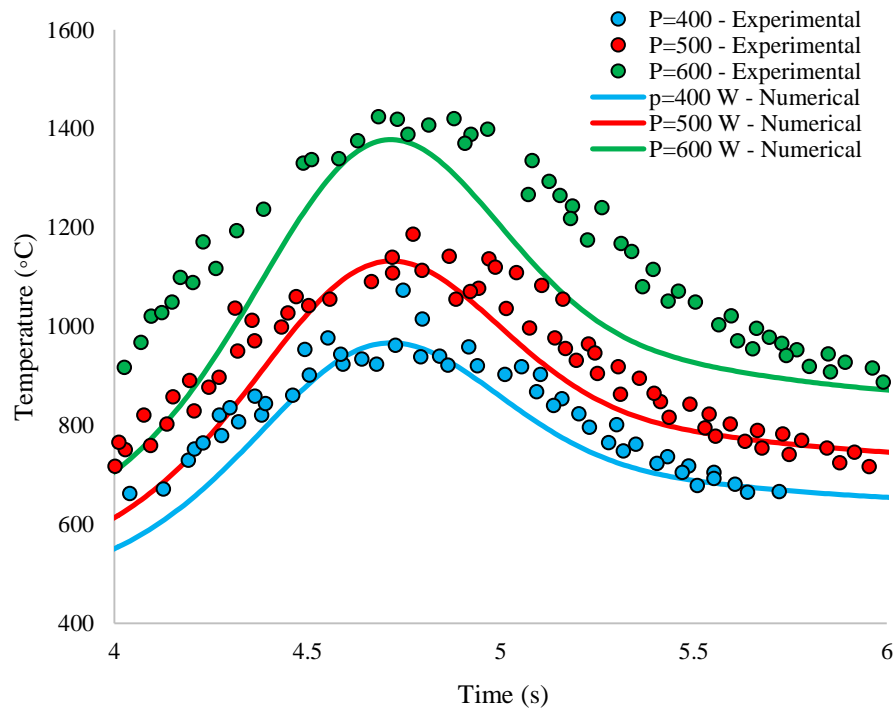


Figure 5. 9 The effect of variation power of laser beam on workpiece surface temperature, at M_2 : $DL=3$ mm, $V_T=100$ mm/min, $\omega= 1000$ rpm (184)

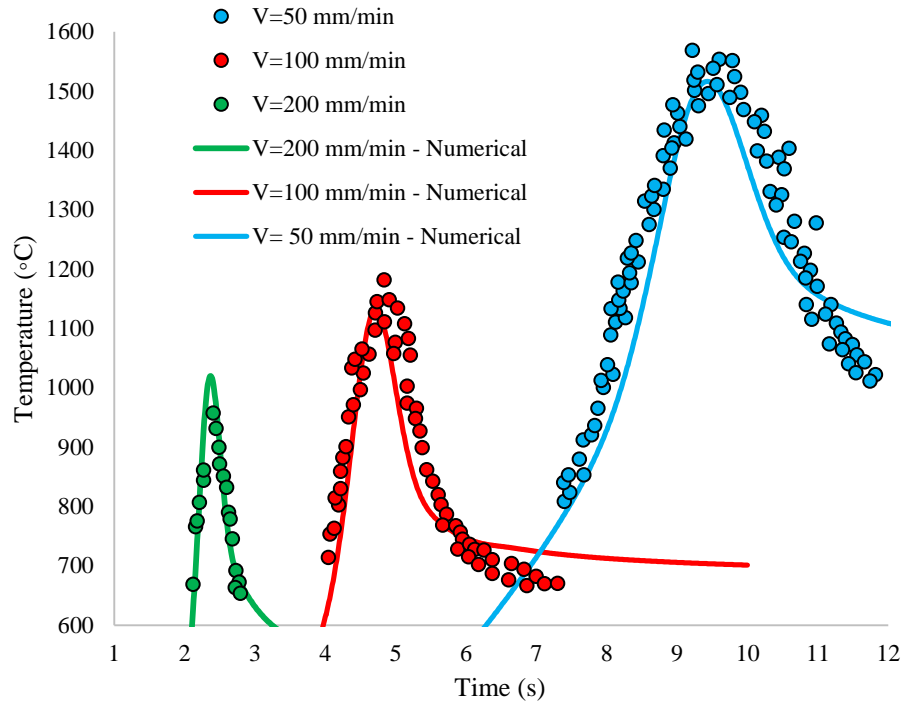


Figure 5. 10 The effect of variation laser scanning velocity on workpiece surface temperature at LP=500 W, $D_L=3$ mm, $\omega= 1000$ rpm (184)

5.16 Deploying the Model

The validation is carried out for a moving laser source combined with a rotational configuration of the rotating cylinder which sets the most complicated motion configuration, anticipated in the LAM process. On the ground of such validation, the proposed thermal model could be deployed for characterisation of LAM process as the applied objective. Comprehensive and detail knowledge of temperature distribution and thermal condition across space and time is a necessity for a reliable assessment of process effectiveness. Among many potential applications, few are suggested here as the key benefits which cannot be easily obtained through experimental or analytical approaches where interrogation area is mostly restricted to the surface area.

5.17 Stationary Laser Heating and Thermal Equilibrium

The pre-heating process of LAM is practically carried out by a stationary laser applied on a rotating workpiece which ultimately reaches a thermal steady-state. The thermal equilibrium between laser (as the heating source) and combined

convective/radiative loss (at heat sink) is expected to set at the steady-state condition, determining the softening condition for the machining process. Figure 5.11 compares temperature trends over finite time for various laser powers at 45° after laser exposure point (in the rotation direction). The dashed line indicates the points over which temperature gets asymptotic to a plateau state, representing a thermal condition.

Variation of surface temperature, as depicted in Figure 5.11, confirms an ultimate convergence of the thermal condition to an equilibrium state. The transition process is characterised by time over which the equilibrium state is reached. For instance, in the case of 100 W heating, the shortest transition and the highest local steady temperature are recorded among the cases. The transient analysis is useful to estimate the time required for LAM preheating and also might be utilised for optimisation of the total energy consumption during the process. However, the final convergence to the thermal equilibrium condition enables a confident use of steady analyses as a reference for all parametric studies in the following sections.

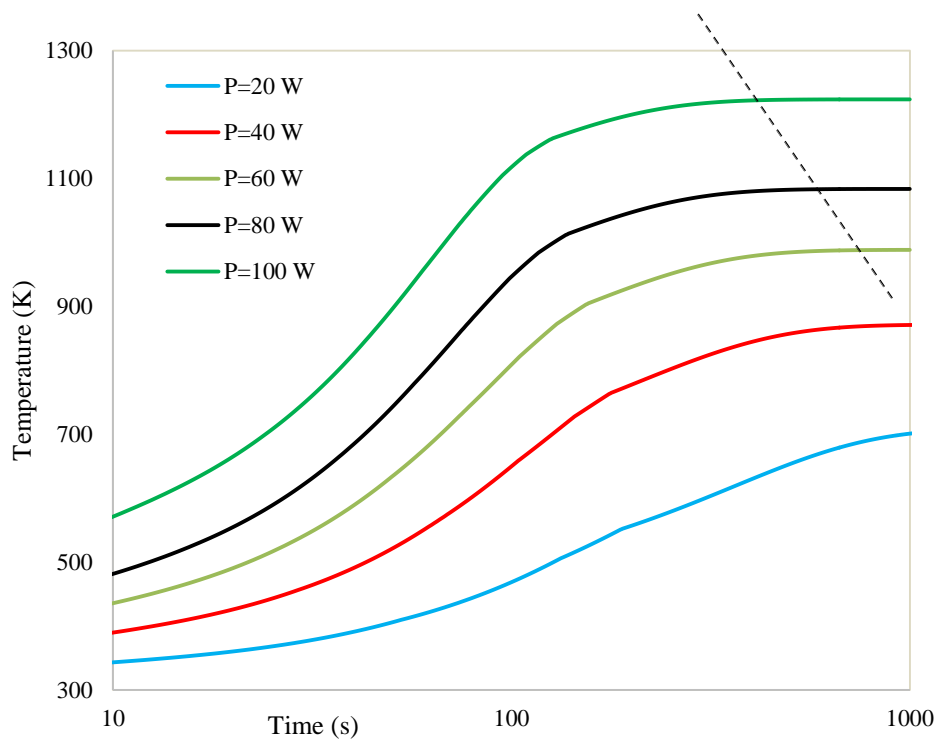


Figure 5. 11 Typical temperature over time for non-traversing laser
 $D_L=2$ mm, $\omega= 1000$ rpm

5.18 Artificial Neural Network

There has been a resurgence of interest in artificial neural networks (ANNs) over the last decades due to their competency to facilitate low-order estimators. An ANN is an information-processing system that has certain performance characteristics in common with biological neural networks. ANNs have developed as generalizations of mathematical models of human cognition or neural biology, utilizing a distributed processing approach to computation. ANNs are capable of solving a board range of engineering problems by “learning” a mathematical model for the problem. This model can then be used to map input data to output data. ANNs are composed of individual interconnected processing elements. These processing elements are analogous to neurons in the brain and are also referred to as artificial neurons, as shown in Figure 5.12. Each artificial neuron sends and/or receives data to/from other elements. An ANN is characterized by some properties (258): (i) a pattern of connections between the neurons (called its architecture), (ii) a method of determining the weights on the connections (called its training, or learning, algorithm), and (iii) an activation function. The network acquires knowledge through a learning process. The inter-neuron connection strengths known as synaptic weight are used to store the knowledge. This learning ability of neural networks gives an advantage in solving complex problems whose analytic or numerical solutions are hard or computationally-demanding to obtain.

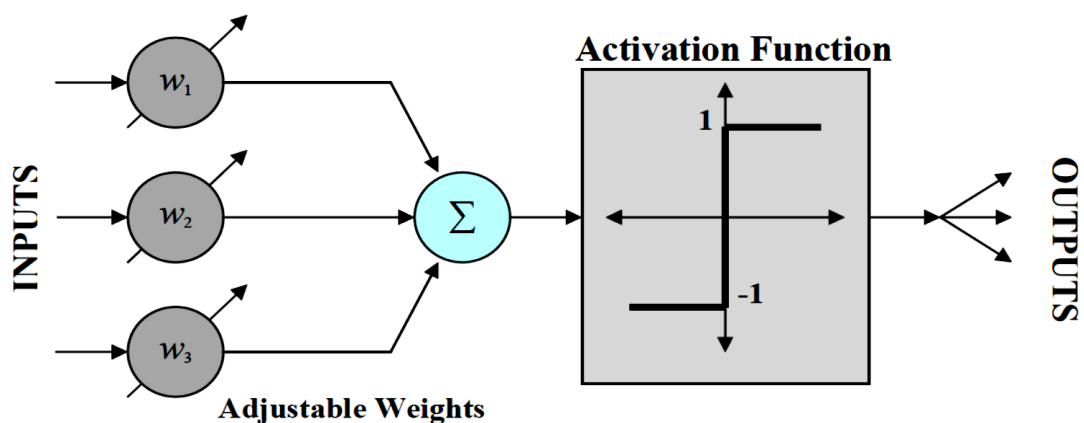


Figure 5. 12 A general neuron model of an ANN

ANN models go by many names, such as connectionist models, parallel distributed processing models, and neuromorphic systems. Whatever the name, all these models attempt to achieve better performance via dense interconnection of the simple computational element. The adjustable multiplication weights (w), it is often convenient to allow positive weights to represent an excitatory connection and negative weights in inhibitory connection. A weight of zero uses when no connection between a pair of neurons is to be made. The input transmitted to a neuron through these weights may come from other neurons, from an external source, or the same neuron. The output of the model neural ranges between limits such as (-1 and 1), that are analogous to a biological neurons minimum and maximum firing rate (259, 260).

The basic operation of an artificial neuron involves summing its input signal $u = [u_1, u_2, \dots, u_p]^T$ multiplied by its weights $w = [w_1, w_2, \dots, w_h]^T$ (T represents the transpose) to applying the net. i.e.

$$\text{Net} = \sum w_h x_p \quad (5-17)$$

The output of neuron (Y) depends on the net, which computes as a function (f) of the net called activation function.

$$Y = f(\text{net}) \quad (5-18)$$

Some examples of commonly used activation $f(\text{net})$ are shown in Figure 5.13. In many cases it is desirable to provide each neuron with a trainable bias. This offset the origin of the activation function, producing an effect that is similar to adjusting the threshold of the neuron, thereby permitting more rapid convergence of the training process.

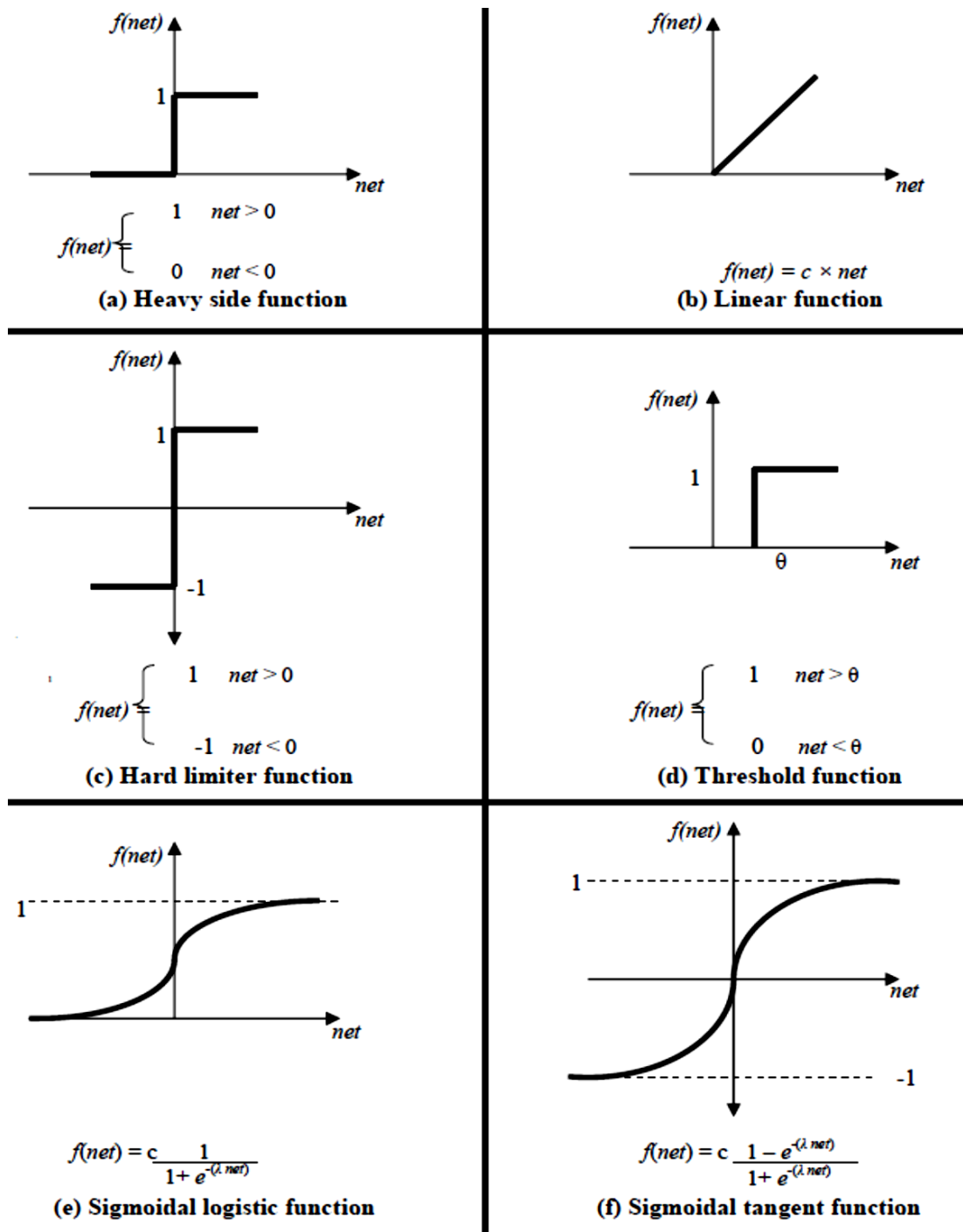


Figure 5. 13 Activation Functions in ANN

Where:

λ : determine the steepness of transition region.

c : neuron gain. θ : constant threshold.

5.18.1 Learning of Neural Networks

Learning is a relatively permanent change in behaviour brought about by experience. Learning in human beings and animals is an inferred process; it cannot see it happening directly and assumes that it has occurred by observing changes in performance. While, learning in ANNs is typically a direct process, and can capture each learning step in a distinct relationship called cause and effect. ANNs are trained using one of the three types of learning algorithms: (1) supervised algorithm, (2) unsupervised algorithm, and (3) reinforcement algorithm (a special form of supervised learning algorithm).

5.18.1.1 Supervised Learning

In supervised learning, the system submits a training pair (consisting of an input pattern and the target output) to the network. The network adjusts weights based upon the process elements error value e (usually the difference between the expected output and the computed output) so that the difference diminishes with each cycle. Thus, supervised learning requires a teacher or supervisor to provide desired or targets output signals. Examples of supervised learning algorithms include the delta rule (Widrow-Hoff (261), the generalized delta rule, or the back-propagation algorithm (BP).

5.18.1.2 Unsupervised Learning

Unsupervised learning procedures classify input patterns without requiring information on target output. In such procedures, the network must detect the pattern regularities and the grouping for each applied input to produce consistent output. The input patterns are automatically adapted to the weights of ANN connections. Examples of unsupervised learning algorithms include the Kohonen and Carpenter-Grossberg Adaptive Resonance Theory (ART) Competitive learning algorithms (262).

5.18.1.3 Reinforcement Learning

Reinforcement learning, or learning with a critic, works by deriving an error when an input target is not available for training (259). In this case, the network obtains an error measure from an application-dependent performance parameter. Weight connections are adjusted, then the network receives a reward/penalty signal. Training proceeds to maximize the likelihood of receiving further reward and minimizing the change of penalty. An example of a reinforcement learning algorithm is the genetic algorithm (GA).

Generally, learning algorithms involve two more functions (in addition to the activation function), namely (i) the error-calculation function (e) controls the updates of weights, and (ii) the increment of the weight Δw function updates the weight.

5.18.2 Laser Preheating Parametric Predictor

The result of computational thermal analysis offers an extensive knowledge of temperature distribution throughout the workpiece which could be utilised for various design predictions and optimisation. Nonetheless, in some application even more minimal thermal prediction would be sufficient for optimisation of the process and hence the field could be summarised into discrete values at critical locations. The low order (i.e. crude yet faster) estimations could be achieved by regression and machine learning (ML) methods (trained by experimental or numerical results) as more affordable prediction options. The functionality expected from preheating, during LAM process, highlights the heated cross section as the critical vicinities where thermal monitoring will be more crucial. The first objective of LAM is to reduce material strength (and to some extent ductility) by applying intense, localised heating source. Besides, it is often desired to remove a finite thickness of material during cutting process while beyond removal thickness, the material should be eluded from overheating which inversely influence the micro-structural and mechanical properties. This could be adopted as the simplest thermal guideline to adjust an informed heating range, rate of application and rotational speed. The field which is reduced to a critical cross-section may need to be discretised into few key points in order to be observed, comprehend and later predicted by lower order

prediction approaches such as machine learning techniques. Figure 5.14 illustrates twelve discrete points across the heated cross section for evaluation of temperature in 3 thickness levels and four circumferential locations. Such combination quantifies the depth of heating intensity around the cross section and indicates the surface thickness of thermally influenced materials.

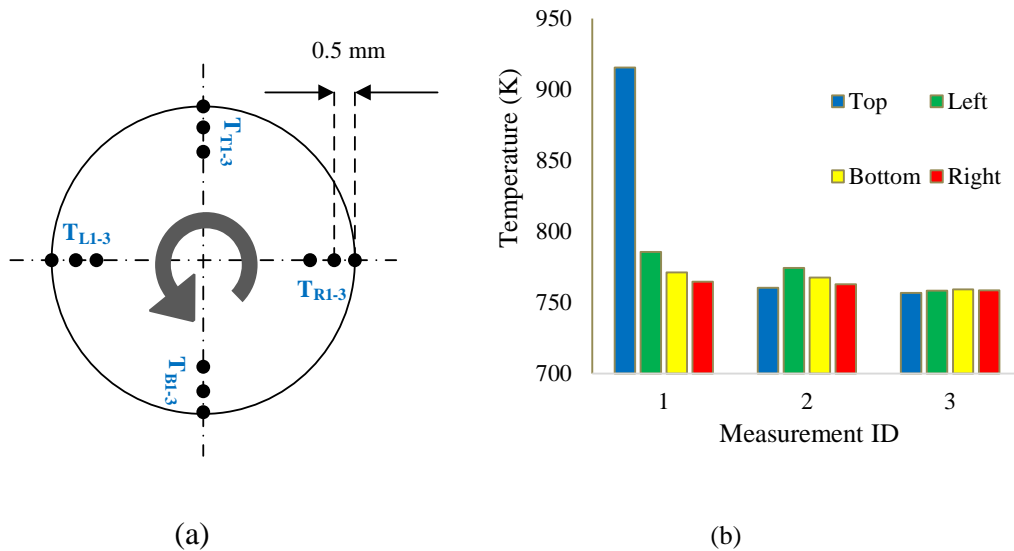


Figure 5. 14 Temperature of selected points at the heating cross section for the discrete thermal summary: (a) temperature points across critical section, (b) discrete thermal summary at point 1 (LP=40W, $\omega=500\text{rpm}$, and $D_L=2\text{mm}$)

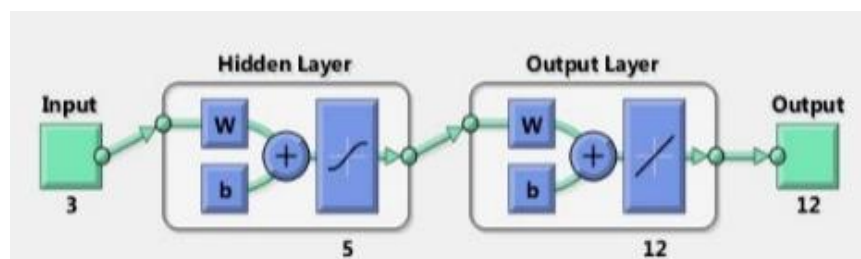
The temperature reading points, as shown in Figure 5.14(a), are named according to their location with respect to the rotational direction (T: Top, L: Left, B: Bottom and R: Right) and spacing from surface of the cylinder (1 to 3: surface-to-core). The point Top-1, which represents the centre of laser exposure area on the surface, is naturally enough captured to have the highest temperature among points, as depicted in Figure 5.14(b). Following the direction of rotation surface temperature drops down steeply (more 100°C within 45°). Circumferential assessment of temperature demonstrates a combination of cooling and heat diffusion to level 2 (0.5 mm away from the surface) and a more uniform temperature pattern around level 3 (1 mm away from the surface). This brief discrete dataset is sufficient to portray the full thermal picture (it is understood that the other areas have lower temperatures) required for controlling LAM. Knowing the temperature value at the given points

will allow estimation of the softened area, the thickness of thermally influenced material and margin to the melting point which are all necessary for informed regulation of LAM operation.

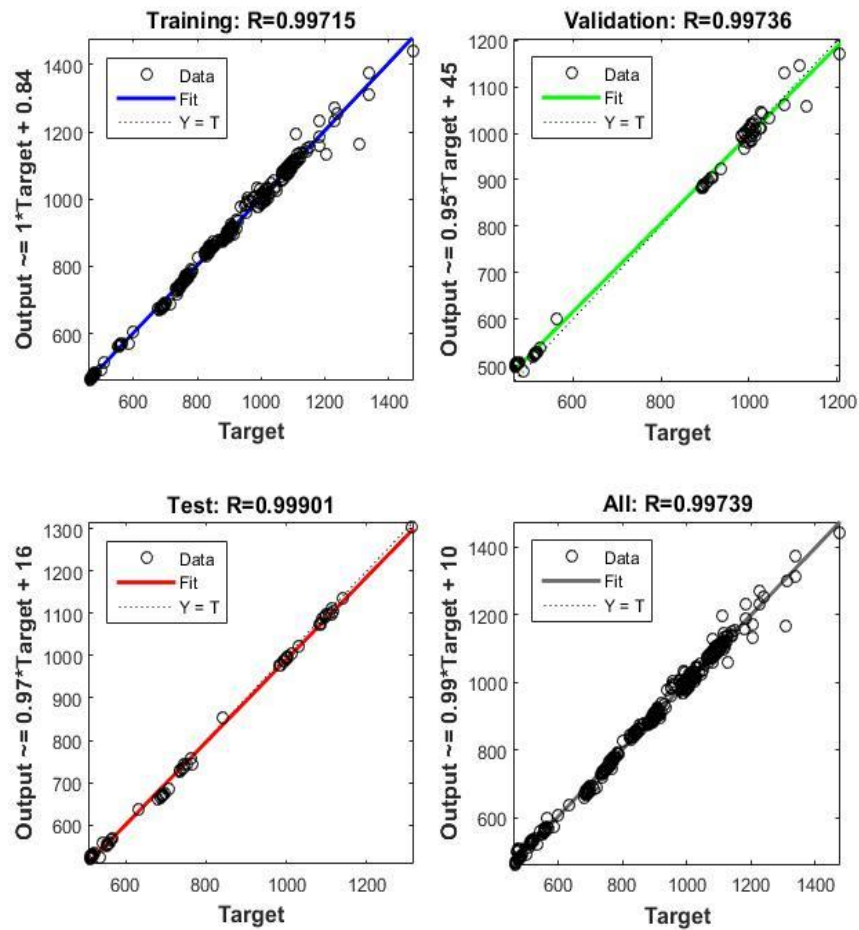
5.18.3 Artificial Neural Network Fitting and Discrete Prediction

Artificial neural network (ANN) is one of the well-trusted methods to develop a low order predictor, for the above-mentioned thermal task. ANN is one of supervised machine learning algorithm which could be briefly characterized as a multi-layer regression tool correlating dataset of input-outputs. The current study utilises the well-validated numerical method for generation of thermal data required for ANN fitting. Repeating parametric analysis and regenerating sufficient data-points enhances accuracy and correctness of fitted correlation between effective (inputs) and affected (outputs) parameters. Not only number of data-point but also a proper understanding of the relation between input-output parameter is necessary for training of an accurate ANN. This has also been tested by numerical parametric analysis which, for instance, reveals dependency of temperatures on heating intensity, rotational speed and laser diameter. This current section is to demonstrate the feasibility of LOFF from the numerical output of the 3D model.

Variable laser power (20, 40, 60, 80, 100)W, rotational speed (500, 1000, 1500) rpm and laser beam diameter (2, 3, 4) mm are the input parameters of the network to be trained, validated and tested for prediction of temperature at 12 discrete points, simply considered as the network outputs. For training, validation and testing process, (45) point data pool is split as 70%-15%-15% respectively where the best model has obtained through five-layer hidden neurons. The network structure and configuration are visualised in Figure 5.15(a).



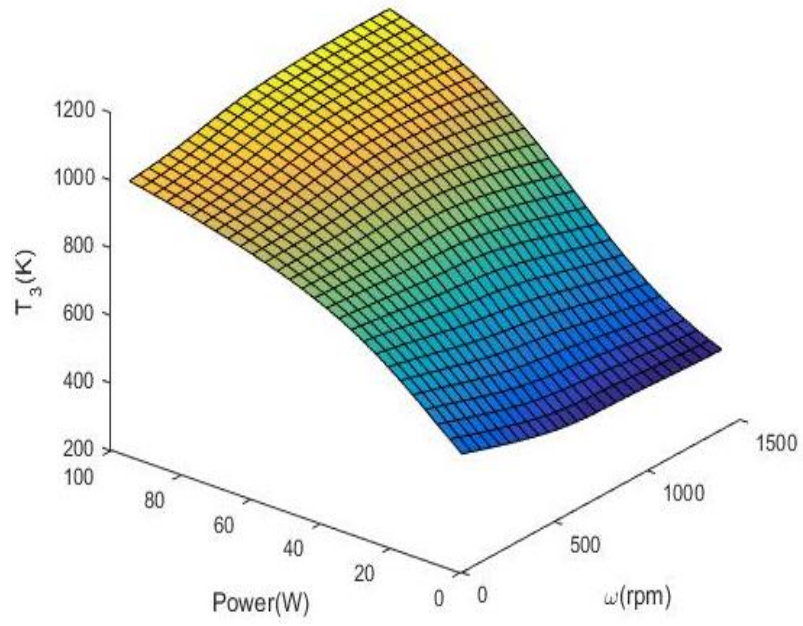
(a)



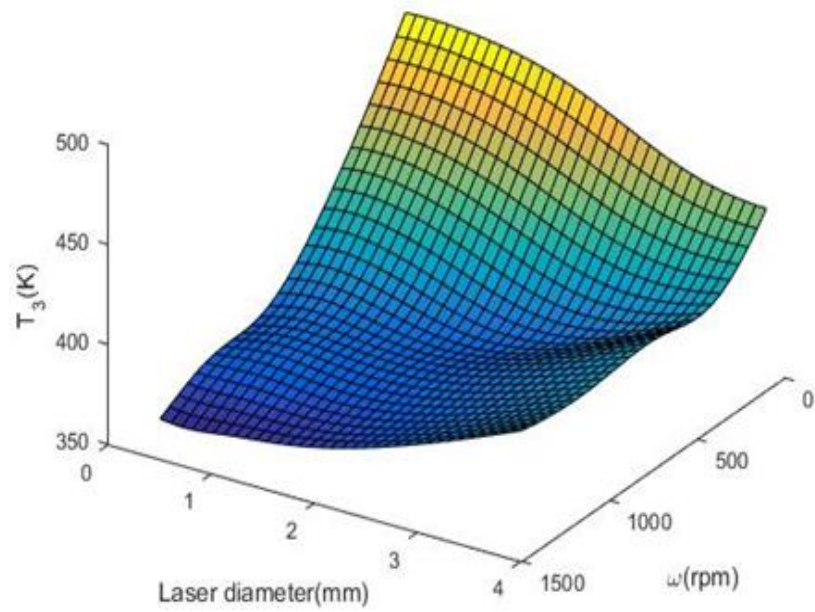
(b)

Figure 5. 15 Framework and examination of ANN fitted though MATLAB, (a) network diagram, (b) regression plots of ANN fitting

By utilising ANN fitting algorithm (Levenberg – Marquardt) (263-265), the appropriate accuracy of the fitted network illustrates in Figure 5.15(b). MATLAB, as a pioneer, robust and widely trusted package, is utilised for data assembling, ANN fitting and checking. This is a satisfactory accuracy for a prediction process, obtained from (45) data point regression which also could be further extended to have extra input parameters (accounting for more physical phenomena) while maintaining/enhancing the accuracy by adding more simulation inputs into fitting process. This brief investigation, nevertheless, emphasizes the applicability of ANN as a tool of lower order for estimation the temperatures of steady-state.



(a)



(b)

Figure 5. 16 LOFF prediction of temperature at TR1, (a) $D_L=2\text{mm}$, varying LP and ω , (b) LP=20W varying D_L and ω

The fitted and verified network could be then used for low order forecast and sensitivity analysis of temperature at given points. Figure 4.16 explain how the ANN could assist to evaluate thermal behaviour against defined input parameter and reversely find safe operational parameters. These types of low order training are computationally affordable, could be extended based on community data reporting various physical consideration and easy to be interpreted. Figure 5.16(a) demonstrates the dependency of temperature values predicted for one single point like the spot diameter of the laser beam is maintained constant at (2 mm) and other inputs are varying. Sensitivity examination of the temperature for the same point is demonstrated in Figure 5.16(b) while heating power the only constant input.

5.19 CFD Analysis of Titanium Alloy Heating

The three-dimension CFD model, which is developed and extensively verified against previously published experimental results, has been utilised for simulating some experiments of this research. The geometry, material properties and operating conditions are set according to what is indicated and measured during the experiment methodology. As explained in Chapters 3 and 4, the current work emphasises on Titanium which, despite its growing applications and importance, has been less investigated in the literature. The investigation (both experimental and numerical) is carried out for a higher range of rotational Reynolds Number (adjusted by combination of the cylinder diameter and rotational speed) which is less examined in the literature. Therefore, two major outcomes are expected by the new sets of simulations; first, broadening validation of the CFD analysis to an extended range of parameters, specifically including the range of our own experiments and the second to attain a better understanding of diffusion pattern inside the titanium workpiece.

5.19.1 Setup and Conditions

The cylindrical workpiece utilised in the experiment is a Titanium alloy (Ti-6Al-4V) of 50 mm of diameter and 250 mm long. The density (ρ), thermal conductivity (k) and specific heat (Cp) of material are respectively set as 4430 kg/m³, 6.6 w/m.K and 565 j/kg.K where the emissivity and absorptivity of the workpiece is measured and adjusted with respective to temperature and surface characteristic as well discussed

in section (3.9). Similarly, the key laser characteristics are roughly indicated as nominal laser power of 55W and diameter of 2 mm which are set accordingly in the simulation. The laser characteristics have the most uncertain parameters which are hard to examine (within the project's facilitation) and hence the potential discrepancy between numerical and experimental results could be mainly correlated to this uncertainty.

5.19.2 Numerical challenges and strategy

The key difference in mesh and setting is larger dimensions of the cylinder which brings concerns of grid and time-step senility to be checked. Following the general approach, spatial analysis is carried out to find and optimised mesh sizing generating results independent of the grid size. Accordingly, the mesh is utilised in a set of transient simulations seeking for valid time step and found it to be 0.001 and 0.0005 seconds respectively for rotational speed of 100 and 1000 rpm. Importance of such setting will be understood by just by looking at the pattern of experimental measurements where temperature is rising rapidly in the early stage and gradually plateaus. Coarsening time-step could cause up to 16 degree difference within 10s of heating under the given conditions, which is significant numerical discrepancy.

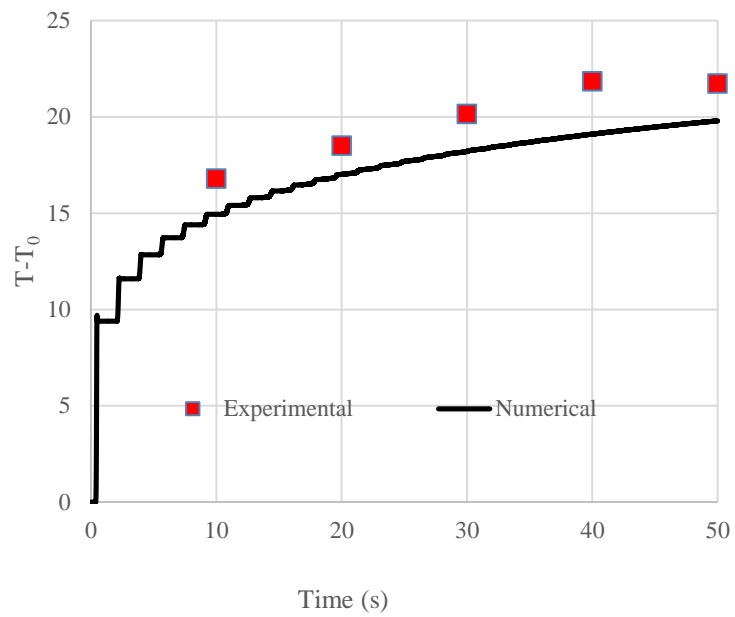
Setting the appropriate time-step makes the numerical model relatively expensive and also time-consuming to simulate, using the given computational resources. Hence, the transient models are used for simulation and comparison of 50 early second where the rate of temperature growth is critical. This strategy is deployed for verification whereas a steady-state model (with the same verified settings) will be used to predict the ultimate thermal state.

5.19.3 Simulation Results

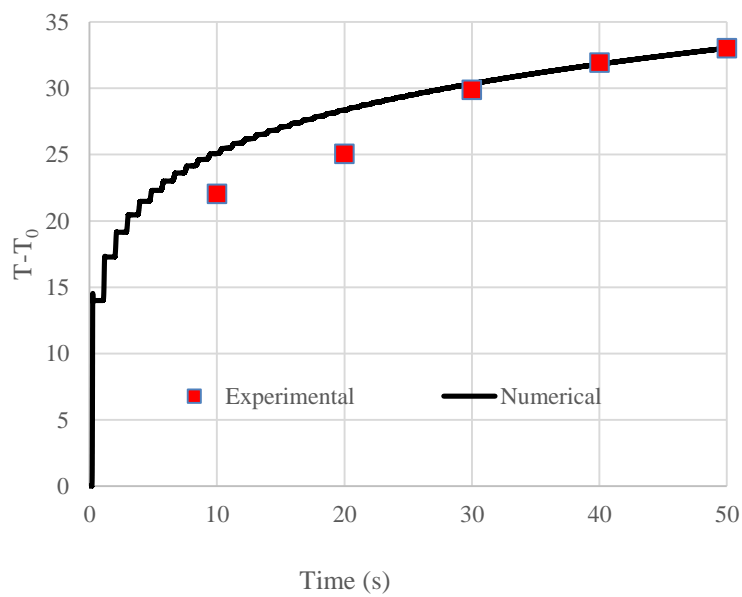
The first set of results which is obtained to compare against experimental transient measurements is the surface temperature at 45° trailing the laser heating point. This has been carried out for Ti-6Al-4V workpieces with rotational speed of 100 rpm, various surface characteristics and laser powers. The surface characteristics are adopted to CFD model by setting temperature-dependent functions of emissivity and absorptivity (determining the thermal source term). Two laser powers are set as 30%

and 50% of the nominal power which are expected to be 16.5 W and 27.5 W, respectively.

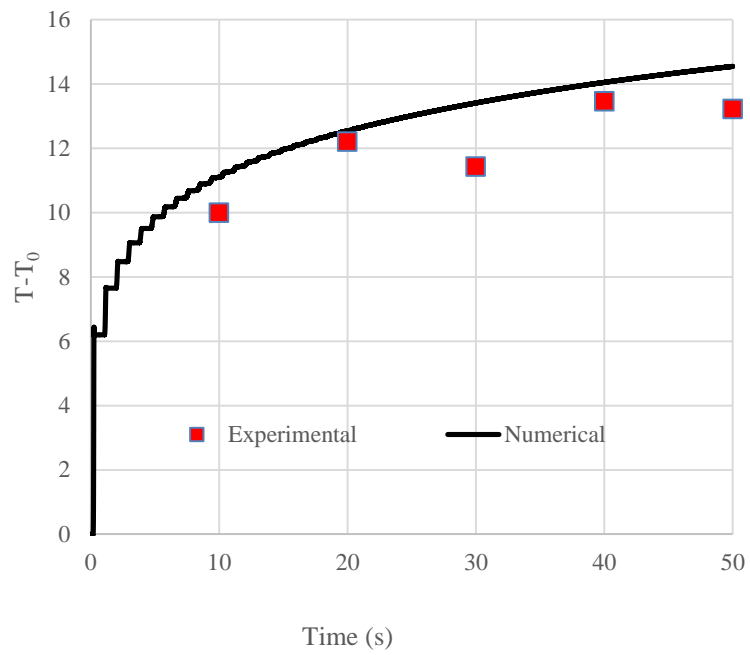
Results visualised in Figure 5.17 reveal satisfactory agreement between numerical and experimental values, especially with such uncertainty in the explained laser characteristics. The predictions of the surface painted in black looks overall better than the rough surface, generated by sand-blasting.



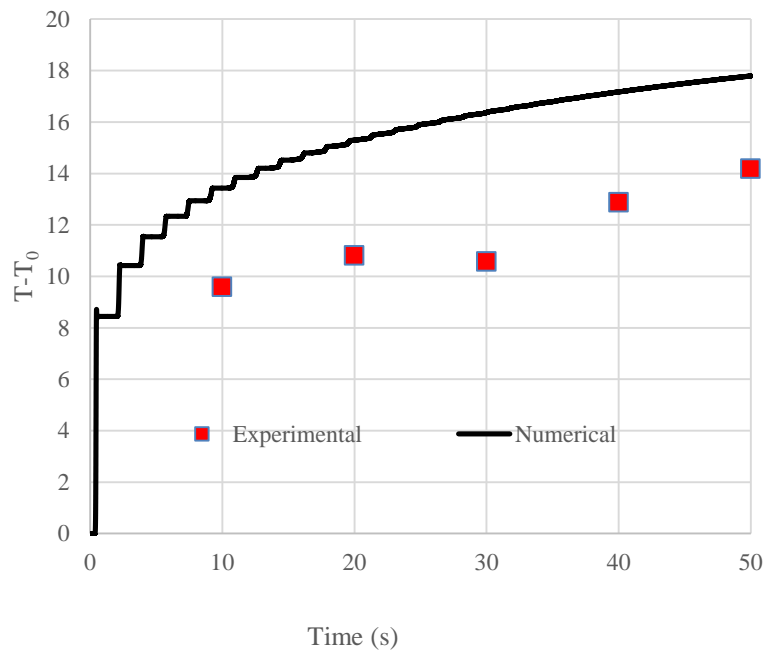
(a) Black-painted – 30% nominal power



(b) Black-painted – 50% nominal power



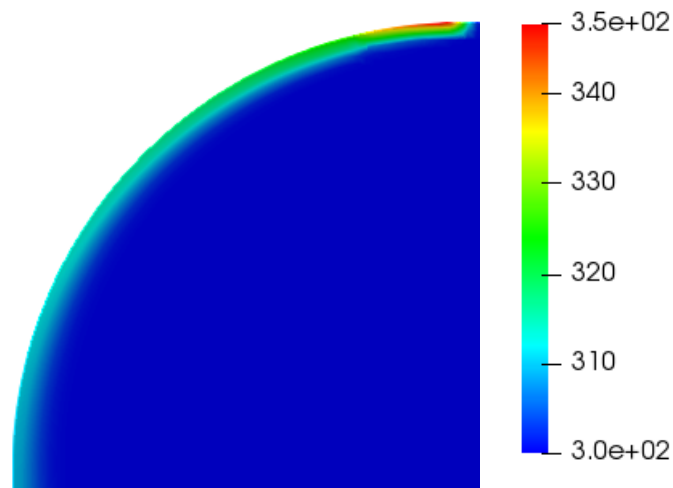
(c) Rough surface – 30% nominal power



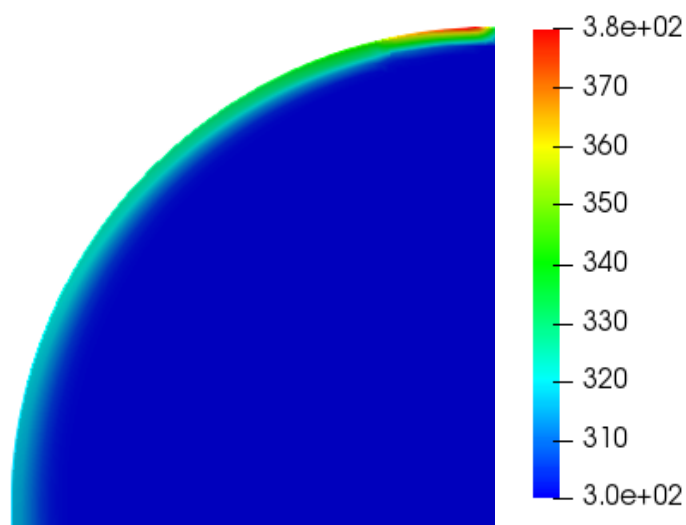
(d) Rough surface – 50% nominal power

Figure 5. 17 Comparison of surface temperature at 45° trailing the laser heating point, $\omega=100$ rpm

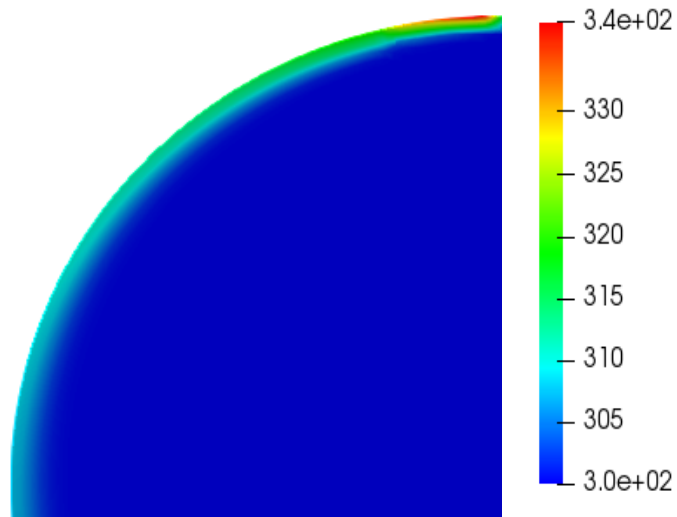
The key difference, imposed by surface characteristics is thermal gain from the identical laser beam through absorption and re-radiation process whereas diffusion pattern/intensity is obviously not affected by the surface characteristics. Temperature contours, visualised in Figure 5.18, shows the thermal diffusion and its intensity for various cases. Typical to the previous thermal diffusion pattern, the lower laser intensity and larger work-piece induce a low-temperature and low-gradient field with the 80 degree as the highest temperature difference associated to the case with 50% of nominal laser power and the surface painted in black.



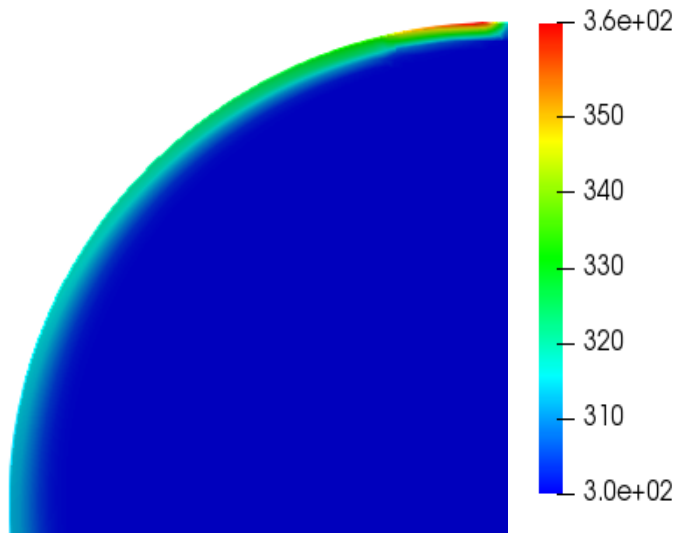
(a) Black-painted – 30% nominal power



(b) Black-painted – 50% nominal power



(c) Rough surface – 30% nominal power



(d) Rough surface – 50% nominal power

Figure 5. 18 Steady-state thermal diffusion patterns and intensity, $\omega=100$ rpm

5.20 Summary

In this chapter, a new numerical investigation has been proposed for the forecast of radiative heat transfer that can be implemented on heated rotating workpiece. Numerical model provides a unique analytical and practical benefits for applications involving LAM. The proposed 3D numerical model is demonstrated to be not only more affordable tools but also offering thermal knowledge which may not be achieved even by decent measurement techniques, for instance, thickness of thermal

diffusion. The process surface behaviour which include absorption, reflection and forced convection (as a result of workpiece rotation) are considered as boundary conditions while heat diffusion across the rotating geometry is simulated. A systematic approach to development, validation and parametric analysis is followed up which could be presented as a generic numerical manifestation applicable for similar thermal modelling manufacturing processes. The key aspects and deliverables of this investigation are concluded as follows:

- The study has formulated a well-validated and accurate numerical model for predicting the transient preheating thermal behaviour of a cylindrical rotating workpiece subjected to a laser heat source, as used in LAM applications.
- Overcoming previous analytical limitations, this model accounts for the complex thermal processes associated with heat absorption over the laser spot area, thermal diffusion into the workpiece and the cylinder surface cooling arising from thermal radiation and rotational convection. Hence, the model warrants an insightful understanding of the transient thermal behaviour of a laser-preheated rotating cylinder, as applied in LAM.
- Advancing the status quo of numerical modelling for this field, this simulation methodology is developed on an SRF, incorporating the combined motion effects of workpiece rotation and traversing laser beam, hence presenting a much realistic treatment of LAM workpiece behaviour subjected to laser spot heating.
- The predictive precision is derived through boundary configuration involving dynamic surface profile and source term that guarantees validity and stability of simulation.
- The simulation model generates data to obtain the depth of thermal penetration for a chosen combination of laser power, laser traversing velocity, workpiece rotational speed and machining material. These data facilitate the determination of laser preheating levels to achieve required material softening depth at the workpiece surface before machining for improved product quality.
- Such depth of information is not practically feasible to capture through even the most sophisticated experimentation.

- For convenient application in workshop floor environment, computationally unsophisticated and practically simpler workpiece preheat forecasting parametric tool is synthesised by correlating the simulation data with ANN principles.
- This ‘trained’ ML approach facilitates the forecasting of LAM preheating requirements as an operational guide for manufacturing processes and identifies the potential for optimisation of LAM variables through preheating.
- Broadening validation of the CFD model analysis for both titanium alloy workpieces (black-painted and rough) shows acceptable agreement between numerical and experimental surface temperatures data.
- Both of lower strength of the laser beam and larger size of titanium workpiece was led to low-temperature and low-gradient field, as illustrated in Figure 5.18.

Chapter 6

Conclusions and Recommendations

This thesis presented a research investigation that examines laser pre-heating technique for enhancing the machinability of hard-to machine (HTM) material, titanium alloy (Ti-6Al-4V). This final chapter outlines and evaluates the technical benefits of this approach and methodology in delivering the objectives identified in Chapter One (section 1.7), along with the possible improvements in the proposed method for future research.

6.1 Introduction

The increased demands on special alloys, such as titanium alloys in the manufacture of engineered components have substantially contributed to innovations and developments in machining techniques. Among these, titanium-based alloys are highly attractive metals for applications, such as in aerospace and biomedical industries that demand extraordinary mechanical properties, namely high corrosion resistance, low weight/volume ratio, high biomechanical and biochemical compatibilities. However, a literature review conducted in the present work has clearly identified that the machining difficulties of titanium alloys is a major obstacle and challenge for its use in applications. This is essentially attributed to the extreme mechanical properties of titanium, such as low thermal conductivity, high hardness, fast hardening, chip morphology generated, auto excited chatter and high chemical reactivity. Owing to these, machining of titanium alloys is also associated with high rate of tool wear, that in turn reduces cutting tool service life. In overcoming such technical problems, titanium alloy machining is usually performed at a slower speed, hence product manufacturing cycle time and costs are major concerns. The thermal condition of titanium alloy workpiece can profoundly affect the dimensional accuracy of machined workpiece. Consequently, regulation of thermal influence has increasingly become an important aspect in modern machining.

Currently, many methods have been introduced and attempted to overcome these difficulties, where thermally assisted machining (TAM) is regarded as an

emerging technology for advanced manufacturing. Workpiece preheating in TAM, either immediately prior to or during cutting operation improves machinability from assisted plastic deformation. In this, the optimum workpiece surface temperature delivers maximum benefits, where thermal assistance would vary from alloy to alloy.

6.1.1 Thermal Assistance Method

From this thesis, a comprehensive appraisal of the current state of development in TAM techniques for improving the machinability of titanium alloys has been provided. It is identified that the main strategy of TAM is to reduce yield strength and the work hardening effects of the workpiece. With appropriate workpiece heating in TAM, plastic deformation is promoted in the cutting zone to reduce shear resistance at the cutting edge thereby lessening the cutting force and specific cutting energy while improving surface finish and tool life.

The optimum benefits of TAM are achieved at certain ranges of feed, speed and the temperature from preheating, depending on the behaviour of titanium alloys, such as the ability to conduct heat and modulus of elasticity. Within these limits, thermal effects produced by surface heating leads to a significant decrease in cutting forces at tool cutting edge. Although below these parametric ranges, a significant reduction of machining forces and machining energy is observed, the surface finish becomes unacceptable. In contrast beyond these ranges, tool wear is observed to be significantly higher. Therefore, prevention of workpiece overheating is critical for successful implementation of TAM that is to be ensured by estimating the peak preheating temperature. As such, careful analysis of surface temperature and workpiece temperatures distribution forms an essential research element in studies to determine optimum preheating conditions and machining parameters. In achieving these objectives, predictive thermal models are viewed to be essential for a clear understanding of heat transfer processes associated with TAM, supported by further experimentation.

The conclusion of previous studies of TAM applications has been shown positive results in terms of the longer tool life, lower cutting forces, smoother machined surface. Among current TAM approaches, Laser-Assisted technique is the most

efficient in improving the machinability of titanium alloys, which this research focus on using it as a preheating method.

6.1.2 Thermal Assistance Techniques

These are: laser assisted machining (LAM), plasma assisted machining (PAM), and induction assisted machining (IAM). These TAM techniques are carried out using a laser beam, plasma torch and an induction coil, respectively. LAM requires complex system components. Nonetheless, controlled operation of heat source movement is much easier than the other two techniques. Due to high laser power, microhardness at cutting zone is minimised, which in turn reduces tool pressure on the machined surface. Therefore, tool life significantly extended as a consequence of reduced cutting forces and rate of tool wear. Similar to LAM, cutting forces are reduced by PAM and IAM techniques.

However, achievable cutting tool life is shorter than with LAM. This is because, rate of flank wear tends to be more due to the high chip temperatures formed with these two techniques. Also, the power density of PAM is low, therefore heating temperatures are difficult to control compared with LAM. Therefore, laser techniques are highly recognised for improved titanium alloy machinability in terms lower machining forces, higher metal removal rate, lesser heat-affected zone, reduced tool wear, and better integrity in machined surface. Table 6.1 summarizes commonly used thermal assistance techniques to advance titanium alloy machinability.

The aforementioned review of experimental studies of LAM identifies a range of parameters, including material properties, operational conditions and laser characteristics, which contribute to the preheating thermal behaviour of a rotating cylinder due to laser spot heating. Due to the interdependency of these parameters, the experimental investigations provide limited scope for isolating such influences and accurate controlling of the variable. In this respect, numerical modelling offers the flexibility and versatility for a comprehensive analysis, whereby individual parametric effects can be appraised and understood with high flexibility. There have been several reported efforts in developing cost-effective and fairly reliable analytical models, albeit ignoring some key thermal and material aspects. In

improving the current knowledge base in this field, this work presents the development of a numerical simulation to describe the preheating thermal behaviour of a rotating cylinder subjected to laser spot as a surface heat source in LAM. The proposed numerical models are demonstrated to be not only more affordable tools but also offering thermal knowledge which may not be achieved even by decent measurement techniques (e.g. thickness of thermal diffusion).

Table 6. 1 Summary of TAM techniques used in titanium alloys machining

Features/ TAM Technique	Critical Parameters	Controlling Heating operation	Shape of Heating Area	Advantages
LAM	<ul style="list-style-type: none"> - Laser beam incident angle - Spot size. - Cutting tool / laser beam distance - Laser power 	Trouble-free operation	Spot area	<ul style="list-style-type: none"> - Improving MRR - Decreasing 30% - 60% in cutting forces - Getting a better surface finish - Reducing tool wear around 90%
PAM	<ul style="list-style-type: none"> - Voltage electric arc. - Type of material - Surface temperature - Emissivity of surface 	Difficult operation	Localised area	<ul style="list-style-type: none"> - Decreasing 20% - 40% in cutting forces - Increasing MRR around 2 times - Enhancing cutting tool life around 1.5 times - Lower power requirement
IAM	<ul style="list-style-type: none"> - Frequency and intensity of the input electric current - Induction coil shape - Specific heat, magnetic permeability, and current flow resistance of the material 	Simple operation	Surface area directly adjacent to the coil shape	<ul style="list-style-type: none"> - Reduction of acceleration of amplitude to range 25% - 80% - Reducing the cutting force in range 36% to 54% - - Increasing by around 206% and 214% for tool life and volume of metal removal, respectively - Decreasing sharply in surface roughness up to certain heating temperature, then beyond this temperature slightly increases - Almost continuous chip produced with increasing heating temperature

6.2 Experimental Work

A small-scale rig has been designed to simulate lathe machine without cutting tool. The test-rig has been designed to make a process of monitoring the heating a rotating workpiece surface by low power laser, the with use IR camera. This test-rig consists of several parts namely: two metallic bases (fixed and mobile), one bearing, two titanium alloy workpieces, DC spinning motor, DC motor for linear velocity, and speed control box. Before doing the experiments, the laser reflection test has been done for safety tests and check the absorptivity for the workpiece surface, as well. Reflection test has been shown that most of the laser energy has reflected from the shiny surface of Ti-6Al-4V workpiece. Therefore, the need to know the emissivity of the workpiece surface was necessary, which prompted the test of emissivity.

The emissivity test measured the normal spectral emissivity of the Ti-6Al-4V alloy and explored the possible reasons for the oscillatory behaviour in emissivity during the thermal process. A simple method has been set up to quickly test the with an infrared thermal imaging system within a small distance according to the theory of measuring temperature by infrared system, which is based on the Planck radiation law and Lambert-beer law. The workpiece temperature has promoted and held on by a heat gun while a temperature difference has been formed between the workpiece and environment. Further, the emissivity and the testing distance between IR camera and workpiece were set at 1.0 & 0.2 m, respectively. In the present test, the effect of surface conditions on the normal spectral emissivity of the Ti-6Al-4V alloy was investigated at a temperature range from 25 °C to 120 °C. This test describes the emissivity estimation of the three workpieces (shiny, rough, painted) to be used for correlation in numerical study of the heating Ti-6Al-4V workpiece by CO₂ laser.

The results of an emissivity test for shiny, painted, and rough workpieces have been plotted in figures (3.33), (3.34) and (3.35), respectively. The measurement results of emissivity test are in good agreement with the data reported by other literatures. As clearly seen in figures (3.34) and (3.35), the normal spectral emissivity results of two different types of the Ti-6Al-4V workpiece surface showed the same rule and trends. The emissivity of rough and painted surfaces decreases with the increase of workpiece temperature. The test results confirmed that both black-painted and rough surfaces have a better value of emissivity compared with a

shiny surface. Additionally, it has found that the absorbance of the black-painted surface higher than the rough one. It is remarkable that, between 25 °C and 120 °C, the emissivity of the rough surface goes to a maximum (0.63) around 64 °C. While the testing results show the emissivity of the black-painted surfaces reached to the maximum (0.91) around 75 °C.

The experimental work of this research has been carried out in four stages with two titanium alloy workpieces. The machine laser Photon Machine (C-55L CO₂ laser) was used as a heating system to preheat workpiece in the experiments. Furthermore, to measure the temperatures distribution at the workpiece surface, the FLIR ThermoVision™ A40V Camera has been utilized for that. All the experiments have done at thermal emissivity (0.5) and fixed distance setting IR camera away from the workpiece.

6.3 Numerical Work

To emulate a typical LAM setup, the modelling configuration used for simulating the preheating thermal behaviour of a cylindrical workpiece subjected to laser beam as a heat surface source in advance of the machining process. As the intended purpose, the model is setup only to examine the laser preheating requirements for appraising the material softening potential in preparation for the subsequent cutting operation. Hence, the cutting-generated heat is not included in the analysis, allowing the examination of laser preheating thermal behaviour in isolation of the cutting tool integration. A finite volume-based numerical simulation that examines and analyses the thermal response imparted by laser spot preheating on a rotating surface. The process surface behaviours which include absorption, reflection and forced convection (as a result of rotation) are considered as boundary conditions while heat diffusion across the rotating geometry is simulated. Thus, the simulation modelling accounts for the radiative heat absorption over the laser spot, the combined convective and radiative surface heat losses from the entire workpiece surface.

This problem has various numerical and physical sensitivity issues that are crucial for obtaining valid results. The model examined the influence of laser power, laser scanning and rotational speed on surface temperatures distribution. The combined cylinder rotation and the laser transverse motion impart a unique fluctuating temperature profile that propagates into the workpiece material. The

numerical analysis is developed using a three-dimensional finite volume framework and the ANSYS FLUENT platform, recognising their advantages as a computational scheme. The FVM is more robust in handling conservation equation and energy diffusion with embedded heat sources. Moreover, it warrants the use of single rotating reference frame (SRF), as required in modelling the workpiece rotation and complex temperature-dependent formulation involving combined convective and radiative thermal boundary condition. Apart from the numerical accuracy and robustness, ANSYS FLUENT is utilised for its ease of implementation, solver compatibility with other multi-physics platforms (Finite element modules for thermostructural behaviours) and the code versatility in customisation.

The three-dimension numerical model developed needs to conform to some critical requirements in order to achieve converging, stable and valid simulation. In spite of the advection term being absent, the transport equation is theoretically prone to be unbound and leads to truncation errors. With low-order discretisation scheme (first order upwind) or insufficient mesh refinement, numerical instability is readily observed as a consequence of large spatial and temporal gradients across the domain that could force the solver into a rapid divergence. Therefore, grid generation was initially set through a global estimation of relative truncation error (as a function of average grid spacing). Accordingly, further grid refinement was applied on domain boundaries to include sufficient resolution for effective management of laser intensity profile and convection heat loss over the curved cylindrical surface.

Application of large energy heat source over a small area of the laser spot at the boundary gives rise to high spatial temperature gradients that leads to mesh-oriented nonlinearity. In avoiding such issues, the radial mesh resolution is increased towards the curved cylindrical surface. These refinements are applied across five layers of cells for smoother transition, starting from a coarser distribution in the centre core. The sensitivity arising from the ratio of angular mesh resolution to rotational velocity has also been considered as a temporal criterion for grid generation. In this, the refinement was kept at not less than 1 angular refinement and within 0.1 mm for laser movement. The final mesh consists of 858.231 hexagonal cells. Temporal refinement of 0.01s is applied for the cases investigated, giving sufficient robustness even for the maximum Courant number (based on heat flux estimations) due to the implicit time scheme utilised. QUICK formulation is used

for spatial discretisation of energy equation with a second-order implicit temporal discretisation. Discretisation scheme of higher than first-order accuracy is necessary for both convergence and validity.

The modelling parameters of laser properties, cylinder dimensions, cutting variable and temperature recording locations are chosen to match those of a previous experimental study, allowing model validation and sensitivity analysis against the known data. Using the experimental data, the simulation model is validated in three stages to establish the prediction accuracy, the assumptions made and the parametric sensitivity, as outlined below. They are as follows: (a) establishing appropriate laser profile, (b) appraisal of transient surface thermal response of the cylinder against the three measured data points and (c) influence from varying laser power output and laser traverse velocity.

With the validated numerical model, this study extends its applied usefulness to formulate a practically usable parametric predictor as a guiding tool for LAM preheating operations. For this, the model is first deployed to produce a vast array of data sets on the thermal behaviour of cylindrical workpiece with laser spot heating encompassing a range of parameters including laser power and rotational velocity. Such a unique collection of information is extremely tedious, costly and time-consuming to obtain through experimental means, thus vindicating the advantages of the simulation methodology presented. These simulated data sets are then correlated through ANN principles and ML algorithm to synthesise the LAM preheating parametric predictor. This tool is trained for assimilating parametric effects over the entire range of simulated data, thus making it capable of forecasting the most effective laser preheating requirements for LAM for a chosen input of cutting parameters. Guided by this tool, the LAM operations can be performed with precise preheating levels necessary to obtain the required depth of thermal penetration into the workpiece for improved machinability.

For illustrating the ANN predictor concept, this study adopts a simplified data set of quasi-steady temperatures of the preheated workpiece, instead of its transient thermal behaviour, without sacrificing the applied practicality and the technical significance. For generating such data, the transient thermal model is executed with non-traversing laser heating applied to the rotating cylinder until thermal equilibrium (quasi-steady state) is reached. The circumferential

temperatures reflect the combined effects of workpiece cooling by convection and radiation from the surface and thermal diffusion into the workpiece core. The radial temperatures essentially capture the thermal diffusion effect and the depth of heat penetration into the workpiece body. Therefore, this discrete data set represents the full steady thermal picture of the preheated cylindrical workpiece and is indicative of the laser heating required to impose targeted thermally softened material depth for LAM.

To attain a better thermal understanding for preheating titanium alloy workpiece by a low-power laser beam, the numerical model has been used and run with new sets of simulations. These simulation sets were built-up according to the experiments explained in Chapter three. This investigation was executed for a higher range of rotational Reynolds Number, which is not many examined in the previous studies of this research area. Two major outcomes have been gained from these sets of emulations, firstly, expanding the effectiveness of the numerical model analysis by comparing the numerical data with the data of our current experiments. Secondly, achieve a good understanding of temperatures distribution inside Ti-6Al-4V workpiece by visual the diffusion pattern.

6.4 Achievements

Preheating of workpiece before initiating cutting process has indicated much more effectiveness in increasing the machinability than other techniques used for HTM materials. In the present experiments, the reproducibility of the surface temperature data of Ti-6Al-4V workpiece was excellent, which showed that the random errors did not bring about any observable effect on the experimental results. One of the most convenient and effective ways to reduce the difficulties of a titanium alloys machining and increase its working accuracy is process of the preheating workpiece, especially for turning process. The results presented here may facilitate improvements in the machining of titanium alloy (Ti-6Al-4V). The detailed conclusions drawn from these experiments are as follows:

- ✓ The behaviour of surface temperatures increasing was found similar during heating black-painted workpiece and rough workpiece, as well.

- ✓ A laser beam with low power is a beneficial heating source to rise surface temperature and soften the workpiece surface layer.
- ✓ The achieved surface temperature will be enough to decrease the cutting tool pressure on the workpiece surface, thus, decrease cutting forces during the machining process.

The main achievement of this thesis is the development of a new three-dimension numerical model for predicting temperatures distribution. The newly developed model has been verified experimentally and efficiently applied in real machining. The numerical investigation and its ensuing outcomes presented in this thesis provide unique analytical and practical benefits for applications involving laser-assisted manufacturing processes. The numerical investigation and its ensuing outcomes presented in this research provide unique analytical and practical benefits for applications involving laser-assisted manufacturing processes. The key aspects and deliverables of this investigation are concluded below:

- The study has formulated a well-validated and accurate numerical model for predicting the transient thermal behaviour of a cylindrical rotating workpiece due to laser preheating, as used in LAM applications. Overcoming previous analytical limitations, the model accounts for the complex thermal processes associated with heat absorption over the laser spot area, thermal diffusion into the workpiece, and the cylinder surface cooling arising from thermal radiation and rotational convection.
- Advancing the status-quo of numerical modelling for this field, this simulation methodology is developed on a single rotating reference frame (SRF), incorporating the combined motion effects of workpiece rotation and traversing laser beam, hence presenting a much realistic treatment of LAM workpiece behaviour subjected to laser spot heating. The predictive precision is derived through boundary configuration involving dynamic surface profile and source term that guarantee validity and stability of simulation.
- This carefully developed simulation delivers flexibility to extract thermal information, hence warranting insightful understanding on the transient thermal behaviour of a laser-preheated rotating cylinder. Such depth of

information is not practically feasible to capture through even the most sophisticated experimentation.

- Covering a wide parametric range for LAM variable, the model is extended to generate an extensive data set, which is correlated and trained using Artificial Neural Network principles to synthesise a parametric predictor. This machine learning approach facilitates the forecasting of LAM preheating requirements as an operational guide for manufacturing processes and identifies the potential for optimisation of LAM variables through preheating.
- Expanding the simulation process by emulating heating cylindrical Ti-6Al-4V workpiece according to the set-up of the experiments of the current study, gives a better picture to understand the thermal gain from the identical laser beam through absorption and re-radiation process.

6.5 Suggested Improvements and Recommendations for Future Research Interests

This work has clearly identified the simulation possibility for modelling the transient thermal problem associated with heated rotating cylinders. Nonetheless, the model validation was limited to data of preheating the workpiece before starting the cutting process, hence comprehensive analysis could not be performed for machining operation. The following suggestions are made to consider developing the numerical model for future expansion of this research work:

- ❖ Improvement the numerical model to simulate a transient thermal behaviour of the preheating rotating workpiece during the cutting process.
- ❖ Considering different heating styles by laser (spots, zig-zag, curves ... etc.) in future cases studies for heating rotating cylindrical workpiece.
- ❖ Further investigation should be taken on the study thermal stresses at the heating area and cutting zone, before and during the preheating process.
- ❖ Monitoring the torsional vibrations of the workpiece before/after cutting operation to study the effect of preheating process.
- ❖ The obvious focus must be on the monitoring plastic deformation at the heating zone and contact spot of a cutting tool and workpiece.

- ❖ Studying the influence of the setting LAM parameters (laser power, wavelength... etc.) on the mechanical properties of the workpiece metal.
- ❖ Further investigation of the transient thermal problem in LAM associated with heated rotating cylinders with a wide range of laser properties and machining parameters.

References

1. Ezugwu E, Wang Z. Titanium alloys and their machinability—a review. *Journal of materials processing technology*. 1997;68(3):262-74.
2. Gorynin I. Titanium alloys for marine application. *Materials Science and Engineering: A*. 1999;263(2):112-6.
3. Yang X, Richard Liu C. Machining titanium and its alloys. *Machining Science and Technology*. 1999;3(1):107-39.
4. Davim JP. *Machining: fundamentals and recent advances*: Springer Science & Business Media; 2008.
5. Lütjering G, Williams JC. *Titanium*: Springer; 2003.
6. Donachie MJ. *Titanium: a technical guide*: ASM international; 2000.
7. Shokrani A, Dhokia V, Newman ST. Environmentally conscious machining of difficult-to-machine materials with regard to cutting fluids. *International Journal of Machine Tools and Manufacture*. 2012;57:83-101.
8. Gurrappa I. Characterization of titanium alloy Ti-6Al-4V for chemical, marine and industrial applications. *Materials Characterization*. 2003;51(2):131-9.
9. Boyer R. An overview on the use of titanium in the aerospace industry. *Materials Science and Engineering: A*. 1996;213(1):103-14.
10. Zhou Y, Zeng W, Yu H. An investigation of a new near-beta forging process for titanium alloys and its application in aviation components. *Materials Science and Engineering: A*. 2005;393(1):204-12.
11. Pérez J, Llorente J, Sanchez J. Advanced cutting conditions for the milling of aeronautical alloys. *Journal of Materials Processing Technology*. 2000;100(1):1-11.
12. Ezugwu E. Key improvements in the machining of difficult-to-cut aerospace superalloys. *International Journal of Machine Tools and Manufacture*. 2005;45(12):1353-67.
13. Rack HJ, Qazi J. Titanium alloys for biomedical applications. *Materials Science and Engineering: C*. 2006;26(8):1269-77.
14. Niinomi M. Mechanical properties of biomedical titanium alloys. *Materials Science and Engineering: A*. 1998;243(1):231-6.
15. Niinomi M. Mechanical biocompatibilities of titanium alloys for biomedical applications. *Journal of the mechanical behavior of biomedical materials*. 2008;1(1):30-42.
16. Liu X, Chu PK, Ding C. Surface modification of titanium, titanium alloys, and related materials for biomedical applications. *Materials Science and Engineering: R: Reports*. 2004;47(3):49-121.
17. Murr L, Quinones S, Gaytan S, Lopez M, Rodela A, Martinez E, et al. Microstructure and mechanical behavior of Ti-6Al-4V produced by rapid-layer manufacturing, for biomedical applications. *Journal of the mechanical behavior of biomedical materials*. 2009;2(1):20-32.
18. Thomas M, Turner S, Jackson M. Microstructural damage during high-speed milling of titanium alloys. *Scripta materialia*. 2010;62(5):250-3.
19. Welsch G, Boyer R, Collings E. *Materials properties handbook: titanium alloys*: ASM international; 1993.
20. Pramanik A. Problems and solutions in machining of titanium alloys. *The International Journal of Advanced Manufacturing Technology*. 2014;70(5-8):919-28.
21. Abele E, Hölscher R. *New Technology for High Speed Cutting of Titanium Alloys. New Production Technologies in Aerospace Industry*: Springer; 2014. p. 75-81.
22. Shams O, Pramanik A, Chandratilleke T. *Thermal-Assisted Machining of Titanium Alloys. Advanced Manufacturing Technologies*: Springer; 2017. p. 49-76.
23. Madhavulu G, Ahmed B. Hot machining process for improved metal removal rates in turning operations. *Journal of materials processing technology*. 1994;44(3):199-206.

24. Amin A, Ginta TL. Heat-assisted machining. Elsevier Ltd.; 2014.
25. Przystacki D, Jankowiak M, editors. Surface roughness analysis after laser assisted machining of hard to cut materials. Journal of Physics: Conference Series; 2014: IOP Publishing.
26. Pfefferkorn FE, Lei S, Jeon Y, Haddad G. A metric for defining the energy efficiency of thermally assisted machining. International Journal of Machine Tools and Manufacture. 2009;49(5):357-65.
27. Krabacher E.J., M.E. M. Basic factor of hot machining of metals. Journal of Engineering for Industry. 1951;73:761-76.
28. Ginta TL, Amin AN. Machinability Improvement in End Milling Titanium Alloy Ti-6Al-4V. 2010;Vol. 3:pp. 25-33.
29. Radovanovic MR, Dašić PV. LASER ASSISTED TURNING. Research and Development in Mechanical Industry; 13 - 17. September 2006; Budva, Montenegro: RaDMI 2006; 2006. p. 312-6.
30. Shin YC. LAM benefits a wide range of difficult-to-machine materials. Journal of Industrial Laser Solution for Manufacturing. 2011.
31. Pentland W., Mehl C., J. W. Hot machining. American Machinist/Metalworking Manufacturing. 1960;1:117-32.
32. Çakır O, Altan E. HOT MACHINING OF HIGH MANGANESE STEEL: A REVIEW. Trends in the Development of Machinery and Associated Technology; Istanbul, Turkey2008. p. 105-8.
33. Özler L, Inan A, Özel C. Theoretical and experimental determination of tool life in hot machining of austenitic manganese steel. International Journal of Machine Tools and Manufacture. 2001;41(2):163-72.
34. Rajopadhye R. D., Telsang M. T., S. DN. Experimental setup for hot machining process to increase tool life with torch flame. Second International Conference on Emerging Trends in engineering (SICETE); 16th to 18th December 2009; Nagpur, Maharashtra, India2009. p. 58-62.
35. Tosun N, Ozler L. Optimisation for hot turning operations with multiple performance characteristics. The International Journal of Advanced Manufacturing Technology. 2004;23(11-12):777-82.
36. Rebro P. A., Pfefferkorn F. E., Shin Y. C., P. IF. Comparative assessment of laser-assisted machining for various ceramics. Transactions of North American Manufacturing Research Institution2002. 153-60 p.
37. Chryssolouris G, Anifantis N, Karagiannis S. Laser assisted machining: an overview. Journal of manufacturing science and engineering. 1997;119(4B):766-9.
38. Dumitrescu P, Koshy P, Stenekes J, Elbestawi M. High-power diode laser assisted hard turning of AISI D2 tool steel. International Journal of Machine Tools and Manufacture. 2006;46(15):2009-16.
39. Warap N, Mohid Z, Rahim EA, editors. Laser assisted machining of titanium alloys. Materials Science Forum; 2013: Trans Tech Publ.
40. Mantle A., D A. Tool life and surface roughness when high speed machining a gamma titanium aluminide, progress of cutting and grinding. In: Turpan Ua, editor. Fourth International Conference on Progress of Cutting and Grinding; China: International Academic Publishers; 1998. p. 89-94.
41. Veiga C, Davim J, Loureiro A. Review on machinability of titanium alloys: the process perspective. Reviews on Advanced Materials Science. 2013;34(2):148-64.
42. Pramanik A, Littlefair G. Machining of Titanium Alloy (Ti-6Al-4V)—Theory to Application. Machining Science and Technology. 2015;19(1):1-49.
43. Verma D.R.S.V., NandaGopal B.G., Srinivasulu K., S. SR. Effect of pre-drilled holes on tool life in turning of aerospace titanium alloys. Proceedings of the National Conference on

- Advances in Manufacturing System; Kolkata, India: Production Engineering Department, Jadavpur University; 2003. p. 42–7.
44. Dornfeld D, Kim J, Dechow H, Hewson J, Chen L. Drilling burr formation in titanium alloy, Ti-6Al-4V. *CIRP Annals-Manufacturing Technology*. 1999;48(1):73-6.
 45. Oosthuizen G. A., Akdogan G., Dimitrov D., F. TN. A review of the machinability of titanium alloys. *R&D Journal of the South African Institution of Mechanical Engineering*. 2010;26:43-52.
 46. Ezugwu E, Bonney J, Yamane Y. An overview of the machinability of aeroengine alloys. *Journal of materials processing technology*. 2003;134(2):233-53.
 47. Gupta K, Laubscher RF. Sustainable machining of titanium alloys: A critical review. *Proceedings of the Institution of Mechanical Engineers, Part B: Journal of Engineering Manufacture*. 2016:0954405416634278.
 48. Dandekar CR, Shin YC. Laser-assisted machining of a fiber reinforced metal matrix composite. *Journal of manufacturing science and engineering*. 2010;132(6):061004.
 49. Khanna N, Garay A, Iriarte LM, Soler D, Sangwan KS, Arrazola PJ. Effect of heat treatment conditions on the machinability of Ti64 and Ti54M alloys. *Procedia CIRP*. 2012;1:477-82.
 50. Brecher C, Emonts M, Rosen C-J, Hermani J-P. Laser-assisted milling of advanced materials. *Physics Procedia*. 2011;12:599-606.
 51. Venugopal K, Paul S, Chattopadhyay A. Growth of tool wear in turning of Ti-6Al-4V alloy under cryogenic cooling. *Wear*. 2007;262(9):1071-8.
 52. Bandapalli C., Sutaria B. M., V. BD. High speed machining of Ti-alloys- A critical review. *Proceedings of the 1 International and 16 National Conference on Machines and Mechanisms (iNaCoMM2013); Dec 18-19; India: IIT Roorkee; 2013. p. 324-31.*
 53. Che-Haron C. Tool life and surface integrity in turning titanium alloy. *Journal of Materials Processing Technology*. 2001;118(1):231-7.
 54. Komanduri R, Von Turkovich B. New observations on the mechanism of chip formation when machining titanium alloys. *Wear*. 1981;69(2):179-88.
 55. Hartung PD, Kramer B, Von Turkovich B. Tool wear in titanium machining. *CIRP Annals-Manufacturing Technology*. 1982;31(1):75-80.
 56. Jawaid A, Che-Haron C, Abdullah A. Tool wear characteristics in turning of titanium alloy Ti-6246. *Journal of Materials Processing Technology*. 1999;92:329-34.
 57. Nabhani F. Machining of aerospace titanium alloys. *Robotics and Computer-Integrated Manufacturing*. 2001;17(1):99-106.
 58. Wang Z, Wong Y, Rahman M. High-speed milling of titanium alloys using binderless CBN tools. *International Journal of Machine Tools and Manufacture*. 2005;45(1):105-14.
 59. Wang Z, Rahman M, Wong Y. Tool wear characteristics of binderless CBN tools used in high-speed milling of titanium alloys. *Wear*. 2005;258(5):752-8.
 60. Che-Haron C. H., A. J. The effect of machining on surface integrity of titanium alloy Ti-6% Al-4% V. *Journal of Materials Processing Technology*. 2005;166:188-92.
 61. Nouari M, Ginting A. Wear characteristics and performance of multi-layer CVD-coated alloyed carbide tool in dry end milling of titanium alloy. *Surface and Coatings Technology*. 2006;200(18):5663-76.
 62. Haron CC, Ginting A, Arshad H. Performance of alloyed uncoated and CVD-coated carbide tools in dry milling of titanium alloy Ti-6242S. *Journal of Materials Processing Technology*. 2007;185(1):77-82.
 63. Amin AN, Ismail AF, Khairusshima MN. Effectiveness of uncoated WC-Co and PCD inserts in end milling of titanium alloy—Ti-6Al-4V. *Journal of Materials Processing Technology*. 2007;192:147-58.
 64. Jianxin D, Yousheng L, Wenlong S. Diffusion wear in dry cutting of Ti-6Al-4V with WC/Co carbide tools. *Wear*. 2008;265(11):1776-83.

65. Dargusch MS, Zhang MX, Palanisamy S, Buddery AJM, StJohn DH. Subsurface deformation after dry machining of grade 2 titanium. *Advanced Engineering Materials*. 2008;10(1-2):85-8.
66. Ibrahim G, Haron CC, Ghani J. Surface integrity of Ti-6Al-4V ELI when machined using coated carbide tools under dry cutting condition. *Int J Mech Mater Eng*. 2009;4(2):191-6.
67. Sun S, Brandt M, Dargusch M. Characteristics of cutting forces and chip formation in machining of titanium alloys. *International Journal of Machine Tools and Manufacture*. 2009;49(7):561-8.
68. Abdel-Aal H, Nouari M, El Mansori M. Tribo-energetic correlation of tool thermal properties to wear of WC-Co inserts in high speed dry machining of aeronautical grade titanium alloys. *Wear*. 2009;266(3):432-43.
69. Fang N, Wu Q. A comparative study of the cutting forces in high speed machining of Ti-6Al-4V and Inconel 718 with a round cutting edge tool. *Journal of Materials Processing Technology*. 2009;209(9):4385-9.
70. Armendia M, Garay A, Iriarte L-M, Arrazola P-J. Comparison of the machinabilities of Ti6Al4V and TIMETAL® 54M using uncoated WC-Co tools. *Journal of Materials Processing Technology*. 2010;210(2):197-203.
71. Özel T, Sima M, Srivastava A, Kaftanoglu B. Investigations on the effects of multi-layered coated inserts in machining Ti-6Al-4V alloy with experiments and finite element simulations. *CIRP Annals-Manufacturing Technology*. 2010;59(1):77-82.
72. Kali D, S R C. Machinability Study of Titanium (Grade-5) Alloy Using Design of Experiment Technique. *Engineering*. 2011;2011.
73. Honghua S, Peng L, Yucan F, Jiuhua X. Tool life and surface integrity in high-speed milling of titanium alloy TA15 with PCD/PCBN tools. *Chinese Journal of Aeronautics*. 2012;25(5):784-90.
74. Mhamdi M, Boujelbene M, Bayraktar E, Zghal A. Surface integrity of titanium alloy Ti-6Al-4V in ball end milling. *Physics Procedia*. 2012;25:355-62.
75. Ugarte A, M'Saoubi R, Garay A, Arrazola P. Machining Behaviour of Ti-6Al-4V and Ti-5553 Alloys in Interrupted Cutting with PVD Coated Cemented carbide. *Procedia CIRP*. 2012;1:202-7.
76. Nouari M, Makich H. Experimental investigation on the effect of the material microstructure on tool wear when machining hard titanium alloys: Ti-6Al-4V and Ti-555. *International Journal of Refractory Metals and Hard Materials*. 2013;41:259-69.
77. Balaji J, Krishnaraj V, Yogeswaraj S. Investigation on high speed turning of titanium alloys. *Procedia Engineering*. 2013;64:926-35.
78. Cotterell M, Ares E, Yanes J, López F, Hernandez P, Peláez G. Temperature and strain measurement during chip formation in orthogonal cutting conditions applied to Ti-6Al-4V. *Procedia Engineering*. 2013;63:922-30.
79. Shetty PK, Shetty R, Shetty D, Rehaman NF, Jose TK. Machinability Study on Dry Drilling of Titanium Alloy Ti-6Al-4V using L 9 Orthogonal Array. *Procedia Materials Science*. 2014;5:2605-14.
80. Li N, Chen Y, Kong D, Tan S. Experimental investigation with respect to the performance of deep submillimeter-scaled textured tools in dry turning titanium alloy Ti-6Al-4V. *Applied Surface Science*. 2017;403:187-99.
81. Lauwers B, Klocke F., A. K. Advanced manufacturing through the implementation of hybrid and media assisted processes. *Int Chemnitz Manufacturing Colloquium*. 2010;54:205-20.
82. Amin A, Abdelgadir M. The effect of preheating of work material on chatter during end milling of medium carbon steel performed on a vertical machining center (VMC). *Journal of manufacturing science and engineering*. 2003;125(4):674-80.

83. Amin AN, Dolah SB, Mahmud MB, Lajis M. Effects of workpiece preheating on surface roughness, chatter and tool performance during end milling of hardened steel D2. *Journal of Materials Processing Technology*. 2008;201(1):466-70.
84. Ginta TL, Amin A, Lajis MA, Karim A, Mohd Radzi H. Improved tool life in end milling Ti-6Al-4V through workpiece preheating. *European Journal of Scientific Research*. 2009;27(3):384-91.
85. Lajis MA, Amin A, Karim A, Daud C, Radzi M, Ginta TL. Hot machining of hardened steels with coated carbide inserts. *American Journal of Engineering and Applied Sciences*. 2009;2(2):421-7.
86. Ktagawa T, Maekawa K. Plasma hot machining for new engineering materials. *Wear*. 1990;139(2):251-67.
87. Popa L. Complex Study of Plasma Hot Machining (PMP). *Revista de Tehnologii Neconventionale*. 2012;16(1):26.
88. Jau B.M., Copley S.M., M. B. Laser assisted machining. *Proceedings of the Ninth North American Manufacturing Research Conference; University Park, Pennsylvania*1981. p. 12–5.
89. Rajagopal S, Plankenhorn D, Hill V. Machining aerospace alloys with the aid of a 15 kW laser. *Journal of Applied Metalworking*. 1982;2(3):170-84.
90. Thomas T, Vignneau JO. Laser-assisted milling process. *Google Patents*; 1999.
91. Nakayama K, Arai M, Kanda T. Machining characteristics of hard materials. *CIRP Annals-Manufacturing Technology*. 1988;37(1):89-92.
92. Darsin M, Basuki HA, editors. *Development Machining of Titanium Alloys: A Review*. *Applied Mechanics and Materials*; 2014: Trans Tech Publ.
93. Pramanik A, Dixit A, Chattopadhyaya S, Uddin M, Dong Y, Basak A, et al. Fatigue life of machined components. *Advances in Manufacturing*. 2017;5(1):59-76.
94. Ulutan D, Ozel T. Machining induced surface integrity in titanium and nickel alloys: a review. *International Journal of Machine Tools and Manufacture*. 2011;51(3):250-80.
95. Jaffery S, Mativenga P. Assessment of the machinability of Ti-6Al-4V alloy using the wear map approach. *The International Journal of Advanced Manufacturing Technology*. 2009;40(7):687-96.
96. Arrazola P-J, Garay A, Iriarte L-M, Armendia M, Marya S, Le Maitre F. Machinability of titanium alloys (Ti6Al4V and Ti555. 3). *Journal of Materials Processing Technology*. 2009;209(5):2223-30.
97. Isbilir O, Ghassemieh E. Comparative study of tool life and hole quality in drilling of CFRP/titanium stack using coated carbide drill. *Machining Science and Technology*. 2013;17(3):380-409.
98. Odelros S. Tool wear in titanium machining. 2012.
99. Balažic M, Kopač J. Machining of Titanium Alloy Ti-6Al-4V for biomedical applications. *Strojniški vestnik-Journal of Mechanical Engineering*. 2010;56(3):202-6.
100. Ying-lin K., Hui-yue D., Gang L., Z. M. Use of nitrogen gas in high-speed milling of Ti-6Al-4V. *Trans Nonferrous Met Soc, China*. 2009;19:530-4.
101. Machado A, Wallbank J. Machining of titanium and its alloys—a review. *Proceedings of the Institution of Mechanical Engineers, Part B: Journal of Engineering Manufacture*. 1990;204(1):53-60.
102. Zhecheva A, Sha W, Malinov S, Long A. Enhancing the microstructure and properties of titanium alloys through nitriding and other surface engineering methods. *Surface and Coatings Technology*. 2005;200(7):2192-207.
103. Kuttolamadom M, Jones J, Mears L, Kurfess T, Choragudi A. Investigation of the Machining of Titanium Components for Lightweight Vehicles. *SAE Technical Paper*; 2010. Report No.: 0148-7191.

104. Kumar J, Kumar V. Evaluating the tool wear rate in ultrasonic machining of titanium using design of experiments approach. *World Academy of Science, Engineering and Technology*. 2011;81:803-8.
105. Komanduri R, Hou Z-B. On thermoplastic shear instability in the machining of a titanium alloy (Ti-6Al-4V). *Metallurgical and Materials Transactions A*. 2002;33(9):2995-3010.
106. El-Wardany T, Mohammed E, Elbestawi M. Cutting temperature of ceramic tools in high speed machining of difficult-to-cut materials. *International Journal of Machine Tools and Manufacture*. 1996;36(5):611-34.
107. Dearnley P, Grearson A. Evaluation of principal wear mechanisms of cemented carbides and ceramics used for machining titanium alloy IMI 318. *Materials Science and Technology*. 1986;2(1):47-58.
108. Bridges P, Magnus B. *Manufacture of Titanium Alloy Components for Aerospace and Military Applications*. Research and Technology Organization, France. 2001.
109. Shaw MC. *Metal cutting principles*: Oxford university press New York; 2005.
110. Amin A, Hossain MI, Patwari AU, editors. Enhancement of Machinability of Inconel 718 in End Milling through Online Induction Heating of Workpiece. *Advanced Materials Research*; 2011: Trans Tech Publ.
111. Trent EM, Wright PK. *Metal cutting*: Butterworth-Heinemann; 2000.
112. Kumar J, Khamba J. An experimental study on ultrasonic machining of pure titanium using designed experiments. *Journal of the Brazilian Society of Mechanical Sciences and Engineering*. 2008;30(3):231-8.
113. Amin AN, Abraham I, Khairusshima N, Ahmed MI. Influence of preheating on performance of circular carbide inserts in end milling of carbon steel. *Journal of materials processing technology*. 2007;185(1):97-105.
114. Rashid RR, Sun S, Wang G, Dargusch M. The effect of laser power on the machinability of the Ti-6Cr-5Mo-5V-4Al beta titanium alloy during laser assisted machining. *International Journal of machine tools and manufacture*. 2012;63:41-3.
115. Pramanik A, Islam M, Basak A, Littlefair G, editors. *Machining and tool wear mechanisms during machining titanium alloys*. *Advanced Materials Research*; 2013: Trans Tech Publ.
116. Corduan N, Himbart T, Poulachon G, Dessoly M, Lambertin M, Vigneau J, et al. Wear mechanisms of new tool materials for Ti-6Al-4V high performance machining. *CIRP Annals-Manufacturing Technology*. 2003;52(1):73-6.
117. Ginta TL, Amin AN, Karim A, Sutjipto AG, editors. Tool life prediction by response surface methodology for end milling titanium alloy Ti-6Al-4V using uncoated carbide inserts. *International Conference on Mechanical Engineering*; 2007.
118. Abd Rahim E, Warap N, Mohid Z. Thermal-assisted machining of nickel-based alloy. 2015.
119. Zanger F, Schulze V. Investigations on mechanisms of tool wear in machining of Ti-6Al-4V using FEM simulation. *Procedia CIRP*. 2013;8:158-63.
120. Ezugwu EO, Bonney J, Da Silva RB, Cakir O. Surface integrity of finished turned Ti-6Al-4V alloy with PCD tools using conventional and high pressure coolant supplies. *International Journal of Machine Tools and Manufacture*. 2007;47(6):884-91.
121. Rahman M, Wang Z-G, Wong Y-S. A review on high-speed machining of titanium alloys. *JSME International Journal Series C Mechanical Systems, Machine Elements and Manufacturing*. 2006;49(1):11-20.
122. Chauhan DK, Chauhan KK. Optimization of Machining Parameters of Titanium Alloy for Tool Life. *Journal of Engineering Computers & Applied Sciences*. 2013;2(6):57-65.
123. Kato K. Wear in relation to friction—a review. *Wear*. 2000;241(2):151-7.

124. Uddin M, Pham B, Sarhan A, Basak A, Pramanik A. Comparative study between wear of uncoated and TiAlN-coated carbide tools in milling of Ti6Al4V. *Advances in Manufacturing*. 2017;5(1):83-91.
125. Shivpuri R, Hua J, Mittal P, Srivastava A, Lahoti G. Microstructure-mechanics interactions in modeling chip segmentation during titanium machining. *CIRP Annals-Manufacturing Technology*. 2002;51(1):71-4.
126. Sun J, Guo Y. A comprehensive experimental study on surface integrity by end milling Ti-6Al-4V. *Journal of Materials Processing Technology*. 2009;209(8):4036-42.
127. Sun S, Brandt M, Dargusch M. The effect of a laser beam on chip formation during machining of Ti6Al4V alloy. *Metallurgical and Materials Transactions A*. 2010;41(6):1573-81.
128. Ke Q, Xu D, Xiong D. Cutting zone area and chip morphology in high-speed cutting of titanium alloy Ti-6Al-4V. *Journal of Mechanical Science and Technology*. 2017;31(1):309-16.
129. Rashid RR, Bermingham M, Sun S, Wang G, Dargusch M. The response of the high strength Ti-10V-2Fe-3Al beta titanium alloy to laser assisted cutting. *Precision Engineering*. 2013;37(2):461-72.
130. Palanisamy S, Dargusch M, McDonald S, Brandt M, StJohn D. A rationale for the acoustic monitoring of surface deformation in Ti6Al4V alloys during machining. *Advanced Engineering Materials*. 2007;9(11):1000-4.
131. Altintas Y, Weck M. Chatter stability of metal cutting and grinding. *CIRP Annals-Manufacturing Technology*. 2004;53(2):619-42.
132. Dogra M, Sharma VS, Sachdeva A, Suri NM, Dureja JS. Tool wear, chip formation and workpiece surface issues in CBN hard turning: A review. *International Journal of Precision Engineering and Manufacturing*. 2010;11(2):341-58.
133. Hong S.Y., Markus I., W-C. J. New cooling approach and tool life improvement in cryogenic machining of titanium alloy Ti-6Al-4V. *International Journal of Machine Tool & Manufacture*. 2001;41:2245-60.
134. Amin A. Investigation of the mechanism of chatter formation during metal cutting process. *Mechanical Engineering Research Bulletin*. 1983;6(1):11-8.
135. Namb M, Paulo D. Influence of coolant in machinability of titanium alloy (Ti-6Al-4V). *Journal of Surface Engineered Materials and Advanced Technology*. 2011;1(01):9.
136. Lei S, Pfeifferkorn F, editors. *A Review on Thermally Assisted Machining*. ASME 2007 International Manufacturing Science and Engineering Conference; 2007: American Society of Mechanical Engineers.
137. Maity K, Swain P. An experimental investigation of hot-machining to predict tool life. *Journal of materials processing technology*. 2008;198(1):344-9.
138. Klocke F, König W. *Fertigungsverfahren 3: Abtragen, Generieren und Lasermaterialbearbeitung*: Springer-Verlag; 2007.
139. Bermingham M, Palanisamy S, Dargusch M. Understanding the tool wear mechanism during thermally assisted machining Ti-6Al-4V. *International Journal of Machine Tools and Manufacture*. 2012;62:76-87.
140. Luo J, Ding H, Shih AJ. INDUCTION-HEATED TOOL MACHINING OF ELASTOMERS—PART 1: FINITE DIFFERENCE THERMAL MODELING AND EXPERIMENTAL VALIDATION. *Machining science and technology*. 2005;9(4):547-65.
141. Luo J, Ding H, Shih AJ. Induction-Heated Tool Machining of Elastomers—Part 2: Chip Morphology, Cutting Forces, and Machined Surfaces. *Machining science and technology*. 2005;9(4):567-88.
142. Kitagawa T, Maekawa K, Kubo A. Plasma hot machining for high hardness metals. *Bulletin of the Japan Society of Precision Engineering*. 1988;22(2):145-51.

143. Brecher C, Rosen C-J, Emonts M. Laser-assisted milling of advanced materials. *Physics Procedia*. 2010;5:259-72.
144. Sun S, Brandt M, Dargusch M. Thermally enhanced machining of hard-to-machine materials—a review. *International Journal of Machine Tools and Manufacture*. 2010;50(8):663-80.
145. Dogra M., S. SV. Techniques to improve the effectiveness in machining of hard to machine materials: A review. *International Journal of Rresearch in Mechanical Engineering & Technology*. 2013;3(2):122-6.
146. Tian Y, Wu B, Anderson M, Shin YC. Laser-assisted milling of silicon nitride ceramics and Inconel 718. *Journal of manufacturing science and engineering*. 2008;130(3):031013.
147. Weck M, Zeppelin W, Hermanns C, editors. *Laser—a tool for turning centres*. Laser Assisted Net Shape Engineering, Proceedings of the LANE; 1994.
148. Tian Y, Shin YC. Laser-assisted burnishing of metals. *International Journal of Machine Tools and Manufacture*. 2007;47(1):14-22.
149. Anderson M, Patwa R, Shin YC. Laser-assisted machining of Inconel 718 with an economic analysis. *International Journal of Machine Tools and Manufacture*. 2006;46(14):1879-91.
150. Dandekar CR, Shin YC, Barnes J. Machinability improvement of titanium alloy (Ti–6Al–4V) via LAM and hybrid machining. *International Journal of Machine Tools and Manufacture*. 2010;50(2):174-82.
151. Amin A. Influence of the instability of chip formation and preheating of work on tool life in machining high temperature resistant steel and titanium alloys. *Mechanical Engineering Research Bulletin*. 1986;9:52-62.
152. Sun S, Brandt M, Barnes J, Dargusch M. Experimental investigation of cutting forces and tool wear during laser-assisted milling of Ti-6Al-4V alloy. *Proceedings of the Institution of Mechanical Engineers, Part B: Journal of Engineering Manufacture*. 2011;225(9):1512-27.
153. Ayed Y, Germain G, Salem WB, Hamdi H. Experimental and numerical study of laser-assisted machining of Ti6Al4V titanium alloy. *Finite Elements in Analysis and Design*. 2014;92:72-9.
154. Wu Z, Xu D, Feng P, Yu D, Zhang C. Evaluation and optimization method of high speed cutting parameters based on cutting process simulation. *Intelligent Robotics and Applications*. 2009:317-25.
155. Rashid RR, Sun S, Wang G, Dargusch M. An investigation of cutting forces and cutting temperatures during laser-assisted machining of the Ti–6Cr–5Mo–5V–4Al beta titanium alloy. *International Journal of Machine Tools and Manufacture*. 2012;63:58-69.
156. Rashid RR, Sun S, Palanisamy S, Wang G, Dargusch M. A study on laser assisted machining of Ti10V2Fe3Al alloy with varying laser power. *The International Journal of Advanced Manufacturing Technology*. 2014;74(1-4):219-24.
157. Lauwers B. Surface integrity in hybrid machining processes. *Procedia Engineering*. 2011;19:241-51.
158. Ginta TL, Amin AN. Surface Integrity in End Milling Titanium Alloy Ti-6Al-4V under Heat Assisted Machining. *Asian Journal of Scientific Research*. 2013;6(3):609.
159. Germain G, Morel F, Lebrun JL, Morel A, Huneau B, editors. Effect of laser assistance machining on residual stress and fatigue strength for a bearing steel (100Cr6) and a titanium alloy (Ti 6Al 4V). *Materials Science Forum*; 2006: Trans Tech Publ.
160. Joshi S, Tewari A, Joshi S. Influence of Preheating on Chip Segmentation and Microstructure in Orthogonal Machining of Ti6Al4V. *Journal of Manufacturing Science and Engineering*. 2013;135(6):061017.
161. Braham-Bouchnak T, Germain G, Morel A, Lebrun J-L. The influence of laser assistance on the machinability of the titanium alloy Ti555-3. *The International Journal of Advanced Manufacturing Technology*. 2013;68(9-12):2471-81.

162. Ginta TL, Amin AN, Lajis M. Suppressed Vibrations During Thermal-assisted Machining of Titanium Alloy Ti-6Al-4V using PCD Inserts. *Journal of Applied Sciences*. 2012;12(23):2418.
163. De Lacalle LNL, Sanchez JA, Lamikiz A, Celaya A. Plasma assisted milling of heat-resistant superalloys. *Journal of manufacturing science and engineering*. 2004;126(2):274-85.
164. Leshock CE, Kim J-N, Shin YC. Plasma enhanced machining of Inconel 718: modeling of workpiece temperature with plasma heating and experimental results. *International Journal of Machine Tools and Manufacture*. 2001;41(6):877-97.
165. Novak J, Shin Y, Incropera F. Assessment of plasma enhanced machining for improved machinability of Inconel 718. *Journal of manufacturing science and engineering*. 1997;119(1):125-9.
166. Shin Y.C., J.-N. K. Plasma enhanced machining of Inconel 718. *manufacturing science and engineering, ASME MED*. 1996;4:243-9.
167. Dubey AK, Yadava V. Laser beam machining—a review. *International Journal of Machine Tools and Manufacture*. 2008;48(6):609-28.
168. Venkatesan K, Ramanujam R, Kuppan P. Laser Assisted Machining of difficult to cut materials: Research Opportunities and Future Directions-A comprehensive review. *Procedia Engineering*. 2014;97:1626-36.
169. Shin YC. Laser assisted machining. *Mach Technol*. 2000;11(3):1-6.
170. Velayudham A. Modern Manufacturing Processes: A Review. *Journal on Design and Manufacturing Technologies*. 2007;Vol. 1(No. 1):30 - 40.
171. Jeon Y, Park HW, Lee CM. Current research trends in external energy assisted machining. *International Journal of Precision Engineering and Manufacturing*. 2013;14(2):337-42.
172. Rozzi JC, Pfefferkorn FE, Shin YC, Incropera FP. Experimental evaluation of the laser assisted machining of silicon nitride ceramics. *Journal of Manufacturing Science and Engineering*. 2000;122(4):666-70.
173. Rebro PA, Shin YC, Incropera FP. Design of operating conditions for crackfree laser-assisted machining of mullite. *International Journal of Machine Tools and Manufacture*. 2004;44(7):677-94.
174. Lei S, Shin YC, Incropera FP. Experimental investigation of thermo-mechanical characteristics in laser-assisted machining of silicon nitride ceramics. *Journal of Manufacturing Science and Engineering*. 2001;123(4):639-46.
175. Wu J-F, Guu Y-B. Laser assisted machining method and device. *Google Patents*; 2006.
176. Kim K-S, Kim J-H, Choi J-Y, Lee C-M. A review on research and development of laser assisted turning. *International Journal of Precision Engineering and Manufacturing*. 2011;12(4):753-9.
177. Shi B, Attia H. Integrated process of laser-assisted machining and laser surface heat treatment. *Journal of Manufacturing science and engineering*. 2013;135(6):061021.
178. Kannan V, Radhakrishnan R, Palaniyandi K. A review on conventional and laser assisted machining of Aluminium based metal matrix composites. *Engineering Review*. 2014;34(2):75-84.
179. Klocke F, Bergs T, editors. *Laser-assisted turning of advanced ceramics. Lasers and Optics in Manufacturing III*; 1997: International Society for Optics and Photonics.
180. Rahim E, Warap N, Mohid Z. Thermal-Assisted Machining of Nickel-based Alloy 2015-11-25.
181. Kong XJ, Zhang HZ, Wu XF, Wang Y, editors. *Laser-Assisted Machining of Advanced Materials. Materials Science Forum*; 2014: Trans Tech Publ.

182. Pfefferkorn FE, Incropera FP, Shin YC. Heat transfer model of semi-transparent ceramics undergoing laser-assisted machining. *International Journal of Heat and Mass Transfer*. 2005;48(10):1999-2012.
183. Gratias J, Fan L, Marot G, Cohen P, Moisan A. Proposition of a method to optimize the machining of XC42 steel with laser assistance. *CIRP Annals-Manufacturing Technology*. 1993;42(1):115-8.
184. Rozzi JC, Pfefferkorn FE, Incropera FP, Shin YC. Transient thermal response of a rotating cylindrical silicon nitride workpiece subjected to a translating laser heat source, part I: comparison of surface temperature measurements with theoretical results. *Journal of heat transfer*. 1998;120(4):899-906.
185. Sun S, Harris J, Brandt M. Parametric Investigation of Laser-Assisted Machining of Commercially Pure Titanium. *Advanced engineering materials*. 2008;10(6):565-72.
186. Yang B, Lei S. Laser-assisted milling of silicon nitride ceramic: a machinability study. *International Journal of mechatronics and manufacturing systems*. 2008;1(1):116-30.
187. Lei S, Shin YC, Incropera FP. Deformation mechanisms and constitutive modeling for silicon nitride undergoing laser-assisted machining. *International Journal of Machine Tools and Manufacture*. 2000;40(15):2213-33.
188. Bejjani R, Shi B, Attia H, Balazinski M. Laser assisted turning of titanium metal matrix composite. *CIRP Annals-Manufacturing Technology*. 2011;60(1):61-4.
189. Attia H, Tavakoli S, Vargas R, Thomson V. Laser-assisted high-speed finish turning of superalloy Inconel 718 under dry conditions. *CIRP Annals-Manufacturing Technology*. 2010;59(1):83-8.
190. Anderson M, Shin Y. Laser-assisted machining of an austenitic stainless steel: P550. *Proceedings of the Institution of Mechanical Engineers, Part B: Journal of Engineering Manufacture*. 2006;220(12):2055-67.
191. Ding H, Shin YC. Laser-assisted machining of hardened steel parts with surface integrity analysis. *International Journal of Machine tools and manufacture*. 2010;50(1):106-14.
192. Germain G, Dal Santo P, Lebrun J-L. Comprehension of chip formation in laser assisted machining. *International Journal of Machine Tools and Manufacture*. 2011;51(3):230-8.
193. Garcí V, Arriola I, Gonzalo O, Leunda J. Mechanisms involved in the improvement of Inconel 718 machinability by laser assisted machining (LAM). *International Journal of Machine Tools and Manufacture*. 2013;74:19-28.
194. Kim D-H, Lee C-M. A study of cutting force and preheating-temperature prediction for laser-assisted milling of Inconel 718 and AISI 1045 steel. *International Journal of Heat and Mass Transfer*. 2014;71:264-74.
195. Venkatesan K, Ramanujam R, Kuppan P. Analysis of Cutting Forces and Temperature in Laser Assisted Machining of Inconel 718 Using Taguchi Method. *Procedia Engineering*. 2014;97:1637-46.
196. Dong-Gyu A, Kyung-Won B. Influence of cutting parameters on surface characteristics of cut section in cutting of Inconel 718 sheet using CW Nd: YAG laser. *Transactions of Nonferrous Metals Society of China*. 2009;19:s32-s9.
197. Kong X, Yang L, Zhang H, Zhou K, Wang Y. Cutting performance and coated tool wear mechanisms in laser-assisted milling K24 nickel-based superalloy. *The International Journal of Advanced Manufacturing Technology*. 2015;77(9-12):2151-63.
198. Thawari G, Sundar JS, Sundararajan G, Joshi S. Influence of process parameters during pulsed Nd: YAG laser cutting of nickel-base superalloys. *Journal of Materials Processing Technology*. 2005;170(1):229-39.

199. Ding H, Shin YC. Improvement of machinability of Waspaloy via laser-assisted machining. *The International Journal of Advanced Manufacturing Technology*. 2013;64(1-4):475-86.
200. Rebro PA, Shin YC, Incropera FP. Laser-assisted machining of reaction sintered mullite ceramics. *Journal of Manufacturing Science and Engineering*. 2002;124(4):875-85.
201. Lee S-J, Kim J-D, Suh J. Microstructural variations and machining characteristics of silicon nitride ceramics from increasing the temperature in laser assisted machining. *International journal of precision engineering and manufacturing*. 2014;15(7):1269-74.
202. Kim J-D, Lee S-J, Suh J. Characteristics of laser assisted machining for silicon nitride ceramic according to machining parameters. *Journal of Mechanical Science and Technology*. 2011;25(4):995-1001.
203. Rashid RAR, Sun S, Wang G, Dargusch MS. Experimental investigation of laser assisted machining of AZ91 magnesium alloy. *International Journal of Precision Engineering and Manufacturing*. 2013;14(7):1263-5.
204. Pfeifferkorn FE, Shin YC, Tian Y, Incropera FP. Laser-assisted machining of magnesia-partially-stabilized zirconia. *Journal of manufacturing science and engineering*. 2004;126(1):42-51.
205. Wang Y, Yang L, Wang N. An investigation of laser-assisted machining of Al₂O₃ particle reinforced aluminum matrix composite. *Journal of materials processing technology*. 2002;129(1):268-72.
206. Chang C-W, Kuo C-P. Evaluation of surface roughness in laser-assisted machining of aluminum oxide ceramics with Taguchi method. *International Journal of Machine Tools and Manufacture*. 2007;47(1):141-7.
207. Hedberg G, Shin Y, Xu L. Laser-assisted milling of Ti-6Al-4V with the consideration of surface integrity. *The International Journal of Advanced Manufacturing Technology*. 2015;79(9-12):1645-58.
208. Nasr M.N.A., M. B. Effect of laser power on residual stresses when laser-assisted turning of AISI 4340 steel. *Proceedings of The Canadian Society for Mechanical Engineering International Congress; Toronto, Ontario, Canada 2014*.
209. Lee J-H, Shin D-S, Suh J, Cho H-Y, Kim K-W. Trends of laser integrated machine. *Journal of the Korean Society for Precision Engineering*. 2008;25(9):20-6.
210. Germain G, Lebrun J-L, Braham-Bouchnak T, Bellett D, Auger S. Laser-assisted machining of Inconel 718 with carbide and ceramic inserts. *International journal of material forming*. 2008;1(1):523-6.
211. Dahotre NB, Harimkar SP. *Laser Fabrication and Machining of Materials*. New York: Springer; 2008.
212. Nath A. High Power Lasers in Material Processing Applications: An Overview of Recent Developments. *Laser-Assisted Fabrication of Materials*: Springer; 2013. p. 69-111.
213. König W, Zaboklicki AK. *Laser Assisted Hot Machining of Ceramics and Composite Materials*. National Institute of Science and Tech Technology, NIST Special Publication 847. 1993.
214. König W, Wageman A. Fine Machining of Advanced Ceramics. *Ceramics Today—Tomorrow's Ceramics*, Vincenzini, P, ed, Montecatini Terme, Italy. 1991:pp. 2769-84.
215. Kennedy E, Byrne G, Collins D. A review of the use of high power diode lasers in surface hardening. *Journal of Materials Processing Technology*. 2004;155:1855-60.
216. Bachmann F. Industrial applications of high power diode lasers in materials processing. *Applied surface science*. 2003;208:125-36.
217. Li L. The advances and characteristics of high-power diode laser materials processing. *Optics and Lasers in Engineering*. 2000;34(4):231-53.

218. Choi S, Cheong S, Kim G, Yang S, Kim J. Characteristics of metal surface heat treatment by diode laser. *Journal of Korean Society of Manufacturing Process Engineers*. 2007;6(3):16-23.
219. Venkatesan K, Ramanujam R, Kuppan P. Parametric modeling and optimization of laser scanning parameters during laser assisted machining of Inconel 718. *Optics & Laser Technology*. 2016;78:10-8.
220. Kannan MV, Kuppan P, Kumar AS, Kumar KR, Jegaraj JJR. Effect of Laser Scan Speed on Surface Temperature, Cutting Forces and Tool Wear During Laser Assisted Machining of Alumina. *Procedia Engineering*. 2014;97:1647-56.
221. Yang J, Sun S, Brandt M, Yan W. Experimental investigation and 3D finite element prediction of the heat affected zone during laser assisted machining of Ti6Al4V alloy. *Journal of Materials Processing Technology*. 2010;210(15):2215-22.
222. Zamani H, Hermani J-P, Sonderegger B, Sommitsch C, editors. Numerical and Experimental Investigation of Laser Assisted Side Milling of Ti6Al4V Alloy. *Proc of Materials Science & Technology Conference and Exhibition*; 2012.
223. Zamani H, Hermani J-P, Sonderegger B, Sommitsch C. 3D simulation and process optimization of laser assisted milling of Ti6Al4V. *Procedia CIRP*. 2013;8:75-80.
224. Joshi A, Kansara N, Das S, Kuppan P, Venkatesan K. A Study of Temperature Distribution for Laser Assisted Machining of Ti-6Al-4V Alloy. *Procedia Engineering*. 2014;97:1466-73.
225. Xi Y, Zhan H, Rashid RR, Wang G, Sun S, Dargusch M. Numerical modeling of laser assisted machining of a beta titanium alloy. *Computational Materials Science*. 2014;92:149-56.
226. Pfender E, Spores R, Chen WLT. A new look at the thermal and gas dynamic characteristics of a plasma jet. *International Journal of Materials and Product Technology*. 1995;10(3-6):548-65.
227. Pfender E, Fincke J, Spores R. Entrainment of cold gas into thermal plasma jets. *Plasma Chemistry and Plasma Processing*. 1991;11(4):529-43.
228. Wang Z, Rajurkar K, Fan J, Lei S, Shin Y, Petrescu G. Hybrid machining of Inconel 718. *International Journal of Machine Tools and Manufacture*. 2003;43(13):1391-6.
229. Hossain MI, Amin AN, Patwari A, Karim A. Enhancement of machinability by workpiece preheating in end milling of Ti-6Al-4V. *Journal of Achievements in Materials and Manufacturing Engineering*. 2008;31(2):320-6.
230. Baili M, Wagner V, Dessein G, Sallaberry J, Lallement D, editors. An experimental investigation of hot machining with induction to improve Ti-5553 machinability. *Applied mechanics and Materials*; 2011: Trans Tech Publ.
231. Gecim B, Winer W. Steady temperature in a rotating cylinder subject to surface heating and convective cooling. *Journal of Tribology*. 1984;106(1):120-6.
232. Pfefferkorn F, Rozzi J, Incropera F, Shin Y. Surface temperature measurement in laser-assisted machining processes. *EXPERIMENTAL HEAT TRANSFER An International Journal*. 1997;10(4):291-313.
233. Rozzi JC, Pfefferkorn FE, Incropera FP, Shin YC. Transient, three-dimensional heat transfer model for the laser assisted machining of silicon nitride: I. Comparison of predictions with measured surface temperature histories. *International Journal of Heat and Mass Transfer*. 2000;43(8):1409-24.
234. Rozzi JC, Incropera FP, Shin YC. Transient, three-dimensional heat transfer model for the laser assisted machining of silicon nitride: II. Assessment of parametric effects. *International Journal of Heat and mass transfer*. 2000;43(8):1425-37.
235. Samanta A, Teli M, Singh R. Experimental characterization and finite element modeling of the residual stresses in laser-assisted mechanical micromachining of Inconel

625. Proceedings of the Institution of Mechanical Engineers, Part B: Journal of Engineering Manufacture. 2017;231(10):1735-51.
236. Shi B, Attia H, Vargas R, Tavakoli S. Numerical and experimental investigation of laser-assisted machining of Inconel 718. *Machining Science and Technology*. 2008;12(4):498-513.
237. Abdulghani O, Sobih M, Youssef A, El-Batahgy A-M. Modeling and simulation of laser assisted turning of hard steels. *Modeling and Numerical Simulation of Material Science*. 2013;3(4):106-13.
238. Arrizubieta J, Klocke F, Gräfe S, Arntz K, Lamikiz A. Thermal Simulation of Laser-assisted Turning. *Procedia Engineering*. 2015;132:639-46.
239. Kashani MM, Movahhedy MR, Ahmadian MT, Razavi RS. Analytical Solution of Transient Three-Dimensional Temperature Field in a Rotating Cylinder Subject to a Localized Laser Beam. *Journal of Heat Transfer*. 2017;139(6):062701.
240. Leyens C, Peters M. Titanium and titanium alloys: fundamentals and applications: John Wiley & Sons; 2003.
241. Fusions 10.6 Series User Manual. In: Photon Machines I, editor. Copyright ed2010. p. 1-28.
242. Teodorescu G. Radiative emissivity of metals and oxidized metals at high temperature 2007.
243. Sha W, Malinov S. Titanium alloys: modelling of microstructure, properties and applications: Elsevier; 2009.
244. Zhang ZM, Tsai BK, Machin G. Radiometric temperature measurements: I. Fundamentals: Academic Press; 2009.
245. Pujana J, Del Campo L, Pérez-Sáez R, Tello M, Gallego I, Arrazola P. Radiation thermometry applied to temperature measurement in the cutting process. *Measurement Science and Technology*. 2007;18(11):3409.
246. Hafez MM, Kwak D. Computational fluid dynamics review 2010: World Scientific; 2010.
247. Anderson D, Tannehill JC, Pletcher RH. Computational fluid mechanics and heat transfer: CRC Press; 2016.
248. ANSYS. ANSYS Fluent 18.0 Getting Started Guide. In: Inc. A, editor. ANsys: Southpointe; 2017.
249. Chung T. Computational fluid dynamics: Cambridge university press; 2010.
250. Versteeg HK, Malalasekera W. An introduction to computational fluid dynamics: the finite volume method: Pearson education; 2007.
251. Moukalled F, Mangani L, Darwish M. The finite volume method in computational fluid dynamics. An Advanced Introduction with OpenFOAM and Matlab. 2016:3-8.
252. Leonard BP. A stable and accurate convective modelling procedure based on quadratic upstream interpolation. *Computer methods in applied mechanics and engineering*. 1979;19(1):59-98.
253. Thakur S, Shyy W. Some implementational issues of convection schemes for finite-volume formulations. *Numerical Heat Transfer, Part B Fundamentals*. 1993;24(1):31-55.
254. Paramane SB, Sharma A. Consistent implementation and comparison of FOU, CD, SOU, and QUICK convection schemes on square, skew, trapezoidal, and triangular lid-driven cavity flow. *Numerical Heat Transfer, Part B: Fundamentals*. 2008;54(1):84-102.
255. ANSYS. ANSYS Fluent 18.0 Tutorial Guide. In: Inc. A, editor. ANsys: Southpointe; 2017.
256. El-Genk MS, Huang L, Guo Z, Pate R, Jenen M. Heat transfer between a square flat plate and a perpendicularly impinging circular air jet. *ASME-PUBLICATIONS-HTD*. 1993;202:33-.

257. Kays W, Bjorklund I. Heat transfer from a rotating cylinder with and without crossflow. *Trans ASME*. 1958;80(1):70-8.
258. Merzouki R, Samantaray AK, Pathak PM, Bouamama BO. *Intelligent mechatronic systems: modeling, control and diagnosis*: Springer Science & Business Media; 2012.
259. Parekh R, Yang J, Honavar V. Constructive neural-network learning algorithms for pattern classification. *IEEE Transactions on neural networks*. 2000;11(2):436-51.
260. El-Masry EI, Yang H-K, Yakout MA. Implementations of artificial neural networks using current-mode pulse width modulation technique. *IEEE transactions on neural networks*. 1997;8(3):532-48.
261. H. Nayef B, Norul Huda Sheikh Abdullah S, Iqbal Hussain R, Sahran S, H. Almasri A, Abdullah N, et al. *Neural Networks for Identification, Prediction and Control*. *Journal of Medical Sciences*. 2011;14(3):pp: 242-7.
262. Fekih A, Xu H, Chowdhury FN. Neural networks based system identification techniques for model based fault detection of nonlinear systems. *International Journal of Innovative Computing, Information and Control*. 2007;3(5):1073-85.
263. Levenberg K. A method for the solution of certain non-linear problems in least squares. *Quarterly of applied mathematics*. 1944;2(2):164-8.
264. Marquardt DW. An algorithm for least-squares estimation of nonlinear parameters. *Journal of the society for Industrial and Applied Mathematics*. 1963;11(2):431-41.
265. Mathworks. *Least-Squares (Model Fitting) Algorithms: User's Guide*. Matlab2017.

Appendix A

This appendix shows the signed attribution forms of the co-authors that contributed in the published papers.



School of Civil and Mechanical

Engineering
Level 4, Building 204
GPO Box U1987
Perth Western Australia

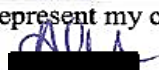
Co-author Attribution Approval Statement

Hereby, I, Dr. Alokesh Pramanik, confirm that the following is my joint publication with Ouf Shams. I, as a co-author, endorse that the level of all authors' contribution is accurately and appropriately addressed in the following table. I also consent this book chapter to be used in the thesis "Machinability Improvement of Hard-to-Machine Materials by Monitoring and Controlling Laser Heating", submitted for the Degree of PhD in Mechanical Engineering of Curtin University.

Book chapter: Ouf Shams, Alokesh Pramanik, Tilak Chandratilleke, "Thermal-Assisted Machining of Titanium Alloys". Advanced Manufacturing Technologies, Springer, p. 49-76, 2017.

Author's affiliation (in order of appearance in published version of book chapter):

- 1- Ouf Shams, Faculty of Science and Engineering, School of Civil and Mechanical Engineering, Curtin University, Perth, Australia.
- 2- Alokesh Pramanik, Faculty of Science and Engineering, School of Civil and Mechanical Engineering, Curtin University, Perth, Australia.
- 3- Tilak Chandratilleke, Faculty of Science and Engineering, School of Civil and Mechanical Engineering, Curtin University, Perth, Australia.
- 4-

		Conception and Design	Acquisition of method	Data manipulation	Interpretation & discussion	Paper drafting	Paper revising	Final approval
Authors	Ouf Shams	X	X	X	X	X	X	X
	Alokesh Pramanik		X		X	X	X	X
		I acknowledge that these represent my contribution to the above research output. Signed  Date06 January 2020.....						
	Tilak Chandratilleke				X	X	X	X


Co-author Attribution Approval Statement

Hereby, I, Dr. Alokesh Pramanik, confirm that the following is my joint publication with Ouf Shams. I, as a co-author, endorse that the level of all authors' contribution is accurately and appropriately addressed in the following table. I also consent this journal paper to be used in the thesis "Machinability Improvement of Hard-to-Machine Materials by Monitoring and Controlling Laser Heating", submitted for the Degree of PhD in Mechanical Engineering of Curtin University.

Journal paper: Nima Nadim, Ouf Shams, Tilak Chandratilleke, Alokesh Pramanik, "Preheating and Thermal Behaviour of a Rotating Cylindrical Workpiece in Laser-Assisted Machining", Journal of Engineering Manufacture. p. 49-76, 2019.

Author's affiliation (in order of appearance in published version of journal paper):

- 1- Nima Nadim, Faculty of Science and Engineering, School of Civil and Mechanical Engineering, Curtin University, Perth, Australia.
- 2- Ouf Shams, Faculty of Science and Engineering, School of Civil and Mechanical Engineering, Curtin University, Perth, Australia.
- 3- Tilak Chandratilleke, Faculty of Science and Engineering, School of Civil and Mechanical Engineering, Curtin University, Perth, Australia.
- 4- Alokesh Pramanik, Faculty of Science and Engineering, School of Civil and Mechanical Engineering, Curtin University, Perth, Australia.

		Conception and Design	Acquisition of method	Data manipulation	Interpretation & discussion	Paper drafting	Paper revising	Final approval
Authors	Nima Nadim	X	X	X	X	X	X	X
	Ouf Shams	X	X	X	X	X	X	X
	Tilak Chandratilleke				X	X	X	X
	Alokesh Pramanik					X	X	X
		I acknowledge that these represent my contribution to the above research output.						
		Signed 						
		Date06 January 2020.....						


Co-author Attribution Approval Statement

Hereby, I, Dr. Alokesh Pramanik, confirm that the following is my joint publication with Ouf Shams. I, as a co-author, endorse that the level of all authors' contribution is accurately and appropriately addressed in the following table. I also consent this book chapter to be used in the thesis "Machinability Improvement of Hard-to-Machine Materials by Monitoring and Controlling Laser Heating", submitted for the Degree of PhD in Mechanical Engineering of Curtin University.

Book chapter: Ouf Shams, Alokesh Pramanik, Tilak Chandratilleke, Nima Nadim, "Comparative Assessment and Merit Appraisal of Thermally Assisted Machining Techniques for Improving Machinability of Titanium Alloys". Introduction to Mechanical Engineering, Springer, p. 297-331, 2018.

Author's affiliation (in order of appearance in published version of book chapter):

- 1- Ouf Shams, Faculty of Science and Engineering, School of Civil and Mechanical Engineering, Curtin University, Perth, Australia.
- 2- Alokesh Pramanik, Faculty of Science and Engineering, School of Civil and Mechanical Engineering, Curtin University, Perth, Australia.
- 3- Tilak Chandratilleke, Faculty of Science and Engineering, School of Civil and Mechanical Engineering, Curtin University, Perth, Australia.
- 4- Nima Nadim, Faculty of Science and Engineering, School of Civil and Mechanical Engineering, Curtin University, Perth, Australia.

		Conception and Design	Acquisition of method	Data manipulation	Interpretation & discussion	Paper drafting	Paper revising	Final approval
Authors	Ouf Shams	X	X	X	X	X	X	X
	Alokesh Pramanik		X		X	X	X	X
		I acknowledge that these represent my contribution to the above research output. Signed  Date ...06 January 2020.....						
	Tilak Chandratilleke				X	X	X	X
	Nima Nadim					X	X	X


Co-author Attribution Approval Statement

Hereby, I, Prof. Tilak Chandratilleke, confirm that the following is my joint publication with Ouf Shams. I, as a co-author, endorse that the level of all authors' contribution is accurately and appropriately addressed in the following table. I also consent this journal paper to be used in the thesis "Machinability Improvement of Hard-to-Machine Materials by Monitoring and Controlling Laser Heating", submitted for the Degree of PhD in Mechanical Engineering of Curtin University.

Journal paper: Nima Nadim, Ouf Shams, Tilak Chandratilleke, Alokesh Pramanik, "Preheating and Thermal Behaviour of a Rotating Cylindrical Workpiece in Laser-Assisted Machining", Journal of Engineering Manufacture. p. 49-76, 2019.

Author's affiliation (in order of appearance in published version of journal paper):

- 1- Nima Nadim, Faculty of Science and Engineering, School of Civil and Mechanical Engineering, Curtin University, Perth, Australia.
- 2- Ouf Shams, Faculty of Science and Engineering, School of Civil and Mechanical Engineering, Curtin University, Perth, Australia.
- 3- Tilak Chandratilleke, Faculty of Science and Engineering, School of Civil and Mechanical Engineering, Curtin University, Perth, Australia.
- 4- Alokesh Pramanik, Faculty of Science and Engineering, School of Civil and Mechanical Engineering, Curtin University, Perth, Australia.

		Conception and Design	Acquisition of method	Data manipulation	Interpretation & discussion	Paper drafting	Paper revising	Final approval
Authors	Nima Nadim	X	X	X	X	X	X	X
	Ouf Shams	X	X	X	X	X	X	X
	Tilak Chandratilleke				X	X	X	X
		I acknowledge that these represent my contribution to the above research output. Signed ...  Date16 January 2020.....						
	Alokesh Pramanik					X	X	X


Co-author Attribution Approval Statement

Hereby, I, Prof. Tilak Chandratilleke, confirm that the following is my joint publication with Ouf Shams. I, as a co-author, endorse that the level of all authors' contribution is accurately and appropriately addressed in the following table. I also consent this book chapter to be used in the thesis "Machinability Improvement of Hard-to-Machine Materials by Monitoring and Controlling Laser Heating", submitted for the Degree of PhD in Mechanical Engineering of Curtin University.

Book chapter: Ouf Shams, Alokesh Pramanik, Tilak Chandratilleke, Nima Nadim, "Comparative Assessment and Merit Appraisal of Thermally Assisted Machining Techniques for Improving Machinability of Titanium Alloys". Introduction to Mechanical Engineering, Springer, p. 297-331, 2018.

Author's affiliation (in order of appearance in published version of book chapter):

- 1- Ouf Shams, Faculty of Science and Engineering, School of Civil and Mechanical Engineering, Curtin University, Perth, Australia.
- 2- Alokesh Pramanik, Faculty of Science and Engineering, School of Civil and Mechanical Engineering, Curtin University, Perth, Australia.
- 3- Tilak Chandratilleke, Faculty of Science and Engineering, School of Civil and Mechanical Engineering, Curtin University, Perth, Australia.
- 4- Nima Nadim, Faculty of Science and Engineering, School of Civil and Mechanical Engineering, Curtin University, Perth, Australia.

		Conception and Design	Acquisition of method	Data manipulation	Interpretation & discussion	Paper drafting	Paper revising	Final approval
Authors	Ouf Shams	X	X	X	X	X	X	X
	Alokesh Pramanik		X		X	X	X	X
	Tilak Chandratilleke	I acknowledge that these represent my contribution to the above research output.						
		Signed 						
		Date16 January 2020.....						
	Nima Nadim					X	X	X

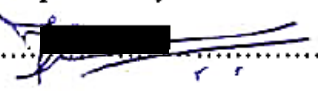
Co-author Attribution Approval Statement

Hereby, I, Prof. Tilak Chandratilleke, confirm that the following is my joint publication with Ouf Shams. I, as a co-author, endorse that the level of all authors' contribution is accurately and appropriately addressed in the following table. I also consent this book chapter to be used in the thesis "Machinability Improvement of Hard-to-Machine Materials by Monitoring and Controlling Laser Heating", submitted for the Degree of PhD in Mechanical Engineering of Curtin University.

Book chapter: Ouf Shams, Alokesh Pramanik, Tilak Chandratilleke, "Thermal-Assisted Machining of Titanium Alloys". Advanced Manufacturing Technologies, Springer, p. 49-76, 2017.

Author's affiliation (in order of appearance in published version of book chapter):

- 1- Ouf Shams, Faculty of Science and Engineering, School of Civil and Mechanical Engineering, Curtin University, Perth, Australia.
- 2- Alokesh Pramanik, Faculty of Science and Engineering, School of Civil and Mechanical Engineering, Curtin University, Perth, Australia.
- 3- Tilak Chandratilleke, Faculty of Science and Engineering, School of Civil and Mechanical Engineering, Curtin University, Perth, Australia.

		Conception and Design	Acquisition of method	Data manipulation	Interpretation & discussion	Paper drafting	Paper revising	Final approval
Authors	Ouf Shams	X	X	X	X	X	X	X
	Alokesh Pramanik		X		X	X	X	X
	Tilak Chandratilleke				X	X	X	X
	<p>I acknowledge that these represent my contribution to the above research output.</p> <p>Signed </p> <p>Date16 January 2020.....</p>							

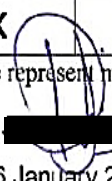
Author Attribution Approval Statement

Hereby, I, Dr. Nima Nadim, confirm that the following is my joint publication with Ouf Shams. I, as a co-author, endorse that the level of all authors' contribution is accurately and appropriately addressed in the following table. I also consent this journal paper to be used in the thesis "Machinability Improvement of Hard-to-Machine Materials by Monitoring and Controlling Laser Heating", submitted for the Degree of PhD in Mechanical Engineering of Curtin University.

Journal paper: Nima Nadim, Ouf Shams, Tilak Chandratilleke, Alokesh Pramanik, "Preheating and Thermal Behaviour of a Rotating Cylindrical Workpiece in Laser-Assisted Machining", Journal of Engineering Manufacture. p. 49-76, 2019.

Author's affiliation (in order of appearance in published version of journal paper):

- 1- Nima Nadim, Faculty of Science and Engineering, School of Civil and Mechanical Engineering, Curtin University, Perth, Australia.
- 2- Ouf Shams, Faculty of Science and Engineering, School of Civil and Mechanical Engineering, Curtin University, Perth, Australia.
- 3- Tilak Chandratilleke, Faculty of Science and Engineering, School of Civil and Mechanical Engineering, Curtin University, Perth, Australia.
- 4- Alokesh Pramanik, Faculty of Science and Engineering, School of Civil and Mechanical Engineering, Curtin University, Perth, Australia.

		Conception and Design	Acquisition of method	Data manipulation	Interpretation & discussion	Paper drafting	Paper revising	Final approval
Authors	Nima Nadim	X	X	X	X	X	X	X
	I acknowledge that these represent my contribution to the above research output.							
	Signed 							
	Date06 January 2020.....							
	Ouf Shams	X	X	X	X	X	X	X
Tilak Chandratilleke				X	X	X	X	
Alokesh Pramanik					X	X	X	

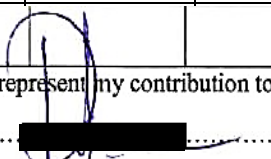
Co-author Attribution Approval Statement

Hereby, I, Dr. Nima Nadim, confirm that the following is my joint publication with Ouf Shams. I, as a co-author, endorse that the level of all authors' contribution is accurately and appropriately addressed in the following table. I also consent this book chapter to be used in the thesis "Machinability Improvement of Hard-to-Machine Materials by Monitoring and Controlling Laser Heating", submitted for the Degree of PhD in Mechanical Engineering of Curtin University.

Book chapter: Ouf Shams, Alokesh Pramanik, Tilak Chandratilleke, Nima Nadim, "Comparative Assessment and Merit Appraisal of Thermally Assisted Machining Techniques for Improving Machinability of Titanium Alloys". Introduction to Mechanical Engineering, Springer, p. 297-331, 2018.

Author's affiliation (in order of appearance in published version of book chapter):

- 1- Ouf Shams, Faculty of Science and Engineering, School of Civil and Mechanical Engineering, Curtin University, Perth, Australia.
- 2- Alokesh Pramanik, Faculty of Science and Engineering, School of Civil and Mechanical Engineering, Curtin University, Perth, Australia.
- 3- Tilak Chandratilleke, Faculty of Science and Engineering, School of Civil and Mechanical Engineering, Curtin University, Perth, Australia.
- 4- Nima Nadim, Faculty of Science and Engineering, School of Civil and Mechanical Engineering, Curtin University, Perth, Australia.

		Conception and Design	Acquisition of method	Data manipulation	Interpretation & discussion	Paper drafting	Paper revising	Final approval
Authors	Ouf Shams	X	X	X	X	X	X	X
	Alokesh Pramanik		X		X	X	X	X
	Tilak Chandratilleke				X	X	X	X
	Nima Nadim					X	X	X
		I acknowledge that these represent my contribution to the above research output. Signed  Date06 January 2020.....						

Appendix B

This appendix shows the permission letters from the publishers of the published papers that used in this thesis.

SPRINGER NATURE LICENSE TERMS AND CONDITIONS

Dec 23, 2019

This Agreement between Curtin University -- OUF SHAMS ("You") and Springer Nature ("Springer Nature") consists of your license details and the terms and conditions provided by Springer Nature and Copyright Clearance Center.

License Number 4734801294828
License date Dec 23, 2019

Licensed Content Publisher:

Springer Nature

Licensed Content Publication:

Springer eBook

Licensed Content Title:

Thermal-Assisted Machining of Titanium Alloys

Licensed Content Author: O. A. Shams, A. Pramanik, T. T. Chandratilleke

Licensed Content Date: Jan 1, 2017

Type of Use: Thesis/Dissertation

Requestor type: academic/university or research institute

Format: print and electronic

Portion: full article/chapter

Will you be translating? no

Circulation/distribution: 500 – 999

Author of this Springer content: yes

Title: Machinability Improvement of Hard-to-Machine Materials by Monitoring
and Controlling Laser Heating

Institution name: Curtin University Expected

presentation date: Jul 2020

Order reference number: 01

Requestor Location: Curtin University
Unit 20, 9-11 Norman Street
St James, WA, Western Australia 6102 Australia
Attn: Curtin University

Total: 0.00 USD

Terms and Conditions

Springer Nature Customer Service Centre GmbH Terms and Conditions

This agreement sets out the terms and conditions of the licence (the **Licence**) between you and **Springer Nature Customer Service Centre GmbH** (the **Licensor**). By clicking 'accept' and completing the transaction for the material (**Licensed Material**), you also confirm your acceptance of these terms and conditions.

1. Grant of License

1. The Licensor grants you a personal, non-exclusive, non-transferable, world-wide licence to reproduce the Licensed Material for the purpose specified in your order only. Licences are granted for the specific use requested in the order and for no other use, subject to the conditions below.

1. 2. The Licensor warrants that it has, to the best of its knowledge, the rights to license reuse of the Licensed Material. However, you should ensure that the material you are requesting is original to the Licensor and does not carry the copyright of another entity (as credited in the published version).

1.3. If the credit line on any part of the material you have requested indicates that it was reprinted or adapted with permission from another source, then you should also seek permission from that source to reuse the material.

2. Scope of Licence

2. 1. You may only use the Licensed Content in the manner and to the extent permitted by these Ts&Cs and any applicable laws.

2. 2. A separate licence may be required for any additional use of the Licensed Material, e.g. where a licence has been purchased for print only use, separate permission must be obtained for electronic re-use. Similarly, a licence is only valid in the language selected and does not apply for editions in other languages unless additional translation rights have been granted separately in the licence. Any content owned by third parties are expressly excluded from the licence.

2. 3. Similarly, rights for additional components such as custom editions and derivatives require additional permission and may be subject to an additional fee. Please apply to Journalpermissions@springernature.com/bookpermissions@springernature.com for these rights.

2. 4. Where permission has been granted **free of charge** for material in print, permission may also be granted for any electronic version of that work, provided that the material is incidental to your work as a whole and that the electronic version is essentially equivalent to, or substitutes for, the print version.

2. 5. An alternative scope of licence may apply to signatories of the [STM Permissions](#)

[Guidelines](#), as amended from time to time.

3. Duration of Licence

3.1. A licence for is valid from the date of purchase ('Licence Date') at the end of the relevant period in the below table:

Scope of Licence	Duration of Licence
Post on a website	12 months
Presentations	12 months
Books and journals	Lifetime of the edition in the language purchased

4. Acknowledgement

4. 1. The Licensor's permission must be acknowledged next to the Licenced Material in print. In electronic form, this acknowledgement must be visible at the same time as the figures/tables/illustrations or abstract, and must be hyperlinked to the journal/book's homepage. Our required acknowledgement format is in the Appendix below.

5. Restrictions on use

5. 1. Use of the Licensed Material may be permitted for incidental promotional use and minor editing privileges e.g. minor adaptations of single figures, changes of format, colour and/or style where the adaptation is credited as set out in Appendix 1 below. Any other changes including but not limited to, cropping, adapting, omitting material that affect the meaning, intention or moral rights of the author are strictly prohibited.

5. 2. You must not use any Licensed Material as part of any design or trademark.

5.3. Licensed Material may be used in Open Access Publications (OAP) before publication by Springer Nature, but any Licensed Material must be removed from OAP sites prior to final publication.

6. Ownership of Rights

6.1. Licensed Material remains the property of either Licensor or the relevant third party and any rights not explicitly granted herein are expressly reserved.

7. Warranty

IN NO EVENT SHALL LICENSOR BE LIABLE TO YOU OR ANY OTHER PARTY OR ANY OTHER PERSON OR FOR ANY SPECIAL, CONSEQUENTIAL, INCIDENTAL OR INDIRECT DAMAGES, HOWEVER CAUSED, ARISING OUT OF OR IN CONNECTION WITH THE DOWNLOADING, VIEWING OR USE OF THE MATERIALS REGARDLESS OF THE FORM OF ACTION, WHETHER FOR BREACH OF CONTRACT, BREACH OF WARRANTY, TORT, NEGLIGENCE, INFRINGEMENT OR OTHERWISE (INCLUDING, WITHOUT LIMITATION, DAMAGES BASED ON LOSS OF PROFITS, DATA, FILES, USE, BUSINESS OPPORTUNITY OR CLAIMS OF THIRD PARTIES), AND WHETHER OR NOT THE PARTY HAS BEEN ADVISED OF THE POSSIBILITY OF SUCH DAMAGES. THIS LIMITATION SHALL APPLY

NOTWITHSTANDING ANY FAILURE OF ESSENTIAL PURPOSE OF ANY LIMITED REMEDY PROVIDED HEREIN.

8. Limitations

8. 1. BOOKS ONLY: Where 'reuse in a dissertation/thesis' has been selected the

following terms apply: Print rights of the final author's accepted manuscript (for clarity, NOT the published version) for up to 100 copies, electronic rights for use only on a personal website or institutional repository as defined by the Sherpa guideline

(www.sherpa.ac.uk/romeo/).

9. Termination and Cancellation

9. 1. Licences will expire after the period shown in Clause 3 (above).

9. 2. Licensee reserves the right to terminate the Licence in the event that payment is not received in full or if there has been a breach of this agreement by you.

Appendix 1 – Acknowledgements:

For Journal Content:

Reprinted by permission from [**the Licensor**]: [**Journal Publisher** (e.g. Nature/Springer/Palgrave)] [**JOURNAL NAME**] [**REFERENCE CITATION**]
(Article name, Author(s) Name), [**COPYRIGHT**] (year of publication)

For Advance Online Publication papers:

Reprinted by permission from [**the Licensor**]: [**Journal Publisher** (e.g. Nature/Springer/Palgrave)] [**JOURNAL NAME**] [**REFERENCE CITATION** (Article name, Author(s) Name), [**COPYRIGHT**] (year of publication), advance online publication, day month year (doi: 10.1038/sj.[**JOURNAL ACRONYM**].)]

For Adaptations/Translations:

Adapted/Translated by permission from [**the Licensor**]: [**Journal Publisher** (e.g. Nature/Springer/Palgrave)] [**JOURNAL NAME**] [**REFERENCE CITATION** (Article name, Author(s) Name), [**COPYRIGHT**] (year of publication)]

Note: For any republication from the British Journal of Cancer, the following credit line style applies:

Reprinted/adapted/translated by permission from [**the Licensor**]: on behalf of Cancer Research UK: : [**Journal Publisher** (e.g. Nature/Springer/Palgrave)] [**JOURNAL NAME**] [**REFERENCE CITATION** (Article name, Author(s) Name), [**COPYRIGHT**] (year of publication)

For **Advance Online Publication** papers:

Reprinted by permission from The [**the Licensor**]: on behalf of Cancer Research UK: [**Journal Publisher** (e.g. Nature/Springer/Palgrave)] [**JOURNAL NAME**] [**REFERENCE CITATION** (Article name, Author(s) Name), [**COPYRIGHT**] (year of publication), advance online publication, day month year (doi: 10.1038/sj. [**JOURNAL ACRONYM**])

For Book content:

Reprinted/adapted by permission from [**the Licensor**]: [**Book Publisher** (e.g. Palgrave Macmillan, Springer etc) [**Book Title**] by [**Book author(s)**] [**COPYRIGHT**] (year of publication)

Other Conditions:

Version 1.2

Questions? customercare@copyright.com or +1-855-239-3415 (toll free in the US) or +1-978-646-2777.

SPRINGER NATURE
LICENSE TERMS
AND CONDITIONS

Dec 23, 2019

This Agreement between Curtin University -- OUF SHAMS ("You") and Springer Nature ("Springer Nature") consists of your license details and the terms and conditions provided by Springer Nature and Copyright Clearance Center.

License Number 4734810192343
License date Dec 23, 2019

Licensed Content Publisher:

Springer Nature

Licensed Content Publication:

Springer eBook

Licensed Content Title:

Comparative Assessment and Merit Appraisal of Thermally Assisted
Machining Techniques for Improving Machinability of Titanium Alloys

Licensed Content Author:

O. A. Shams, A. Pramanik, T. T. Chandratilleke et al

Licensed Content Date: Jan 1, 2018

Type of Use: Thesis/Dissertation

Requestor type: academic/university or research institute

Format: print and electronic

Portion: full article/chapter

Will you be translating? no

Circulation/distribution: 500 – 999

Author of this Springer content: yes

Title: Machinability Improvement of Hard-to-Machine Materials by Monitoring
and Controlling Laser Heating

Institution name: Curtin University Expected

presentation date: Jul 2020

Order reference number: 01

Requestor Location: Curtin University
Unit 20, 9-11 Norman Street
St James, WA, Western Australia 6102 Australia
Attn: Curtin University

Total: 0.00 USD

Terms and Conditions

Springer Nature Customer Service Centre GmbH Terms and Conditions

This agreement sets out the terms and conditions of the licence (the **Licence**) between you and **Springer Nature Customer Service Centre GmbH** (the **Licensor**). By clicking 'accept' and completing the transaction for the material (**Licensed Material**), you also confirm your acceptance of these terms and conditions.

1. Grant of License

1. The Licensor grants you a personal, non-exclusive, non-transferable, world-wide licence to reproduce the Licensed Material for the purpose specified in your order only. Licences are granted for the specific use requested in the order and for no other use, subject to the conditions below.

1. 2. The Licensor warrants that it has, to the best of its knowledge, the rights to license reuse of the Licensed Material. However, you should ensure that the material you are requesting is original to the Licensor and does not carry the copyright of another entity (as credited in the published version).

1.3. If the credit line on any part of the material you have requested indicates that it was reprinted or adapted with permission from another source, then you should also seek permission from that source to reuse the material.

2. Scope of Licence

2. 1. You may only use the Licensed Content in the manner and to the extent permitted by these Ts&Cs and any applicable laws.

2. 2. A separate licence may be required for any additional use of the Licensed Material, e.g. where a licence has been purchased for print only use, separate permission must be obtained for electronic re-use. Similarly, a licence is only valid in the language selected and does not apply for editions in other languages unless additional translation rights have been granted separately in the licence. Any content owned by third parties are expressly excluded from the licence.

2. 3. Similarly, rights for additional components such as custom editions and derivatives require additional permission and may be subject to an additional fee. Please apply to Journalpermissions@springernature.com/
bookpermissions@springernature.com for these rights.

2. 4. Where permission has been granted **free of charge** for material in print, permission may also be granted for any electronic version of that work, provided that the material is incidental to your work as a whole and that the electronic version is essentially equivalent to, or substitutes for, the print version.

2. 5. An alternative scope of licence may apply to signatories of the [STM Permissions](#)

[Guidelines](#), as amended from time to time.

3. Duration of Licence

3.1. A licence for is valid from the date of purchase ('Licence Date') at the end of the relevant period in the below table:

Scope of Licence	Duration of Licence
Post on a website	12 months
Presentations	12 months
Books and journals	Lifetime of the edition in the language purchased

4. Acknowledgement

4. 1. The Licensor's permission must be acknowledged next to the Licenced Material in print. In electronic form, this acknowledgement must be visible at the same time as the figures/tables/illustrations or abstract, and must be hyperlinked to the journal/book's homepage. Our required acknowledgement format is in the Appendix below.

5. Restrictions on use

5. 1. Use of the Licensed Material may be permitted for incidental promotional use and minor editing privileges e.g. minor adaptations of single figures, changes of format, colour and/or style where the adaptation is credited as set out in Appendix 1 below. Any other changes including but not limited to, cropping, adapting, omitting material that affect the meaning, intention or moral rights of the author are strictly prohibited.

5. 2. You must not use any Licensed Material as part of any design or trademark.

5.3. Licensed Material may be used in Open Access Publications (OAP) before publication by Springer Nature, but any Licensed Material must be removed from OAP sites prior to final publication.

6. Ownership of Rights

6.1. Licensed Material remains the property of either Licensor or the relevant third party and any rights not explicitly granted herein are expressly reserved.

7. Warranty

IN NO EVENT SHALL LICENSOR BE LIABLE TO YOU OR ANY OTHER PARTY OR ANY OTHER PERSON OR FOR ANY SPECIAL, CONSEQUENTIAL, INCIDENTAL OR INDIRECT DAMAGES, HOWEVER CAUSED, ARISING OUT OF OR IN CONNECTION WITH THE DOWNLOADING, VIEWING OR USE OF THE MATERIALS REGARDLESS OF THE FORM OF ACTION, WHETHER FOR BREACH OF CONTRACT, BREACH OF WARRANTY, TORT, NEGLIGENCE, INFRINGEMENT OR OTHERWISE (INCLUDING, WITHOUT LIMITATION, DAMAGES BASED ON LOSS OF PROFITS, DATA, FILES, USE, BUSINESS OPPORTUNITY OR CLAIMS OF THIRD PARTIES), AND WHETHER OR NOT THE PARTY HAS BEEN ADVISED OF THE POSSIBILITY OF SUCH DAMAGES. THIS LIMITATION SHALL APPLY

NOTWITHSTANDING ANY FAILURE OF ESSENTIAL PURPOSE OF ANY LIMITED REMEDY PROVIDED HEREIN.

8. Limitations

8. 1. BOOKS ONLY: Where 'reuse in a dissertation/thesis' has been selected the

following terms apply: Print rights of the final author's accepted manuscript (for clarity, NOT the published version) for up to 100 copies, electronic rights for use only on a personal website or institutional repository as defined by the Sherpa guideline

(www.sherpa.ac.uk/romeo/).

9. Termination and Cancellation

9. 1. Licences will expire after the period shown in Clause 3 (above).

9. 2. Licensee reserves the right to terminate the Licence in the event that payment is not received in full or if there has been a breach of this agreement by you.

Appendix 1 – Acknowledgements:

For Journal Content:

Reprinted by permission from [**the Licensor**]: [**Journal Publisher** (e.g. Nature/Springer/Palgrave)] [**JOURNAL NAME**] [**REFERENCE CITATION**]
(Article name, Author(s) Name), [**COPYRIGHT**] (year of publication)

For Advance Online Publication papers:

Reprinted by permission from [**the Licensor**]: [**Journal Publisher** (e.g. Nature/Springer/Palgrave)] [**JOURNAL NAME**] [**REFERENCE CITATION** (Article name, Author(s) Name), [**COPYRIGHT**] (year of publication), advance online publication, day month year (doi: 10.1038/sj.[**JOURNAL ACRONYM**].)]

For Adaptations/Translations:

Adapted/Translated by permission from [**the Licensor**]: [**Journal Publisher** (e.g. Nature/Springer/Palgrave)] [**JOURNAL NAME**] [**REFERENCE CITATION** (Article name, Author(s) Name), [**COPYRIGHT**] (year of publication)]

Note: For any republication from the British Journal of Cancer, the following credit line style applies:

Reprinted/adapted/translated by permission from [**the Licensor**]: on behalf of Cancer Research UK: : [**Journal Publisher** (e.g. Nature/Springer/Palgrave)] [**JOURNAL NAME**] [**REFERENCE CITATION** (Article name, Author(s) Name), [**COPYRIGHT**] (year of publication)

For **Advance Online Publication** papers:

Reprinted by permission from The [**the Licensor**]: on behalf of Cancer Research UK: [**Journal Publisher** (e.g. Nature/Springer/Palgrave)] [**JOURNAL NAME**] [**REFERENCE CITATION** (Article name, Author(s) Name), [**COPYRIGHT**] (year of publication), advance online publication, day month year (doi: 10.1038/sj. [**JOURNAL ACRONYM**])

For Book content:

Reprinted/adapted by permission from [**the Licensor**]: [**Book Publisher** (e.g. Palgrave Macmillan, Springer etc) [**Book Title**] by [**Book author(s)**] [**COPYRIGHT**] (year of publication)

Other Conditions:

Version 1.2

Questions? customercare@copyright.com or +1-855-239-3415 (toll free in the US) or +1-978-646-2777.



Preheating and thermal behaviour of a rotating cylindrical workpiece in laser-assisted machining

Author: Nima Nadim, Ouf A Shams, Tilak T Chandratilleke, et al

Publication: Proceedings of the Institution of Mechanical Engineers, Part B: Journal of Engineering Manufacture

Publisher: SAGE Publications

Date: 07/16/2019

Copyright © 2019, © SAGE Publications

If you are a SAGE journal author requesting permission to reuse material from your journal article, please note you may be able to reuse your content without requiring permission from SAGE. Please review SAGE's author re-use and archiving policies at <https://us.sagepub.com/en-us/nam/journal-author-archiving-policies-and-re-use> for more information.

If your request does not fall within SAGE's reuse guidelines, please proceed with submitting your request by selecting one of the other reuse categories that describes your use. Please note, a fee may be charged for reuse of content requiring permission. Please contact permissions@sagepub.co.uk if you have questions.

[BACK](#)

[CLOSE WINDOW](#)